STRESS-STRAIN CHARACTERISTICS OF COHESIONLESS GRANULAR MATERIALS SUBJECTED TO STATICALLY APPLIED HOMOGENEOUS LOADS IN AN OPEN SYSTEM

Thesis by

James M. Bell

In Partial Fulfillment of the Requirements

For the Degree of

Doctor of Philosophy

California Institute of Technology

Pasadena, California

1965

(Submitted September 1, 1964)

ACKNOWLEDGEMENTS

The author takes pleasure in acknowledging his thesis committee including Professors R. F. Scott, G. W. Housner, C. W. McCormick, N. H. Brooks and J. K. Knowles who reviewed the entire study and offered constructive criticism towards improvement of the manuscript. Thanks are especially due to Dr. R. F. Scott who served as project advisor during the course of the work and to Dr. G. W. Housner who introduced the author to invariant functions.

The author is sincerely grateful for the personal financial support received from the Ford Foundation, which provided a fellowship loan program for two years, and from the National Science Foundation which provided a NSF Science Faculty Fellowship for one year. Thanks are extended to the Engineering Division of the California Institute of Technology for providing funds and facilities for the construction of the spherical and three-dimensional compression apparatus, and especially to Dr. F. C. Lindvall, Chairman of the Division of Engineering and Applied Science, for his encouragement towards the completion of this work. The author is indebted to Mr. J. W. McClanahan, Photography Lab Supervisor, for taking the majority of photographs included herein; and to Mr. D. W. Laird, Supervisor, Mechanical Engineering Shop, for technical advice on difficult details of construction.

The author expresses thanks to the Engineering Experiment Station of the University of Idaho which provided facilities for standard triaxial compression tests, and especially to Mrs. Ann Kennaly, secretary, who aided in the typing of the figures. The author is also indebted to Mr. R. G. Thomson, a student of civil engineering at the University, who assisted in the performance of the most laborious calculations.

Finally, the author wishes to acknowledge his wife, Janet, who offered constant encouragement during the entire course of graduate study and who aided materially in the preparation and typing of this work.

ABSTRACT

A general stress-strain relationship in incremental and invariant form is derived for sand on the basis of experimental evidence. The resulting expression does not include the yield condition but makes allowance for the direction of loading and the state of stress. Two new modified and dimensionless invariant functions are introduced and a detailed description and classification of stress paths presented. A new first yield criterion for sand stressed to yield along one stress path is developed from experimental evidence. The friction angle in triaxial compression was minimum and 14° less than that in triaxial extension. The Mohr-Coulomb yield criterion extended to three dimensions is rejected.

Emphasis is placed on the importance of obtaining homogeneous stress in physical experiments. A new spherical compression apparatus was developed to study the behavior of sand under spherical compression. Disadvantages of former apparatuses were largely overcome by elimination of frictional loading, and a homogeneous state of stress was obtained. A new stress controlled three-dimensional compression apparatus capable of applying principal stresses to a rectangular plate sample was developed to study the behavior of sand under a general stress state, particularly under deviatoric stress. This apparatus provided for the independent measurement of volumetric strain and allowed for the development of considerable deformation in obtaining yield.

TABLE OF CONTENTS

1. INTRODUCTION

1.1 GRANULAR MATERIALS

Granular material consists of solid particles or grains and the inter-space between, or voids. The granular material of primary interest here is sand. Sand is composed of particles of various sizes and shapes. The grains are relatively large (diameters exceeding 0.074 mm) with respect to colloidal sizes and are primarily composed of quartz minerals. Grain size distributions are commonly obtained in the laboratory by use of square mesh sieves. Grain shape may be observed under a low power microscope.

A particular granular material may be considered as homogeneous or non-homogeneous, and as isotropic or anisotropic. The definitions of these terms are first made in a geometrical frame of reference and are closely related to the scale in whic the material is viewed. If the grains of various sizes and shapes are randomly distributed in space, the material is defined as geometrically homogeneous. If the grains are randomly oriented in space, the material is defined as geometrically isotropic. It is doubtful that any granular material found in nature is perfectly homogeneous or isotropic in this sense.

The scale of view is significant to the foregoing definitions of homogenity and isotropy. The word random has statistical implications, and the number of particles involved must therefore be great enough to give a valid statistical representation of the material.

If only several grains existing within a real granular mass were viewed, the picture would necessarily be both non-homogeneous and anisotropic. The same material viewed on a larger scale might be essentially homogeneous and isotropic.

Consider a particular granular material existing in nature, and the question of classification in terms of homogenity and isotropy. A three-dimensional picture of the grain structure would provide a basis of classification; however, this is not practically obtained. Certain physical tests are suggested. A grain size analysis performed on samples obtained at various locations within the material in space very likely provides the most direct answer to the question of homogenity. The results are, of course, physically related to the size of samples obtained and the spacial locations represented. The question of isotropy is far more difficult because any sampling technique is essentially destructive with respect to the maintenance of grain orientation. Physical tests, for example the determination of the resistance to fluid flow in various directions, might yield unequal results which would indicate the material to be geometrically anisotropic on a scale corresponding to the size of the test sample. The reverse physical indication might not, however, be geometrically conclusive. A material which is geometrically homogeneous and isotropic will, under spherical states of stress (equal, all-around pressure), be strained equally in all directions. The reverse statement again, however, may not lead to a definite geometric conclusion. Many physical tests might be considered in

this light. A substantial problem exists in obtaining relatively undisturbed samples of the granular material for testing. Field (in-situ) tests might be considered in order to eliminate some of the undesirable effects of sample disturbance.

1.2 STRESS AND STRAIN IN GRANULAR MATERIALS

The relationship between stress and strain for sand is indeed complex. Previous laboratory investigations have considered special cases; however, certain experimental limitations and a lack of generality have left much to be desired. Theoretical investigations have necessarily been limited to the study of simplified models. For the most part past studies of the stress-strain problem in granular materials have been concerned with failure, the limiting or the ultimate state.

The most well-known relationship between stress and strain is perhaps that represented by Hooke's law. This linear relationship is not often used beyond the proportional limit for the materials to which it applies, and certainly it does not contain any statement about yield or the failure condition. Various empirical criteria are used in engineering works to predict failure in solids which closely follow Hooke's law at small strains, and for the most part these are finally expressed as functional relationships between the stresses. In engineering practice the Mohr-Coulomb failure criterion has long been used to express the limiting condition for soils in general.

It is unlikely that soil of any type follows Hooke's law closely even at very small strains, and it would be fortunate indeed

if a single stress-strain functional relationship could be developed which would apply over wide ranges of deformation including the limit condition. Osborne Reynolds (1)* observed that granular materials undergo volume change upon shearing, and it is now well known that the relationship between stress and strain in sand is non-linear over a considerable range in deformation.

The term stress without qualifying phrases is herein defined as force per total unit area. The area involved is mostly void area and is large with respect to the actual area of grain contacts. Stress so defined is a statistical quantity which necessarily must be obtained as an average to include many grain contacts. The statistical nature of the definition places an obvious limitation on the size of the real problems to be solved in that a truly representative number of particles must be present. The usual procedure in continuum mechanics is adopted herein in that stress will be mathematically treated as a differential quantity, the area shrinking to zero in the limit. The expression "stress at a point" and the use of calculus should not, however, be allowed to erase the physical meaning of quantities thus operated upon.

The term strain without qualifying phrases is herein defined as a change in length per initial unit length, and like stress will be mathematically treated as a true limit value. This definition corresponds with that commonly used in the theory of elasticity and

---

*Reference numbers used in the text refer to correspondingly numbered items in the reference list which follows the appendixes.

has proven suitable in theoretical developments where the square of the strains are small with respect to unity.

Consider a granular system which contains fluid within the voids. In practice the fluid may be restricted from free motion by many factors. An open system is defined as a system in which, during the process of straining, the pore fluid pressure at a point in space remains constant in time. A closed system is defined as a system in which the mass of pore fluid within remains constant in time. The terms open and closed system are attributed to Kezdi (2). Normally the open system is free to drain at the boundaries while the closed system is normally sealed from drainage at the boundaries. Whether or not a system in practice is considered essentially open or closed depends considerably on the rate of loading or deformation and the compressibility of the pore fluid.

Throughout this work the well-known effective stress principle attributed to Terzaghi will be assumed valid.

1.3 LIMITED SUMMARY OF PREVIOUS WORK

1.31 EARLY WORK

Scientific progress in understanding the behavior of granular materials was very slow until the latter part of the eighteenth century. In 1776 C. A. Coulomb (3) published his famous essay which dealt in large part with the problem of earth pressure on retaining walls. In this work Coulomb suggested the failure law bearing his name which separated the strength of soil into components of cohesion

and friction. He applied the laws of friction and cohesion as they are known for solid bodies.

In 1857 Rankine (4) published a notable theory of earth pressure which stated in part that the shearing resistance was proportional to the normal pressure along the surface of rupture. Basically, this reiterated Coulomb's assumption about the strength of soil disregarding cohesion; however, Rankine's work dealt directly with stress while Coulomb's work dealt with total force. About 1881, Mohr (5) published his "Circle of Stress" method of stress analysis--a tool commonly used today in dealing with two-dimensional stress problems.

According to Capper and Cassie (6), the measurement of the shearing strength of sand utilizing what is commonly known as a direct shear box appears to have been accomplished first in France by Leygue about 1895. It is noteworthy and somewhat surprising that the classical theories of earth pressure were developed prior to the performance of physical laboratory tests on soil. In some respects this was putting the cart before the horse; nevertheless, in considerable measure the vision of the classical figures, i.e. Coulomb and Rankine, was born out in practice.

Since these early times, the entire subject of soil mechanics was placed in perspective perhaps more by the late Karl Terzaghi than by any other individual. Physical laboratory and full-scale field investigations have followed, many of which deal with the strength of granular materials. The art of testing soils was much improved

by the advent of the triaxial compression test. A brief history of the triaxial test is given by Haythornthwaite (7).

1.32 SPECIFIC EXPERIMENTAL STUDIES ON SAND

Experimental studies involving the relationship between the state of stress and the failure condition for sands were performed by Kjellman (8), Habib (11), Bishop and Eldin (10), Jakobson (12), Kirkpatrick (13), Peltier (14), Haythornthwaite (7), and Wu, Loh, and Malvern (18). These particular works are summarized in Table 3.1.

Roscoe, Schofield and Wroth (15) indicated the existence of a unique critical voids ratio line for sand as based upon tests carried out in a simple shear apparatus. Hvorslev (16) summarized the results of strength studies on sand previous to 1960.

Tests performed by Kjellman (8) and Jakobson (12) for the most part did not reach yield and are regarded mainly as stress-strain studies. Wilson and Sutton (9) considered the tangent modulus of elasticity for two sands over a wide range in porosity as based upon triaxial compression test results. Chaplin (17) discussed the compressibility of sands and considered the change in number of grain contacts with porosity.

1.33 GENERAL RELATIONSHIP BETWEEN STRESS AND STRAIN IN SOILS

Hoshino (19, 20, 21) presented hypothetical theories of deformation for soils. In the final paper his previous theories are modified somewhat to account for volume change induced by shearing in the triaxial compression test.

Newmark (22) introduced a failure hypothesis for soils, and a stress-strain relationship in the form of invariant functions. This paper is believed to be particularly significant in that it suggests an approach in which a general stress-strain relationship might be obtained from experimental evidence.

Meyerhof (23) emphasized the importance of the general three-dimensional stress-strain problem in soil mechanics. Kondner (24) suggested a hyperbolic stress-strain relationship which might be applied in specific cases to certain soils over their entire range in deformation.

1.34 YIELD AND PLASTICITY THEORIES

Ideal theories of plasticity are advanced in standard texts, i.e. Prager and Hodge (25). Which ideal theory might be applied to soil in general or sand in particular is still open to question. Kezdi (2) clearly states the arbitrary nature of plasticity theories as applied to soil mechanics. Coleman (26) and Coleman and Russam (27) indicate a possible yield criterion for soils in invariant form. Hu (28) discussed the significance of the spherical stress state in the plastic flow of metals. Haythornthwaite (29) expressed doubt as to the validity of the Coulomb failure criterion as applied to soil for complex stress states. Haythornthwaite (30) also considered the range of the yield condition in ideal plasticity.

DeWet (31) discussed the use of the energy concept in soil mechanics. Takagi (32) dealt with the plane plastic deformation of

soils and suggested a general yield criterion in arbitrary invariant form.

1.35 THE STUDY OF SIMPLIFIED GRANULAR MATERIALS

Deresiewicz (33) summarized current knowledge as well as presenting the possible direction of future work with respect to granular materials composed of groups of spherical particles. Newland and Allely (34, 35) studied triaxial compression tests on lead shot and discussed the effects of membrane penetration. Rowe (36) performed a theoretical and experimental study of ideal assemblies of rods and uniform spheres. The removal of end plate restraint was attempted in triaxial tests. Laszlo (37) also studied the stability of groups of cylinders and spheres.

1.4 PURPOSE AND SCOPE OF THIS STUDY

The purpose of this investigation was to obtain a relationship between statically applied stress and the resulting strain in sand. General relationships were formulated which contain arbitrary functions. A limited number of physical laboratory tests were carried out to empirically define the form of these functions, and a new yield criterion was obtained. A spherical compression apparatus was developed to define the relationship between spherical stress and spherical strain for samples of sand at various degrees of initial porosity. A three-dimensional compression apparatus was developed to study the more general relationship between stress and strain; however, the initial porosity in the three-dimensional tests was

relatively low (dense sand) and essentially constant. Theoretical developments based upon simplified models of granular material were not attempted.

At the outset, strains were assumed small in order that the usual engineering definition of strain might be utilized. Theories of finite deformation provide better definitions of strain where the deformations become relatively large; however, these theories give rise to certain analytical complexities usually resulting in the study of special cases.

The physical laboratory tests were stress controlled, thus the approach adopted throughout this study was to proceed in discussion from stress to strain. The test specimens were saturated with water, but the stresses were applied slowly, and the strains were essentially static prior to yield. All tests were considered to be fully drained and the systems completely open. Physical laboratory tests were not purposely carried beyond yield.

Symbols will be defined where they first appear and are summarized in the appendix. Tables, figures and equations are numbered separately for each chapter; the number before the period denotes the chapter and the number following the period gives the number of the item in the chapter.

2. A DIRECT RELATIONSHIP BETWEEN STRESS AND STRAIN FOR GRANULAR MATERIAL SUBJECTED TO CONTROLLED STATICALLY APPLIED LOADS IN AN OPEN SYSTEM

The load-deformation behavior of a representative sample of granular material subjected to a homogeneous state of external stress must necessarily represent the integrated action of its constituant parts. The following discussion thus proceeds from small scale to large scale behavior. It has been previously suggested that the relationship between stress and strain is dependent on the scale in which the material is viewed.

2.1 SMALL SCALE BEHAVIOR--A SINGLE PARTICLE

Consider a single grain subjected to concentrated loads and torques as shown in Figure 2.1. Each force is inclined from the normal to the contact surface (envisioned as a plane bounded area) by an angle of obliquity.

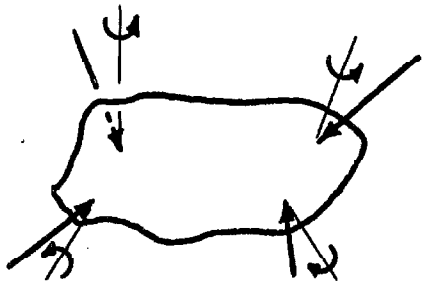

Figure 2.1 Single Particle under Load

Internal grain deformations consist of elastic (returnable) and plastic (non-returnable) components. Elastic deformations occur throughout the grain, and may be associated primarily with

the present loading*. Plastic deformations are largely the result of stress concentration, i.e. at particle contacts, and depend considerably on the entire history of loading. The stresses existing within the real grain at any given time are indeterminate. It is possible that weak grains may fracture when subjected to relatively low loads, and factors conducive to such undesirable behavior are:

1. Sudden irregularities in grain shape
2. Internal non-homogenities or irregularities existing with the grain
3. Structural grain shapes leading to the development of high bending stresses, i.e. needles or plates (not common in sand).

The particular grain shown in Figure 2.1 must be in static equilibrium unless yield is in progress. It is important to note that yield referred to in this context is associated primarily with grain to grain slippage and occurs on a relatively small scale. Here the ability of a contact to support surface stress without the occurrence of a discontinuity in deformation is of critical

---

*An elasticity theory due to Hertz (38) expresses the relative approach Δ of two spheres, each of radius R, compressed statically by a force N which is directed along their line of centers as

$$\Delta = 2\left[\frac{3(1-\nu^2)}{4E}\,\frac{N}{R^{1/2}}\right]^{2/3}$$

Here ν and E denote Poisson's ratio and Young's modulus respectively, the power relationship is due to the increase in contact area with load. Deresiewicz (33) summarizes this and later developments for deformation under inclined load and torsion.

importance*. If the torques were absent, it might be presumed that the angle of obliquity must be limited such that $\tan \alpha \leq f$ where f is the static coefficient of grain to grain friction. It is suggested, however, that the presence of torque increases the deviatoric state of grain contact stress, and thus decreases the effective limit value f.

A classification of contact stability with respect to grain to grain slippage is given as follows: A sub-critical contact exists where the interface stresses are below yield, and where there is no danger of impending relative motion. A critical contact exists where the interface stresses have approached yield as a limit and where slippage is impending. A super-critical contact exists where the contact surfaces are in a state of relative motion.

If a certain contact becomes critical, a minute additional obliquity in loading or a minute additional adverse torque will cause the contact to become super-critical. Should the particle yield, certain adjustments are required if static equilibrium is to be attained once again. These adjustments likely involve one or a combination of the following factors:

1. Number of particle contacts
2. Location of particle contacts
3. Orientation of particle contacts

---

*According to Gemant (39), the basic mechanism of external friction is so complex that there is yet no generally accepted theory available. The well-known Coulomb law of solid friction is still empirically based. Numerous experimental studies have indicated that the static Coulomb coefficient of friction is essentially independent of load and dependent upon the nature of the surface and temperature in addition to other factors.

4. Magnitude of loads

5. Direction of loads

6. Magnitude of torques

7. Direction of torques

It seems reasonable that a grain which has yielded on a small scale will require less adjustment to reach a new equilibrium if the number of contacts is initially high, and if the contacts are uniformly spaced and symmetrically oriented about the particle.

2.2 INTERMEDIATE SCALE BEHAVIOR--A FEW PARTICLES

Consider now increasing the scale of view to include a few particles as shown in Figure 2.2 External loads and torques are applied to the system by adjacent particles. The deformation of the group with respect to some reference stage in past history includes that previously mentioned for each individual particle plus the integrated effects of relative grain to grain displacement. Relative grain movements may occur with translation and/or rotation. Those displacements associated with frictional energy dissipation result in plastic group deformation.

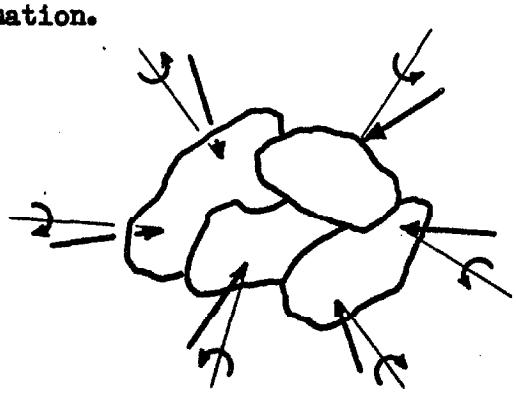

Figure 2.2 A Few Particles under Load

The geometric grain structure for such a small group of sand particles must necessarily be non-homogeneous and anisotropic. An engineering definition of stress and strain in the context of Section 1.2 is not possible for such a group of particles which does not statistically represent the material. The field of view must be enlarged.

2.3 LARGE SCALE BEHAVIOR--A NUMBER OF PARTICLES SUFFICIENT TO STATISTICALLY REPRESENT THE BEHAVIOR OF THE SYSTEM

Consider now a cube-shaped model of the material statistically containing a large number of particles as illustrated in Figure 2.3. For convenience the cube may be taken of unit dimensions.

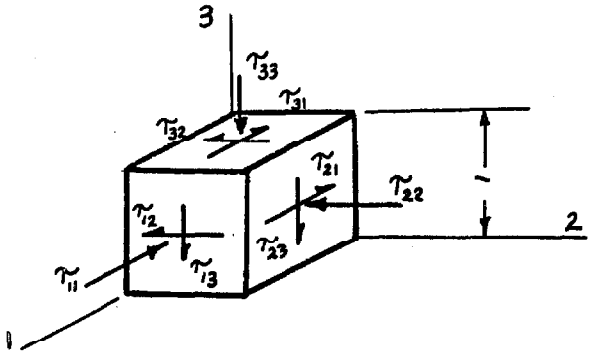

Figure 2.3 A Representative Number of Particles under Stress

The existing state of stress* can now be defined in engineering terms, and the stress components τ_{ij} (i, j = 1, 2, 3) may be considered as externally applied. Stress will be transmitted

---

*The notation for stress and strain here is the same as that used by Sokolnikoff (40) except that the sign convention for stress is reversed, i.e. τ_{ij} refers to stress on the i plane in the -j direction, thus resulting in positive signs for the usual compression stress.

throughout the model by certain particles, and a system of internal contact forces and torques serves to transmit the loads from particle to particle. All particles are not necessarily loaded--some groups may be entirely free from load. If each particle is in a state of static equilibrium, there are no super-critical contacts; and it follows that the entire system must be in a state of static equilibrium. The effects of vibration are neglected. The stiffness of the model depends on many factors. The actual paths of force transmission are indeterminate; however, the number, location and direction of the paths must be related to the size, shape, orientation and location of each particle. The elastic and plastic properties of the grains and the coefficients of grain to grain friction also have a bearing on the stiffness of the sample. The possibility of grain slippage at a given grain to grain contact is dependent primarily upon the angle of obliquity of the contact force, and this in turn is dependent upon the existing state of applied external stress.

Now let it be assumed that the boundary stress components τ_{ij} are changed by $\Delta\tau_{ij}$ in such a way that certain internal contacts become super-critical. If relatively small groups of particles, including these critical grains, are able to adjust in such a way that motion is damped on a relatively small scale, the boundaries will sense motion followed by static equilibrium once again. In other words, the rate of strain as sensed at the boundaries will essentially decrease in time after application of the boundary load increment. On a large scale this behavior is defined as static or below yield.

If the boundary stresses are returned to their former values, the model is not expected to return precisely to its original configuration. The degree of elasticity is primarily dependent upon the relative amounts of elastic and plastic deformation which occurred due to the previous stress increment.

Suppose now that the boundary components of stress are changed in such a way that, at a certain state of stress, yield spreads to a large number of particles and equilibrium cannot be maintained within the sample as a whole. Even though the boundary loads are held constant, the sample deforms at a rate which increases with time. That condition where at a fixed state of stress the state of strain becomes continuously dependent upon time is herein defined as first yield.

After first yield has been obtained, the strain response of the model is dependent upon time and the state of stress which is applied. Physical tests which are stress controlled by dead load are generally terminated soon after first yield due to equipment limitations and the following discussion is hypothetical. It is assumed that the state of stress is subject to control at all times.

Figure 2.4 a) represents the hypothetical and idealized stress-strain behavior of an initially dense sand in a stress controlled environment. An equal all-around pressure is first applied to the model, point O representing the initial state. As deviatoric or shearing stress is slowly applied, the strain response is essentially static and is given by Oa. At a, the rate of strain increases in time, and first yield is uniquely defined for the stress path previously

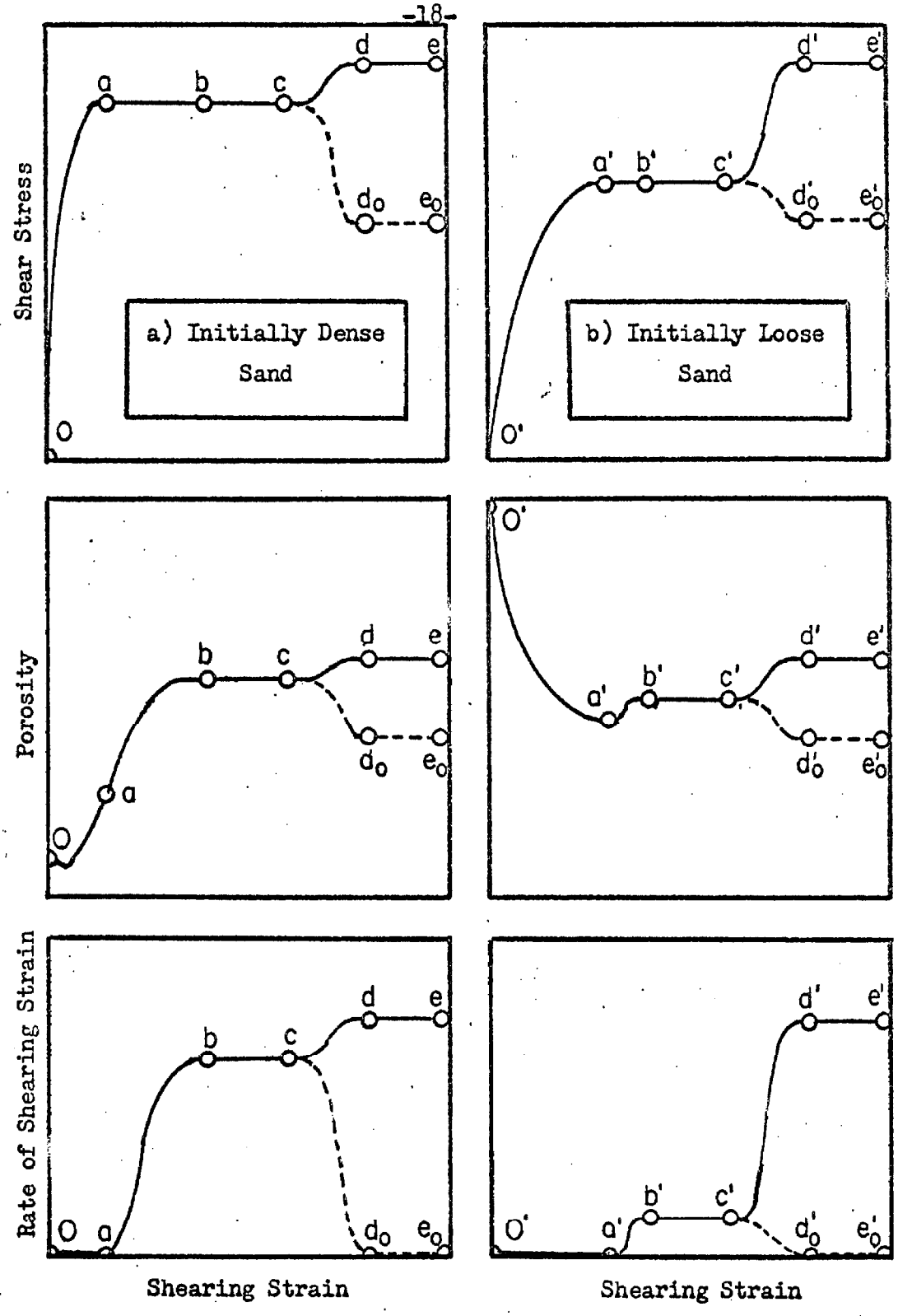

Figure 2.4 Simplified Stress-Strain Relationships for Initially Dense and Initially Loose Sands.

traced. The state of stress is held constant at the first yield value, and the rate of strain increases to reach a constant value at b, continuing to point c where the shearing stress is then either increased or decreased. Curve cd represents response to an increased deviatoric stress at c, while cd_o represents response to a particular decreased deviatoric stress causing the rate of strain to approach zero asymptotically. The horizontal curves bc, de and d_oe_o all represent ultimate yields, and the corresponding states of stress are related to porosity and rate of strain. It is suggested that the particular ultimate yield obtained from a decreasing state of deviatoric stress following first yield such that the rate of strain approaches zero in time be defined as static ultimate yield.

2.4 THE SEARCH FOR A QUANTITATIVE AND GENERAL STRESS-STRAIN RELATIONSHIP

The purpose of this section is to develop a mathematical expression of a general nature to represent the relationship between statically applied stress and the resulting strain for granular materials in an open system. The approach taken is in large part empirical, and certain unspecified functions must eventually be determined, at least approximately, by the performance of physical laboratory experiments.

2.41 ELASTIC SOLIDS

The state of stress and the state of strain both possess the properties of a tensor, each involving nine components--six of which

are independent. The usual engineering definition of strain has been adopted here which assumes that the square of the strains are negligible with respect to unity (small superposable strains).

$$\epsilon_{ij} = \frac{1}{2}\left(\frac{\partial u_i}{\partial x_j} + \frac{\partial u_j}{\partial x_i}\right) \tag{2.1}$$

where u_i (u_j) represents the displacement of a point in the i (j) direction, and x_j (x_i) represents the initial j (i) co-ordinate of the point. The sign convention is chosen such that an increase in volume (positive dilatancy) will be associated with extension strain.

It is assumed here that the relationship between stress and strain for anisotropic but elastic solids may be expressed by a generalized Hooke's law (40) modified so as to contain certain arbitrary and possibly non-linear coefficient functions.

$$\epsilon_{ij} = b_{ijkL}\,\tau_{kL} \qquad (i, j, k, L = 1, 2, 3) \tag{2.2}$$

or

$$\epsilon = B\tau \tag{2.3}$$

where ϵ is the strain tensor, B is the transformation matrix composed of 81 coefficient functions, and τ is the stress tensor. Since $\epsilon_{ij} = \epsilon_{ji}$ and $\tau_{ij} = \tau_{ji}$, it may be shown that the 81 coefficient functions b_{ijkL} in the B matrix contain at most 36 independent functions. If the conditions of anisotropy are fixed with respect to the 1, 2 and 3 axes, the number of independent functions may be appropriately reduced by further analysis, see Love (41). For a linearly elastic and isotropic medium it is well known that there exist only two independent coefficient functions in the B matrix.

2.42 NON-ELASTIC SOLIDS

In the case of non-elastic materials a unique relationship between stress and strain may not be written in the form of Equation 2.2 because the behavior is dependent upon the direction as well as the magnitude of load variation. The direction of loading is perhaps best reflected in differential form for a single stress increment.

$$d\epsilon_{ij} = d_{ijkL}\, d\tau_{kL}, \quad (i, j, k, L = 1, 2, 3) \tag{2.4}$$

where

$$d_{ijkL} = d_{ijkLC}, \qquad d\tau_{kL} > 0 \tag{2.5}$$

$$d_{ijkL} = d_{ijkLR}, \qquad d\tau_{kL} < 0 \tag{2.6}$$

In this form each coefficient function d_{ijkL} is given a double identity, one function, d_{ijkLC}, corresponding to an increase in the corresponding stress, the other function, d_{ijkLR}, corresponding to a decrease in the corresponding stress. In this formulation there would be at most 72 possible functions to be determined by physical experimentation.

2.43 GRANULAR MATERIALS

The stress-strain relationship for granular materials may be described in general form by Equations 2.4 through 2.6. The coefficient functions d_{ijkL} are measures of stiffness and thus may be taken to be mechanical properties of the material. For granular materials it is assumed that these are in turn related to variables previously mentioned in Sections 2.1 through 2.3. (Initially all variables thought likely to bear upon the stiffness of sand will be

included. Numerous simplifications will be made later for purposes of analysis.) Let it be assumed that the following set of variables is equivalent to those of Sections 2.1 through 2.3:

1. Modulus of elasticity of the grain material, E
2. Poisson's ratio of the grain material, ν
3. Yield strength of the grain material, s
4. Coefficient of grain to grain friction, f
5. Actual state of existing stress, τ_{ij} (components)
6. State of strain measured from an isotropic state, ϵ''_{ij} (components)
7. Porosity of the material, n
8. Coefficients representing particle shape, a_n
9. Coefficients representing grain size distribution, b_n.

The modulus of elasticity E and Poisson's ratio ν of the grain material are involved in the elastic deformation of a single particle as may be seen by the simplest of theories, i.e. the Hertz theory. The yield strength of the grain material s is related to the plastic deformation of the grains where highly stressed, and may also be related to the coefficient of grain to grain friction f. The existing stress components τ_{ij} are included to account for shear and normal forces existing between the grains in addition to other factors--friction and slippage being highly dependent on contact loads. The strain components ϵ''_{ij} measured from an isotropic state are given to represent the effect of orientation or anisotropy of the grain structure. The porosity of the material n is included primarily as a

measure of the number of grain contacts. The factors required to represent the effect of particle shape a_n increase with the complexity of the shape, i.e. one diameter required for a sphere, two for a cylinder, three for an ellipsoid, etc. The factors required to represent the effect of grain size distribution b_n increase with the complexity of the grain size distribution curve.

The following direct relationship between stress and strain is proposed:

$$d\epsilon_{ij} = d_{ijkL}\, d\tau_{kL}, \qquad (i, j, k, L = 1, 2, 3)$$

(Equation 2.4) where

$$d_{ijkL} = d_{ijkLC}\ (E, \nu, s, f, a_n, b_n, n, \epsilon''_{ij}, \tau_{ij}), \quad d\tau_{kL} > 0 \qquad (2.7)$$

$$d_{ijkL} = d_{ijkLR}\ (E, \nu, s, f, a_n, b_n, n, \epsilon''_{ij}, \tau_{ij}), \quad d\tau_{kL} \leq 0 \qquad (2.8)$$

For a particular granular material the coefficient functions may be reduced to

$$d_{ijkL} = d_{ijkLC}\ (n, \epsilon''_{ij}, \tau_{ij}), \qquad d\tau_{kL} > 0 \qquad (2.9)$$

$$d_{ijkL} = d_{ijkLR}\ (n, \epsilon''_{ij}, \tau_{ij}), \qquad d\tau_{kL} \leq 0 \qquad (2.10)$$

In this case the variables E, ν, s, f, a_n and b_n, all dealing with certain physical and mechanical properties of the grains themselves, are assumed to remain constant during the process of straining. The possibility of grain fracture has been neglected.

In order to further simplify the relationship between stress and strain, and in order to facilitate the planning of a limited number of laboratory experiments, it is desirable to carefully consider the utility of stress and strain invariant functions.

2.5 YIELD CRITERIA

2.51 FIRST YIELD

Stress-strain diagrams in simplified form were given in Figure 2.4. The curves Oa and O'a' are considered to represent that portion of the stress-strain behavior included within the range of the relationships expressed in the previous section. Points a and a' represent first yield as defined by Section 2.3 for initially dense and initially loose sands respectively. If the curves Oa and O'a' are assumed horizontal at a and a', then according to Equation 2.4 the requirement that at least one coefficient function d_{ijkL} becomes infinitely large defines first yield. On this basis, the first yield condition may be included within the range of the general stress-strain relationships of the previous section. It should be mentioned that these relationships based on the engineering definition of strain become less accurate with increasing strain.

Unfortunately, near the limit condition, certain practical difficulties are associated with the generality of the stress-strain relationships previously presented. Consider, for example, the dense sand at first yield. The stress-strain relationship may break sharply at a and thus may not be clearly defined by experimental data. If the sharp curvature could be detected, still it would be difficult to empirically fit a continuous function to the entire range of deformation including first yield--a limit condition. The loose sand is more desirable in this respect, but the strains are larger.

In search for a practical first yield criterion and considering the possible requirement that a single coefficient function d_{ijkL} in Equation 2.4 becomes infinitely large at first yield, then in the limit it follows that

$$\frac{1}{d_{ijkL}} = d_{1y}\,(n,\ \epsilon''_{ij},\ \tau_{ij}) = 0 \qquad (2.11)$$

where d_{1y} is regarded as a single functional relationship to be obtained empirically from physical experiments. If geometric isotropy is neglected the strain components ϵ''_{ij} are dropped resulting in

$$d_{1y}\,(n,\ \tau_{ij}) = 0 \qquad (2.12)$$

2.52 ULTIMATE YIELD

According to Section 2.3, an ultimate yield criterion corresponding to a fixed state of stress rationally includes a statement on the state of rate of strain. Equation 2.11 so modified gives

$$d_{uy}\,(n,\ \dot{\epsilon}_{ij},\ \tau_{ij}) = 0, \qquad \dot{\epsilon}_{ij} = \frac{d\,\epsilon_{ij}}{dt} \qquad (2.13)$$

In this formulation for ultimate yield the state of rate of strain has replaced the state of non-isotropic strain in the equation for first yield. For a fixed rate of strain, for example, static ultimate yield as defined by Section 2.3 (points d_o and d_o' of Figure 2.4), Equation 2.13 is further modified giving

$$d_{suy}\,(n,\ \tau_{ij}) = 0 \qquad (2.14)$$

The consideration of isotropy has disappeared. If the porosity at

static ultimate yield is considered constant for a particular granular material then Equation 2.14 may be reduced finally to

$$f(\tau_{ij}) = 0 \qquad (2.15)$$

Ideal theories of plasticity for isotropic materials which assume constant volume during yield, i.e. Kezdi (2), give the following empirical relationship for the limiting state

$$f(\sigma_1, \sigma_2, \sigma_3) = 0 \qquad (2.16)$$

where σ_1, σ_2 and σ_3 are principal stresses. The latter form is equivalent to Equation 2.15. The experimental works of Hvorslev (16) and Roscoe, Schofield and Wroth (15) for limited stress states support the hypothesis represented by Equation 2.14.

3. THE RELATIONSHIP BETWEEN STRESS AND STRAIN IN INVARIANT FORM FOR GRANULAR MATERIAL SUBJECTED TO CONTROLLED STATICALLY APPLIED LOADS IN AN OPEN SYSTEM

3.1 STRESS INVARIANT FUNCTIONS

Stress and strain invariant functions are developed in standard texts: see Timoshenko and Goodier (38), Sokolnikoff (40), and Love (41). Newmark (22) discussed the possible use of invariant functions in stress-strain studies of cohesive soils. Sections 3.11 and 3.12 are not original with the author, and are included to provide a brief introduction to invariant functions and a certain continuity of presentation.

Relationships between the principal stress ratio β, originally presented by Lode (42), and various stress invariants are developed in Section 3.13 where a new modified and dimensionless third stress invariant function I_3^* is introduced. Relationships between the friction angle Φ, well known as a parameter in the Mohr-Coulomb strength criterion, and the principal stress ratio β are developed in Section 3.14 where a new modified and dimensionless second stress invariant function I_2^* is introduced.

The relationships given in Sections 3.13 and 3.14 allow the investigator using variables different from those of this study an avenue of comparison. In combination with the first invariant function, the author later adopts the second and third modified and dimensionless invariant functions as convenient variables, and these are used where possible in the presentation of test results. Physical

justification for the use of these particular invariant functions is given in Section 3.4.

3.11 THE ORIGINAL STRESS INVARIANT FUNCTIONS I_{1n}, I_{2n}, I_{3n}

The original stress invariant functions arise from a statement of force equilibrium in three dimensions. Given a cubic element, i.e. Figure 2.3, subjected to stress components τ_{ij}, it is possible to find three orthogonal and principal stresses T from solution of the cubic equation

$$T^3 + I_{1n}T^2 + I_{2n}T + I_{3n} = 0 \tag{3.1}$$

where the first, second, and third normal stress invariants are respectively

$$I_{1n} = \tau_{11} + \tau_{22} + \tau_{33} \tag{3.2}$$

$$I_{2n} = \tau_{11}\tau_{22} + \tau_{22}\tau_{33} + \tau_{11}\tau_{33} - \tau_{12}^2 - \tau_{23}^2 - \tau_{13}^2 \tag{3.3}$$

$$I_{3n} = \begin{Vmatrix} \tau_{11} & \tau_{12} & \tau_{13} \\ \tau_{12} & \tau_{22} & \tau_{23} \\ \tau_{13} & \tau_{23} & \tau_{33} \end{Vmatrix} \tag{3.4}$$

Principal stresses as determined from Equation 3.1 do not require specification of the orientation of axes 1, 2 or 3 except that they be mutually orthogonal; therefore the stress functions I_{1n}, I_{2n} and I_{3n} given by Equations 3.2, 3.3 and 3.4 are invariant from the axes of orientation.

If the axes of orientation are principal axes, the shear stress components may be eliminated from Equations 3.2, 3.3 and 3.4 giving

$$I_{1n} = \tau_{11} + \tau_{22} + \tau_{33} \tag{3.2}$$

$$I_{2n} = \tau_{11}\tau_{22} + \tau_{22}\tau_{33} + \tau_{11}\tau_{33} \tag{3.5}$$

$$I_{3n} = \tau_{11}\tau_{22}\tau_{33} \tag{3.6}$$

3.12 MODIFIED STRESS INVARIANTS I_1, I_2, I_3

Specification of any three linearly independent functions of the three original stress invariants allows for the determination of the three original invariants and thus for the state of stress at a point independent from the orthogonal axes of orientation. Three such functions which have proven to be of considerable value in material studies are designated as the first, second and third modified stress invariants and are given respectively by

$$I_1 = I_{1n} \tag{3.7}$$

$$I_2 = I_{2n} - \frac{1}{3} I_{1n}^2 \tag{3.8}$$

$$I_3 = I_{3n} - \frac{I_{1n} I_{2n}}{3} + \frac{2}{27} I_{1n}^3 \tag{3.9}$$

The utility of this particular scheme of modified stress invariants is based primarily upon the physical behavior of isotropic materials where spherical stresses cause only spherical strains, and where deviatoric stresses cause only deviatoric strains. The division of stress is given by

$$\tau_{ij}' = \frac{I_1}{3} \delta_{ij} \tag{3.10}$$

and

$$\tau_{ij}'' = \tau_{ij} - \frac{I_1}{3} \delta_{ij} \tag{3.11}$$

where

τ_{ij}' = spherical stress

τ_{ij}'' = deviatoric stress

δ_{ij} = Kroenecker delta function $\qquad \delta_{ij}\begin{cases} = 1, & i=j \\ = 0, & i\neq j \end{cases}$

The first modified stress invariant is dependent only upon the spherical state of stress while the second and third modified stress invariants are dependent only upon the deviatoric state of stress as it can be shown that

$$I_1 = \tau_{11} + \tau_{22} + \tau_{33} \tag{3.12}$$

$$I_2 = \tau_{11}''^2 + \tau_{22}''^2 + \tau_{33}''^2 + 2\,\tau_{12}''^2 + 2\,\tau_{23}''^2 + 2\,\tau_{13}''^2 \tag{3.13}$$

$$I_3 = \begin{Vmatrix} \tau_{11}'' & \tau_{12}'' & \tau_{13}'' \\ \tau_{12}'' & \tau_{22}'' & \tau_{23}'' \\ \tau_{13}'' & \tau_{23}'' & \tau_{33}'' \end{Vmatrix} \tag{3.14}$$

If the 1, 2 and 3 axes are principal axes then the preceding expressions are simplified

$$I_1 = \tau_{11} + \tau_{22} + \tau_{33} \tag{3.12}$$

$$I_2 = \tau_{11}''^2 + \tau_{22}''^2 + \tau_{33}''^2$$

$$= \frac{1}{3}\left[(\tau_{11}-\tau_{22})^2+(\tau_{22}-\tau_{33})^2+(\tau_{11}-\tau_{33})^2\right] \tag{3.15}$$

$$I_3 = \tau_{11}''\,\tau_{22}''\,\tau_{33}'' = \left(\tau_{11}-\frac{I_1}{3}\right)\left(\tau_{22}-\frac{I_1}{3}\right)\left(\tau_{33}-\frac{I_1}{3}\right) \tag{3.16}$$

3.13 RELATIONSHIPS INVOLVING THE PRINCIPAL STRESS RATIO

Consider the state of stress such that

$$\sigma_3 \leq \sigma_2 \leq \sigma_1 \tag{3.17}$$

where σ_1, σ_2 and σ_3 are defined by the inequality as major, intermediate and principal stresses respectively. The principal stress ratio* is given by

$$\beta = 1 - 2\left(\frac{\sigma_2-\sigma_3}{\sigma_1-\sigma_3}\right) = \frac{\sigma_1 - 2\sigma_2 + \sigma_3}{\sigma_1-\sigma_3}\ , \tag{3.18}$$

$$-1 \leq \beta \leq 1$$

and solving for σ_2 then

$$\sigma_2 = \frac{\sigma_1 + \sigma_3}{2} - \left(\frac{\sigma_1 - \sigma_3}{2}\right) \tag{3.19}$$

The first invariant stress function I_1 may be expressed according to Equation 3.12 as

$$I_1 = \sigma_1 + \sigma_2 + \sigma_3 \tag{3.20}$$

and upon substitution of Equation 3.19 for σ_2 gives

$$I_1 = 3\left(\frac{\sigma_1+\sigma_3}{2}\right) - \beta\left(\frac{\sigma_1-\sigma_3}{2}\right) \tag{3.21}$$

The deviatoric stresses are from Equation 3.11

$$\sigma_1'' = \sigma_1 - \frac{I_1}{3}\ ,\quad \sigma_2'' = \sigma_2 - \frac{I_1}{3}\ ,\quad \sigma_3'' = \sigma_3 - \frac{I_1}{3} \tag{3.22}$$

and upon substitution of Equation 3.21 for I_1 become

$$\sigma_1'' = \frac{3+\beta}{6}(\sigma_1-\sigma_3) = 1 + \frac{\beta}{3}\left(\frac{\sigma_1-\sigma_3}{2}\right) \tag{3.23}$$

---

*Lode (42) utilized parameters μ and ν for principal stress and principal strain ratios respectively in a study of the effect of the intermediate principal stress on the yield properties of metals.

$$\sigma_2'' = -\frac{\beta}{3}(\sigma_1-\sigma_3) = -\frac{2}{3}\beta\left(\frac{\sigma_1-\sigma_3}{2}\right) \tag{3.24}$$

$$\sigma_3'' = \frac{3-\beta}{6}(\sigma_1-\sigma_3) = 1-\frac{\beta}{3}\left(\frac{\sigma_1-\sigma_3}{2}\right) \tag{3.25}$$

The second modified invariant function is rewritten from Equation 3.15 as

$$I_2 = \sigma_1''^2 + \sigma_2''^2 + \sigma_3''^2 \tag{3.26}$$

Upon substitution of Equations 3.23, 3.24 and 3.25 one obtains

$$I_2 = \frac{3+\beta^2}{6}(\sigma_1-\sigma_3)^2 \tag{3.27}$$

The third modified invariant function is rewritten from Equation 3.16 as

$$I_3 = \sigma_1''\,\sigma_2''\,\sigma_3'' \tag{3.28}$$

Upon substitution of Equations 3.23, 3.24 and 3.25 one obtains

$$I_3 = \frac{1}{27}\beta\left(\frac{3+\beta}{2}\right)\left(\frac{3-\beta}{2}\right)(\sigma_1-\sigma_3)^3$$

$$-\frac{1}{108}\beta(9-\beta^2)(\sigma_1-\sigma_3)^3 \tag{3.29}$$

Equating $(\sigma_1-\sigma_3)$ obtained from Equations 3.27 and 3.29 leads to

$$I_3^* = \frac{3\sqrt{6}\,I_3}{I_2^{3/2}} = \frac{\beta(9-\beta^2)}{(3+\beta^2)^{3/2}} \tag{3.30}$$

where I_3^* is defined as the third modified and dimensionless stress invariant function. The function I_3^* was normalized for the sake of simplicity such that the range in I_3^* and β coincide. Also, in this way I_3^* represents the ratio of I_3 to its maximum positive value with I_2 fixed.

Figure 3.1 gives $I_2/(\sigma_1-\sigma_3)^2$ and $I_3/(\sigma_1-\sigma_3)^3$ as functions of β. Figure 3.2 gives I_3^* as a function of β.

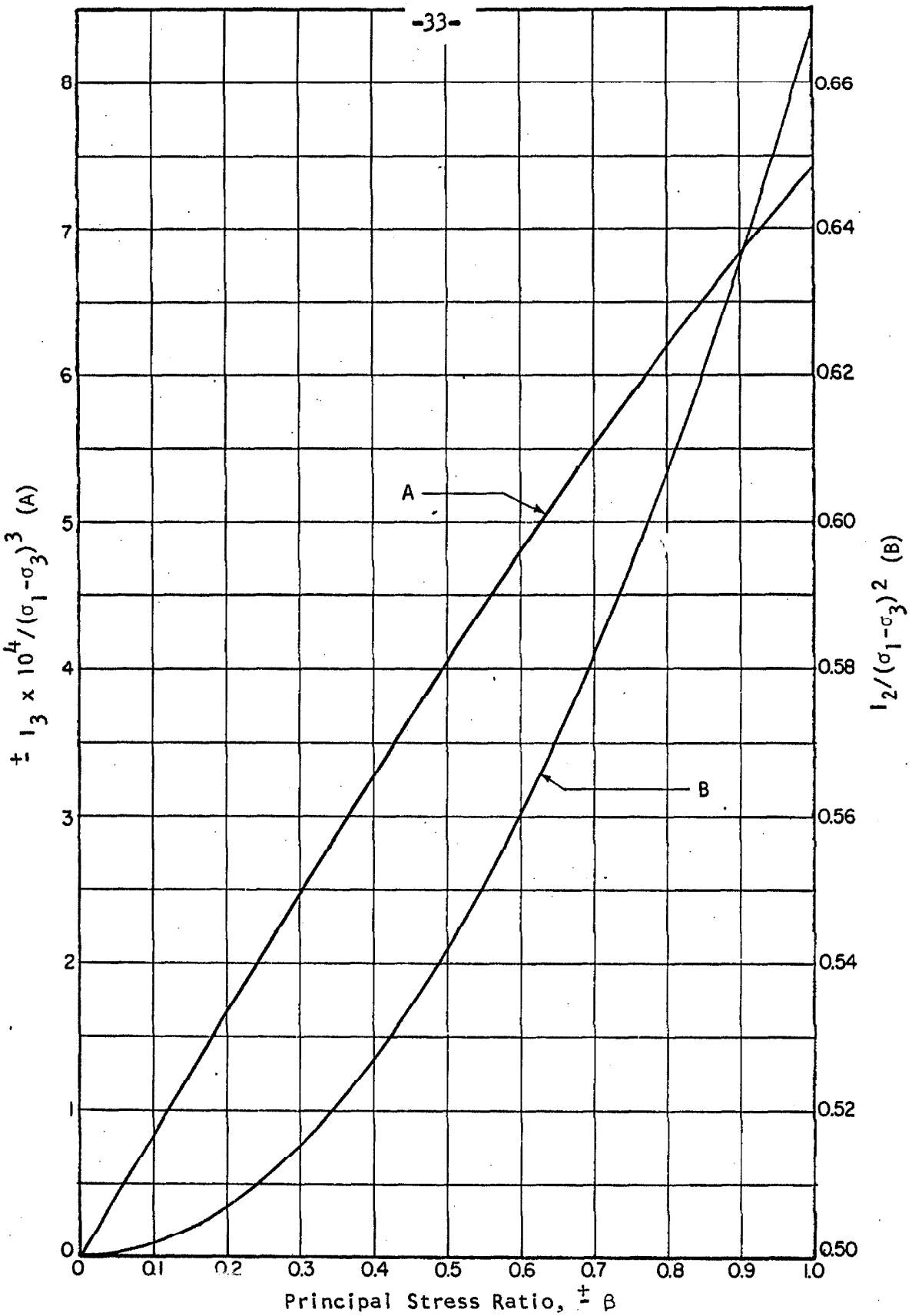

Figure 3.1 Second and Third Stress Invariants as Functions of the Maximum Principal Stress Difference and the Principal Stress Ratio.

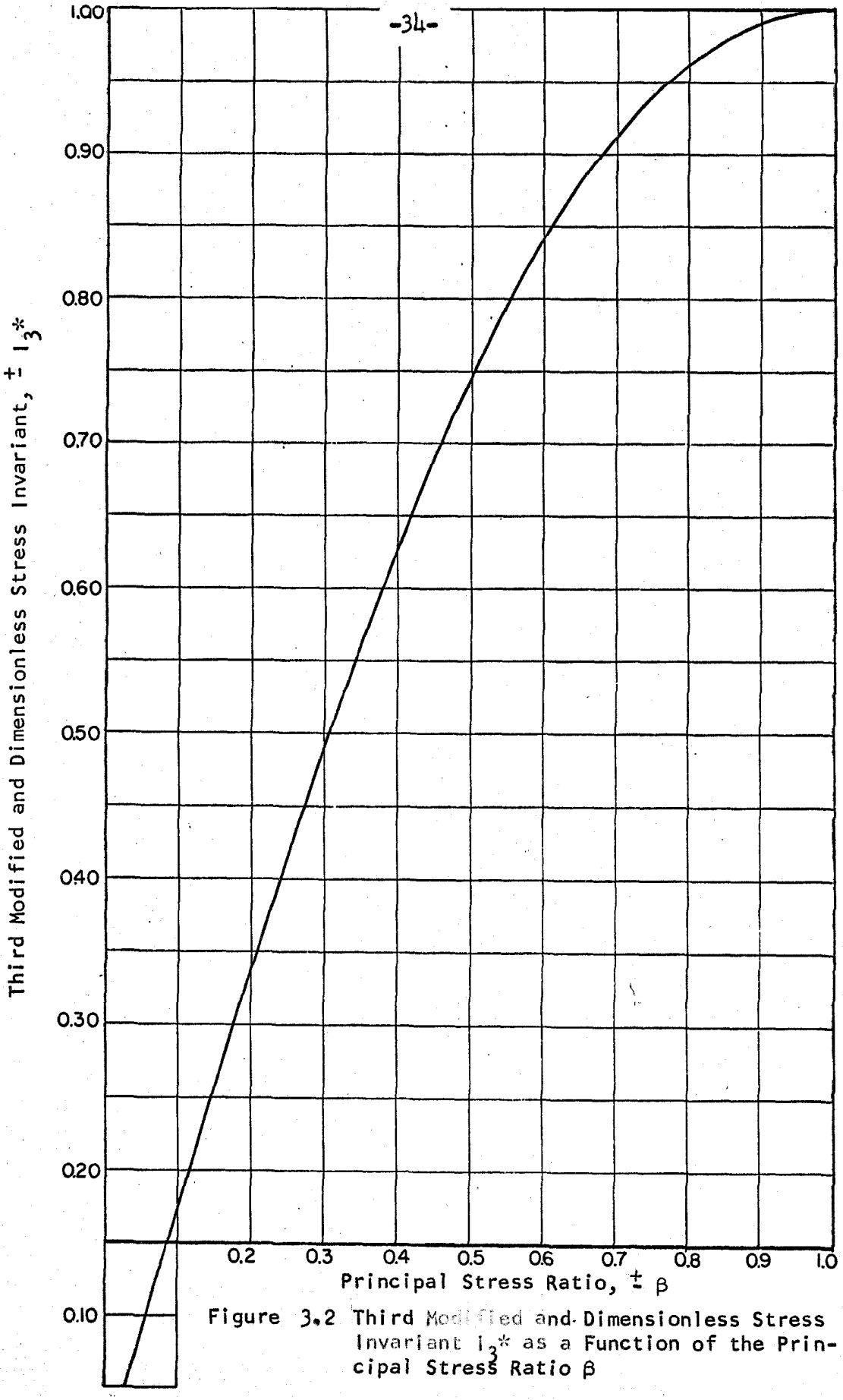

Figure 3.2 Third Modified and Dimensionless Stress Invariant I_3^* as a Function of the Principal Stress Ratio β

The principal stress ratio β is dependent only upon the deviatoric state of stress since I_1 is absent from Equation 3.30. This can be shown directly if σ_1, σ_2 and σ_3 from Equation 3.22 are substituted into Equation 3.18 giving

$$\beta = \frac{\sigma_1''-2\sigma_2''+\sigma_3''}{\sigma_1''-\sigma_3''} \tag{3.31}$$

3.14 RELATIONSHIPS INVOLVING THE FRICTION ANGLE $\bar{\Phi}$

In general the friction angle $\bar{\Phi}$ is defined in soil mechanics literature by

$$\sin \bar{\Phi} = \frac{\sigma_1-\sigma_3}{\sigma_1+\sigma_3} \tag{3.32}$$

and physically this represents the maximum ratio of shear to normal stress as viewed in two dimensions, i.e. by use of the Mohr Circle of Stress.

Substituting Equations 3.19, 3.20 and 3.27 into Equation 3.32 results in

$$\sin \bar{\Phi} = \frac{3}{\sqrt{\frac{2}{3}\frac{(\beta^2+3)}{I_2^*}}+\beta} \tag{3.33}$$

where the second modified and dimensionless stress invariant function I_2^* is defined by

$$I_2^* = I_2/I_1^2 \tag{3.34}$$

This relationship expresses the friction angle in terms of the principal stress ratio and the second modified and dimensionless stress invariant function.

By holding β (or I_3^*) constant, the following equations for particular states of stress are obtained:

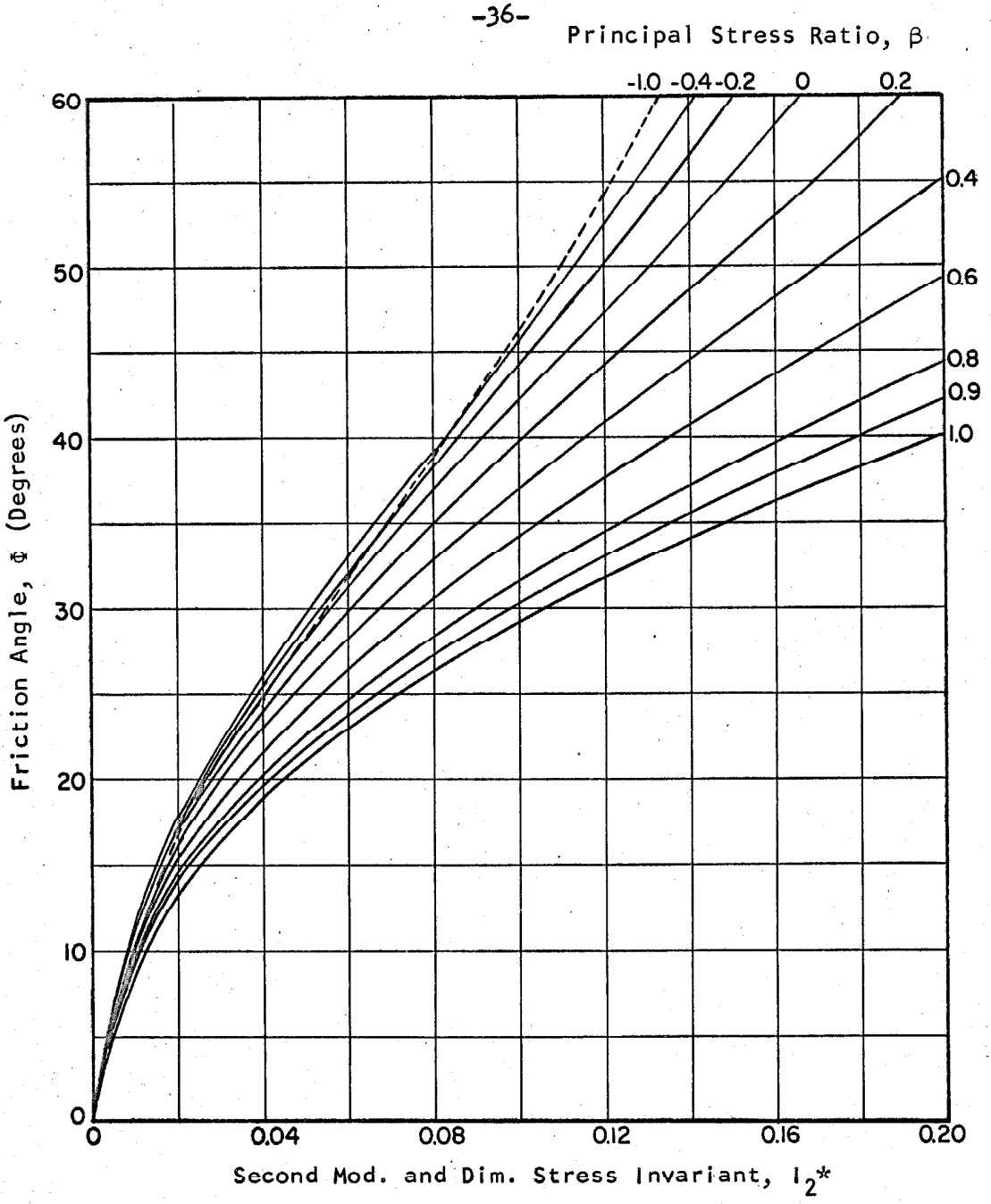

Figure 3.3 Friction Angle Φ as a Function of the Second Modified and Dimensionless Stress Invariant I_2^* and the Principal Stress Ratio β

Triaxial Compression, $\sigma_2=\sigma_3$; β, $I_3^* = 1$

$$\sin \Phi_1 = \frac{3}{(2\sqrt{\frac{2}{3}})\left[\frac{1}{\sqrt{I_2^*}}\right]+1} \tag{3.35}$$

Average Compression, $\sigma_2 = \sigma_1+\sigma_3/2$; β, $I_3^* = 0$

$$\sin \Phi_0 = \frac{3}{\sqrt{2}}\sqrt{I_2^*} \tag{3.36}$$

Triaxial Extension, $\sigma_2=\sigma_3$; β, $I_3^* = -1$

$$\sin \Phi_{-1} = \frac{3}{(2\sqrt{\frac{2}{3}})\left[\frac{1}{\sqrt{I_2^*}}\right]-1} \tag{3.37}$$

Figure 3.3 gives Φ as a function of I_2^* for fixed values of β.

3.2 STRAIN INVARIANT FUNCTIONS

The three original strain invariant functions are obtained from a statement of deformation geometry. The preceding three sections may be used directly to express the relationships between strains and strain invariants if τ_{ij} is replaced by ϵ_{ij}, σ_i is replaced by ϵ_i, the term I is replaced by the term J, and the term β is replaced by -k. The latter sign switch is a result of the author's sign convention which requires that limits be reversed in Equation 3.24. It should be remembered that tensile stress was taken negative and tensile strain was taken positive.

3.3 THE GENERAL RELATIONSHIP BETWEEN STRESS AND STRAIN IN INVARIANT FORM FOR LINEARLY ELASTIC SOLIDS

The purpose of this section is to present a stress-strain relationship in terms of invariant functions for a material which in the

past has been studied in considerable detail. The relationship between stress and strain for isotropic, linearly elastic solids is well known in the theory of elasticity and is given by standard texts (38, 40, 41). Poisson's ratio ν and the modulus of elasticity E are the two material parameters which allow for the unique relationship between stress and strain. It is simply demonstrated that principal stresses are coincident with the corresponding principal strains. Consider the element shown in Figure 3.4 subjected to principal stresses τ_{11}, τ_{22}, τ_{33}.

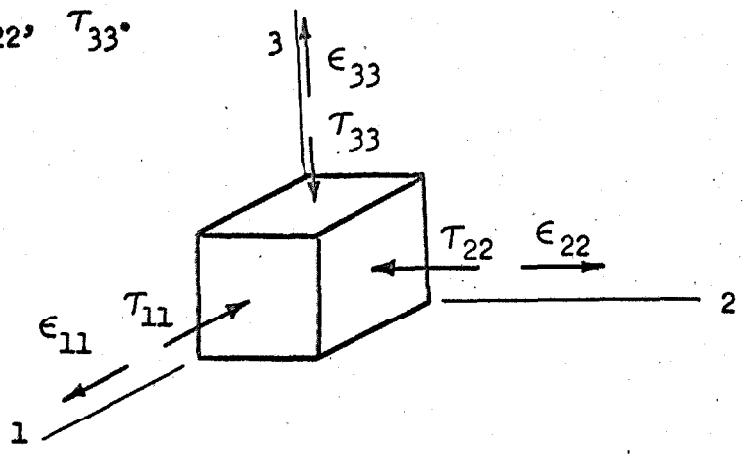

Figure 3.4 Element Subjected to Mutually Orthogonal Principal Stresses

Hooke's law states that

$$-\epsilon_{11} = \frac{\tau_{11}}{E} - \nu\frac{\tau_{22}}{E} - \nu\frac{\tau_{33}}{E} \tag{3.38}$$

$$-\epsilon_{22} = \frac{\tau_{22}}{E} - \nu\frac{\tau_{11}}{E} - \nu\frac{\tau_{33}}{E} \tag{3.39}$$

$$-\epsilon_{33} = \frac{\tau_{33}}{E} - \nu\frac{\tau_{11}}{E} - \nu\frac{\tau_{22}}{E} \tag{3.40}$$

$$\epsilon_{12} = \epsilon_{21} = \epsilon_{23} = \epsilon_{32} = \epsilon_{13} = \epsilon_{31} = 0 \tag{3.41}$$

From these equations the following relationships may be derived:

$$\epsilon_{11}+\epsilon_{22}+\epsilon_{33}=-\left(\frac{1-2\nu}{E}\right)(\sigma_1+\sigma_2+\sigma_3) \tag{3.42}$$

$$\frac{1}{3}\left[(\epsilon_{11}-\epsilon_{22})^2+(\epsilon_{22}-\epsilon_{33})^2+(\epsilon_{11}-\epsilon_{33})^2\right]$$

$$=\left(\frac{1+\nu}{E}\right)^2 \frac{1}{3}\left[(\tau_{11}-\tau_{22})^2+(\tau_{22}-\tau_{33})^2+(\tau_{11}-\tau_{33})^2\right] \tag{3.43}$$

$$\left[\epsilon_{11}-\left(\frac{\epsilon_{11}+\epsilon_{22}+\epsilon_{33}}{3}\right)\right]\left[\epsilon_{22}-\left(\frac{\epsilon_{11}+\epsilon_{22}+\epsilon_{33}}{3}\right)\right]\left[\epsilon_{33}-\left(\frac{\epsilon_{11}+\epsilon_{22}+\epsilon_{33}}{3}\right)\right]$$

$$=-\left(\frac{1+\nu}{E}\right)^3\left[\tau_{11}-\left(\frac{\tau_{11}+\tau_{22}+\tau_{33}}{3}\right)\right]\left[\tau_{22}-\left(\frac{\tau_{11}+\tau_{22}+\tau_{33}}{3}\right)\right]\left[\tau_{33}-\left(\frac{\tau_{11}+\tau_{22}+\tau_{33}}{3}\right)\right] \tag{3.44}$$

which may then be written in invariant form as

$$J_1=-\left(\frac{1-2\nu}{E}\right) I_1=-(M-3N)\, I_1 \tag{3.45}$$

$$J_2=\left(\frac{1+\nu}{E}\right)^2 I_2=M^2\, I_2 \tag{3.46}$$

$$J_3=-\left(\frac{1+\nu}{E}\right)^3 I_3=-M^3\, I_3 \tag{3.47}$$

where M and N are mechanical properties of the material defined by

$$M=\frac{1+\nu}{E} \quad \text{and} \quad N=\frac{\nu}{E} \tag{3.48}$$

Equations 3.45, 3.46 and 3.47 indicate that the first strain invariant (spherical) is dependent only upon the first stress invariant (spherical), and that the second and third modified strain invariants (deviatoric) are dependent only upon the second and third modified stress invariants (deviatoric) respectively.

The appearance of the same material property M in Equations 3.46 and 3.47 suggests a simple relationship between the second

and third modified stress and strain invariant functions. From Equation 3.46

$$M = \left(\frac{J_2}{I_2}\right)^{1/2}$$

and upon substitution into Equation 3.47 leads to

$$-\frac{J_3}{J_2^{3/2}} = \frac{I_3}{I_2^{3/2}} \quad \text{or} \quad -J_3^* = I_3^* \tag{3.49}$$

where $$J_3^* = \frac{3\sqrt{6}\, J_3}{J_2^{3/2}} \quad \text{and} \quad I_3^* = \frac{3\sqrt{6}\, I_3}{I_2^{3/2}} \tag{3.50}$$

The terms J_3^* and I_3^* are modified and dimensionless strain and stress invariant functions respectively. It should be noted that I_3^* proved to be a convenient variable in the developments of Section 3.13.

In summary, a most simplified and complete relationship between stress and strain for an isotropic and linearly elastic material is given in invariant form by

$$J_1 = -(M-3N)\, I_1 \tag{3.45}$$

$$J_2 = M^2\, I_2 \tag{3.46}$$

$$-J_3^* = I_3^* \tag{3.51}$$

3.4 THE GENERAL RELATIONSHIP BETWEEN STRESS AND STRAIN IN INVARIANT FORM FOR GRANULAR MATERIALS

3.41 INTRODUCTION

Certain difficulties are encountered in the use of invariant functions to obtain a stress-strain relationship for sand. The significant property of invariants, independence of orientation, results

in the assumption that principal stresses are coincident with corresponding principal strains; and this assumption is strictly valid only for isotropic materials. It is not possible, even for linearly elastic anisotropic solids, to obtain relationships of the form of Equations 3.45, 3.46 and 3.51 solely in terms of invariant functions from a generalized Hooke's law.

A paper of particular interest which discussed the complex behavior of soil was given by Newmark (22). His suggested stress-strain relationship for cohesive soil follows:

$$\epsilon_{OCT} = f_1(\sigma_{OCT}) + f_2(\tau_{OCT}) + f_3(\Phi) \tag{3.52}$$

$$\frac{1}{2}\gamma_{OCT} = f_4(\sigma_{OCT}) + f_5(\tau_{OCT}) + f_6(\Phi) \tag{3.53}$$

$$\theta = f_7(\sigma_{OCT}) + f_8(\tau_{OCT}) + f_9(\Phi) \tag{3.54}$$

In these equations the functions f_1 to f_9 are arbitrary functions and

$$\epsilon_{OCT} = \frac{1}{3} J_1, \qquad \gamma_{OCT} = \sqrt{\frac{J_2}{3}}, \qquad \theta = J_3$$

$$\sigma_{OCT} = \frac{1}{3} I_1, \qquad \tau_{OCT} = \sqrt{\frac{I_2}{3}}, \qquad \Phi = \frac{3I_3}{I_2}$$

Converting Equations 3.52, 3.53 and 3.54 into invariant form

$$\frac{1}{3} J_1 = f_1\left(\frac{1}{3} I_1\right) + f_2\left(\sqrt{\frac{I_2}{3}}\right) + f_3\left(3\,\frac{I_3}{I_2}\right) \tag{3.55}$$

$$\frac{1}{2}\sqrt{\frac{J_2}{3}} = f_4\left(\frac{1}{3} I_1\right) + f_5\left(\sqrt{\frac{I_2}{3}}\right) + f_6\left(3\,\frac{I_3}{I_2}\right) \tag{3.56}$$

$$J_3 = f_7\left(\frac{1}{3} I_1\right) + f_8\left(\sqrt{\frac{I_2}{3}}\right) + f_9\left(3\,\frac{I_3}{I_2}\right) \tag{3.57}$$

Upon generalizing Equations 3.55, 3.56 and 3.57 somewhat

$$J_1 = g_1(I_1) + g_2(I_2) + g_3(\frac{I_3}{I_2}) \tag{3.58}$$

$$J_2 = g_4(I_1) + g_5(I_2) + g_6(\frac{I_3}{I_2}) \tag{3.59}$$

$$J_3 = g_7(I_1) + g_8(I_2) + g_9(\frac{I_3}{I_2}) \tag{3.60}$$

Newmark's formulation implies a unique relationship between stress and strain and thus does not allow for inelastic behavior. The author prefers not to place undue importance upon the values of stress and strain corresponding to any particular plane. It is perhaps better to deal directly with the three invariant functions of stress and strain in functional relationships. The third invariant functions deserve careful consideration in a study of this type.

It is worthwhile to assign some physical significance to the various modified invariant functions in order to better understand their possible relationship to the behavior of granular materials. The first stress invariant function I_1 represents the sum of the normal stresses occurring on any three mutually orthogonal planes through a point, and thus represents a measure of normal stress averaged over all planes through a point. The second modified stress invariant I_2 is three times the square of the resultant shear stress occurring on those planes subjected to a normal stress $I_1/3$.

The ratio of shear stress to a corresponding mean normal stress $\sqrt{3} \cdot \sqrt{I_2/I_1}$ is significant to the behavior of granular materials

as this physically represents some measure of angle of obliquity, and thus of friction and grain to grain slippage.

The third modified stress invariant is a measure of the distribution of shear and normal stresses occurring on all planes through a point. If a sand is strained in three dimensions, it is suggested that the stress-strain behavior reflects in considerable measure that which occurs on all planes through a point (not a single plane as in the Mohr-Coulomb theory), and thus the third invariant stress function obtains significance. The distribution of shear and normal stresses is a function of the stress ratio β, and according to Equation 3.37 then is also a function of the third modified and dimensionless stress invariant.

3.42 PROPOSED GENERAL RELATIONSHIPS--CONSIDERING TOTAL STRAIN HISTORY

Based upon Equations 2.4, 2.9 and 2.10, and by the use of physical reasoning suggested in the preceding section, the following relationship is proposed to represent the stress-strain behavior of a particular granular material in invariant form.

$$dJ_1 = C_{11}dI_1 + C_{12}dI_2^* + C_{13}dI_3^* \tag{3.61}$$

$$dJ_2 = C_{21}dI_1 + C_{22}dI_2^* + C_{23}dI_3^* \tag{3.62}$$

$$dJ_3^* = C_{31}dI_1 + C_{32}dI_2^* + C_{33}dI_3^* \tag{3.63}$$

where

$$C_{ij} = C_{ijC}(n, J_2, J_3^*, I_1, I_2^*, I_3^*), \quad dI_j > 0 \tag{3.64}$$

and

$$C_{ij} = C_{ijR}(n, J_2, J_3^*, I_1, I_2^*, I_3^*), \quad dI_j < 0 \tag{3.65}$$

In this formulation the modified strain invariant functions J_2 and J_3^* replace the strain components ϵ''_{ij}, while the modified stress invariant functions I_1, I_2^* and I_3^* replace the stress components τ_{ij} in Equations 2.9 and 2.10. In this case physical experiments are required to establish at most 18 coefficient functions. The advantage of invariant functions in reducing the amount of data to be obtained by experimentation is apparent.

3.43 PROPOSED GENERAL RELATIONSHIPS--CONSIDERING SPHERICAL STRAIN HISTORY

A reduction is proposed to simplify the program of laboratory experimentation and the analysis of data. If the terms J_2 and J_3^* are removed from Equations 3.64 and 3.65, the effect of deviatoric strain history has been neglected. The resulting relationship between stress and strain is given by Equations 3.61, 3.62 and 3.63 where

$$C_{ij} = C_{ijC}(n, I_1, I_2^*, I_3^*), \quad dI_j > 0 \tag{3.66}$$

and

$$C_{ij} = C_{ijR}(n, I_1, I_2^*, I_3^*), \quad dI_j < 0 \tag{3.67}$$

If a limited number of laboratory experiments are to be performed, and if the porosity is essentially constant, then Equations 3.66 and 3.67 are finally reduced to

$$C_{ij} = C_{ijC}(I_1, I_2^*, I_3^*), \quad dI_j > 0 \tag{3.68}$$

$$C_{ij} = C_{ijR}(I_1, I_2^*, I_3^*), \quad dI_j < 0 \tag{3.69}$$

It must be realized that the end product of this section is indeed the result of extensive simplification. The amount of reduction

justified is certainly open to question. The amount of reduction necessary in planning a limited program of experimentation is nevertheless considerable. The relative importance of the terms I_1, I_2^* and I_3^* depends upon the state of stress in addition to other factors.

3.5 YIELD CRITERIA

3.51 FIRST YIELD

Following the discussion of Section 2.51, and proceeding to the general stress-strain relationship in invariant form as suggested by Equations 3.61 through 3.65, first yield might be defined by the requirement that at least one of the coefficient functions C_{ij} becomes infinitely large. Difficulties associated with this approach to a first yield criterion are the same as those listed in Section 2.51.

In search of a more practical criterion, and considering the possible requirement that one coefficient function in Equations 3.61 through 3.63 becomes infinitely large at first yield, then it follows that in the limit

$$\frac{1}{C_{ij}} = C_{1y}(n, J_2, J_3^*, I_1, I_2^*, I_3^*) = 0 \qquad (3.70)$$

where C_{1y} is regarded as a single functional relationship to be obtained from physical experiments. If deviatoric strain history is neglected, the modified strain invariant functions J_2 and J_3^* are neglected resulting in

$$C_{1y}(n, I_1, I_2^*, I_3^*) = 0 \qquad (3.71)$$

3.52 ULTIMATE YIELD

Following the discussion of Section 2.52, Equation 3.70 is modified to account for the influence of the rate of strain by

$$C_{uy}(n, \dot{J}_2, \dot{J}_3^*, I_1, I_2^*, I_3^*) = 0 \qquad (3.72)$$

In this relationship for ultimate yield the state of rate of deviatoric strain as given by $\dot{J}_2$, $\dot{J}_3^*$ has replaced the state of deviatoric strain as given by J_2, J_3^* in Equation 3.70 for first yield. For a fixed rate of strain, for example, static ultimate yield as defined by Section 2.3, Equation 3.72 is further modified giving

$$C_{suy}(n, I_1, I_2^*, I_3^*) = 0 \qquad (3.73)$$

If the porosity at static ultimate yield were a fixed value for a particular granular material, Equation 3.73 would finally be reduced to

$$C_{suy}(I_1, I_2^*, I_3^*) = 0 \qquad (3.74)$$

which is totally lacking in reference to strain history and is equivalent to the ideally plastic formulation given in terms of principal stresses, Equation 2.16.

3.53 PAST WORK ON THE FORM OF THE YIELD SURFACE

For purposes of comparison Table 3.1 presents a summary of the results of certain laboratory investigations which might be useful in attempts to define the so-called yield surface in the form of Equation 2.16 or 3.74. Of principal interest is the shape of the yield surface $f(\sigma_1, \sigma_2, \sigma_3)$ which is cut by an octahedral plane ($\sigma_1+\sigma_2+\sigma_3$=constant). This envelope of intersection has conventionally been compared with the Mohr-Coulomb theory. Variance of the friction angle ϕ along the

envelope essentially represents variance from the Mohr-Coulomb theory of failure. In comparing experimental studies the effects of several variables--not always well defined--must be considered:

1. Type of soil tested
2. Initial porosity
3. Stress path ideally followed
4. Definition of shear failure
5. Stress concentration, i.e. as related to the various equipment
6. Methods of calculation and correction of test results.

It is suggested that the effect of non-homogeneous loading presents the most difficult problem in comparison, particularly for the denser sands. Several investigators indicate that the intermediate principal stress is an important factor in determining the shearing strength of sand. If this be true, then the friction angle actually depends upon the stress ratio β or the modified and dimensionless stress invariant function I_3*.

Hvorslev (16) summarized ideas prior to 1960 regarding the shape of the failure surface in principal stress space. His Figure 40 c) is reproduced with minor modification here as Figure 3.5.

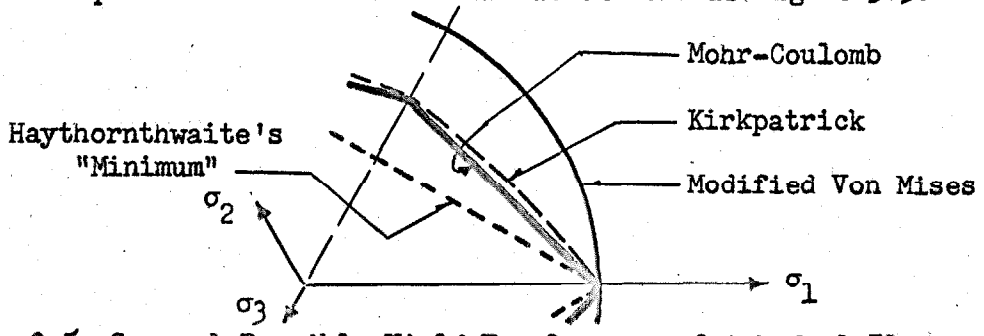

Figure 3.5 Several Possible Yield Envelopes on Octahedral Plane

Table 3.1 Comparison of Past Experimental Investigations on the Strength of Sands at Different States of Stress

Investigator Reference and Date	Type of Soil**	Type of Apparatus	Principal Stress Ratio β	Friction Angle Φ_β Degrees	Initial Void Ratio e or Porosity n	Density Compared with Critical	Comments
Kjellman (8) 1936	Quartz Sand D ≐ 1mm	Three-Dimen. Compr.	1 0.24 0	35 43 43	e=0.67	Dense	
		Direct Shear	?	34			Movement 10x larger than 3-D compression
Habib (11) 1953	Leucate Sand well graded round grains	Triaxial	1 -1	38 30			
	River Sand round grains		1 -1	39 30			
	Fontainbleau Sand		1 -1	31 24-1/2		Near Critical	
	angular C_u = 1.54 dense	Triaxial with Torsion	1 0.82 0.56 0 -0.24 -0.60 -1	32 33 36 31 28 27 25			

**Grain diameter D based on mechanical analysis using square meshed sieves. Hazen's coefficient of uniformity $C_u = D_{60}/D_{10}$.

Table 3.1 continued

Investigator Reference and Date	Type of Soil	Type of Apparatus	Principal Stress Ratio β	Friction Angle Φ_β Degrees	Initial Void Ratio e or Porosity n	Density Compared with Critical	Comments
Bishop and Eldin (10) 1953	Folkestone Sand med to fine well graded D≐0.06–0.8mm C_u = 2 n_{max} = 0.46 n_{min} = 0.33	Triaxial			n=0.37–0.46	Mostly dense	$\Phi_1 \doteq \Phi_{-1}$ over a wide range in initial density
Jakobson (12) 1957	Sand A, Quartz w/some feldspar Some polish. gr. D=0.6–1.0mm C_u = 1.2 e_{max} = 0.78 e_{min} = 0.59	Three-Dimen. Compr. (Kjellman Apparatus)	1	34	e=0.57	Dense	*Estimates by the author based on Jakobson's Fig. 6. These tests did not reach a failure condition.
			1 -1	34* 43*	e=0.61–0.65	Dense	
	Sand B, Quartz w/some feldspar, No polished gr. D=0.5–1.0mm C_u = 1.2 e_{max} = 0.86 e_{min} = 0.66		1	40-1/2	e=0.67	Dense	
			1 -1	37* 54*	e=0.69	Dense	

Table 3.1 continued

Investigator Reference and Date	Type of Soil	Type of Apparatus	Principal Stress Ratio σ_3	Friction Angle Φ_σ Degrees	Initial Void Ratio e or Porosity n	Density Compared with Critical	Comments
Kirkpatrick (13) 1957	Loch Aline Sand med fine D=0.06–0.6mm C_u = 1.5	Triaxial	1 -1	39 38.7	n=0.35	Dense	
		Thick Cylinder	.26– .30 -.28–-.36	40–42-1/2* 40–42-1/2*	n=0.36	Dense	Author's calcs based on Kirkpatrick's Tab.2
Peltier (14) 1957	Various Sands	Triaxial					$\Phi_1 - \Phi_{-1} \doteq 7°$
	Leucate Sand D=1.6–2.0mm		1 -1	37 28			Triaxial shear box indicates opposite results compared with normal triaxial compression and extension equipment
		Triaxial Shear Box	1 -1	31 38			
	Seine Sand D=0.5–1.0mm		1 -1	33-1/2 41-1/2			
	Leucate Sand D=1.6–2.0mm		1 -1	34-1/2 45-1/2			
Haythornthwaite (7) 1960	Lantern Hill Sand Crush. Quartz D=0.3–0.35mm	Triaxial	1 -1	36* 24–31*	n=0.47–0.52	Relative Density 70%	* Author's estimates based on Haythornthwaite's Figure 10
Wu, Loh, Malvern (18) 1936	Ottawa Sand D=0.3–0.6mm	Thick Cylinder	1 -1 0	37 37 42	e=0.45–0.52	Dense ?	$\Phi_1 \doteq \Phi_{-1}$ $\Phi_0 - \Phi_1 \doteq 5°$

4. CONSIDERATION OF LABORATORY TESTS AND THE STUDY OF CONTROLLED STRESS PATHS IN OBTAINING A STRESS-STRAIN RELATIONSHIP

4.1 INTRODUCTION

Apart from inaccuracies in measurement, a physical laboratory test cannot be devised which is ideal. It is not possible to form a sample which is perfectly in accordance with preconceived desires. Each sample will likely have inhomogenities. An unknown degree of initial anisotropy may result during the process of forming. In addition, the sample may not be stressed or strained in the desired homogeneous manner. Physical equipment most often limits the magnitude of loads and deformations obtainable.

It is not possible to exercise a great deal of control over the methods of forming sand samples; however, it is perhaps possible by indirect means to determine the degree of isotropy obtained.

4.11 NON-HOMOGENEOUS APPLICATION OF STRESS

If the apparatus performs in such a way that non-uniform boundary loads are applied, there will be unknown variations in stress and strain occurring within the test specimen. It is not possible in severe cases of stress concentration to accurately interpret the average stress-strain data obtained. Every effort should thus be made to design physical test equipment first which is capable of applying a homogeneous state of stress. This conclusion was clearly stated by Kjellman (8) in 1936.

4.12 TEST COMPARISON--DENSE SAND

The results of two hypothetical shear tests performed on initially dense sand are to be compared: the first using equipment which imposes homogeneous boundary loads, and the second using equipment which imposes non-homogeneous boundary loads. It is further specified that both tests are to follow the same paths of average stress.

It is assumed that the first test would produce a valid stress-strain relationship for the stress path chosen. Non-homogeneous boundary loading in the second test would lead to stress variation within the specimen. On a small scale, certain zones may be relatively free from shearing distortion while certain zones may yield prematurely at relatively small average strains. In dense sands local yield is associated with volumetric expansion (positive dilatancy) and leads to progressive weakening. The manner in which the yield zone grows is related to the magnitude and manner of boundary load application, and thus must be related to the details of the particular test equipment involved. When the local yield zone extends entirely through the sample the results may be spectacular. It is suggested that the average shear stress causing such a progressive failure is most often low compared with that required to develop yield in the homogeneous case where the average shear strain may be noticeably higher. The effects of non-homogeneous loading vary, however, with the average state of stress as will be discussed in Chapter 9.

This process of progressive yielding in dense sand is undesirable in a strength experiment because it is dependent upon the

particular details of the mechanical equipment involved. A similar process occurs in nature, and the difficulties in correlation of the two cases are thought primarily due both to differences in scale and in stress concentration.

4.13 TEST COMPARISON--LOOSE SAND

The results of two hypothetical shear tests performed on initially loose sand are to be compared under the same conditions as those of Section 4.12.

Again, it is assumed that the first test would produce a valid stress-strain relationship for the stress path chosen. It is well known that the initial shearing of a loose sand is associated with consolidation (negative dilatancy) which must effectively increase the overall distortional rigidity of the sample. It is suggested that the non-homogeneous test might tend to accelerate the growth of stability zones; however, there is little reason to believe that the stress-strain results obtained in the two tests would differ appreciably. On this basis, perhaps both tests would reach yield at nearly the same average state of stress and strain.

Practical problems are encountered in the formation of loose sands as the material is highly sensitive to vibration. Vibration occurring during a stress-strain experiment may also result in the tabulation of misleading data. To a considerable degree the behavior of loose sand in nature must represent the combined effect of static loading and vibration. Difficulties in correlating associated natural phenomena with laboratory test results, in addition to other factors,

are likely due to differences in vibration. This study is primarily concerned with dense sand, and the effects of vibration are neglected.

4.2 CONSIDERATION OF PARTICULAR LABORATORY TESTS

Laboratory apparatus developed and utilized by the author in this study included spherical compression test equipment to study the stress-strain relationship for the special case of spherical stress, and three-dimensional compression test equipment to study primarily the stress-strain relationships for cases involving the variation of deviatoric stress. Both sets of apparatus are fully described in the following chapters. Tests considered for possible use in this study are covered in the ensuing discussion.

4.21 THREE-DIMENSIONAL COMPRESSION

The three-dimensional compression test is a stress controlled experiment in which three mutually orthogonal and principal stresses may be arbitrarily varied on a plate-or cube-shaped specimen. It is not possible to vary the orientation of the applied stresses, but in other respects the test is completely general. Kjellman developed a test of this type (8), and further work utilizing this equipment has been continued by Jakobson (12).

Stress paths are not limited by the three-dimensional test apparatus except as to magnitude. The most useful stress paths* for this study are believed to be those recommended in Figure 4.1, and are based on the use of stress invariant functions.

*A summary of stress path notation used by the author with a suggested system of stress path classification is given in Section 4.3.

4.22 TRIAXIAL COMPRESSION

The triaxial compression test is ideally a stress controlled experiment in which three orthogonal principal stresses are applied to a test specimen in such a way that the intermediate principal stress σ_2 is equivalent to the minor principal stress σ_3. In terms of invariants this restriction may be stated

$$I_3^* = \frac{3\sqrt{6}\, I_3}{I_2^{3/2}} = 1 \qquad (4.1)$$

In practice the normal triaxial compression test is far from ideal. Stress control is desired; nowever, strain control is introduced due to end-plate restraint. Friction between the end plates and the sample results in introducing an unknown shear stress distribution on two faces of the test specimen.

Balla (43) and Haythornthwaite (7) discuss the mechanics of the linearly elastic and ideally plastic triaxial specimen respectively. Bjerrum and Kummeneje (44) compare the shearing resistance of sand samples with circular and rectangular cross section. Bishop and Henkel (45) give thorough treatment to triaxial test procedures in a complete text.

The key to improvement of normal triaxial compression test equipment lies first in the elimination of end-plate friction. A substantial step in this direction appears to have been taken by Rowe and Barden (46). Much more work along this line is required before conclusive evidence is obtained.

Ideal triaxial compression stress path diagrams are given in Figure 4.2 and include those recommended for this study as well as those commonly used.

4.23 TRIAXIAL EXTENSION

The triaxial extension test is ideally a stress controlled experiment in which three orthogonal principal stresses are applied to a test specimen in such a way that the intermediate principal stress σ_2 is equivalent to the major principal stress σ_1. In terms of stress invariants this restriction may be stated

$$I_3^* = \frac{3\sqrt{6}\, I_3}{I_2^{3/2}} = -1 \qquad (4.2)$$

In practice the normal triaxial extension test is performed utilizing equipment similar to that for the normal triaxial compression test. In fact, the equipment is most often identical, and similar problems involving the effects of end-plate friction are introduced. The effects of stress variation are not comparable in the two tests. Improvement of normal triaxial extension tests again lies first in the elimination of end-plate friction.

Ideal triaxial extension stress path diagrams are given by Figure 4.3 and include those recommended for this study as well as those commonly used.

4.24 AVERAGE COMPRESSION

The average compression test ideally is a stress controlled experiment in which three orthogonal principal stresses are applied

to a test specimen in such a way that the intermediate principal stress σ_2 is the average of the major and minor principal stresses σ_1 and σ_3 respectively. In terms of stress invariants this restriction may be stated

$$I_3^* = \frac{3\sqrt{6}\, I_3}{I_2^{3/2}} = 0 \qquad (4.3)$$

There is no laboratory test equipment yet designed specifically to follow the average compression stress path. A simple test of this type would seem desirable as the state of stress is midway between triaxial compression and triaxial extension. Such a test may more nearly approach a state of plane strain than either the triaxial compression or triaxial extension test.

Ideal stress path diagrams are given in Figure 4.4 and include those recommended for this study as well as those which might possibly be used if specific test equipment were developed.

4.3 CLASSIFICATION OF STRESS OR STRAIN PATHS

In the future it is likely that numerous studies will be carried out in which various paths of stress and strain are followed. It seems desirable to put forth a system of classification now which possesses some generality in order that future work may be referenced quickly and in brief fashion.

The suggested system of classification is based upon the stresses or strains or functions thereof, i.e. invariant functions. The first term in the following classification deals with the type of function which is controlled. The subscripts appearing on this

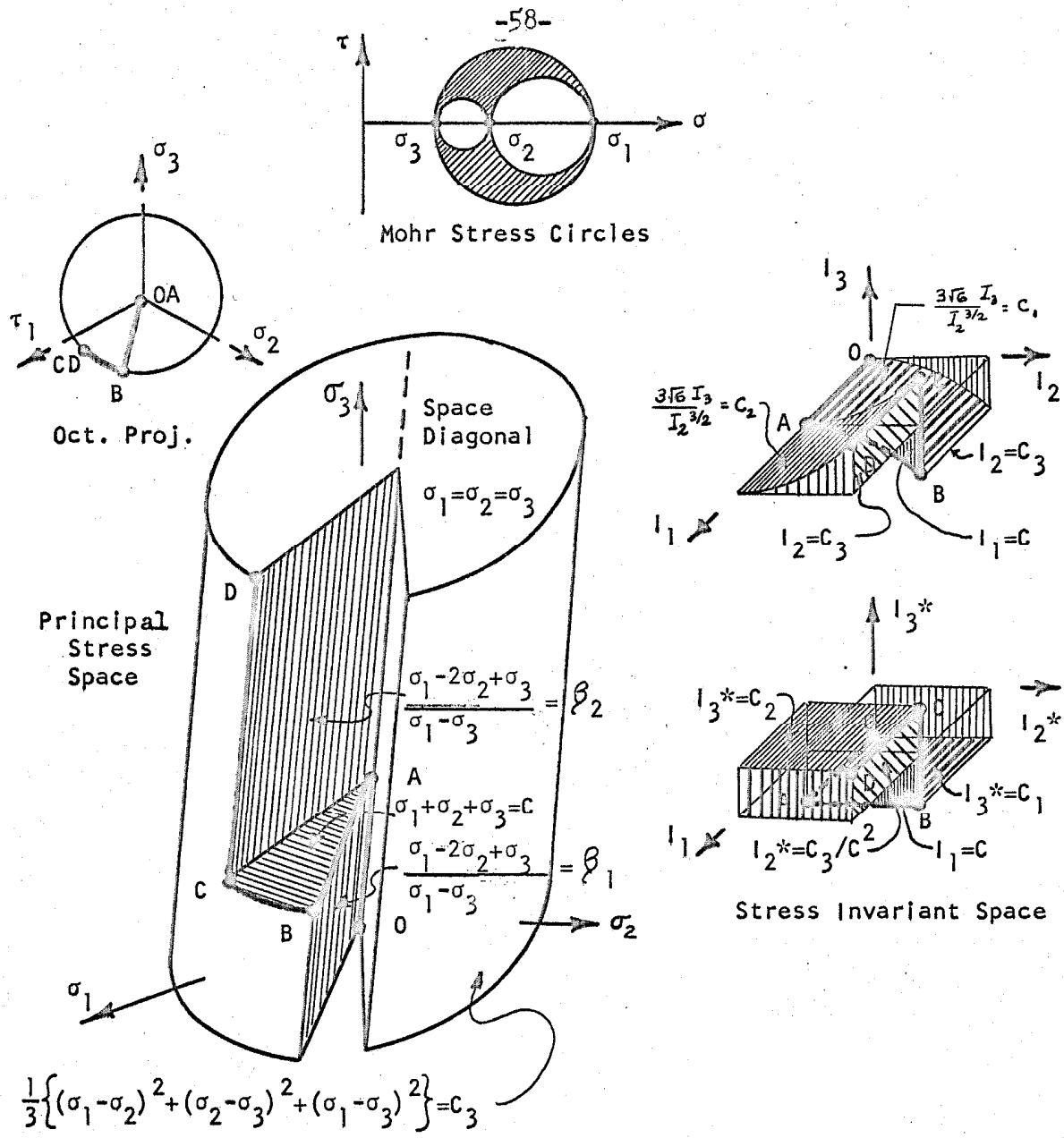

Stress Path Summary

Path	Symbol	Properties
OA	SC	I_2 (I_2*), I_3 = 0
AB	I_{13}*	I_1, I_3* constant
BC	I_{12}	I_1, I_2 (I_2*) constant
CD	I_{23}	I_2, I_3, (I_3*) constant

Figure 4.1 Three Dimensional Compression Stress Path Diagrams

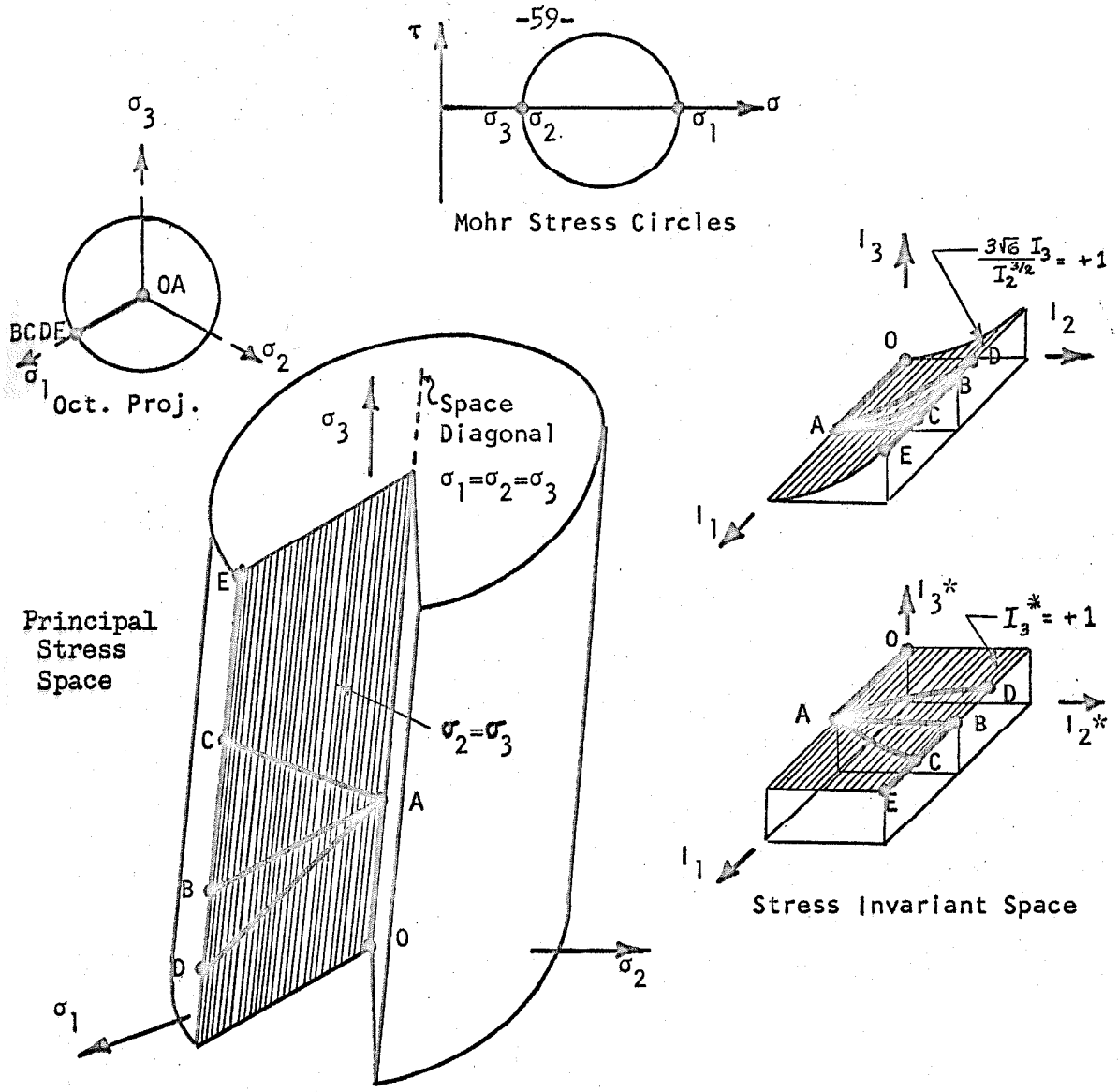

Stress Path Summary

Path	Symbol	Properties
OA	SC	$I_2(I_2^*)$, $I_3 = 0$
AB	I_{13}^*(TC)	I_1 constant
AC	TC_{NA}	σ_2, σ_3 constant
AD	TC_{NB}	σ_1 constant
BE	I_{23}^*(TC)	I_2, I_3 constant

Figure 4.2 Triaxial Compression Stress Path Diagrams

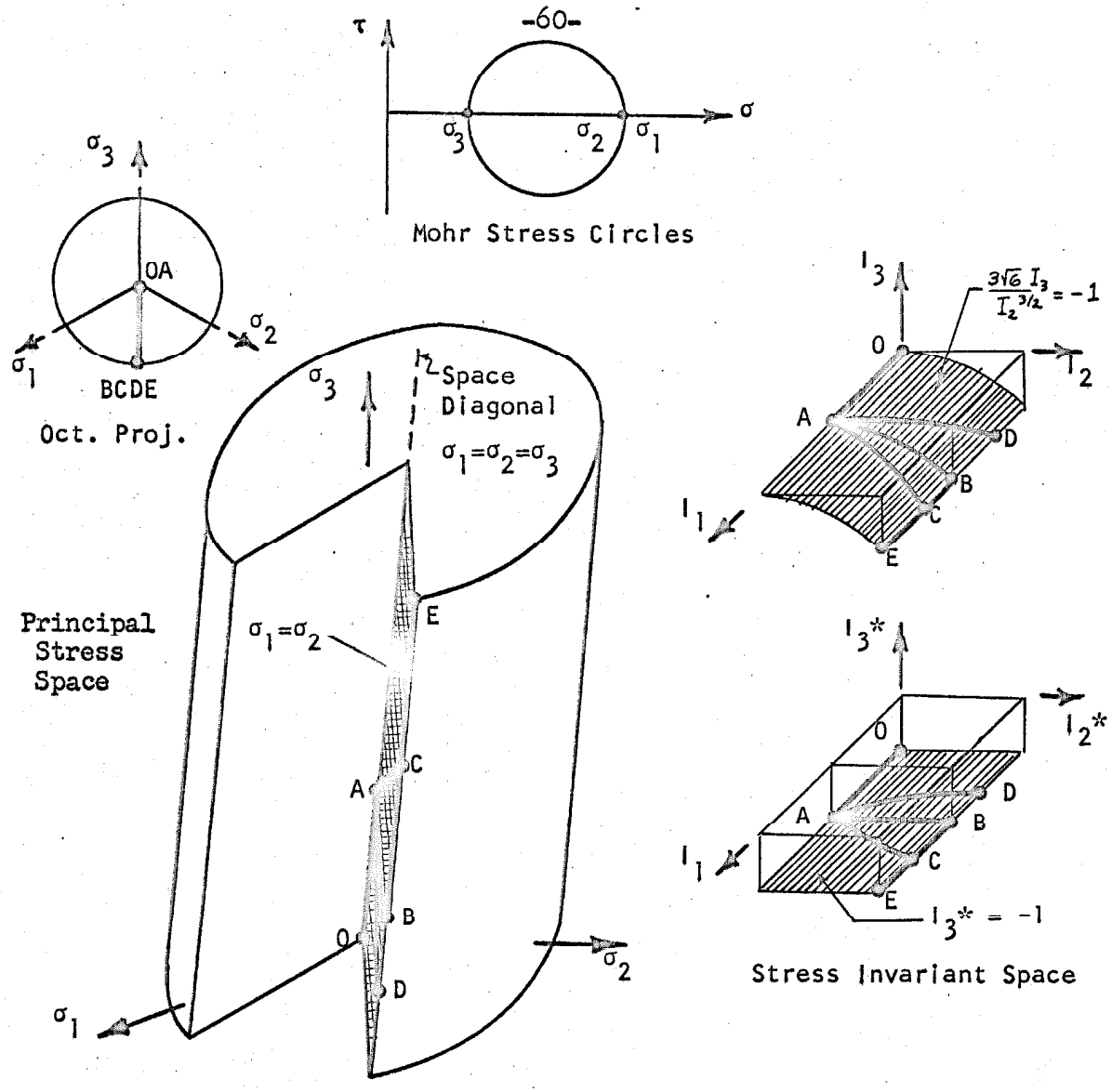

Stress Path Summary

Path	Symbol	Properties
OA	SC	$I_2(I_2^*)$, $I_3 = 0$
AB	I_{13^*}(TE)	I_1 constant
AC	TE_{NA}	σ_3 constant
AD	TE_{NB}	σ_1, σ_2 constant
BE	I_{23^*}(TE)	I_2, I_3 constant

Figure 4.3 Triaxial Extension Stress Path Diagrams

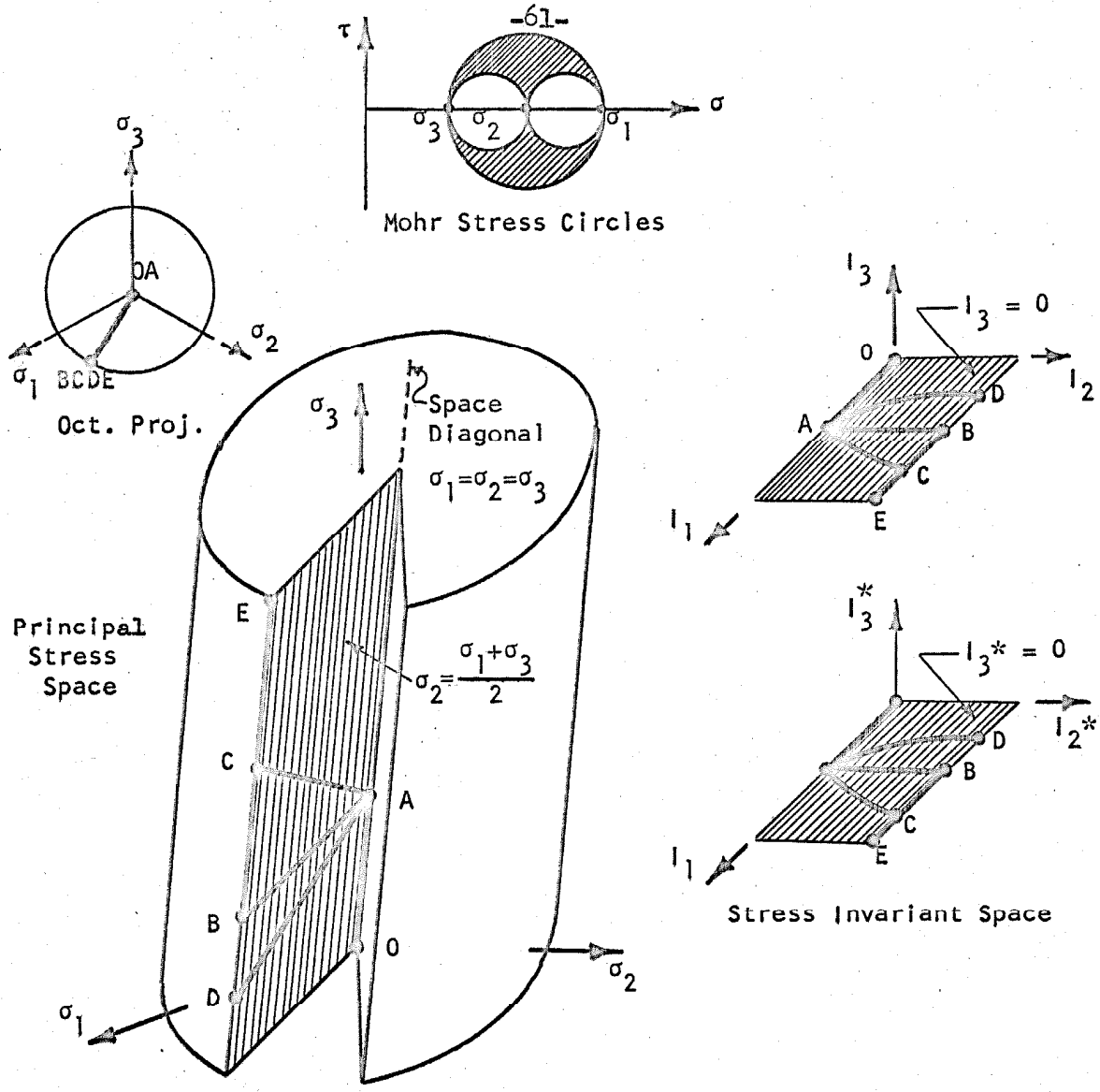

Stress Path Summary

Path	Symbol	Properties
OA	SC	$I_2(I_2^*)$, $I_3 = 0$
AB	$I_{13}^*(AC)$	I_1 constant
AC	AC_{NA}	σ_3 constant
AD	AC_{NB}	σ_1 constant
BE	$I_{23}^*(AC)$	I_2, I_3 constant

Figure 4.4 Average Compression Stress Path Diagrams

function signify the specific functions held constant. The final subscript is either null or R which signifies an increase or decrease respectively in the remaining and variable function. A statement regarding the variable function is therefore included only by omission. This method of classification is suitable only where three independent variables are involved, and where there is little doubt as to the identity of the "remaining" variable.

For example, consider the stress path designation I_{13*}. In this case the I signifies that the invariant stress functions are controlled. The subscripts 1 and 3* signify that the first stress invariant and the third modified and dimensionless stress invariant are held constant. Only by omission is it observed that the variable is the second stress invariant I_2 (or the second modified and dimensionless stress invariant I_2*); and only by omission is it seen that this variable is increased during the test thus giving direction to the path designated. The term $I_{13*}(TC)$ signifies all of the preceding, and in addition specifies that the stress path belongs to the triaxial compression state of stress.

As a further example consider the term ϵ_{23R}. In this case the ϵ signifies that the linear strains are controlled. The subscripts 2 and 3 signify that strains in the 2 and 3 directions are held constant. Only by omission is it ascertained that the variable is the strain in the 1 direction; and by including the subscript R it is shown that the strain ϵ_1 is decreased during the test thus giving direction to the path designated. The specific term $\epsilon_{23R}(OD)$ might

Table 4.1 Stress Path Classification

Type of Stress Path		Symbol	Constants			Variables	
			Stress Invariants	Principal Stresses	Prin. Stress Ratio	Increasing Stress Invariants	Increasing Principal Stresses
Invariant Based Stress Paths	Normal Compression	I_{23}	I_2, I_3, I_3^*		β	I_1	$\sigma_1, \sigma_2, \sigma_3$
		$I_{23}(SC)$	$I_2, I_3=0$		—	I_1	$\sigma_1, \sigma_2, \sigma_3$
		$I_{23}(TC)$	I_2, I_3, I_3^*		$\beta = 1$	I_1	$\sigma_1, \sigma_2, \sigma_3$
		$I_{23}(AC)$	I_2, I_3, I_3^*		$\beta = 0$	I_1	$\sigma_1, \sigma_2, \sigma_3$
		$I_{23}(TE)$	I_2, I_3, I_3^*		$\beta = -1$	I_1	$\sigma_1, \sigma_2, \sigma_3$
	Radial Compression	I_{13}^*	I_1, I_3^*		β	I_2, I_2^*	$\sigma_1, I_3^* > 0$; $\sigma_1, \sigma_2, I_3^* < 0$
		$I_{13}^*(TC)$	$I_1, I_3^*=1$		$\beta = 1$	I_2, I_2^*	σ_1
		$I_{13}^*(AC)$	$I_1, I_3=I_3^*=0$	σ_2	$\beta = 0$	I_2, I_2^*	σ_1
		$I_{13}^*(TE)$	$I_1, I_3^* = -1$		$\beta = -1$	I_2, I_2^*	$\sigma_1=\sigma_2$
	Circular Compression	I_{12}	I_1, I_2, I_2^*			$I_3(I_3^*)$	
Triaxial Compression		TC_{NA}	$I_3^*=1$	$\sigma_2=\sigma_3$	$\beta = 1$	I_1, I_2, I_2^*	$\sigma_1, \sigma_1-\sigma_3$
		TC_{NB}	$I_3^*=1$	σ_1	$\beta = 1$	I_2, I_2^*	$\sigma_1-\sigma_3$
		TC	$I_3^*=1$		$\beta = 1$	I_2	$\sigma_1-\sigma_3$
Average Compression		AC_{NA}	$I_3^*=0$	σ_3	$\beta = 0$	I_1, I_2, I_2^*	σ_1, σ_2
		AC_{NB}	$I_3^*=0$	σ_1	$\beta = 0$	I_2, I_2^*	$\sigma_1-\sigma_3$
		AC	$I_3^*=0$		$\beta = 0$	I_2	$\sigma_1-\sigma_3$
Triaxial Extension		TE_{NA}	$I_3^* = -1$	σ_3	$\beta = -1$	I_1, I_2, I_2^*	$\sigma_1=\sigma_2$
		TE_{NB}	$I_3^* = -1$	$\sigma_1=\sigma_2$	$\beta = -1$	I_2, I_2^*	$\sigma_1-\sigma_3$
		TE	$I_3^* = -1$		$\beta = -1$	I_2	$\sigma_1-\sigma_3$

be used to specify that the strain path belongs to the one-dimensional strain case with $\epsilon_2 = \epsilon_3 = 0$.

It is suggested that specific and particularly well known tests might be classified apart from this basic system avoiding the use of numerals. For example, use SC for a spherical compression test where the stresses are increased, and SC_R for a similar test where the stresses are decreased.

Table 4.1 is designed primarily for stress controlled tests and contains suggested stress path classifications, all of which are referenced to the stress invariant functions for comparison, including those commonly used in the past as well as those considered most likely to be used in the near future.

4.4 SOLUTION FOR PRINCIPAL STRESSES USING CONTROLLED STRESS INVARIANT FUNCTIONS

The use of invariant functions in material studies has been previously emphasized. If it is desired to control the stress invariant functions during the progress of a stress controlled test, then it is necessary to pre-calculate the principal stresses.

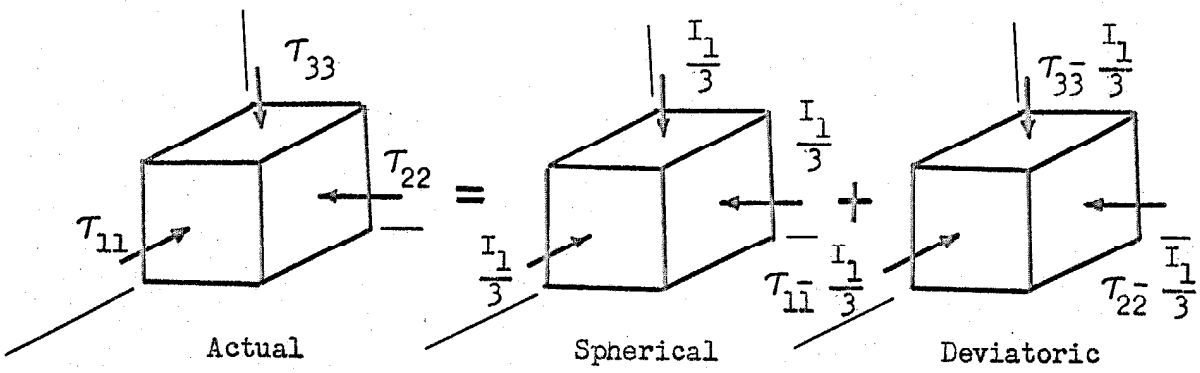

Figure 4.5 Principal Stress Division

Consider a cube-shaped element subjected to principal stresses τ_{11}, τ_{22}, τ_{33} as shown in Figure 4.5. For convenience, the state of stress is first divided into spherical and deviatoric components. The principal stresses for the spherical state of stress are given by τ_{11}', τ_{22}', $\tau_{33}' = I_1/3$ and are later to be added to those obtained for the deviatoric state of stress.

For the deviatoric state of stress the following set of equations represents the first stress invariant, the second modified stress invariant, and the third modified stress invariant respectively.

$$\tau_{11}'' + \tau_{22}'' + \tau_{33}'' = 0 \tag{4.4}$$

$$I_2 = \tau_{11}''^2 + \tau_{22}''^2 + \tau_{33}''^2 \tag{4.5}$$

$$I_3 = \tau_{11}'' \tau_{22}'' \tau_{33}'' \tag{4.6}$$

Solution of these equations for the deviatoric principal stress τ_{11}'' in terms of the invariants results in the cubic expression

$$\tau_{11}''^3 - \frac{I_2}{2} \tau_{11}'' - I_3 = 0 \tag{4.7}$$

A stress solution in dimensionless form is desired for the sake of generality. The following dimensionless variables are advanced

$$\tau_{ii}''^* = \frac{\tau_{ii}''}{I_1} \tag{4.8}$$

$$I_2^* = \frac{I_2}{I_1^2} \tag{4.9}$$

$$I_3^* = \frac{3\sqrt{6}\, I_3}{I_2^{3/2}} \tag{4.10}$$

and upon substitution into Equation 4.7 one obtains

$$I_1^3(\tau_{11}''^{*3} - \frac{I_2^* \tau_{11}''^*}{2} - \frac{I_2^{*3/2} I_3^*}{3\sqrt{6}} = 0 \qquad (4.11)$$

and since physically $I_1 \neq 0$ then

$$\tau_{11}''^{*3} - \frac{I_2^* \tau_{11}''^*}{2} - \frac{I_2^{*3/2} I_3^*}{3\sqrt{6}} = 0 \qquad (4.12)$$

The three real roots $\tau_{11}''^*$ of this equation are given by

$$\sqrt{\frac{2}{3} I_2^*} \cos \frac{\theta}{3}, \quad \sqrt{\frac{2}{3} I_2^*} \cos \left(\frac{\theta}{3} + 120°\right)$$

and $$\sqrt{\frac{2}{3} I_2^*} \cos \left(\frac{\theta}{3} + 240°\right) \qquad (4.13)$$

where

$$\theta = \cos^{-1} I_3^* \qquad (4.14)$$

Finally, the original stresses in dimensionless form are obtained by addition of the spherical stress in dimensionless form to the deviatoric stress in dimensionless form or

$$\tau_{ii}^* = \frac{1}{3} + \tau_{ii}''^* \qquad (4.15)$$

The following convention of principal stress control was adopted

$$\sigma_3 \leq \sigma_2 \leq \sigma_1 , \quad \text{or } \sigma_3^* \leq \sigma_2^* \leq \sigma_1^* .$$

Table 4.2 gives the dimensionless principal stresses σ_1^*, σ_2^* and σ_3^* for the range of variables $0 \leq I_2^* \leq 0.25$ and $-1 \leq I_3^* \leq 1$. Solutions corresponding to negative (tensile) stress values are not included for physical reasons. To obtain principal stresses for a specific experiment multiply the dimensionless values taken from the table by the first stress invariant I_1.

Table 4.2 Dimensionless Principal Stresses as Functions of the Second and Third Modified and Dimensionless Stress Invariant Functions

I_2^*	σ	I_3^* (Table values = $\sigma^* \times 10^5$)										
		-1.0	-0.8	-0.6	-0.4	-0.2	0	0.2	0.4	0.6	0.8	1.0
0.00	1*	33333	33333	33333	33333	33333	33333	33333	33333	33333	33333	33333
	2*	33333	33333	33333	33333	33333	33333	33333	33333	33333	33333	33333
	3*	33333	33333	33333	33333	33333	33333	33333	33333	33333	33333	33333
0.01	1*	37416	38827	39373	39779	40114	40404	40662	40896	41111	41311	41498
	2*	37416	35817	35071	34449	33881	33333	32785	32217	31595	30849	29250
	3*	25168	25355	25555	25770	26004	26262	26552	26887	27293	27839	29250
0.02	1*	39107	41103	41875	42450	42923	43333	43698	44029	44333	44615	44880
	2*	39107	36846	35791	34912	34107	33333	32559	31754	30875	29820	27560
	3*	21786	22051	22333	22637	22698	23333	23743	24216	24791	25563	27560
0.03	1*	40404	42849	43795	44498	45079	45580	46027	46432	46805	47151	47475
	2*	40404	37635	36343	35267	34281	33333	32385	31399	30323	29031	26262
	3*	19191	19515	19861	20234	20639	21086	21587	22168	22871	23817	26262
0.04	1*	41498	44321	45413	46226	46896	47475	47991	48459	48889	49289	49663
	2*	41498	38301	36809	35566	34428	33333	32238	31100	29857	28365	25168
	3*	17003	17377	17777	18207	18675	19191	19770	20440	21253	22345	25168
0.05	1*	42462	45618	46839	47748	48497	49144	49721	50244	50725	51172	51590
	2*	42462	38887	37219	35830	34557	33333	32109	30836	29447	27779	24204
	3*	15076	15494	15941	16422	16945	17522	18169	18918	19827	21048	24204
0.06	1*	43333	46791	48128	49123	49944	50654	51285	51858	52385	52875	53333
	2*	43333	39417	37590	36068	34674	33333	31992	30598	29076	27249	23333
	3*	13333	13791	14281	14808	15381	16013	16722	17543	18538	19875	23333
0.07	1*	44134	47869	49313	50389	51275	52041	52724	53343	53912	54441	54936
	2*	44134	39904	37931	36287	34782	33333	31884	30379	28735	26762	22532
	3*	11730	12225	12754	13323	13942	14625	15391	16277	17353	18797	22532
0.08	1*	44880	48872	50417	51566	52513	53333	54062	54724	55333	55898	56427
	2*	44880	40358	38249	36491	34882	33333	31784	30175	28417	26308	21786
	3*	10239	10768	11333	11942	12604	13333	14153	15100	16249	17794	21786

Table 4.2 continued

I_2^*	σ	I_3^* (Table values = $\sigma^* \times 10^5$)										
		-1.0	-0.8	-0.6	-0.4	-0.2	0	0.2	0.4	0.6	0.8	1.0
0.09	1*	45580	49815	51453	52672	53677	54546	55320	56022	56667	57267	57828
	2*	45580	40784	38547	36682	34976	3333	31690	29984	28119	25882	21086
	3*	08838	09399	09599	10644	11346	11820	12989	13994	15213	16851	21086
0.10	1*	46243	50707	52433	53718	54777	55694	56509	57249	57929	58561	59153
	2*	46243	41187	38829	36864	35064	33333	31602	29802	27837	25479	20433
	3*	07513	08105	08737	09417	10157	10973	11889	12948	14233	15959	20423
0.11	1*	46873	51555	53366	54713	55824	56785	57640	58416	59130	59793	60413
	2*	46873	41571	39097	37036	35149	33333	31517	29630	27569	25095	19793
	3*	06253	06873	07536	08250	09026	09881	10842	11953	13300	15111	19793
0.12	1*	47475	52365	54256	55664	56824	57828	58721	59532	60277	60969	61617
	2*	47475	41937	39354	37201	35230	33333	31436	29465	27312	24729	19191
	3*	05049	05697	06389	07134	07945	08838	09842	11002	12410	14301	19191
0.13	1*	48053	53142	55111	56576	57783	58828	59758	60601	61377	62098	62772
	2*	48053	42288	39599	37359	35307	33333	31359	29307	27067	24378	18613
	3*	03894	04568	05289	06065	06908	07838	08883	10090	11555	13524	18513
0.14	1*	48608	53890	55933	57453	58706	59791	60755	61631	62436	63184	63884
	2*	48608	42626	39836	37510	35382	33333	31284	29156	26830	24040	18058
	3*	02782	03482	04230	05035	05911	06875	07960	09213	10733	12776	18058
0.15	1*	49144	54611	56726	58300	59597	60719	61718	62624	63457	64231	64956
	2*	49144	42953	40064	37657	35454	33333	31212	29009	26602	23713	17522
	3*	01710	02435	03209	04042	04948	05947	07069	08366	09940	12055	17522
0.16	1*	49663	55309	57493	59119	60458	61617	62649	63585	40285	65245	65993
	2*	49663	43268	40285	37799	35523	33333	31143	28867	26381	23398	17003
	3*	00673	01421	02221	03081	04017	05049	06208	07547	09173	11375	17003
0.17	1*		55986	58237	59912	61293	62488	63551	64516	65403	66227	66998
	2*		43574	40499	37936	35591	33333	31075	28730	26167	23092	16500
	3*		00439	01263	02150	03115	04178	05373	06754	08429	10680	16500

Table 4.2 continued

I_2^*	σ	I_3^* (Table values = $\sigma^* \times 10^5$)										
		-1.0	-0.8	-0.6	-0.4	-0.2	0	0.2	0.4	0.6	0.8	1.0
0.18	1*			58959	60683	62104	63333	64427	65420	66332	67180	67974
	2*			40707	38070	35656	33333	31010	28596	25959	22795	16012
	3*			00334	01246	02239	03333	04562	05983	07707	10024	16012
0.19	1*				61432	62892	64155	65279	66299	67237	68108	68923
	2*				38200	35720	33333	30946	28466	25757	22506	15538
	3*				00367	01387	02511	03774	05234	07005	09385	15538
0.20	1*					63660	64956	66190	67155	68117	69011	69848
	2*					35782	33333	30884	28340	25560	22225	15076
	3*					00557	01710	03006	04504	06321	08763	15076
0.21	1*						65737	66919	67990	68976	69892	70750
	2*						33333	30824	28217	25369	21951	14625
	3*						00929	02257	03792	05654	08156	14625
0.22	1*						66499	68806	68806	69815	70753	71630
	2*						33333	30765	28096	25181	21683	14184
	3*						00167	01526	03097	05003	07564	14184
0.23	1*							68481	69603	70635	71594	72491
	2*							30707	27979	24998	21421	13754
	3*							00811	02417	04366	06984	13754
0.24	1*								70383	71437	72417	73333
	2*								27863	24819	21165	13333
	3*								01752	03743	06418	13333
0.25	1*								71147	72223	73223	74158
	2*								27751	24643	20914	12921
	3*								01101	03133	05863	12921

5. SPHERICAL COMPRESSION APPARATUS AND EXPERIMENTAL PROCEDURE

The spherical compression apparatus included that equipment necessary to experimentally determine the relationship between stress and strain for sand samples subjected to a spherical state of stress. The relationship was expected to be dependent upon porosity, and provisions were included for the measurement of sample volume.

The apparatus was designed and constructed to meet the following requirements:

1. Allow for the formation of a relatively homogeneous and isotropic sample of Ottawa sand
2. Maintain the sample in a fixed shape prior to the application of external or internal pressure
3. Allow for the application of a specified and measurable normal stress to the sand skeleton
4. Allow for the measurement of strain induced by changes in the applied state of stress
5. Allow for the determination of the total sample volume.

5.1 DESIGN

Normal triaxial compression equipment was used as a basis for design of the spherical compression apparatus with one notable exception, the end plates. It was desired to eliminate, as much as possible, the boundary friction associated with the rigidity of triaxial end plates. A schematic section of the spherical compression

apparatus is given by Figure 5.1. Photographs of the test equipment are included in Section 5.4.

5.11 SAMPLE MEMBRANE

The 0.032-in. thick latex rubber membrane was cylindrical in shape, and was approximately 2-3/4 in. in diam by 10-1/2 in. in height. The membrane was necked down at the top to 1 in. in diam in order to reduce the effect of end restraint and still allow space for the placement and compaction of sand. A uniform section approximately 1 in. long at the top allowed for the connection of a drainage cap in the usual manner. The base of the membrane was provided with a 1/4-in. tube connection to allow for saturation of the test specimen and for the measurement of internal volume change.

5.12 SAMPLE FORM

A rigid aluminum cylinder 2-3/4 in. ID and 10-1/2 in. in height was provided to contain the test sample and fix the boundaries during sand placement.

5.13 COMPRESSION CHAMBER

The lucite compression chamber was approximately 4-1/2 in. ID and 20 in. in height, and was designed to carry approximately 200 psi static internal pressure with a factor of safety of 4 against failure. Rubber O-rings were provided to seal the chamber.

Two valves were provided on the top plate to allow for application of air pressure and ventilation of the chamber. Three valves were provided on the base plate, one for filling and emptying the

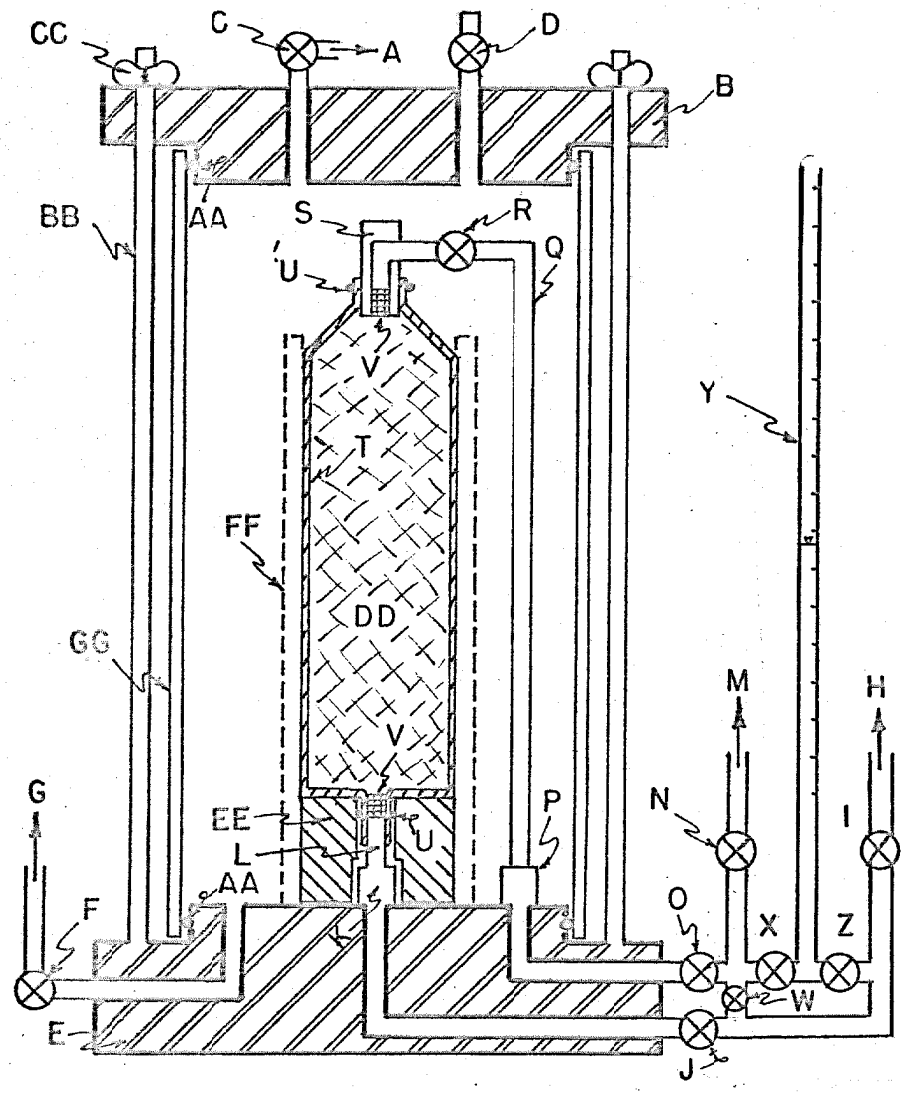

A. To air supply (pressure gage and regulator)
B Cap plate
C Air pressure valve
D Relief valve
E Base plate
F Chamber fill valve
G To chamber fill reservoir (P-V Tank No. 3)
H To sample supply reservoir (P-V Tank No. 1)
I Sample supply reservoir valve
J Sample supply valve
K Internal supply fitting
L Internal supply line
M To vac. and drainage reservoir (P-V Tank No. 4)
N Vacuum valve
O Sample drain valve
P Internal base drain fitting
Q Internal drain line (flexible)
R Internal drain valve
S Sample drainage cap
T Sample membrane
U Rubber strip binding
V Filter screen
W Division valve
X Burette drain valve
Y Volumetric strain burette
Z Burette supply valve
AA O-Ring seal
BB Tie rod
CC Wing nut
DD Sand sample
EE Split-cylinder base
FF Sample-cylinder form (position)
GG Lucite cylinder

Figure 5.1 Schematic Section-Spherical Compression Apparatus

compression chamber with water, one for admittance of water to the base of the sample, and one to allow for drainage of air and water from the top of the sample during the process of saturation.

Two fittings on the base plate and inside the test chamber were provided to allow for connection of supply and drainage lines to the test sample. A drainage cap was provided with an attached valve for connection to the top of the sample and to the internal drain line. This valve allowed for the application of vacuum to the base of the dry test specimen and the subsequent removal of the rigid aluminum form prior to assembly of the compression chamber. Screens were placed at the base and at the top of the specimen to prevent movement of sand from the sample. A split-cylinder base was provided to support the sample and allow for alignment of the sample form.

5.14 ACCESSORY EQUIPMENT

Air Pressure Gage and Regulator

An air pressure regulator provided controlled application of air pressure (up to 100 psi) to the compression chamber. Several laboratory type Bourdon gages were furnished for measurement of air pressure. The low range gage had a capacity of 60 psi and a least division of 0.25 psi, while the high range gage had a capacity of 100 psi and a least division of 0.5 psi.

Pressure-Volume Tanks and Piping System

Three pressure-volume tanks, described in Chapter 6, served for filling the spherical compression chamber with water and emptying it, for supplying water to the base of the sample, and for the removal

of air and water purged from the top of the test specimen during the process of saturation.

The piping system allowed for the application of vacuum to the sample, saturation of the test specimen, and measurement of volume changes occurring within the test specimen.

Volumetric Strain Burette

A 10-cc burette was provided to accurately measure the volume changes occurring within the pores of the test specimen. The least reading of the burette was 0.05 cc, which corresponded to a non-corrected volumetric strain of approximately 5×10^{-5}.

5.2 STRESS-STRAIN EXPERIMENTAL PROCEDURE

Where possible the following experimental procedure was adopted as standard after Spherical Compression Test No. 4-2; exceptions will be noted in the presentation of particular test results. Frequent reference will be made in the ensuing discussion to Figure 5.1, and capital letters refer directly to this figure.

5.21 SAMPLE FORMING

The base of the compression chamber was cleaned and placed on the table. The sample membrane T, Figure 5.2, was sealed to the supply line L by binding with a thin rubber strip U. Half of the split-cylinder base EE was set in place on the base plate E, and the supply tubing L was clamped at the proper elevation by tightening the internal supply fitting K. Figure 5.3 shows the base connection prior to clamping. The remaining half of the split-cylinder base was

inserted to form a base for the test specimen, Figure 5.4, and the sample cylinder form FF was bound to the split-cylinder base with masking tape (not shown).

Approximately 2000 gm of oven dry sand was weighed out in a glass beaker and poured through a glass funnel into the sample membrane, Figure 5.5. Various degrees of initial density were obtained by tamping with a 1/2-in. diam steel rod at regular intervals during the placement process. When the sand reached a level approximately 1 in. below the top of the membrane, the sand remaining in the glass beaker was weighed.

The sample drainage cap S with valve R closed was inserted into the membrane until the base of the cap rested lightly on the sand surface. The membrane was then carefully sealed to the cap by binding with thin rubber stripping U. Valves O, X, Z and I were closed, and valves N, W and J were opened. A vacuum of 5 psi was applied to the base of the sample from the drainage reservoir. The vacuum source was provided by an aspirator attached to a sink faucet, Figure 6.8, and the vacuum was measured with a Bourdon gage. Upon application of vacuum the specimen contracted somewhat, and the sample cylinder form was removed.

The internal drain line Q was carefully coupled to the internal drain valve R at the top of the specimen, and to the internal base drain fitting P, Figure 5.6. Valves O and R were opened, thus applying vacuum to the top of the specimen, then valves J and W were closed.

5.22 COMPRESSION CHAMBER ASSEMBLY

The lucite cylinder, lubricated with silicone grease over areas to be in contact with the rubber O-ring seals AA, was set in place on the base plate and the cap plate B was inserted. The tie rod wing nuts CC were hand tightened against the top plate.

The compression chamber was then lifted and placed upon a metric balance. The air relief valve D was opened. Valve C was closed and the air pressure supply line A was attached. The sample supply line from pressure-volume tank no. 1 was filled with water and attached to closed valve I. The chamber fill line leading from pressure-volume tank no. 3 was filled with water and attached to closed valve F. Figure 5.7 shows the assembled compression chamber. Photographs of the spherical apparatus were taken after the performance of the experiments and at that time the pressure-volume tanks were in use in the three-dimensional compression tests. Reference is made to Figure 5.1 for the actual piping details which the photographs do not accurately describe.

5.23 INITIAL SAMPLE VOLUME DETERMINATION

The weight of the compression chamber and its contents was recorded, and the water volume in the fill reservoir was noted. The chamber fill valve F was then opened, and upon overflow at valve D, both valves F and S were closed. The weight of the compression chamber and its contents was recorded once again and the water volume in the fill reservoir was noted.

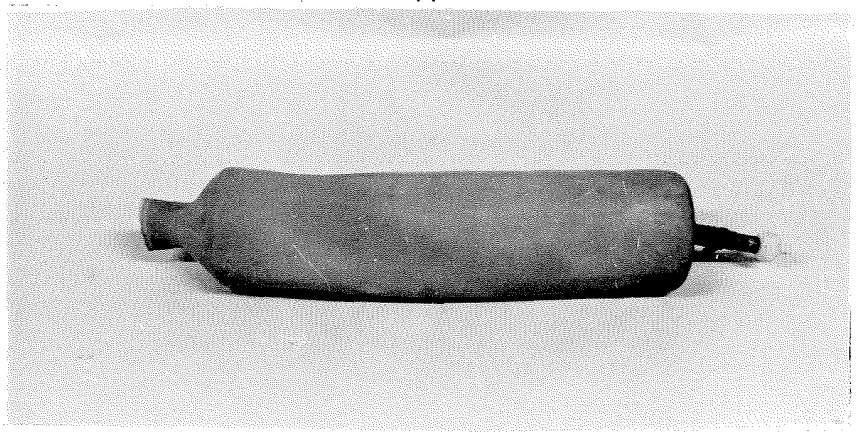

Figure 5.2 Sample Membrane, Spherical Compression Apparatus

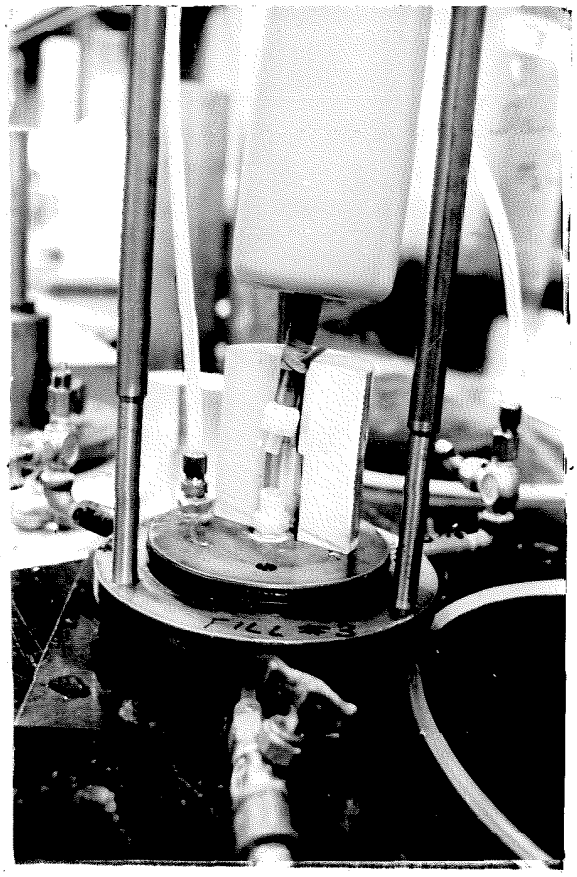

Figure 5.3 Base Prior to Connection, Spherical Compression Apparatus

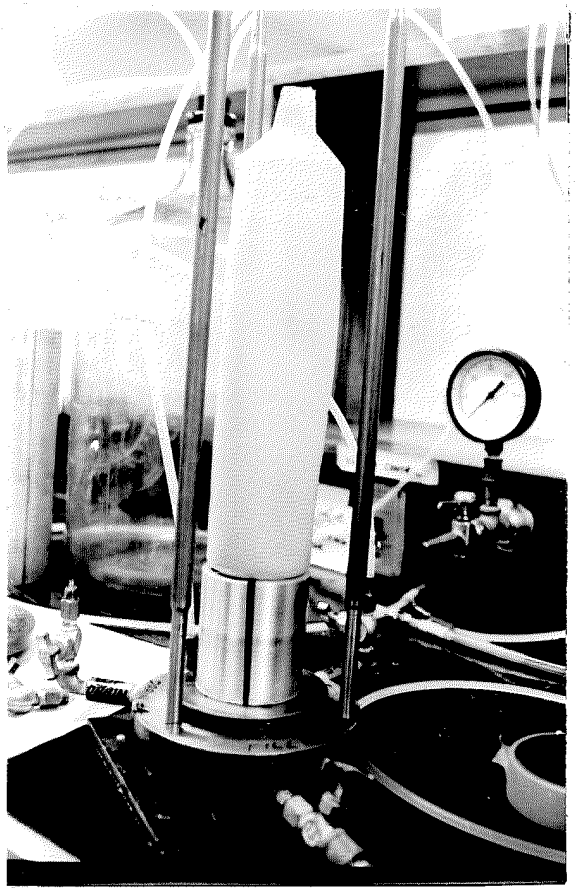

Figure 5.4 Base After Connection, Spherical Compression Apparatus

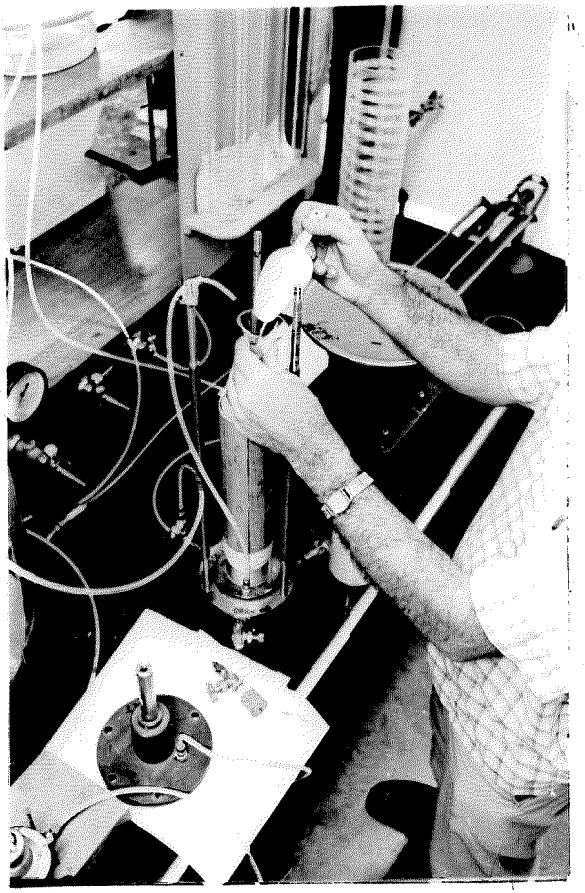

Figure 5.5 Placement of Sand, Spherical Compression Apparatus

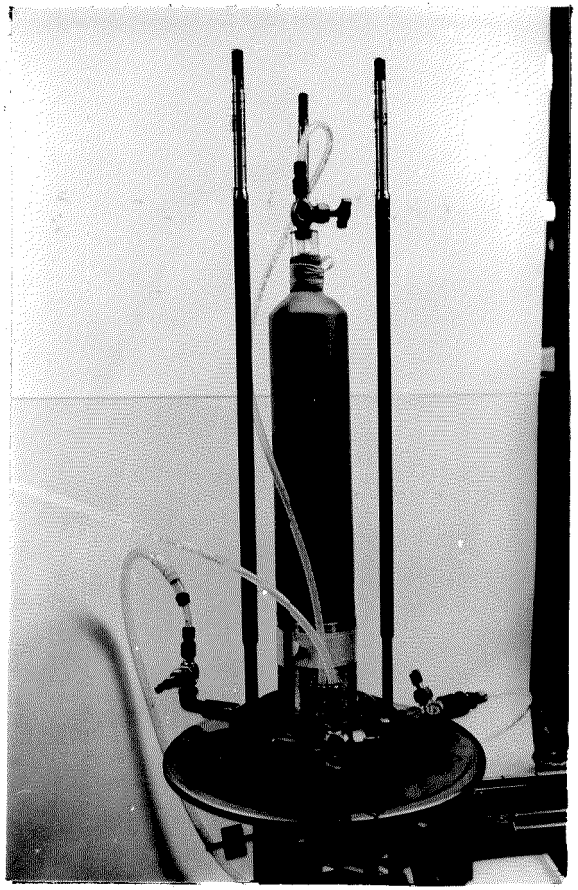

Figure 5.6 Sand Sample Under Vacuum, Spherical Compression Apparatus

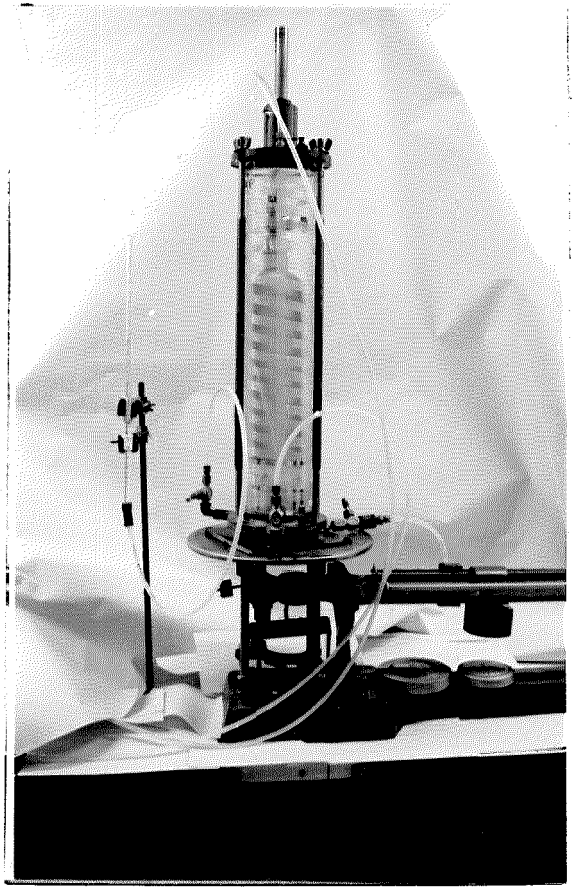

Figure 5.7 Assembled Compression Chamber, Spherical Compression Apparatus

5.24 SATURATION OF THE SAND SAMPLE

Air pressure valve C was opened and an external pressure of 4.5 psi was applied. Valves I and J were opened until water appeared at the base of the compression chamber, then valve J was closed. The sample supply reservoir volume was recorded and the metric scale weight was noted. The sample supply valve J was then opened and water was allowed to enter the specimen. When water appeared at the drainage cap the scale weight and supply reservoir volumes were recorded. Water was allowed to flow through the test specimen until air bubbles were no longer visible within the internal drain line. At this point sample supply valve J and sample drain valve O were closed and the scale weight recorded.

The burette Y was filled with water and valves X, Z and W were opened momentarily, allowing water to fill the measurement system. The burette was again filled with water, the reading recorded. Valves X, Z, O and J were opened allowing water to move freely from both ends of the specimen. As the sample had been under vacuum at the top, the specimen expanded due to the decrease in effective stress, and water moved from the burette to the sample. When the burette volume reached equilibrium in time, the burette reading and metric weight were recorded.

The burette was made movable in a vertical direction in order that a constant pore fluid pressure might be maintained within the test specimen, thus reducing the possible adverse effects of air compressibility within the fluid measurement system. Atmospheric

pressure was maintained near the center of the sample in order that the effects of pore-water pressure might be neglected.

5.25 STRESS-STRAIN EXPERIMENT

The initial pressure was 4.5 psi in all experiments; however, the stress path was varied in different experiments. The maximum number of loading intervals was ten. The lowest applied external pressure was 1-1/3 psi, and each successively higher pressure was 1-1/2 times as large as the previous one. The highest applied external pressure was 76.9 psi. Load increments were applied slowly (10-15 sec), and were maintained for approximately 2 min. Burette readings were recorded prior to and following each load application.

5.3 EXPERIMENTAL DETAILS

The spherical compression chamber volume determination given in Appendix A4 was used in the estimation of sample volume.

Strain effects including rubber penetration, drain line compression and temperature change are given in Appendix A3. A discussion of vibration and steps taken to reduce the effects of vibration on experimental results is presented in Section 9.3.

Rubber penetration normally accounted for 20-50% of the total volume change as recorded at the burette, and test data were corrected for this effect (see Appendix A6). Test results were not corrected for other effects which were considered negligible in comparison.

6. THREE-DIMENSIONAL COMPRESSION APPARATUS AND EXPERIMENTAL PROCEDURE

The three-dimensional compression apparatus included that equipment necessary to experimentally determine the relationship between stress and strain for a sample of sand subjected to a general state of statically applied stress. The author designed and constructed apparatus to meet the following essential requirements:

1. Allow for the formation of a relatively homogeneous and isotropic sample of Ottawa sand
2. Maintain the sample in a fixed shape prior to the application of confining pressure
3. Allow for the application of an arbitrary state of principal stress
4. Allow for the measurement of principal strains induced by changes in the applied state of principal stress
5. Allow for the determination of sample volume.

6.1 DESIGN

6.11 GENERAL

Rubber pressure cells were used to apply principal stresses to five faces of a square, plate-shaped sample contained within a rubber membrane. A relatively rigid chamber provided space for containment of the sample and the pressure cells. Three principal strains were measured from the volume changes occurring within the pressure cells, and volumetric strain was measured directly by the movement of water

from the void spaces within the test specimen. A check was thus provided on the measurement of strain. The specimen could conceivably undergo considerable deformation without the development of mechanical interference at the corners.

The three-dimensional compression apparatus was composed of eight major components:

1. Sample membrane
2. Sample form
3. Compression chamber
4. Pressure cells
5. Pressure-volume tanks
6. Volumetric strain burette
7. Saturation-rotation device
8. Press frame.

Schematic drawings and photographs are given early in the chapter so that the reader may quickly gain a comprehensive view of the apparatus. Numerous photographs are presented later in the chapter for illustration of experimental procedure. Photographs of particular details are given in Appendix 7.

Schematic diagrams first given illustrate:

1. The compression chamber containing a test specimen, but with cover plates removed, Figure 6.1
2. A typical pressure-volume tank, Figure 6.2
3. Overall piping system including air pressure control and measurement, Figure 6.3.

Photographs first given illustrate:

1. A side view of the compression chamber, saturation-rotation device and press frame, Figure 6.4
2. A top view of the compression chamber, Figure 6.5
3. The four pressure-volume tanks and their relationship to the compression apparatus, Figure 6.6
4. A front view of three pressure-volume tanks including the air pressure control panel behind, Figure 6.7
5. The vacuum source, Figure 6.8.

6.12 SAMPLE MEMBRANE

The sample membrane, Figure A7.12, was formed of 0.055-in. thick latex to sheath a sand specimen approximately 2 in. in height and 15-1/2 in. sq. Two openings were provided in diagonal corners for placement and removal of sand, for saturation of the test sample, and for volumetric strain measurement.

6.13 SAMPLE FORM

A wood form consisting of two parts was designed to hold the sample membrane in a relatively fixed position during sand placement, Figure 6.9. It was approximately 16 in. sq and 2 in. thick in inside dimensions when assembled.

6.14 COMPRESSION CHAMBER

A compression chamber, composed primarily of steel, was designed to contain the sand specimen and the rubber pressure-cells. The inside dimensions were approximately 2 in. in thickness by 20 in. square.

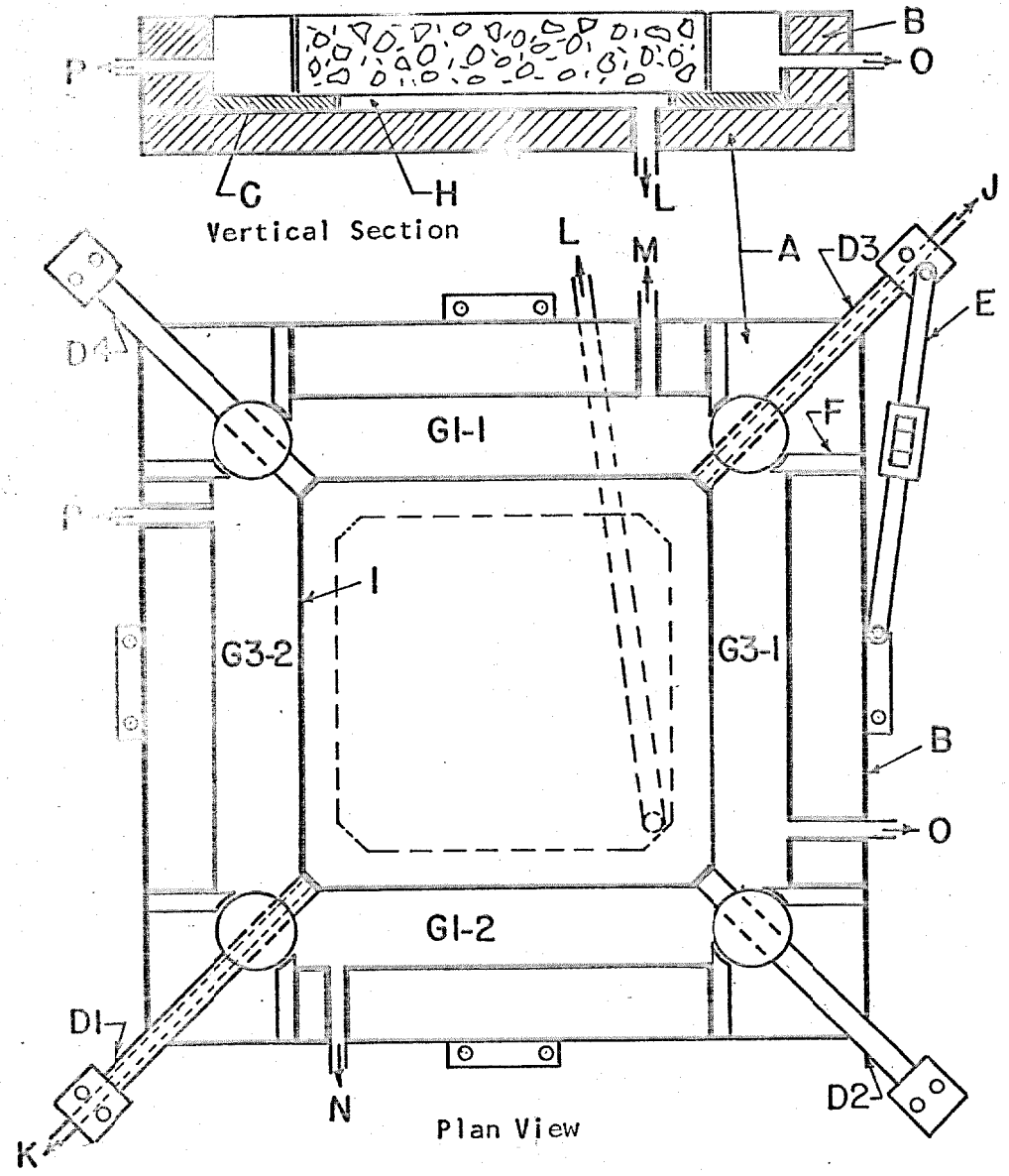

A Base plate
B Side bar
C Spacer plate
D Piston assembly
E Piston control
F Pressure seal
G Side pressure cells (major and minor principal stress)
H Base pressure cell (intermediate principal stress)
I Sample membrane
J To sample supply reservoir (P-V TK. 4, Valve 3, Front)
K To sample drainage reservoir (P-V TK. 4, Valve 25, rear)
L To intermediate pressure volume tubes (P-V TK. 2, Valve 3)
M To major pressure-volume tubes (P-V TK. 1, Valve 1)
N To major pressure-volume tubes (P-V TK. 1, Valve 2)
O To minor pressure-volume tubes (P-V TK. 3, Valve 1)
P To minor pressure-volume tubes (P-V TK. 3, Valve 2)

Note: Cover plates removed and press frame not shown.

Figure 6.1 Schematic Diagram - Compression Chamber, Three-Dimensional Compression Apparatus

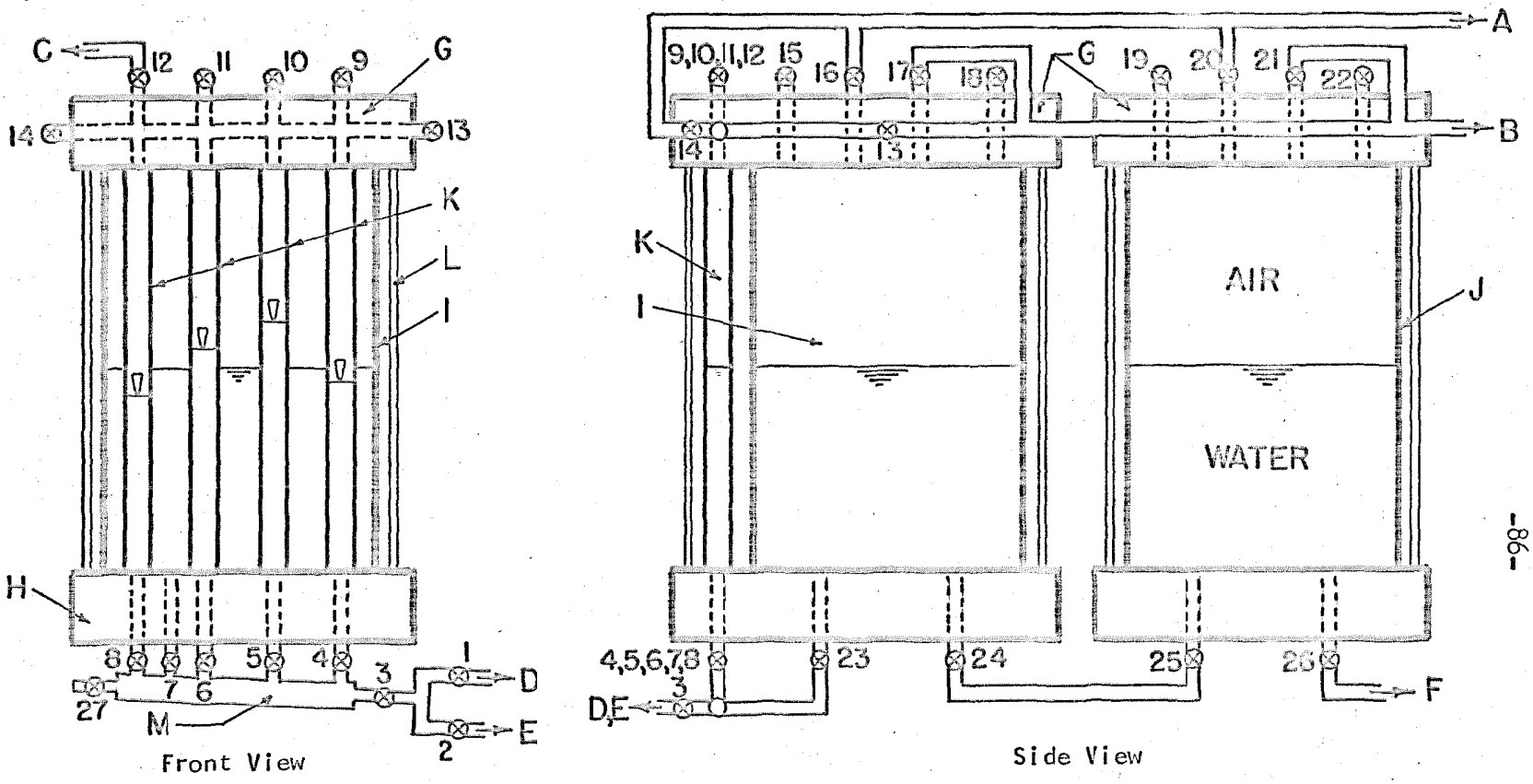

Key:

A	To vacuum supply	G	Top plate	M	Valve manifold
B	To air pressure supply	H	Base plate		
C	To P-V TK. 2, Valve 9	I	Front reservoir		Valves numbered 1-27
D	To pressure cell G1-1	J	Rear reservoir		
E	To pressure cell G1-2	K	Graduated tube		
F	To P-V TKS. 2, 3, 4, Valve 26	L	Tie rod		

Figure 6.2 Schematic Diagram of Pressure Volume Tank No. 1. Three-Dimensional Compression Apparatus

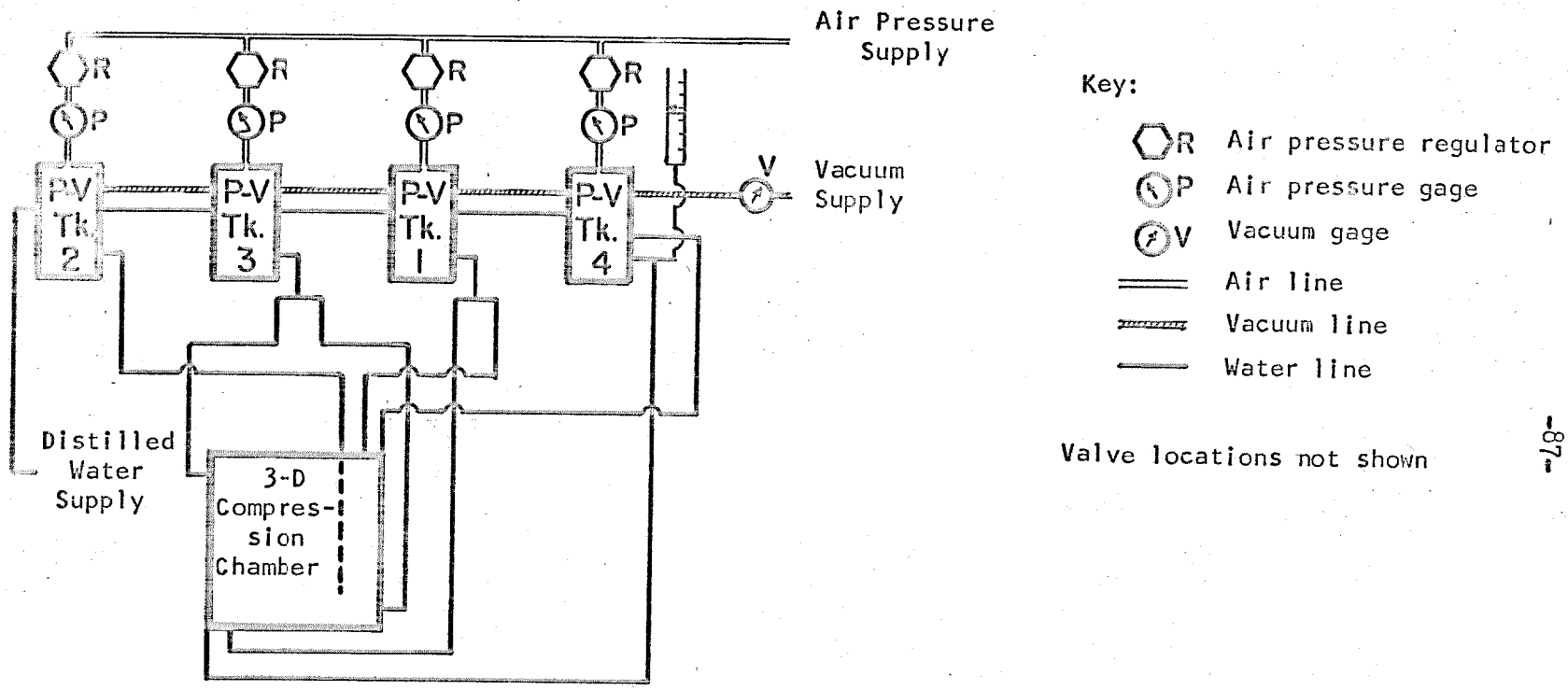

Figure 6.3 Schematic Diagram - Piping System for Three-Dimensional Compression Apparatus

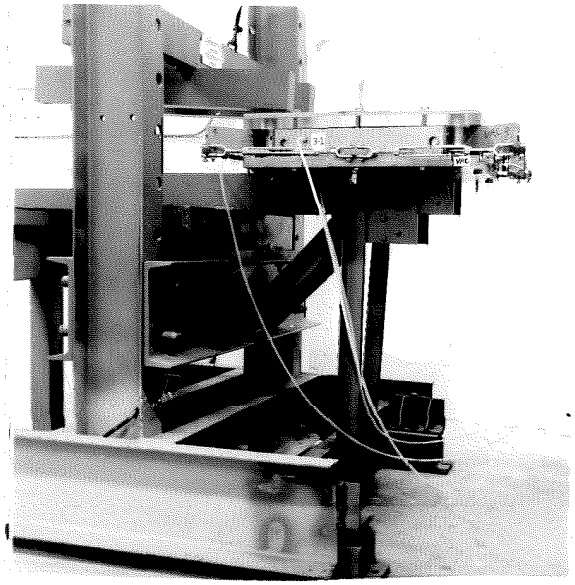

Figure 6.4 Side View of Compression Chamber, Saturation-Rotation Device and Press Frame, Three-Dimensional Compression Apparatus

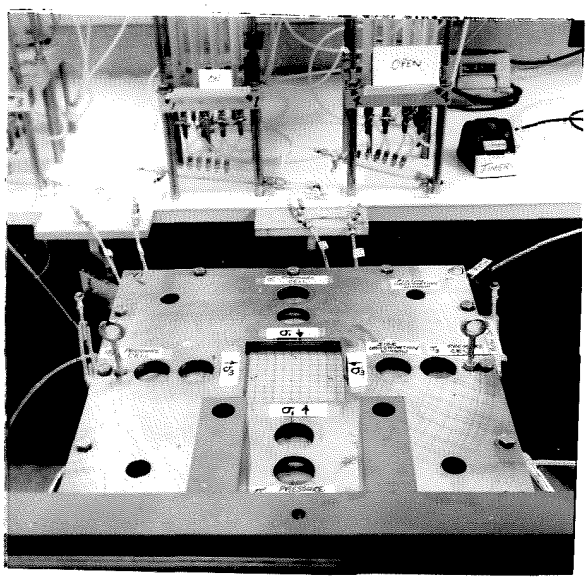

Figure 6.5 Top View of Compression Chamber, Three-Dimensional Compression Apparatus

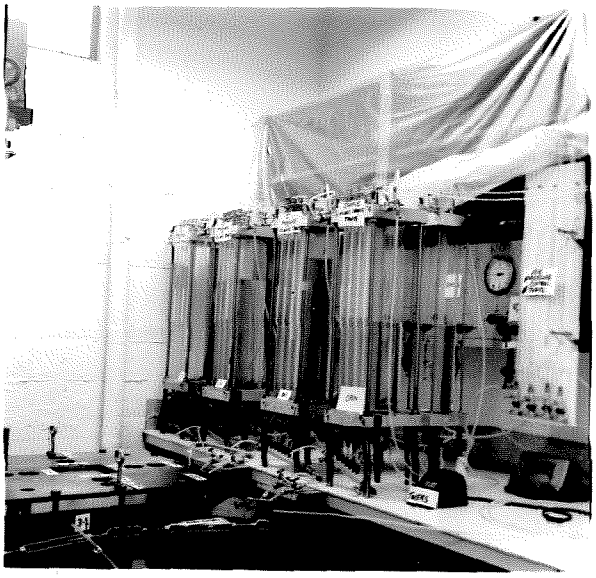

Figure 6.6 Four Pressure-Volume Tanks and Compression Chamber, Three-Dimensional Compression Apparatus

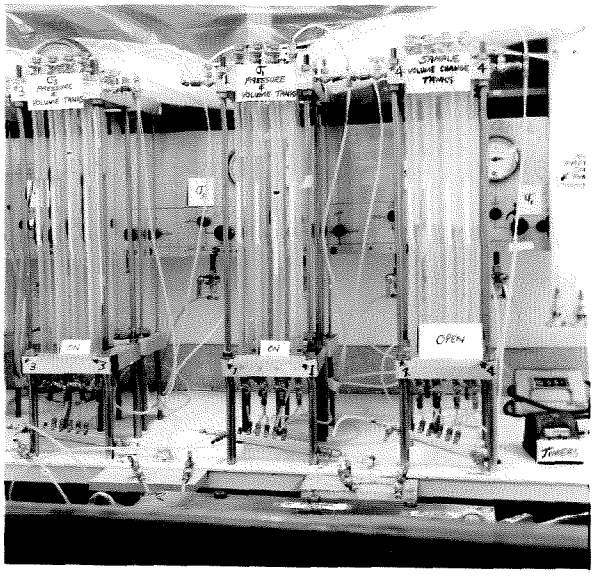

Figure 6.7 Front View of Pressure-Volume Tanks 3, 1 and 4, and Air Pressure Control Panel, Three-Dimensional Compression Apparatus

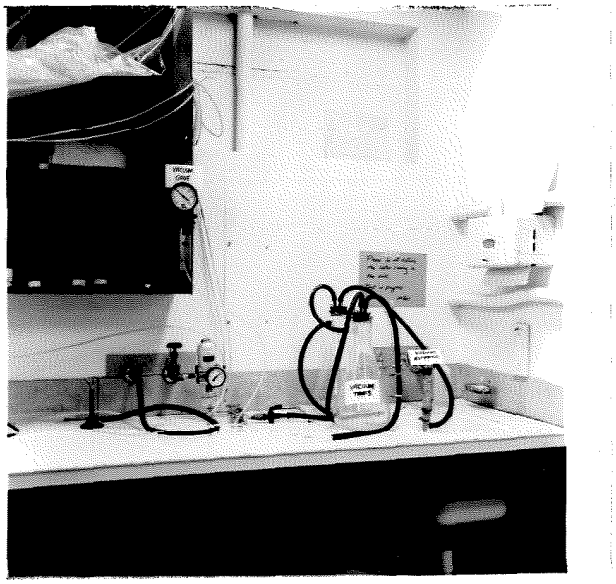

Figure 6.8 Vacuum Source, Three-Dimensional Compression Apparatus

Rectangular pistons, Figures A7.1 and A7.2, entered the chamber through cylinders at the corners to provide separation for the side pressure-cells. Control of piston motion was provided by the installation of turnbuckles outside the chamber. Holes were provided through the pistons for passage of water lines from the test specimen.

A recess was provided in the base of the chamber adjacent to the test specimen for containment of the base pressure-cell which was approximately 12 in. sq and 1/2 in. deep. Two cover plates were provided, a lucite plate which was placed next to the sample, and a steel plate with cutouts to serve as observation windows. The side pressure-cells were sealed inside the test chamber at the piston cylinders with acrylic plastic plates. Holes were provided in the compression chamber for the admittance of a water line to each pressure-cell.

6.15 PRESSURE-CELLS

The compromise necessary in obtaining ideal boundary conditions is somewhat dependent upon the range in expected deformation. This equipment was designed to allow approximately 20% strain (3 to 3-1/2 in.)

The side pressure-cells, Figure A7.10, were made larger than the spaces allowed within the compression chamber in order that cell skin tension might be neglected, thus allowing direct measurement of applied pressure. The base pressure-cell was made smaller than the base of the test specimen (see Figure 6.14) in order that considerable deformation might be permitted without the occurrence of pressure-cell interference. Latex equipment used in forming rubber components is shown by Figures A7.9 and A7.11.

6.16 PRESSURE-VOLUME TANKS

Four identical pressure-volume tanks were designed to form a part of the three-dimensional compression apparatus. Pressure-volume tanks 1, 2 and 3 were used in connection with the application of three principal stresses to the test specimen, and for the measurement of the resulting three principal strains. The fourth tank was used primarily in saturating the sand sample.

A typical tank, pressure-volume tank no. 1 of Figure 6.2, was composed of two reservoirs and four relatively small tubes. Regulated air pressure was applied at the top and thus to the water interface near the center of the tank. Water filled the pressure-cells G1-1 and G1-2, Figure 6.1, and was continuous into the base of pressure-volume tank no. 1. Numerous valves were provided for experimental

flexibility, Figures A7.7 and A7.8. Provisions were made to supply the cells with relatively large volumes of water from the reservoirs or relatively small volumes from the graduated tubes. The tubes could be operated individually or in combination. Each tube had a least reading of 1 cc and a capacity of 150 cc, corresponding approximately to a non-corrected least strain of 1.4×10^{-4} and a strain capacity of 2.1%. The foregoing information applies as well to tank no. 3 except that it was connected to side pressure-cells G3-1 and G3-2 of Figure 6.1.

Pressure-volume tank no. 2 was connected to base pressure-cell H. The corresponding least strain in this case was approximately 2.2×10^{-4} and the strain capacity of a single tube was 3.3%.

In the initial saturation of a test specimen, the front reservoir of pressure-volume tank no. 4 served as a water supply source, the rear reservoir for drainage.

The four tanks were supplied with a common vacuum and a common distilled water line, Figure 6.3. In order that water could be periodically de-aired, the rear reservoirs were placed on vacuum while the front reservoirs were active and under positive pressure. Each tank had a separate air pressure regulator and Bourdon pressure gage.

6.17 VOLUMETRIC STRAIN BURETTE

A 25 cc burette was put in line with the sample supply in order to allow for an accurate measurement of internal volume change, and thus volumetric strain during a stress-strain experiment. The least reading of the burette was 0.1 cc, corresponding approximately to a

non-corrected volumetric strain of 1.4×10^{-5}. The full range of the burette corresponded to a volumetric strain of 3.5×10^{-4}.

6.18 SATURATION-ROTATION DEVICE

The compression chamber including the test specimen weighed over 300 lb assembled. In order to fill the sample voids with water while the sample was in place within the compression chamber it was necessary to provide a handling tool. The saturation-rotation device, Figures A7.5 and A7.6, allowed for rotation of the compression chamber about two mutually orthogonal and horizontal axes in such a way that the diagonal corner membrane openings might be high and low points within the test specimen.

6.19 PRESS FRAME

Deformation of the compression apparatus under internal pressure was minimized by addition of a press frame, Figure A7.3, for lateral restraint. With the frame fully bolted a spherical compression chamber pressure of 100 psi was calculated to produce only 0.01 in. expansion at the center of the test chamber, and this corresponded approximately to 0.5% equivalent sample strain. Spherical chamber pressures during this study did not exceed 18 psi on the average, and only half of the press frame bolts were utilized.

Ease in handling the top portion of the press frame was provided by an existing box frame already equipped with a lifting device which also provided a convenient level of support for the compression apparatus. Vibration isolators, Figure A7.4, were placed under the corners

of the box frame to reduce the effects of structural vibration occurring at the floor.

6.2 STRESS-STRAIN EXPERIMENTAL PROCEDURE

The following experimental procedure was adopted as standard following Experiment No. 2, and major exceptions will be given in the presentation of particular test results. Frequent reference will be made to the schematic drawings, Figures 6.1 and 6.2. Where valves are referred to by two numbers separated by a dash the first number indicates the pressure-volume tank number, and the second number indicates the valve number corresponding to Figure 6.2. For example, valve 3-1 refers to valve number 1 of pressure-volume tank no. 3.

6.21 SAMPLE FORMING

The sample membrane was wiped clean of grease and placed in the lower half of the wood form, Figure 6.9. A piece of 100-mesh/in. brass screen material was cut, rolled and fit into the end of a section of polyflow tubing approximately 10 ft in length. The screened end of the tubing was inserted in one of the two open membrane corner tubes and the joint was bound with thin rubber stripping, Figure 6.10. A second piece of polyflow tubing was cut to a length of 12 in. and inserted into the diagonally opposite corner tube, and this joint was similarly sealed. The top half of the wood form was set in place and the two units were bolted together. Thick rubber stripping was bound to the polyflow tubing at the diagonal ends, Figure 6.11, and was pushed tight against the form to provide some rigidity in the connection. The form,

with one diagonal end resting on a table, was clamped to a wooden support such that the short open tube was at the top. A funnel was bound to the short tube with masking tape and clamped to the wooden support.

Fifteen lb of dry Ottawa sand was weighed out in an aluminum pan and poured into the funnel with a scoop, Figure 6.12. When the pan was empty, 13.31 lb of dry sand was weighed out and poured into the funnel. Upon filling the membrane, the form was vibrated with a rubber hammer, Figure 6.13, over its entire surface and sand was added until 28.31 lb of dry sand was in place within the rubber membrane. At this stage the funnel was removed and a small piece of sieve material was cut, rolled and placed tight against the sand within the upper polyflow tube. A wooden plug was inserted in the end of the longer tube at the base. The form was then released from the wooden support and moved in a horizontal position to a table adjacent to the compression apparatus.

6.22 CONTAINMENT OF SAND SAMPLE WITHIN THE COMPRESSION CHAMBER

The plastic dust cover was removed from the compression chamber in the horizontal preparation position, Figure 6.14, and silicon grease was applied to all inside parts. The corner piston assembly, D of Figure 6.1, was removed from the chamber and placed on the pressure-volume table. The longer drain tube from the sand sample was passed through this piston from the side to be adjacent to the sample and connected to the vacuum manifold.. A vacuum of 12 psi was slowly applied to the sand sample and the form bolts were removed. The top half of the form was lifted from the sample, Figure 6.15, and the test

specimen was examined. If there were visible depressions on the surface, the test was aborted and a new sample formed.

Upon obtaining a suitable sample, the top face of the membrane was greased and the sample was carefully lifted from the form, turned over and placed within the compression chamber by hand. The corner piston assembly was set in place within the compression chamber, Figure 6.16, and all pistons were adjusted to meet the diagonal corners of the test specimen. Silicon grease was then applied to the top and sides of the sample membrane. The lucite cover plate was lubricated on the lower surface with silicon grease and set in place, Figure 6.17. The steel cover plate was installed and bolted down, Figure 6.18.

Frequent reference will now be made to Figure 6.2. In the beginning, valves 1 through 26 (all four units) were closed. Valves 13, 17, 23, 1 and 2 were then opened and an air pressure of 5 psi was applied through B (first three units). Valve 3 was opened (first three units) allowing water to flow from the front reservoirs to the pressure cells. The test sample at this stage was confined by an internal vacuum of 12 psi and an externally applied pressure of 5 psi.

Vacuum pressure was reduced to atmospheric and the vacuum line was separated about 20 in. from the end of the piston bracket D1 of Figure 6.1. An open needle valve (drain valve) was installed at this location and the tubing was re-connected. The wood plug was then removed from the supply tube at the base of the test specimen and a needle valve (supply valve) was attached and closed. The vacuum was again increased to 12 psi.

At this point the first three pressure-volume tanks were connected by attachment of a short piece of polyflow tubing from valve 1-12 to valve 3-9 and from valve 3-12 to valve 2-9. These valves were then opened and valves 2-13 and 3-13 were closed resulting in the application of a common pressure to all graduated tubes. Valve 23 was closed and valve 4 was opened (first three units) thus connecting the right graduated tubes directly to the pressure-cells.

6.23 SATURATION OF SAND SAMPLE

Valves 1-3, 1-1 and 1-2 were closed and the compression chamber was rotated by hand about a horizontal axis parallel to the box frame, Figure 6.19, to a vertical position. The chamber was then rotated about a horizontal axis normal to the box frame so that the supply tubing was low and the drain tubing was high, Figure 6.20.

Pressure-volume tank no. 4 was now prepared for use as a sample supply source. First all valves were closed, and an air pressure of 5 psi was applied through B of Figure 6.2. Valves 15, 21, 24 and 25 were opened allowing water to flow from the rear to the front reservoir. Upon filling the front reservoir, valves 21, 24 and 25 were closed and valve 23 was opened. A piece of polyflow tubing about 6 ft in length was connected directly to valve 24 of the front reservoir. Valve 24 was opened and upon filling, the line was connected to the supply valve at the base of the test specimen. A note was made of the supply reservoir volume, and then the supply valve was opened allowing water to enter the sample.

Upon observation of water at the top drain valve, the supply reservoir volume was again recorded. Water was allowed to flow through the sample under vacuum until water appeared in the vacuum bottles, Figure 6.8. At this point the drain valve was closed and the line extending from the drain valve to the bottles was removed and attached to valve 25 (rear reservoir). This line was filled with water by opening valves 19 and 25, and upon filling was attached to the drain valve once again. The drain valve was then opened allowing water to flow back into the sample due to the existing partial vacuum.

6.24 PLACEMENT OF CHAMBER WITHIN PRESS FRAME

The compression chamber was rotated to a horizontal position and moved to the center of the box frame. The top half of the press frame was lowered by means of a crank to rest on the compression chamber, Figure 6.21, and four tie bolts were inserted and tightened to provide lateral restraint, Figure 6.22.

Valves 1-3, 1-1 and 1-2 were re-opened and equilibrium was usually obtained in about 1 hr. The drain valve and the supply valve were closed and the supply line was connected to a 25 cc burette. The burette was filled with water to the same level as that normally used in the pressure-volume tubes (base level) thus providing a balance of pore-water pressure with the head of water normally existing on the pressure-cells. The supply valve was then opened and the right-hand pressure-volume tube was adjusted to base level by varying the pressures in the front reservoir and cracking valve 23 momentarily (first three units).

6.25 AIR VOLUME DETERMINATION

A sample air volume determination was made essentially by changing the pore fluid pressure and noting the corresponding volume change. The pressure change was accomplished by simply raising and lowering the burette a few inches within its holder; the volume change was obtained directly from the burette readings, Appendix All.

6.26 INITIAL SPHERICAL COMPRESSION CYCLES

Water was withdrawn from the burette to the 25 cc mark by use of a polyethylene bottle connected to a small diameter plastic tube. The burette and the pressure-volume tubes were again adjusted to base level.

Pressure was applied to all cells to 30 psi in increments of 5 psi and released to 5 psi in increments of 5 psi. Each load increment was maintained for approximately 15 min. Readings of the three right-hand pressure-volume tubes and the volumetric strain burette were taken prior to and following each load increment.

Approximately four complete cycles of compression and extension were made prior to the performance of each specific deviatoric stress-strain experiment. Water was taken from the burette when its range of operation was threatened and the water level was periodically adjusted to base level. The final compression cycle was performed to leave each pressure-cell at 18 psi, the spherical stress normally used in the deviatoric stress-strain experiments.

6.27 DEVIATORIC STRESS-STRAIN EXPERIMENT

With the sample under 18 psi all around pressure, regulators 2 and 3 were adjusted to develop pressures of 18 psi, valves 2-13

and 3-13 were opened, and valves 2-9, 3-12, 3-9 and 1-12 were closed. The pressure-volume tubes were adjusted to base level and the burette was filled to the 5 cc mark and adjusted to base level. Each parallel pair of side pressure-cells were always used to apply the major and minor principal stresses, and the base cell was always used to apply the intermediate principal stress: Figure 6.1, G1-1 and G1-2 for σ_1, G3-1 and G3-2 for σ_3 and H for σ_2.

The initial stress path invariably was of the type I_{13}*(I_1 and I_3* constant, I_2 or I_2* increased). The subsequent stress paths were varied in the different experiments. The effective principal stresses used were pre-calculated by use of Table 4.2 with knowledge of the particular stress path desired. Each load increment was maintained for a period of approximately 15 min. Readings of the three right-hand pressure-volume tubes and of the burette volume were taken prior to and following each increment of loading. The burette and the graduated tubes were periodically adjusted to base level. The difference of head caused by a graduated tube level other than base zero was normally taken into account by correction of the applied air pressure at the beginning of a load increment. For the yield tests, however, several adjustments were normally required at relatively high deviatoric stress states. When the rate of volume change as recorded by the burette did not decrease in time after the application of a deviatoric stress increment, it was assumed that first yield had been obtained and all flow valves were shut as quickly as possible. The loads were then reduced by one load decrement, the flow valves opened and the test continued.

If the volume change indicated by the burette continued to increase, the loads were immediately reduced by the next load decrement. Upon obtaining a static condition once again, the usual 15 min load interval was normally adopted. The state of stress was always returned to the spherical state existing prior to the deviatoric cycle.

6.28 FINAL SPHERICAL COMPRESSION CYCLES

Several experiments included a series of spherical compression cycles following the deviatoric stress paths. These were performed in the same manner as initial spherical compression cycles. In each case the supply valve was finally closed at a common cell pressure of 5 psi, sealing the sample, and the air pressure was then reduced to atmospheric in all pressure-volume units. Valves 1, 2, 4, 13 and 17 were closed and valve 23 was opened.

6.29 COMPRESSION CHAMBER DISASSEMBLY

The press frame was unbolted and lifted above the compression chamber. The chamber was moved to the preparation position and the steel cover plate was removed. The sample was visually examined through the lucite cover plate for zones of progressive failure. Figure 6.23 shows the only sample which exhibited such a failure, Sample No. 10.

A vacuum of 2 psi was applied to pressure-volume tanks 1, 2 and 3. Valve 16 was opened and valves 1 and 2 were opened in sequence for a few moments drawing water from the pressure-cells into the front reservoirs. Valve 16 was closed and valves 10 and 15 were opened.

The lucite plate was carefully lifted from the chamber, wrapped with a plastic cover and stored. The sample supply and drain valves were disconnected from the sample. The extended pistons were retracted into the piston cylinders, and the piston assembly was carefully removed from the compression chamber.

The sample was lifted from the chamber and placed on a platform scale. The polyflow drain and supply tubes were removed from the membrane, and the wet test specimen and membrane were weighed together.

The sheathed sample was taken to a sink platform where the sand was washed into an aluminum pan. When the membrane was completely free of sand it was hung up to dry overnight. The pan of wet sand was placed in a ventilated oven at 100°C to dry. In the morning the membrane was weighed and the sand removed from the oven and stored.

6.3 EXPERIMENTAL DETAILS

Various effects were considered for possible correction of measured stress-strain data. Strain effects including rubber penetration, pressure-cell behavior and temperature change are given in Appendix A8. Stress effects including membrane behavior and boundary friction are given in Appendix A9. Photographic measurement of principal strains was attempted unsuccessfully and is reported in Appendix A10. Air volume determination is given in Appendix A11. Measures were taken to minimize the effects of vibration by the installation of vibration isolators, as is discussed in Chapter 9.

Errors due to temperature change were considered negligible. Test results were normally corrected for strain effects attributed to rubber penetration and pressure-cell behavior. Variations from this procedure are reported in Chapter 7. At small strains, the pressure-cell correction was of the same order of magnitude as the measured strain, while at relatively high strains (near yield) the pressure-cell corrections were on the order of 4% of the measured principal strains and the rubber penetration correction was on the order of 1% of the measured volumetric strains. (See Appendix A.3)

Boundary friction was estimated to be less than 0.2 psi on the basis of supplemental tests and was neglected in calculations. Stress effects attributed to membrane behavior were taken into account only in the development of a first yield criterion, Section 8.5, and at yield accounted for approximately 5% of the applied major principal stress and 10% of the applied minor principal stress.

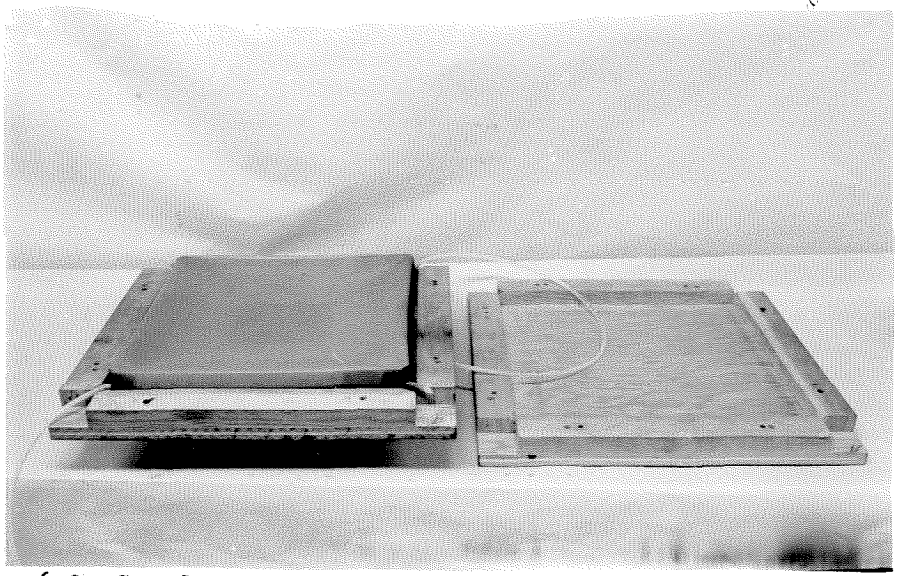

Figure 6.9 Sample Membrane in Place within Bottom Half of Wood Form, Three-Dimensional Compression Apparatus

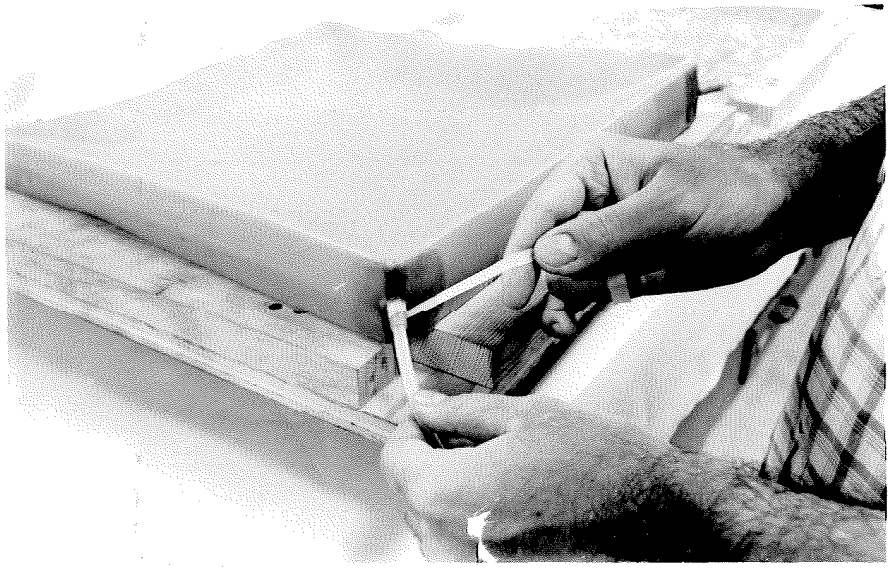

Figure 6.10 Attachment of Drain Line to Sample Membrane, Three-Dimensional Compression Apparatus

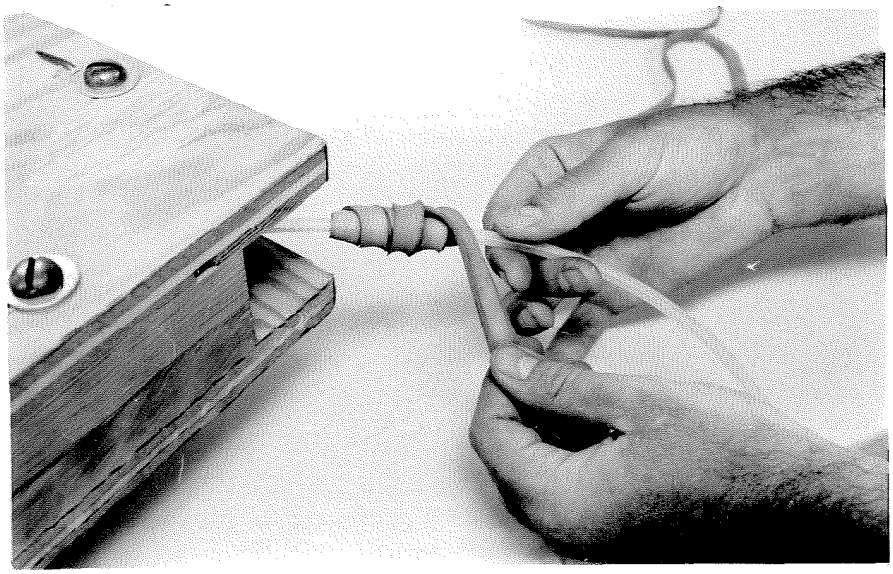

Figure 6.11 Stiffening the Drain Line Connection at the Sample Form, Three-Dimensional Compression Apparatus

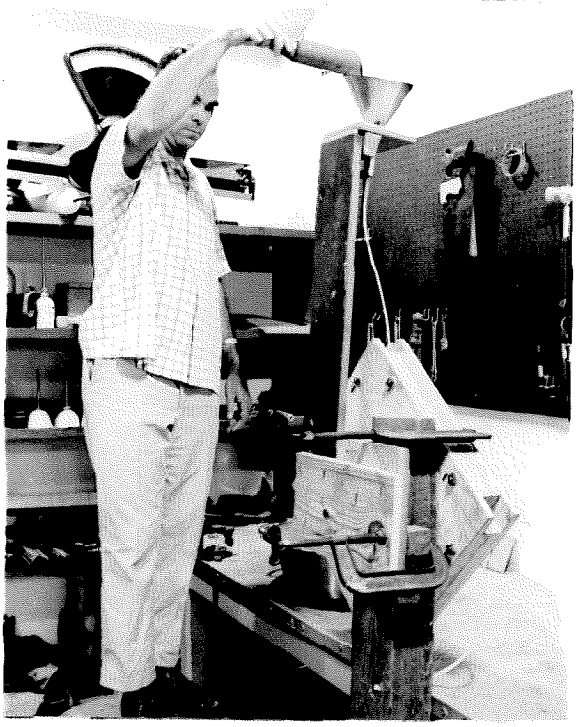

Figure 6.12 Placement of Sand, Three-Dimensional Compression Apparatus

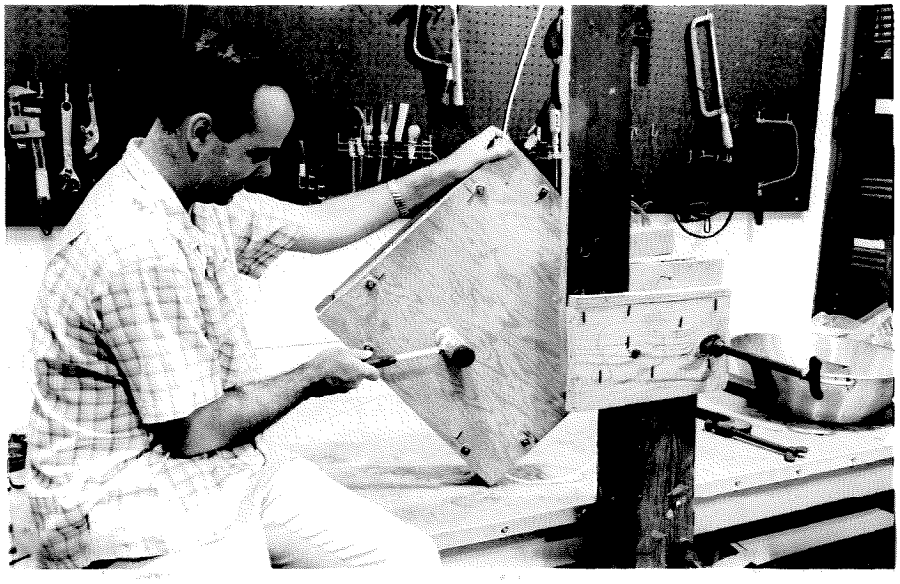

Figure 6.13 Vibration of Mold Form with Rubber Mallet, Three-Dimensional Compression Apparatus

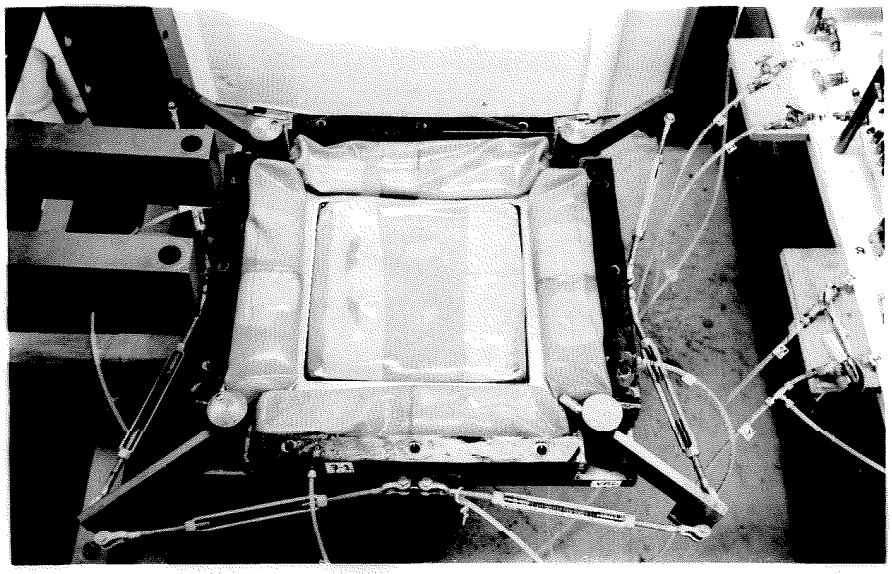

Figure 6.14 Compression Chamber Prepared for Sample, Three-Dimensional Compression Apparatus

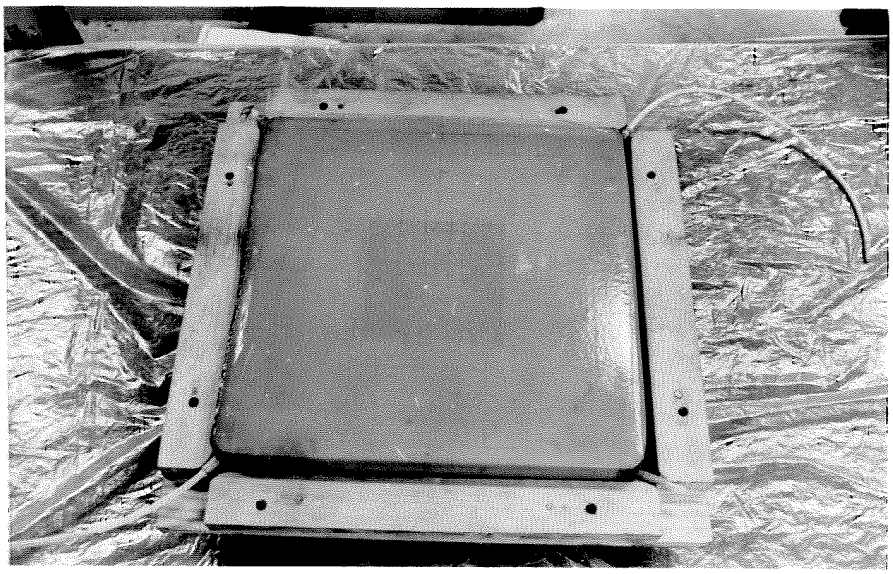

Figure 6.15 Formed Test Specimen under Vacuum, Three-Dimensional Compression Apparatus

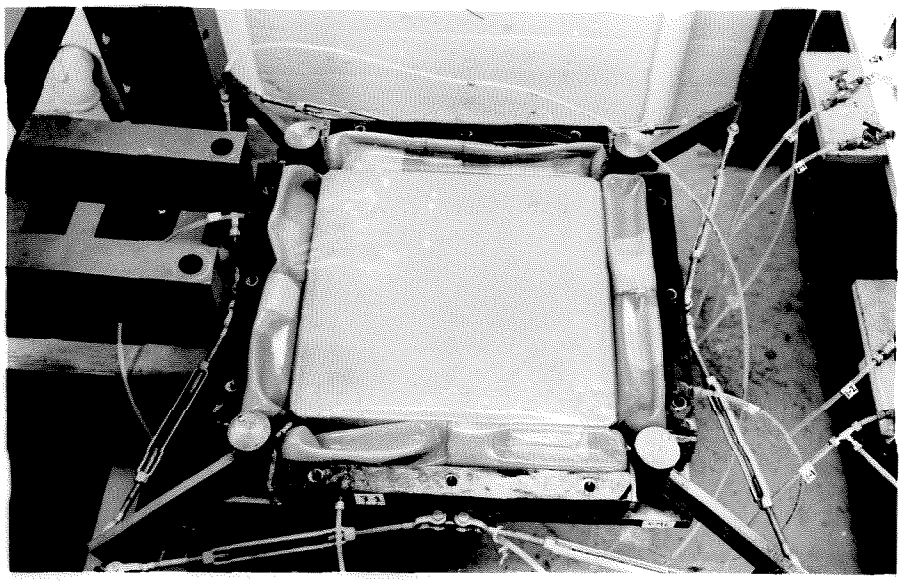

Figure 6.16 Test Specimen in Place within Compression Chamber, Three-Dimensional Compression Apparatus

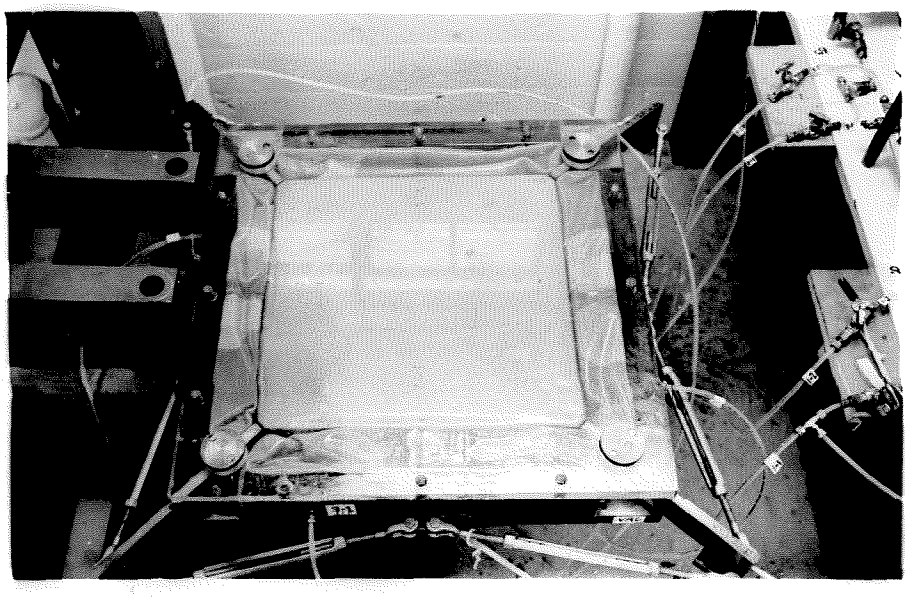

Figure 6.17 Lucite Cover Plate Installed on Compression Chamber, Three-Dimensional Compression Apparatus

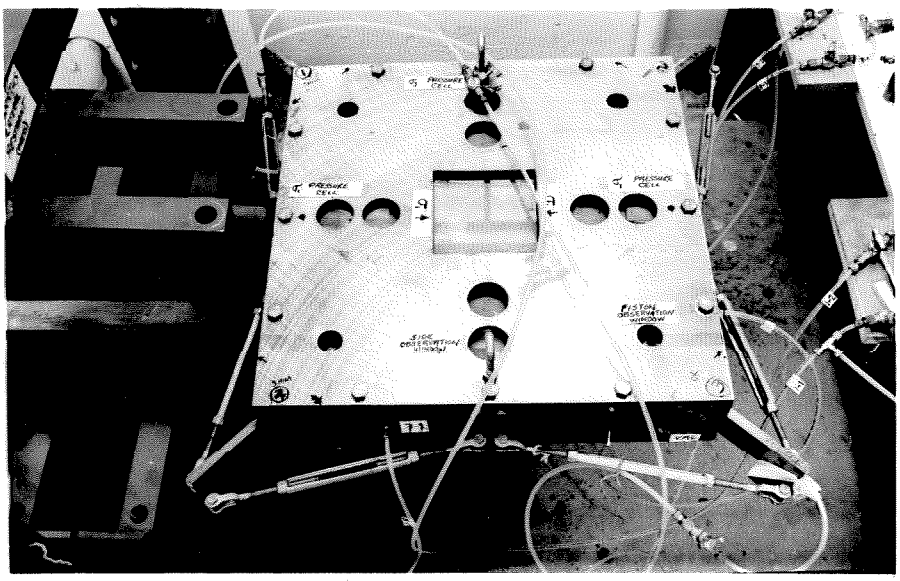

Figure 6.18 Steel Cover Plate Bolted to Compression Chamber, Three-Dimensional Compression Apparatus

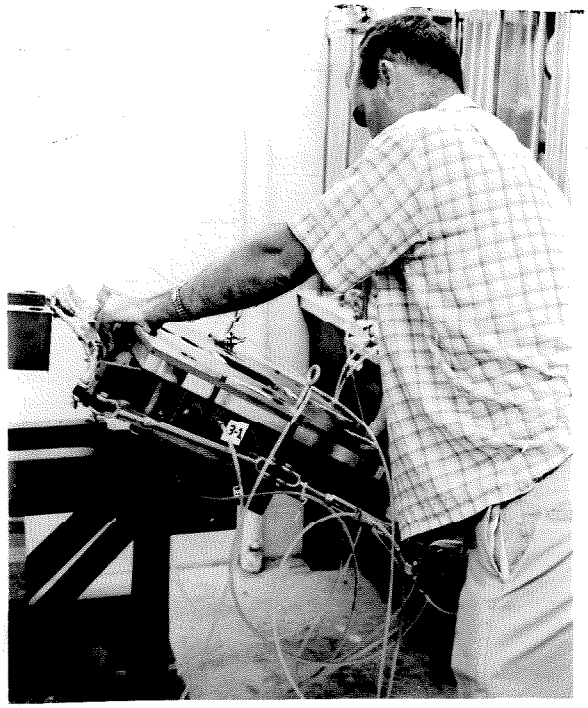

Figure 6.19 Rotation of Compression Chamber to Vertical Position, Three-Dimensional Compression Apparatus

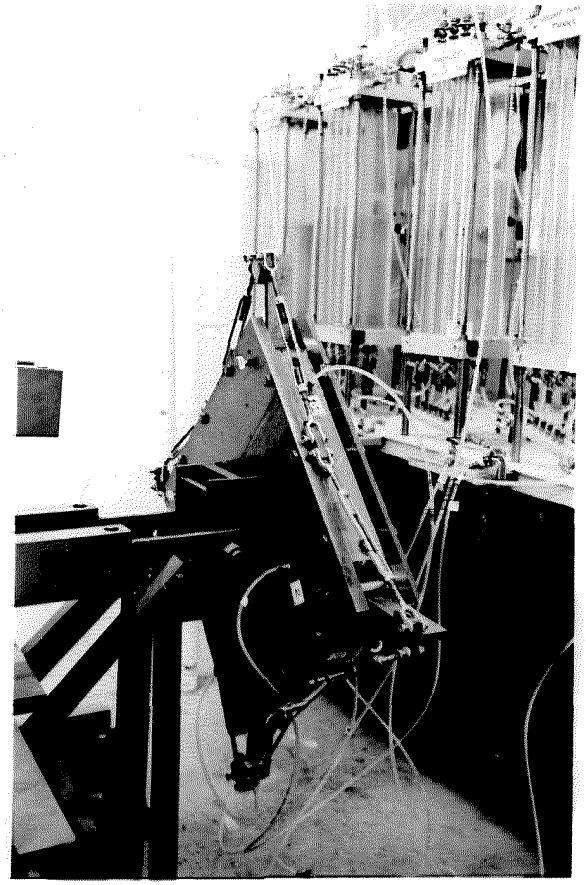

Figure 6.20 Compression Chamber in Saturation Position, Three-Dimensional Compression Apparatus

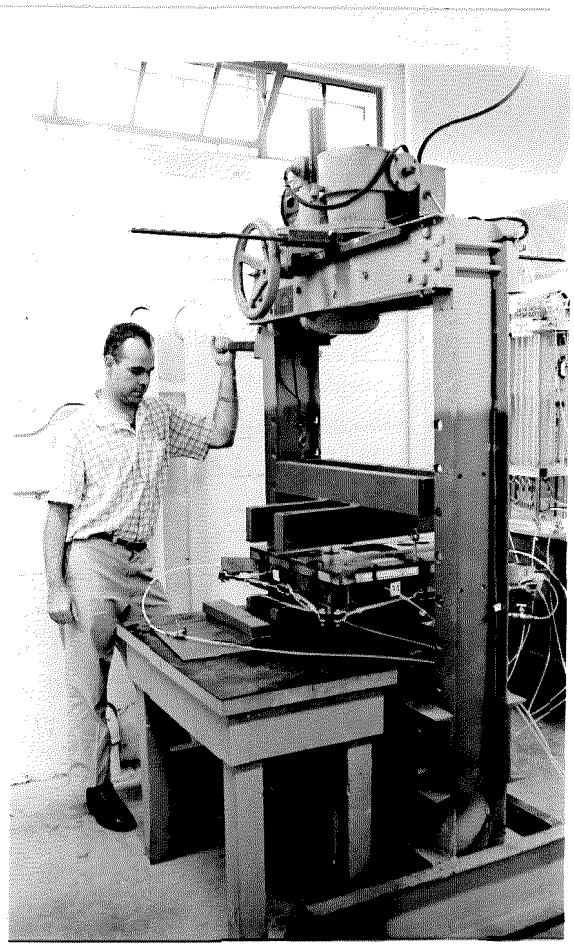

Figure 6.21 Lowering Top Half of Press Frame to Rest on Compression Chamber, Three-Dimensional Compression Apparatus

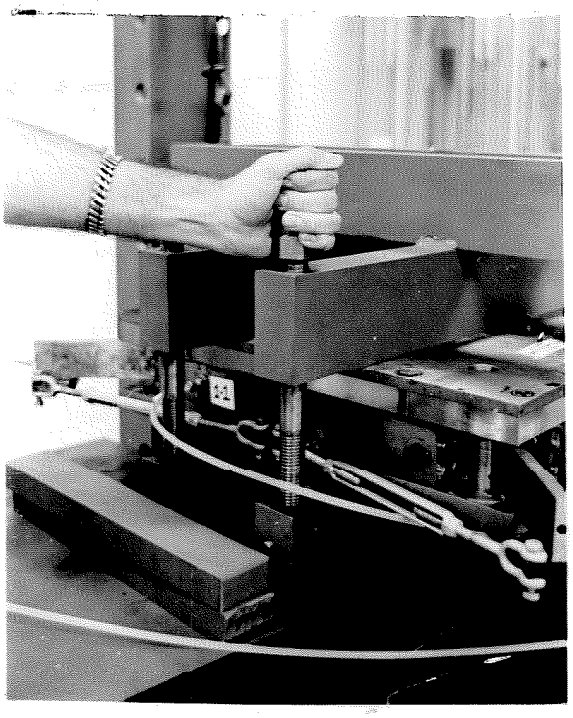

Figure 6.22 Bolting the Press Frame, Three-Dimensional Compression Apparatus

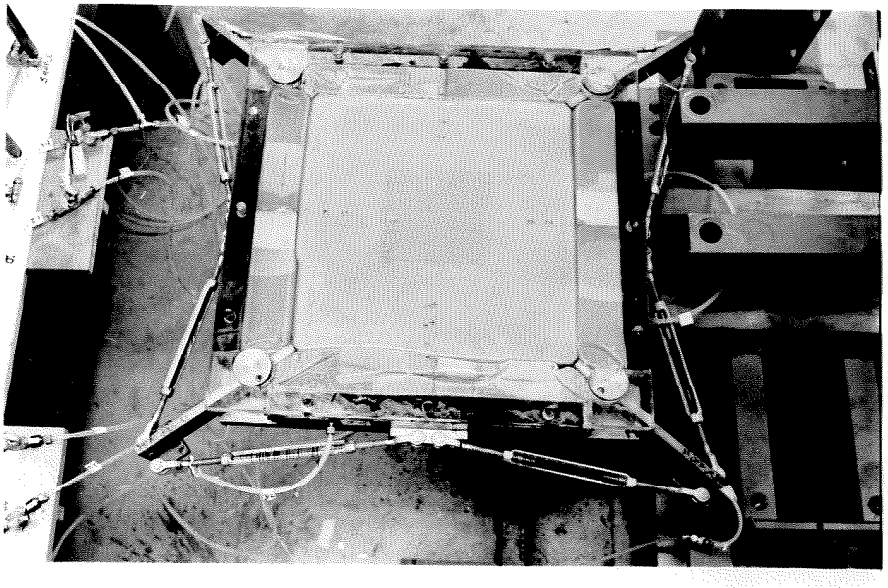

Figure 6.23 Local Failure of Three-Dimensional Compression Test Sample No. 10

7. RESULTS OF LABORATORY EXPERIMENTS

7.1 PRELIMINARY TESTS AND DESCRIPTION OF SAND

The granular material used in both the spherical and three-dimensional compression stress-strain experiments was Ottawa sand composed chiefly of subangular and subrounded quartz particles.

7.11 GRAIN SIZE AND SHAPE

A photograph of representative Ottawa sand grains used in the laboratory investigations is given in Figure 7.1.

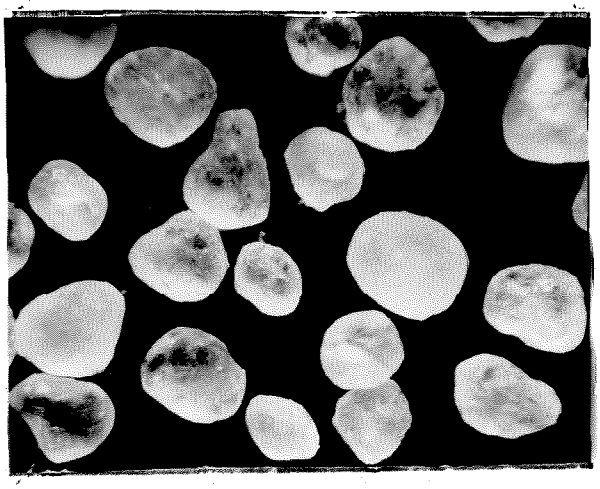

Figure 7.1 Representative Ottawa Sand Grains

A mechanical analysis was performed using standard square mesh sieves, and the results of five separate tests are shown in Figure 7.2. The effective diameters fell between 0.3 and 1.0 mm which appeared to be in agreement with the direct observation mentioned above. According to the Unified System of Classification, and based upon the grain size distribution curve, the material was classified as a fine to medium

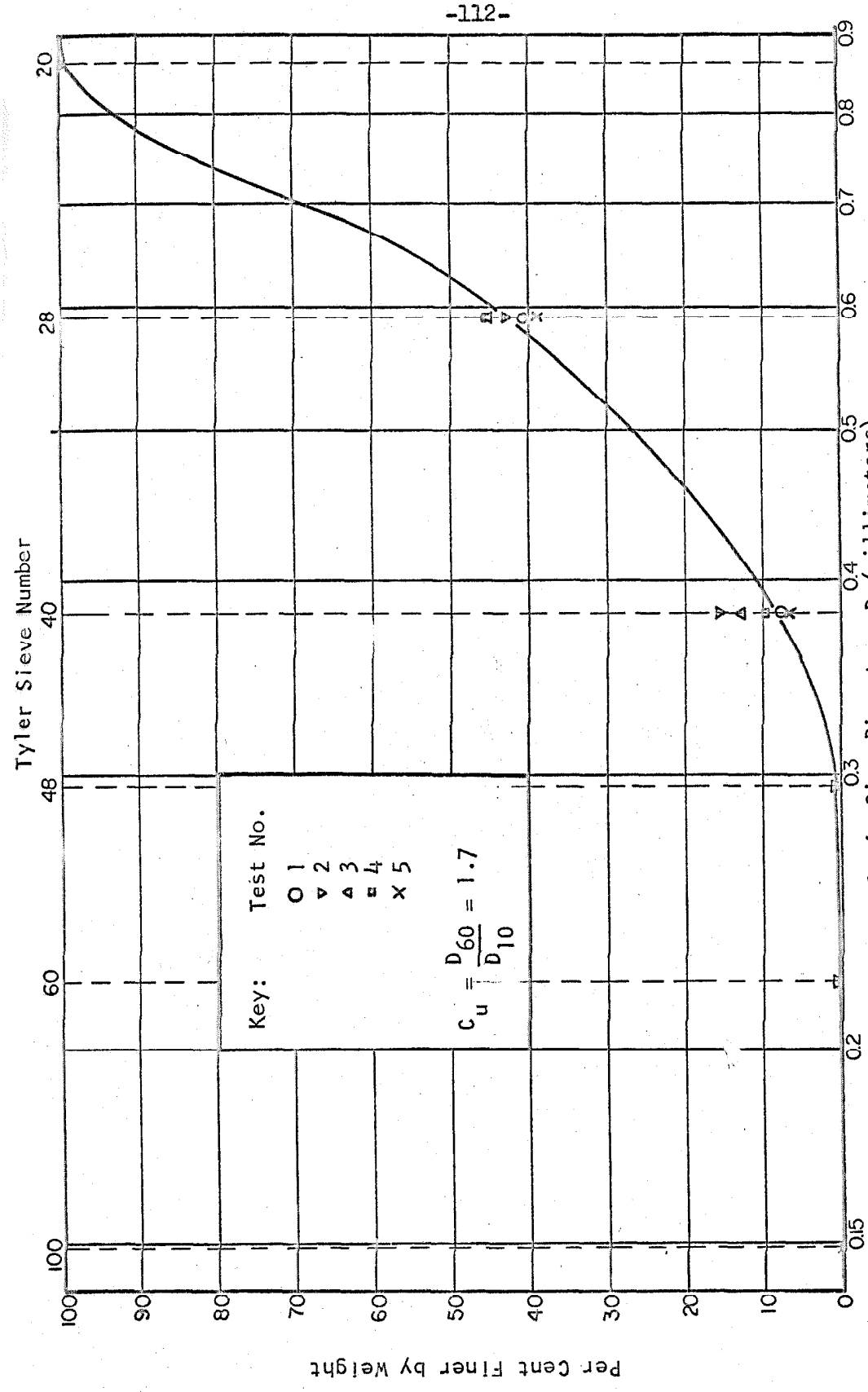

Figure 7.2 Grain Size Distribution of Ottawa Sand Determined by Use of Square Mesh Sieves.

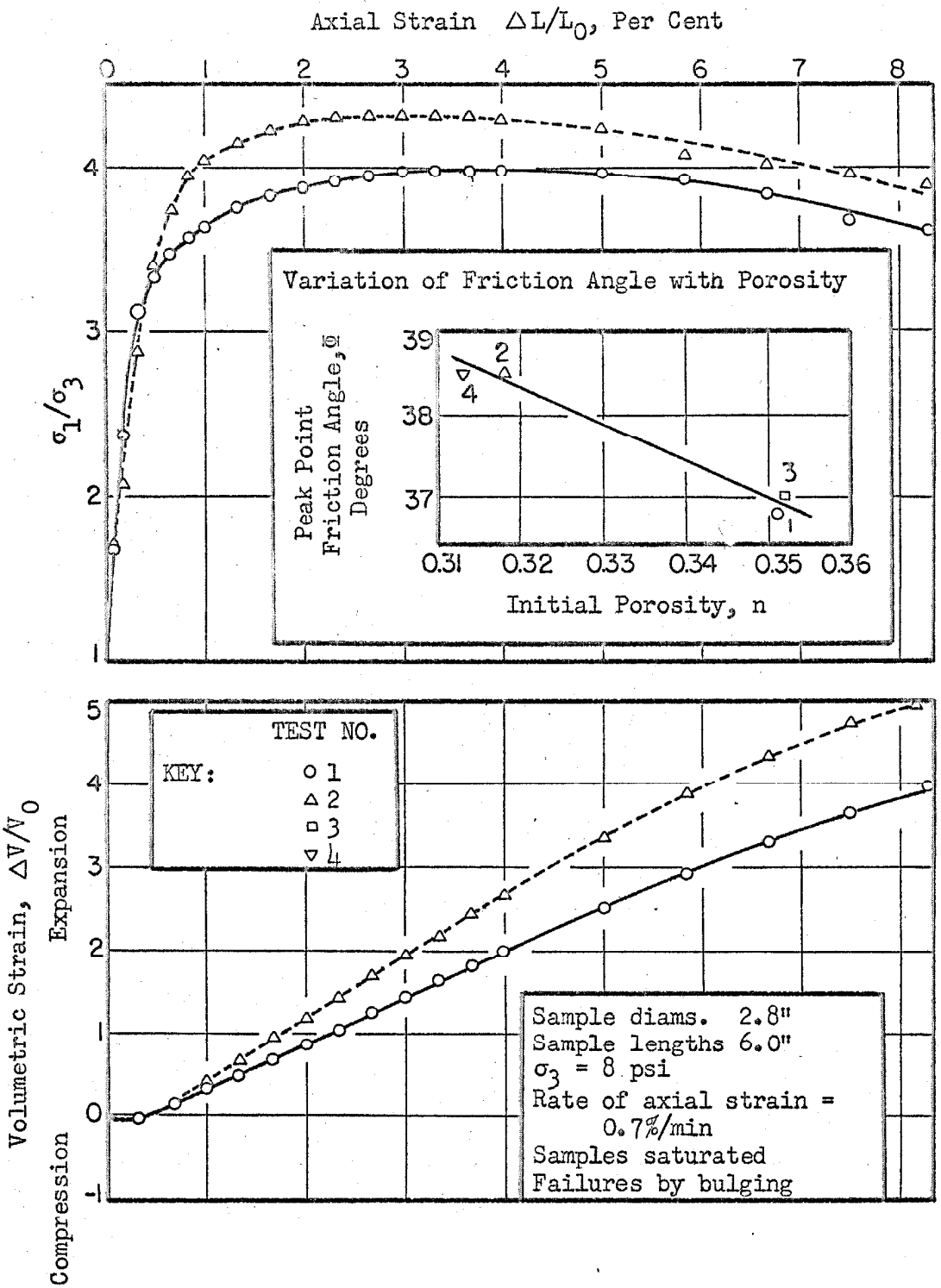

Figure 7.3 Standard Triaxial Compression Results, Constant σ_3--Tests Fully Drained

sand of uniform gradation. Hazen's uniformity coefficient $C_u(D_{60}/D_{10})$ was 1.7, and the effective size D_{10} was 0.4 mm.

7.12 SPECIFIC GRAVITY OF SOLIDS

Two specific gravity tests were performed, each on approximately 200 gm of representative material, utilizing a volumetric (water) displacement method. The results were 2.64 and 2.66. A specific gravity of 2.65 was assumed throughout the remainder of the test program.

7.13 DENSITY, VOID RATIO AND POROSITY

Density tests were performed on representative samples of oven dry sand utilizing a steel unit weight cylinder of about 0.1 cu ft in volume. The highest dry density obtained by vibration of the bucket with a rubber mallet was 110 lb/cu ft and was indicative of maximun densities practically obtainable in the three-dimensional compression apparatus. The lowest dry density obtained by careful placement of dry sand without impact or vibration was 95 lb/cu ft. The corresponding values of porosity were 0.34 and 0.43 respectively.

7.14 PRELIMINARY STRENGTH TESTS

The angle of repose determined by pouring sand into a large pan was approximately 30°. Several direct shear tests were performed at a shearing displacement of 0.05 in. per min on cylindrical samples of dry sand 2.41 in. in diam and 1 in. in height. Absolute porosities and normal displacements were not measured. Peak point friction angles obtained for normal pressures ranging from 11 to 55 psi were from 25° for the loosest test condition to 33° for the most dense test condition.

Corresponding peak point shearing displacements were from 0.12 in. (5.0%) to 0.03 (1.3%) and the ultimate friction angle was on the order of 24° for all samples.

Four drained triaxial compression tests were performed on saturated cylindrical samples of sand using standard equipment. Variations in initial density were obtained by compaction with a 2-in. diam steel plunger. Detailed results for two tests are given by Figure 7.3 as is normal--where a plot of initial porosity versus peak point friction angle for all tests is also presented. For an initial porosity of 0.35 and a constant lateral pressure of 8 psi, the peak point friction angle was 37° and occurred at approximately 4% axial strain and 2% volumetric strain.

7.2 STRESS-STRAIN EXPERIMENTS, SPHERICAL COMPRESSION APPARATUS

Six spherical compression tests were attempted, the first three of which failed due to apparatus malfunctions. A brief resume of the entire program is followed by the presentation of experimental logs and test results for Experiments 4, 5 and 6. Complete data and example calculations of test results for Experiment No. 6 are given in Appendixes A5 and A6 respectively. Test results were corrected for the effects of rubber penetration, Appendix A2.1; volume changes occurring over long periods of time were neglected.

7.21 RESUME OF LABORATORY PROGRAM

Experiment No. 1.--Leakage occurred in the volume measurement system at an undetermined location within the compression chamber. The test failed to produce useful data.

Experiment No. 2.--The vacuum pump failed during the saturation period and the sample was seriously distorted due to lack of confinement. The test was aborted.

Experiment No. 3.--Once again leakage occurred in the volume measurement system at an undetermined location within the compression chamber. The rate of flow was slight, but varied in time. The test was discontinued.

Experiment No. 4.--Difficulties were encountered early during this experiment; however, these were later corrected and useful data were obtained. A pattern for subsequent work was established. The final porosity of this test sample was 0.37.

Experiment No. 5.--This experiment was performed successfully on the least dense material, and the final porosity was 0.39.

Experiment No. 6.--This experiment was performed successfully on the most dense material; the final porosity was 0.34.

7.22 EXPERIMENTAL LOGS AND TEST RESULTS

Experimental logs, Tables 7.1, 7.2 and 7.3, give the test series, stress history and comments for each experiment. A new test series indicates a considerable lapse of time or a change in the loading program.

The test results are given graphically, Figures 7.4 through 7.16. Plots giving porosity n as a function of applied spherical stress σ for the entire experiment are followed by a plot giving volumetric compressibility $-\Delta n/\Delta\sigma$ as a function of applied spherical stress σ for final cycles of stress.

Table 7.1 Log of Experiment No. 4

Test Series	Stress History* and Comments
4-1	5(83), 10(26), 15(13), 20(15), 30(9-840)[1], 40(22), 50(53), 58.5(60)[2], 50(5), 40(5), 30(5), 20(17), 15(5), 10(5), 5(162)[3]: Initially used 25 cc burette and 100 psi air pressure gage. 1. Installed 10 cc burette. Bur. vol. change, 1.6 cc. 2. Noted deformation increase upon starting vibrator above lab, noted some air in top drain line. 3. Placed vibration pads under compression apparatus, applied 4 psi vacuum to top drain line and allowed water to percolate through sample.
4-2	10(12), 15(18), 20(40), 25(30), 30(23), 35(33-810)[4], 40(39), 45(11), 50(17), 55(10), 50, 45, 40, 35, 30, 25, 20, 15, 10, 5(5), 1(4): 4. Bur. vol. change, 2.98 cc. Rapid increase in rigidity with pressure indicated a logarithmic pressure increment practical. Recorded vol. changes in time indicated that at 2 min, 88-100% of the asymptotic values were obtained.
4-3	2, 3, 4.5, 6.8, 10.1, 15.2, 22.8, 34.2, 51.3, 34.2, 22.8, 15.2, 10.1, 6.8, 4.5, 3, 2, 1, 2, 3, 4.5(2-287)[5]: 5. Bur. vol. change, 1.62 cc.
4-4	3, 2, 1.3, 2, 3, 4.5, 6.8, 10.1(5), 15.2, 22.8, 34.2, 22.8, 15.2, 10.1, 6.8, 4.5, 3, 2, 1.3, 2, 3, 4.5(2-990)[6]: 6. Bur. vol. change, 0.53 cc. Installed air pres. gage, 60 psi

*Stress history is given in terms of applied pressures in psi followed by a number in parentheses indicating the time of load application in minutes. The first parenthetical number indicates the time interval elapsed to the burette reading--which was used in the calculation and plotting of test results; the second number indicates the long term load interval (usually overnight). No( )=2min.

Table 7.1 continued

Test Series	Stress History and Comments
4-5	3, 2, 1.3, 2, 3, 4.5, 6.8, 10.1, 15.222.8, 34.2, 51.3[7], 76.9, 51.3, 34.2, 22.8, 15.2, 10.1, 6.8, 4.5, 3, 2, 1.3, 2, 3, 4.5(2-1380)[8]: 7. Noticed air bubble in tcp drain line. 8. Bur. vol. change, 0.82 cc. Applied vacuum of 4 psi and allowed water tc percolate through sample.
4-6	3, 2, 1.3, 2, 3, 4.5, 5.8, 10.1, 15.2, 22.8, 34.2, 51.3, 76.9[9]: 9. Air line disconnected at 88 psi upon increasing pressure. Sample saved serious distortion by sealing sample drainage; but load sequence was interrupted. Max. pressure of 76.9 used in future work.
4-7	1.3, 2, 3, 4.5, 3, 2, 1.3, 2, 3, 4.5, 6.8, 10.1, 15.2, 22.8, 34.2, 51.3, 76.9, 51.3, 34.2, 22.8, 15.2, 10.1, 6.8, 4.5, 3, 2, 1.3, 2, 3, 4.5(2-4020)[10]: 10. Bur. vol. change, 9.63 cc
4-8	3, 2, 1.3, 2, 3, 4.5, 6.8, 10.1, 6.8, 4.5, 3, 2, 1.3, 2, 3, 4.5, 6.8, 10.1, 15.2, 10.1, 6.8, 4.5, 3, 2, 1.3, 2, 3, 4.5, 6.8, 10.1, 15.2, 22.8, 15.2, 10.1, 6.8, 4.5, 3, 2, 1.3, 2, 3, 4.5, 6.8, 10.1, 15.2, 22.8, 34.2, 22.8, 15.2, 10.1, 6.8, 4.5, 3, 2, 1.3, 2, 3, 4.5, 6.8, 10.1, 15.2, 22.8, 34.2, 51.3, 34.2, 22.8, 15.2, 10.1, 6.8, 4.5, 3, 2, 1.3, 2, 3, 4.5, 6.8, 10.1, 15.2, 22.8, 34.2, 51.3, 76.9, 51.3, 34.2, 22.8, 15.2, 10.1, 6.8, 4.5, 3, 2, 1.3, 2, 3, 4.5

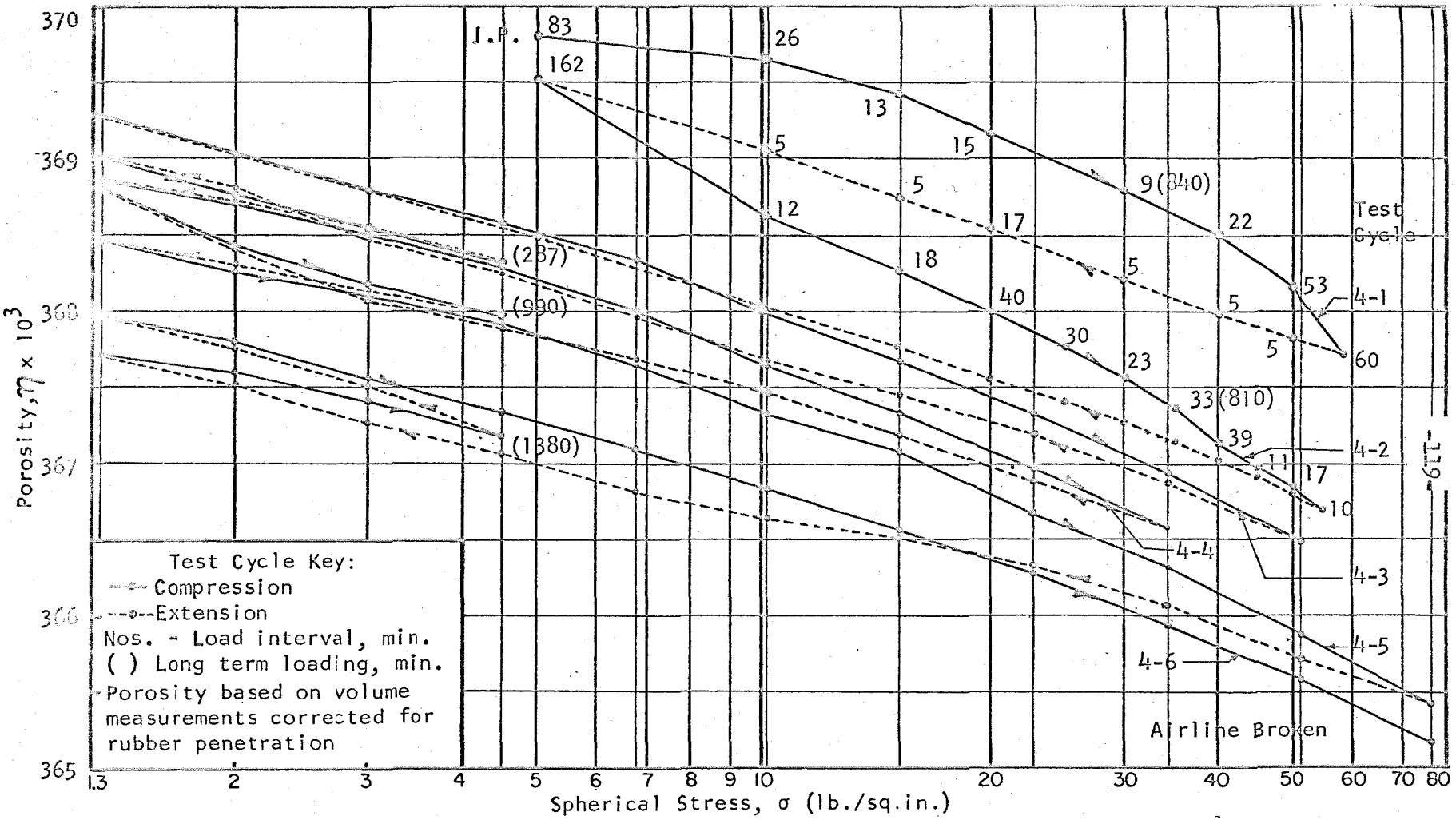

Figure 7.4 Porosity as a Function of Applied Spherical Stress
Spherical Compression Test Nos. 4-1 through 4-6

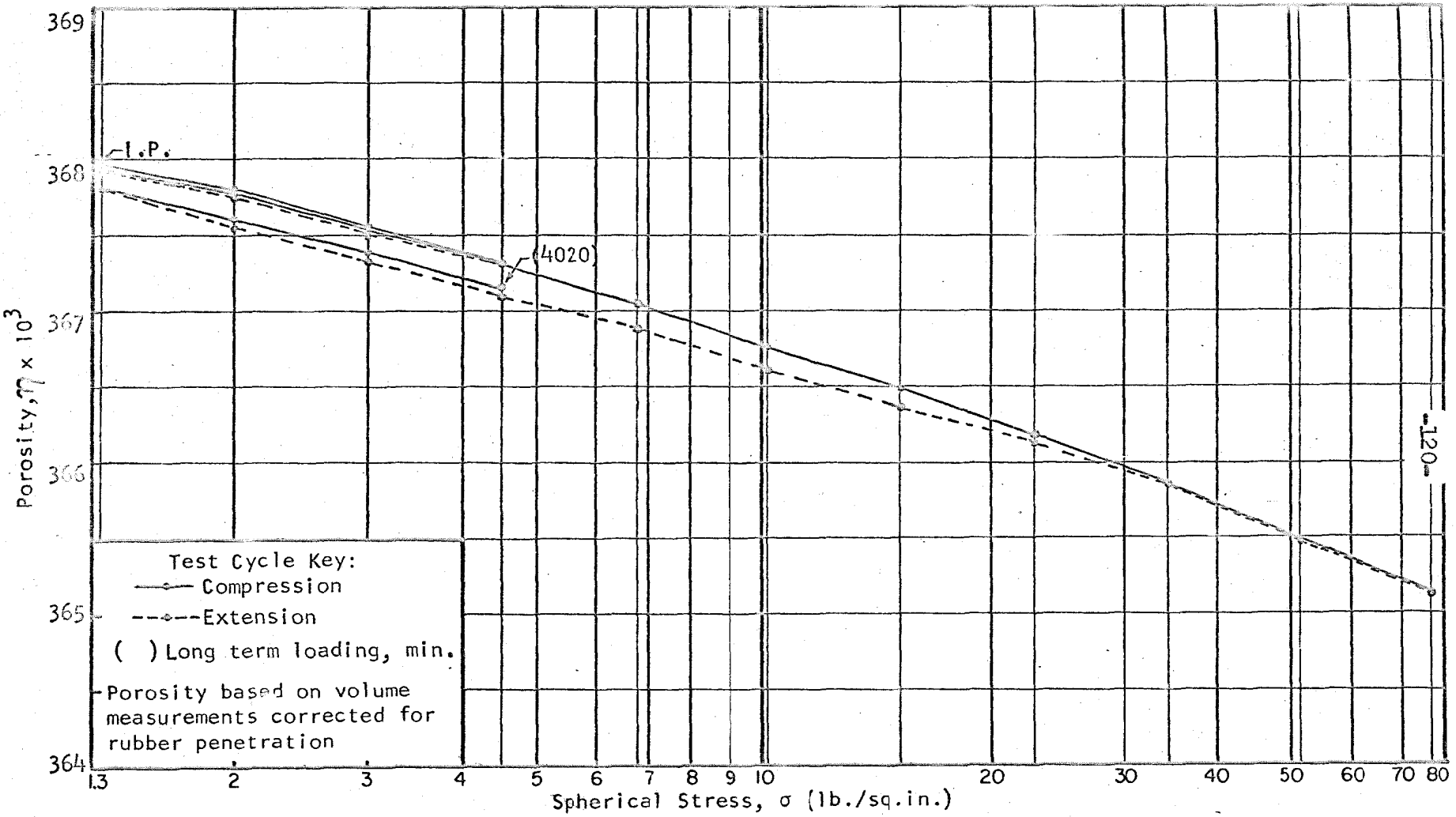

Figure 7.5 Porosity as a Function of Applied Spherical Stress
Spherical Compression Test Nos. 4-7

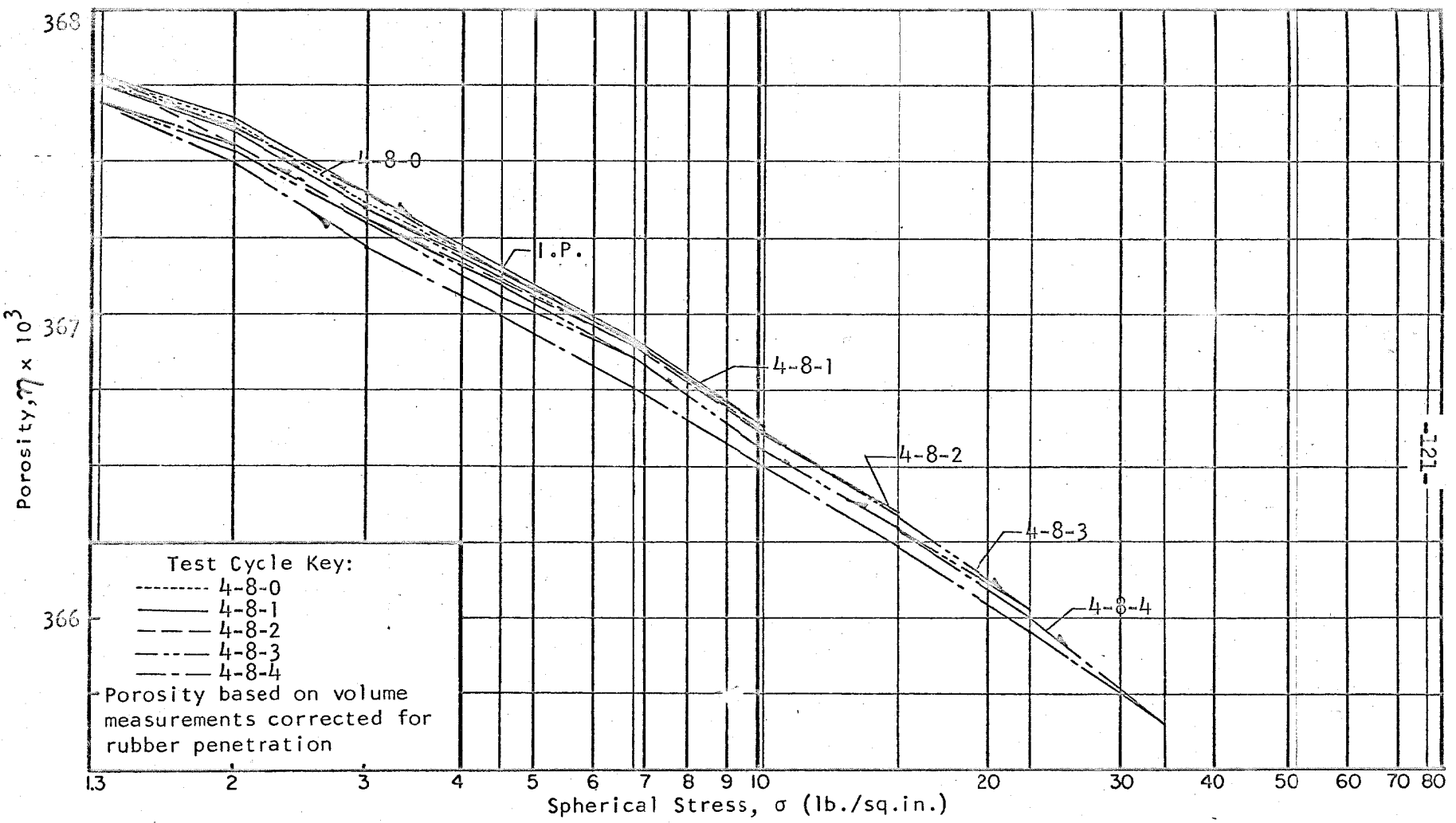

Figure 7.6 Porosity as a Function of Applied Spherical Stress
Spherical Compression Test Nos. 4-8-0 through 4-8-4

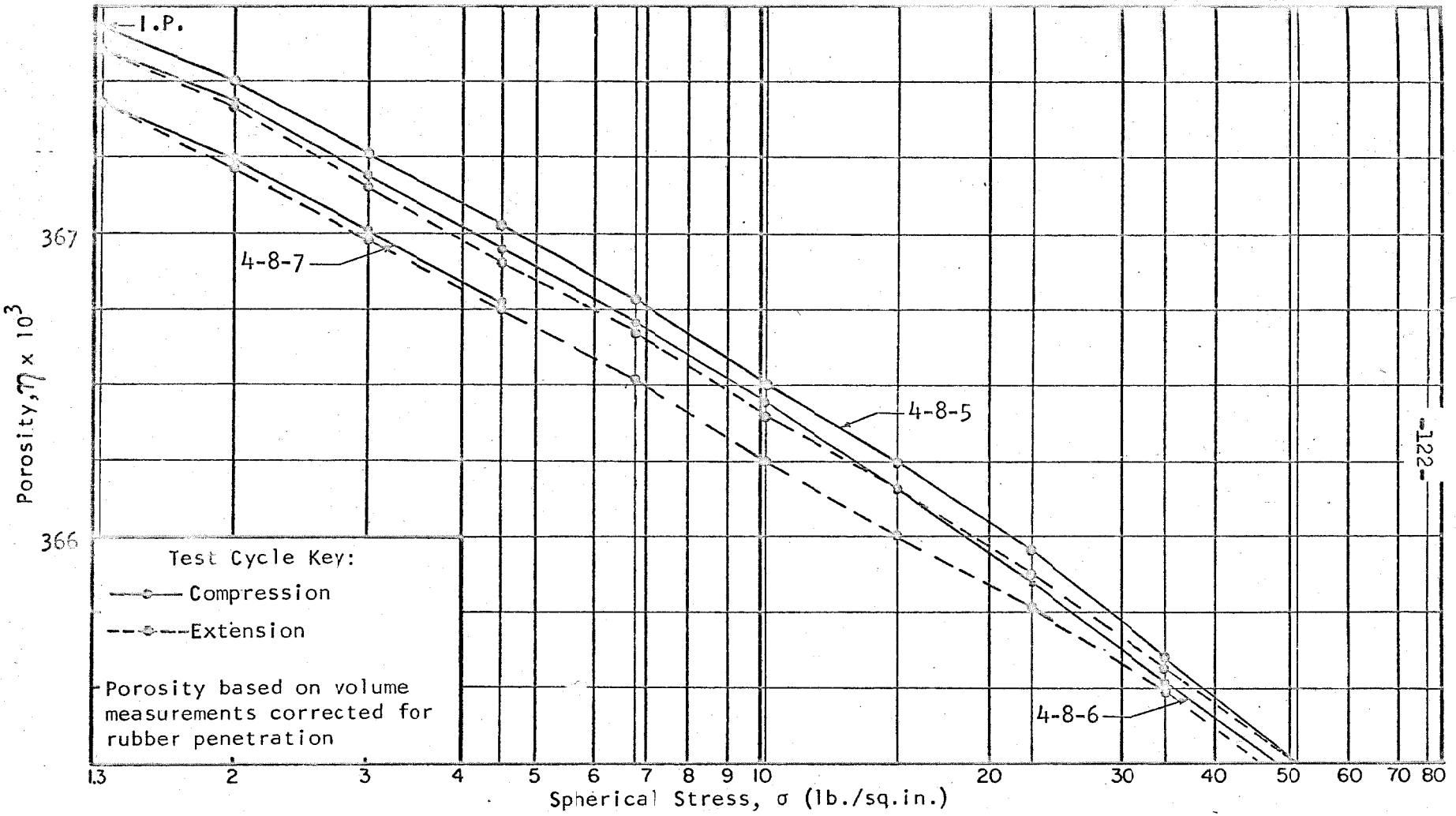

Figure 7.7 Porosity as a Function of Applied Spherical Stress
Spherical Compression Test Nos. 4-8-5 through 4-8-7

Test Cycle Key: ○ ● 4-8-5
ⴰ ⴰ 4-8-6
⊙ 4-8-7

Clear Circles - Compression
Solid Circles - Extension
Compressibility based on volume measurements corrected for rubber penetration.

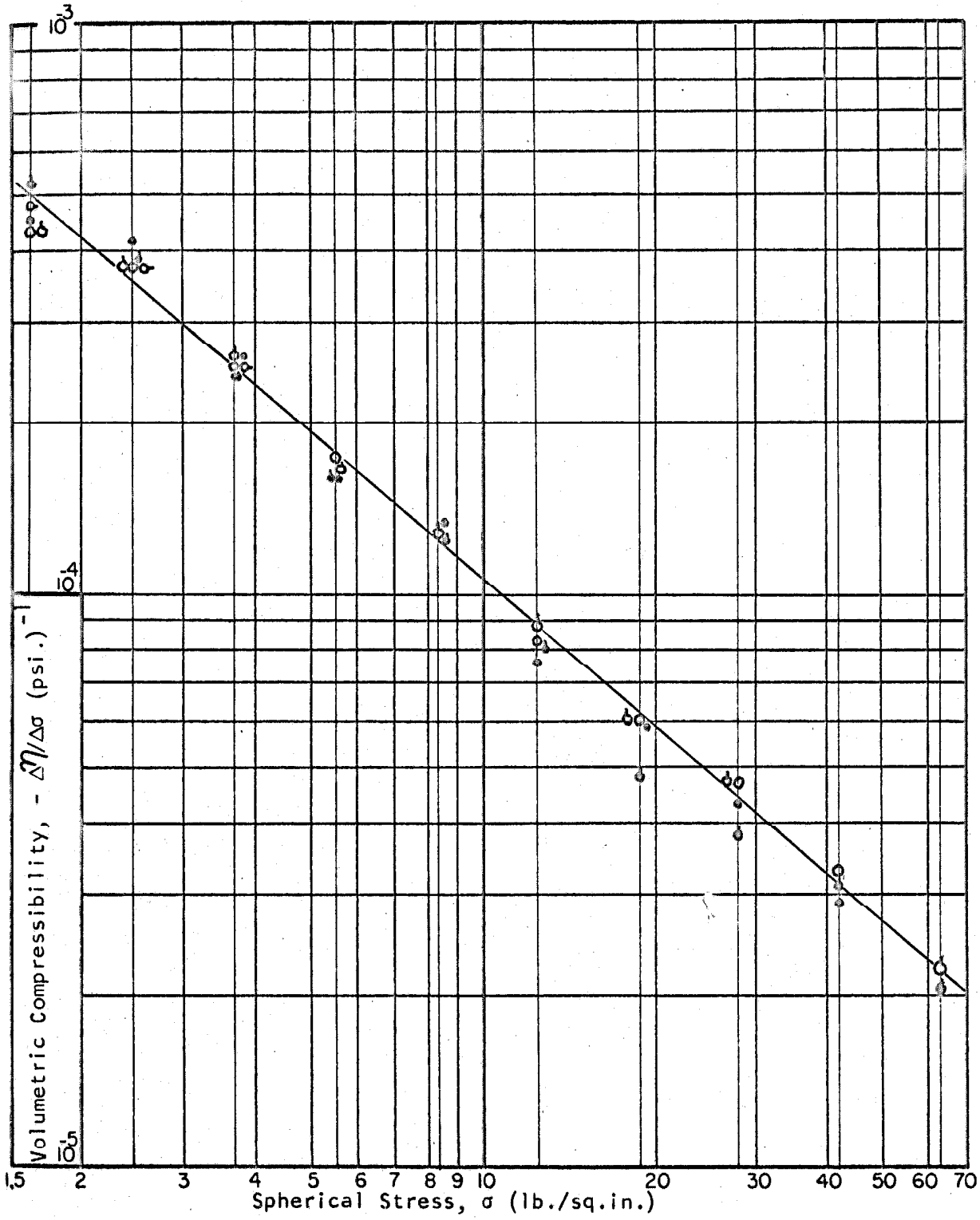

Figure 7.8 Volumetric Compressibility as a Function of Applied Spherical Stress.

Spherical Compression Test Nos. 4-8-5 through 4-8-7

Table 7.2 Log of Experiment No. 5

Test Series	Stress History (see footnote page 117) and Comments
5-1-0	4.5, 3, 2, 1.3
5-1-1	2, 3, 4.5, 6.8, 10.1, 6.8, 4.5, 3, 2, 1.3
5-1-2	2, 3, 4.5, 6.8, 10.1, 15.2, 10.1, 6.8, 4.5, 3, 2, 1.3
5-1-3	2, 3, 4.5, 6.8, 10.1, 15.2, 22.8, 15.2, 10.1, 6.8, 4.5, 3, 2, 1.3
5-1-4	2, 3, 4.5, 6.8, 10.1, 15.2, 22.8, 34.2, 22.8, 15.2, 10.1, 6.8, 4.5, 3, 2, 1.3
5-1-5	2, 3, 4.5, 6.8, 10.1, 15.2, 22.8, 34.2, 51.3, 34.2,22.8, 15.2, 10.1, 6.8, 4.5, 3, 2, 1.3
5-1-6	2, 3, 4.5, 6.8, 10.1, 15.2, 22.8, 34.2, 51.3, 34.2, 22.8, 15.2, 10.1, 6.8, 4.5(2-2520)[1]: 1. Bur. vol. change, 0.43 cc
5-2	3, 2, 1.3, 2, 3, 4.5, 6.8, 10.1, 15.2, 22.8, 34.2, 51.3, 76.9, 51.3, 34.2, 22.8, 15.2, 22.8, 15.2, 22.8, 15.2, 22.8, 15.2, 22.8, 15.2, 22.8, 15.2(2-1020)[2]: 2. Bur.vol. change, 0.27 cc
5-3-0	10.1, 6.8, 4.5, 3, 2, 1.3
5-3-1	2, 3, 4.5, 6.8, 10.1, 15.2, 22.8, 34.2, 51.3, 76.9, 51.3, 34.2, 22.8, 15.2, 10.1, 6.8
5-3-2	10.1, 15.2, 22.8, 34.2, 51.3, 76.9, 51.3, 34.2, 22.8, 15.2, 10.1
5-3-3	15.2, 22.8, 34.2, 51.3, 76.9, 51.3, 34.2, 22.8, 15.2
5-3-4	22.8, 34.2, 51.3, 76.9, 51.3, 34.2, 22.8
5-3-5	34.2, 51.3, 76.9, 51.3, 34.2
5-3-6	51.3, 76.9, 51.3

Table 7.2 continued

Test Series	Stress History and Comments
5-3-7	76.9, 51.3, 34.2, 22.8, 15.2, 10.1, 6.8, 4.5, 3, 2, 1.3
5-3-8	2, 3, 4.5, 6.8, 10.1, 15.2, 22.8, 34.2, 51.3, 76.9, 51.3, 34.2, 22.8, 15.2, 10.1, 6.8, 4.5, 3, 2, 1.3
5-3-9	2, 3, 4.5$(2\text{-}1140)^3$:3. Bur. vol. change, 2.22 cc
5-4-0 through 5-4-15	3, 4.5, 6.8, 4.5, 6.8, 10.1, 6.8, 10.1, 15.2, 10.1, 15.2, 22.8, 15.2, 22.8, 34.2, 22.8, 34.2, 51.3, 34.2, 51.3, 76.9, 51.3, 76.9, 51.3, 34.2, 51.3, 34.2, 22.8, 34.2, 22.8, 15.2, 22.8, 15.2, 10.1, 15.2, 10.1, 6.8, 10.1, 6.8, 4.5, 6.8, 4.5, 3, 4.5, 3, 2, 1.3
5-4-16	2, 3, 4.5, 6.8, 10.1, 15.2, 22.8, 34.2, 51.3, 76.9, 51.3, 34.2, 22.8, 15.2, 10.1, 6.8, 4.5, 3, 2, 1.3
5-4-17	2, 3, 4.5, 6.8, 10.1, 15.2, 22.8, 34.2, 51.3, 76.9, 51.3, 34.2, 22.8, 15.2, 10.1, 6.8, 4.5$(2\text{-}2400)^4$: 4. Bur. vol. change, 1.85 cc

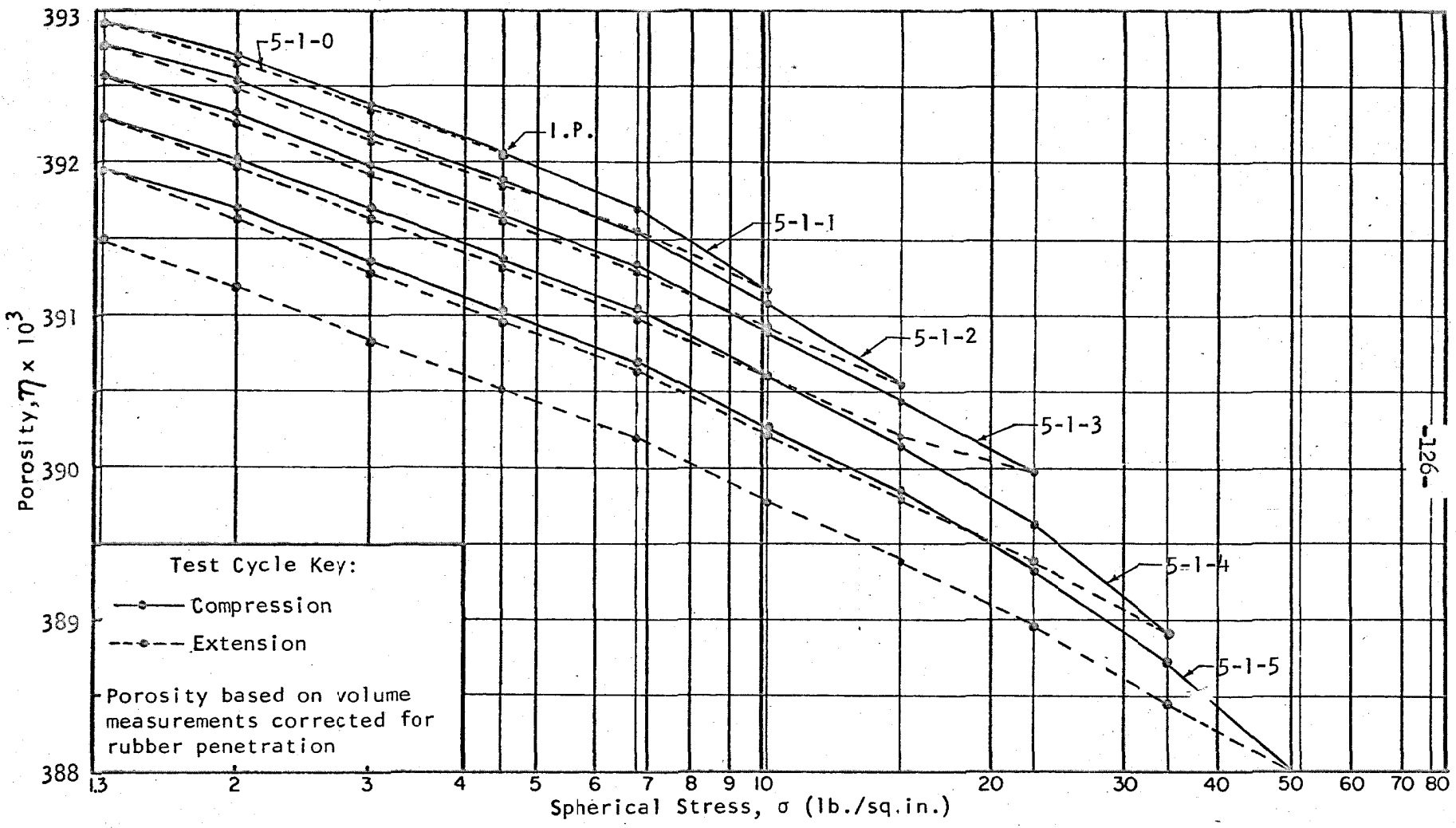

Figure 7.9 Porosity as a Function of Applied Spherical Stress
Spherical Compression Test Nos. 5-1-0 through 5-1-5

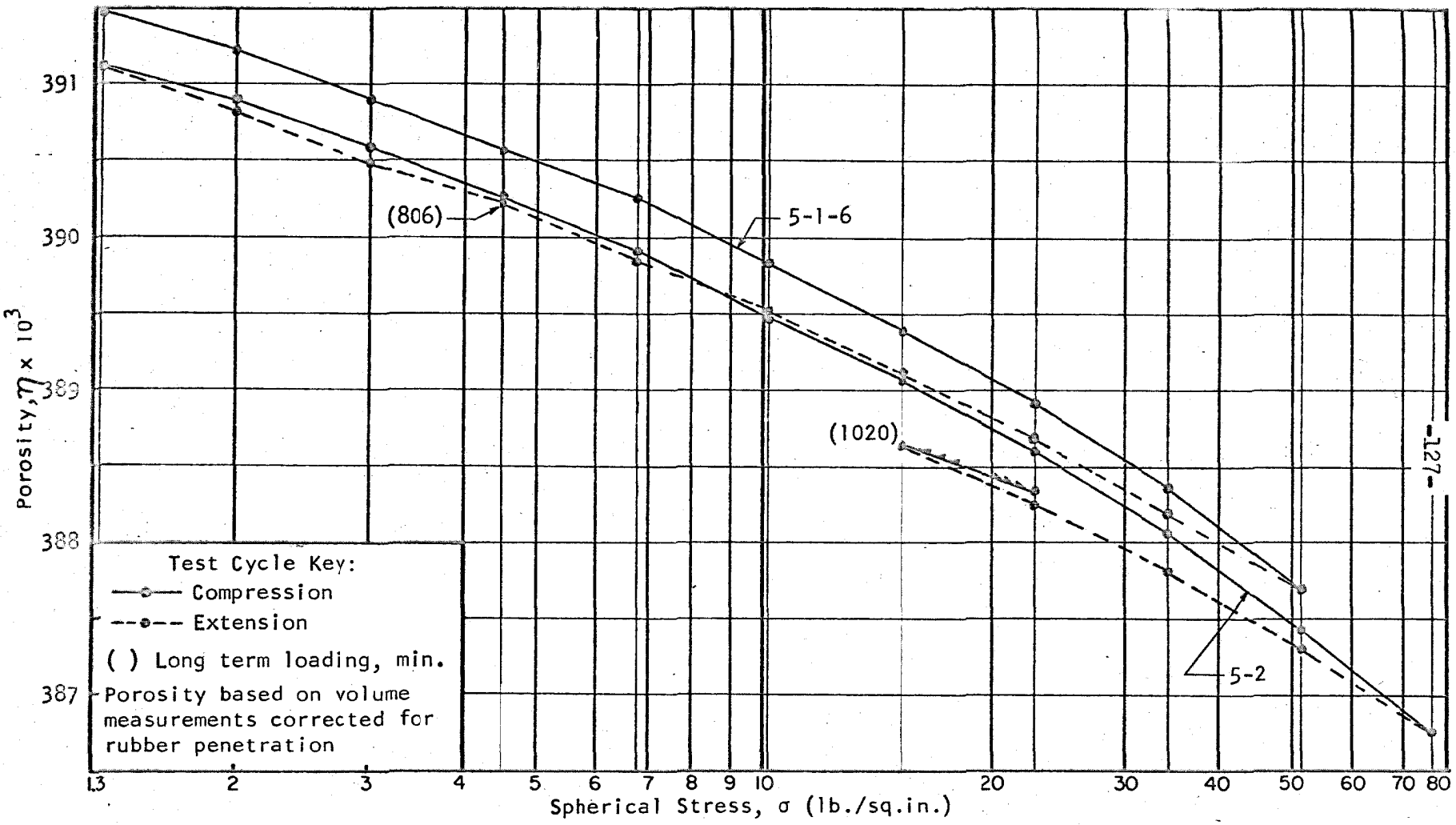

Figure 7.10 Porosity as a Function of Applied Spherical Stress
Spherical Compression Test Nos. 5-1-6 and 5-2

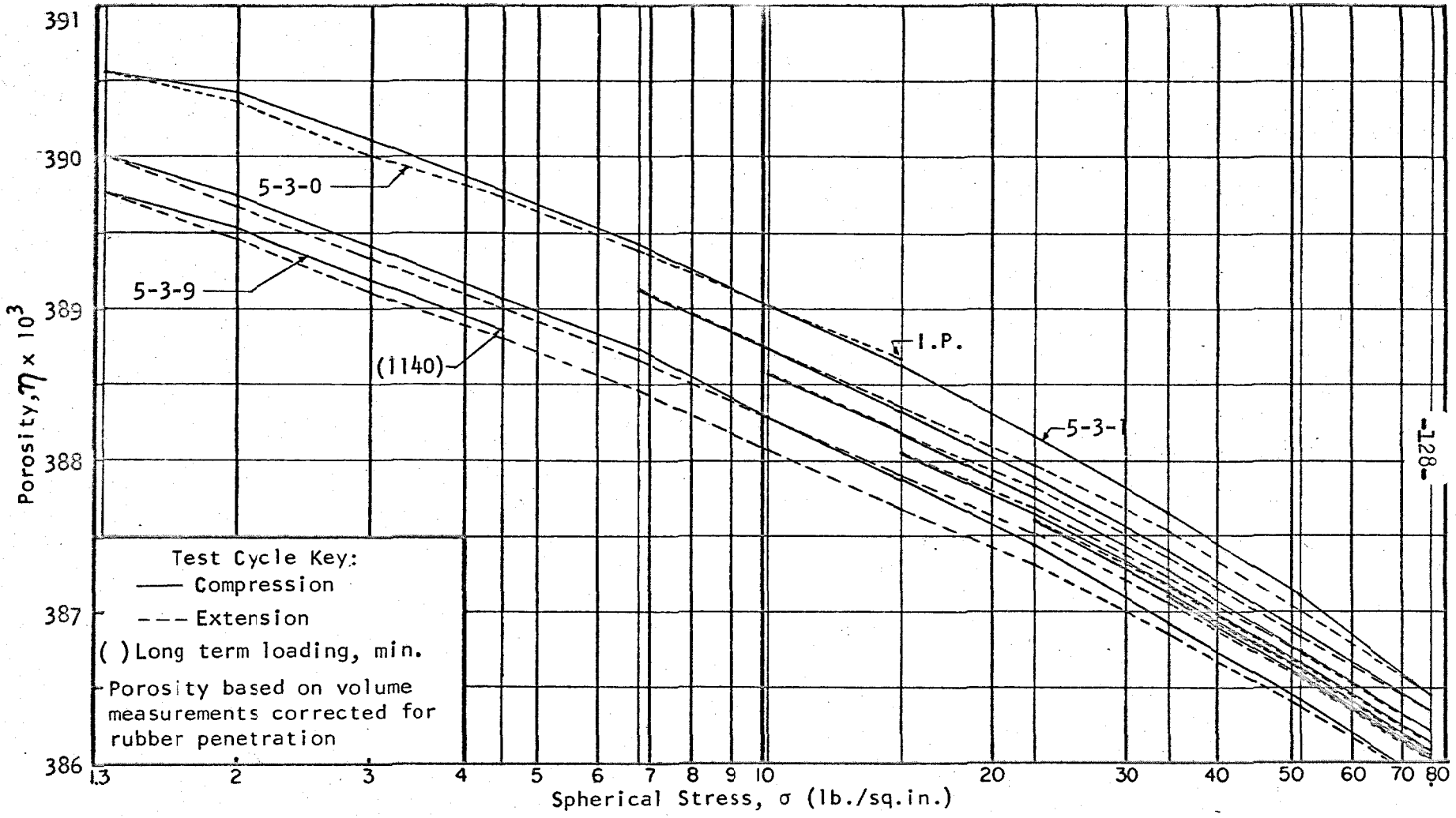

Figure 7.11 Porosity as a Function of Applied Spherical Stress
Spherical Compression Test Nos. 5-3-0 through 5-3-9

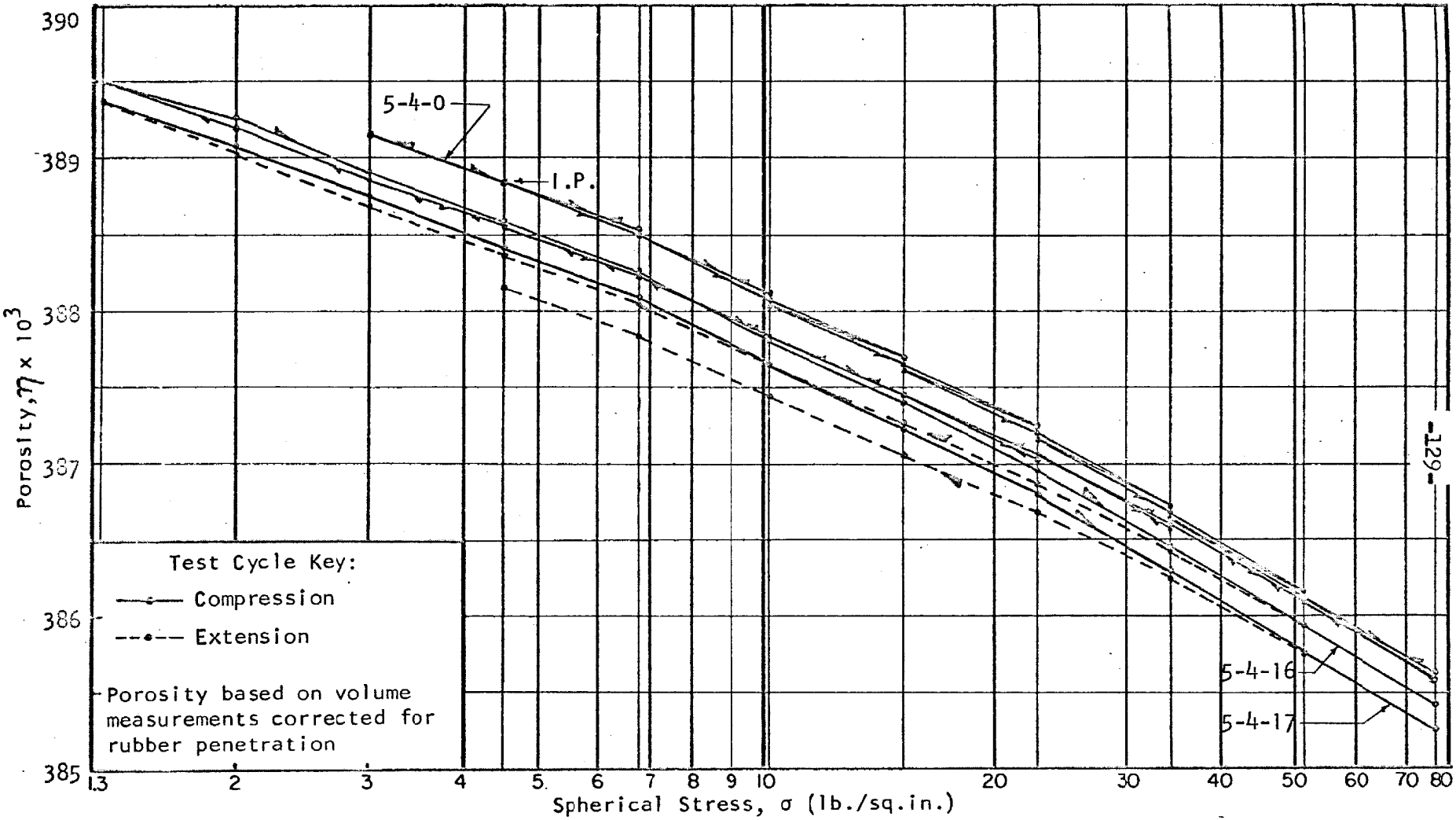

Figure 7.12 Porosity as a Function of Applied Spherical Stress
Spherical Compression Test Nos. 5-4-0 through 5-4-17

Test Cycle Key: ○ ● 5-4-16
δ ♦ 5-4-17

-130-

Clear Circles - Compression
Solid Circles - Extension
Compressibility based on volume measurements corrected for rubber penetration.

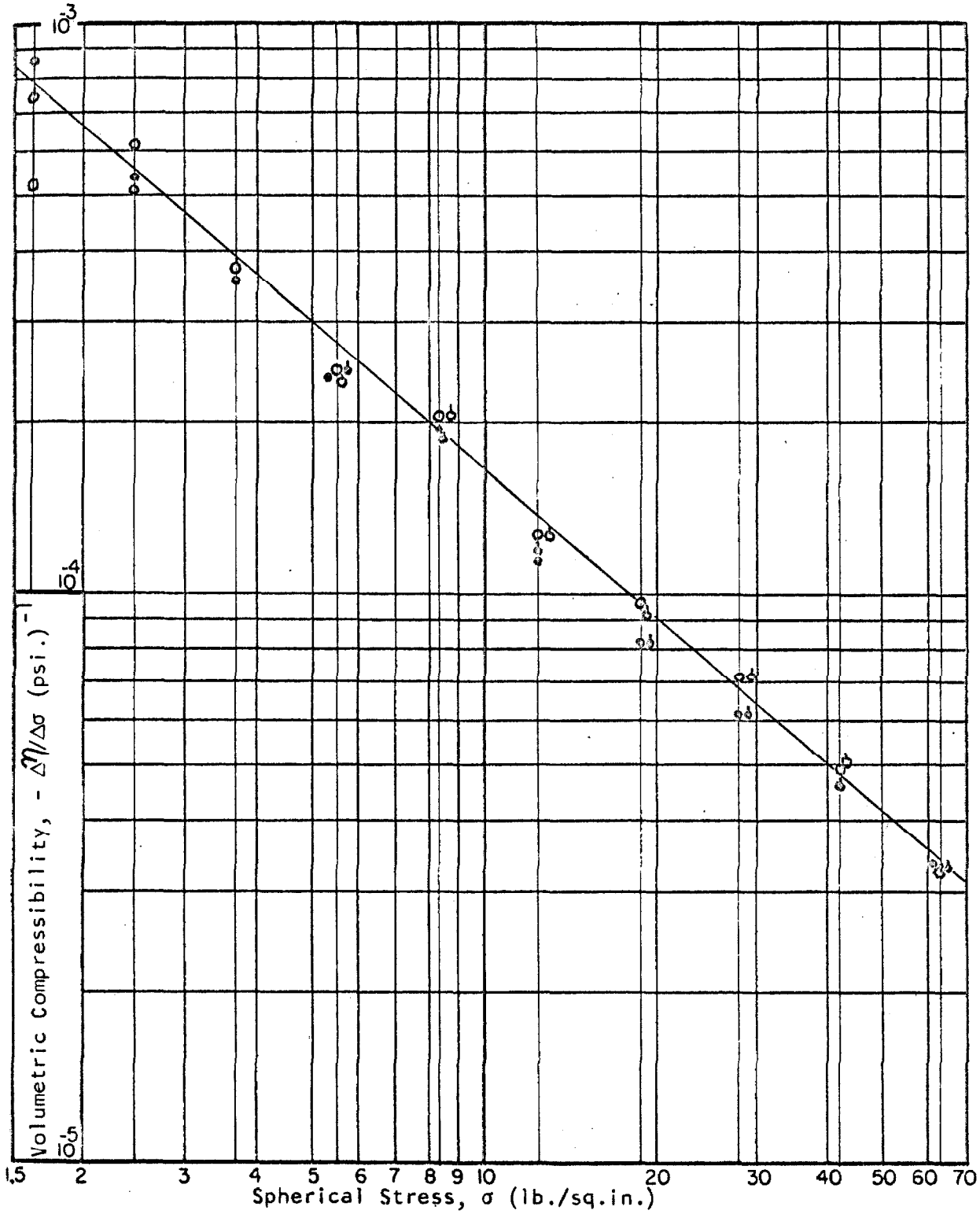

Figure 7.13 Volumetric Compressibility as a Function of Applied Spherical Stress.

Spherical Compression Test Nos. 5-4-16 and 5-4-17

Table 7.3 Log of Experiment No. 6

Test Series	Stress History (see footnote page 117) and Comments
6-1-0	4.5, 3, 2, 1.3
6-1-1	2, 3, 4.5, 6.8, 10.1, 15.2, 22.8, 34.2, 51.3, 76.9, 51.3, 34.2, 22.8, 15.2, 10.1, 6.8, 4.5, 3
6-1-2 through 6-1-15	4.5, 6.8, 4.5, 6.8, 10.1, 6.8, 10.1, 15.2, 10.1, 15.2, 22.8, 15.2, 22.8, 34.2, 22.8, 34.2, 51.3, 34.2, 51.3, 34.2, 51.3, 76.9, 51.3, 76.9, 51.3, 34.2, 51.3, 34.2, 22.8, 34.2, 22.8, 15.2, 22.8, 15.2, 10.1, 15.2, 10.1, 6.8, 10.1, 6.8, 4.5, 6.8, 4.5, 3, 2, 1.3
6-1-16	2, 3, 4.5, 6.8, 10.1, 15.2, 22.8, 34.2, 51.3, 76.9, 51.3, 34.2, 22.8, 15.2, 10.1, 6.8, 4.5, 3, 2, 1.3
6-1-17	2, 3, 4.5, 6.8, 10.1, 15.2, 22.8, 34.2, 76.9, 51.3, 34.2, 22.8, 15.2, 10.1, 6.8, 4.5, 3
6-1-18	4.5

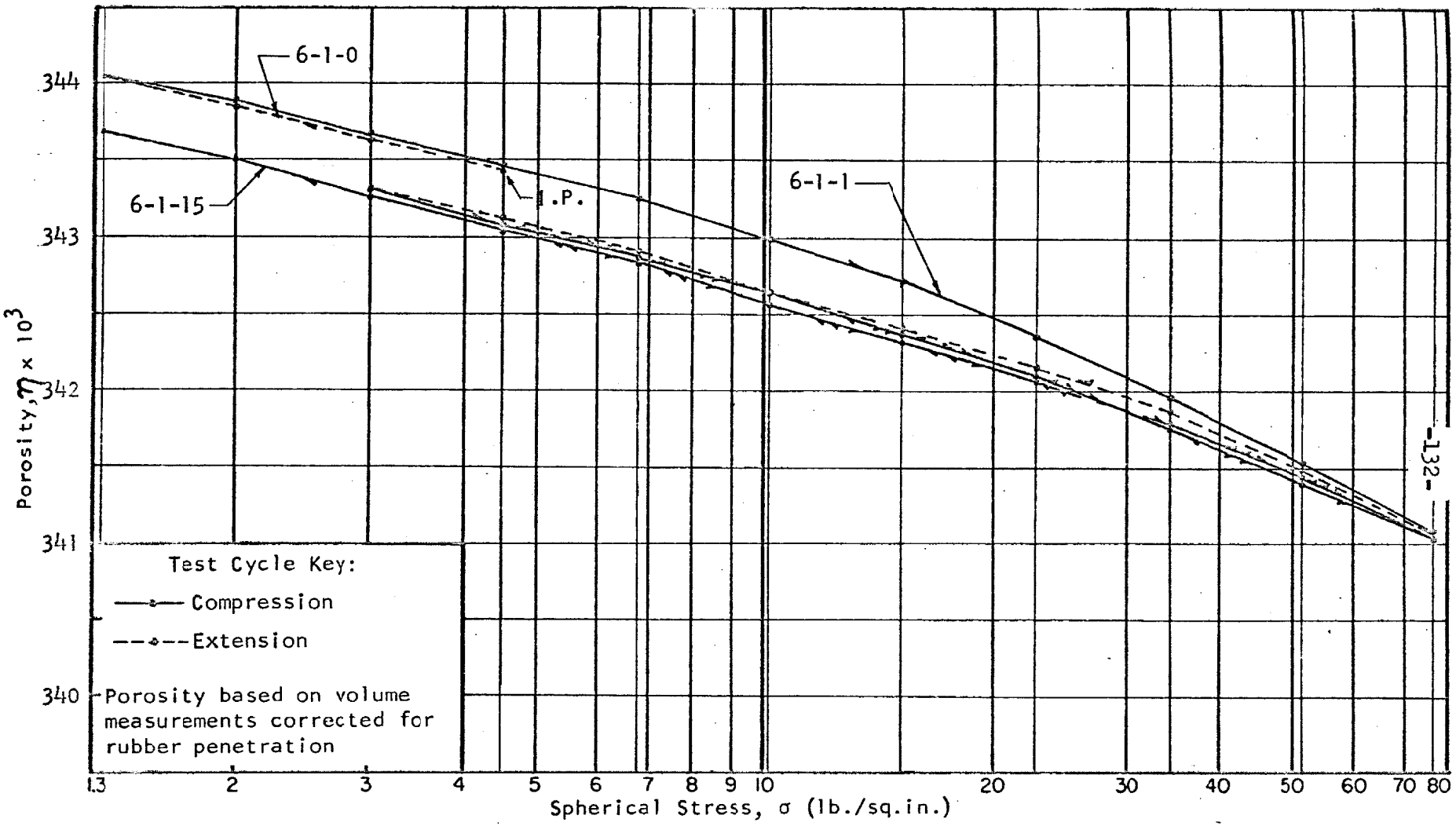

Figure 7.14 Porosity as a Function of Applied Spherical Stress
Spherical Compression Test Nos. 6-1-0 through 6-1-15

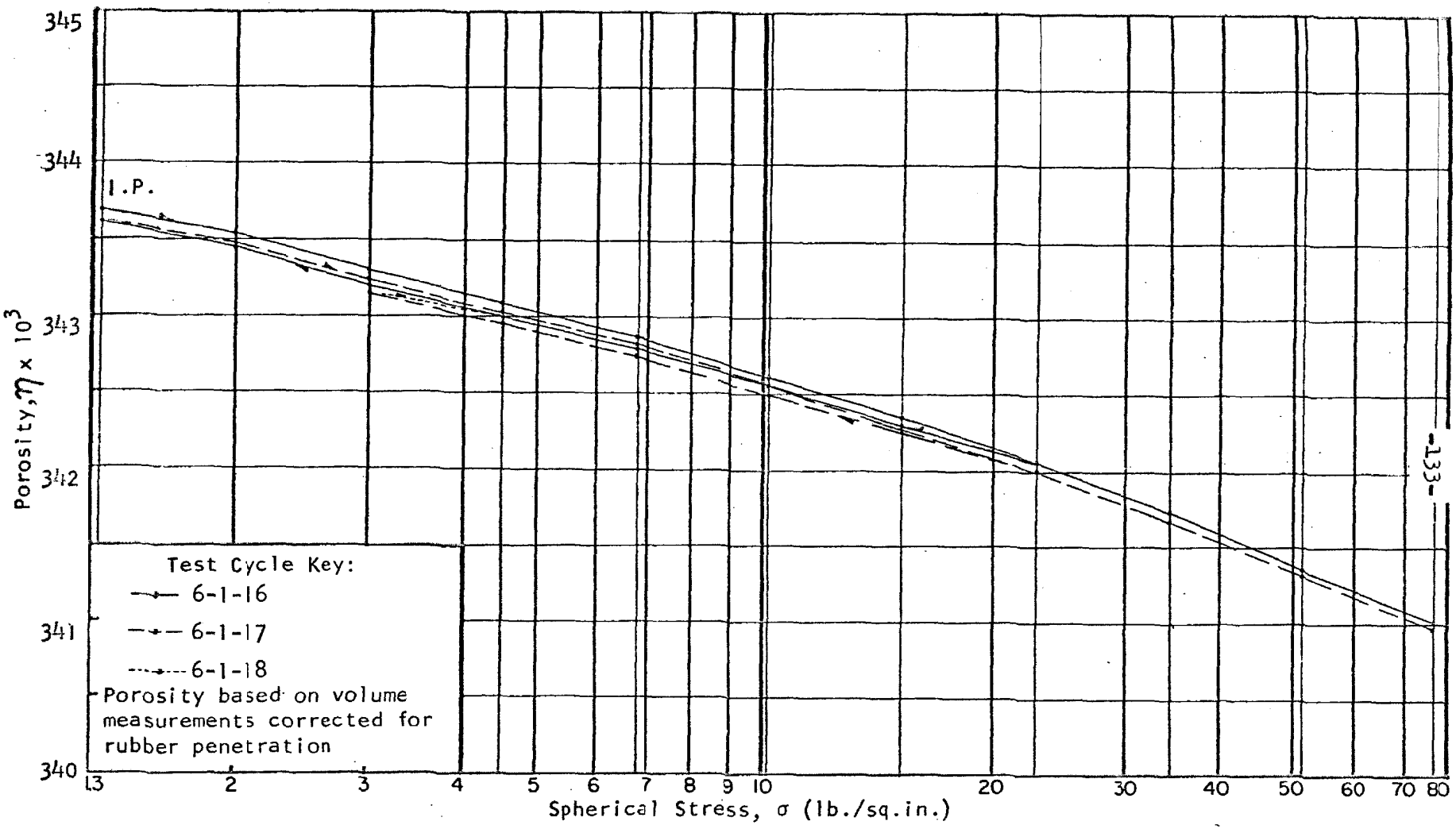

Figure 7.15 Porosity as a Function of Applied Spherical Stress
Spherical Compression Test Nos. 6-1-16 through 6-1-18

Test Cycle Key: ○ ● 6-1-16
◔ ◕ 6-1-17
◎ 6-1-18

Clear Circles - Compression
Solid Circles - Extension
Compressibility based on volume measurements corrected for rubber penetration.

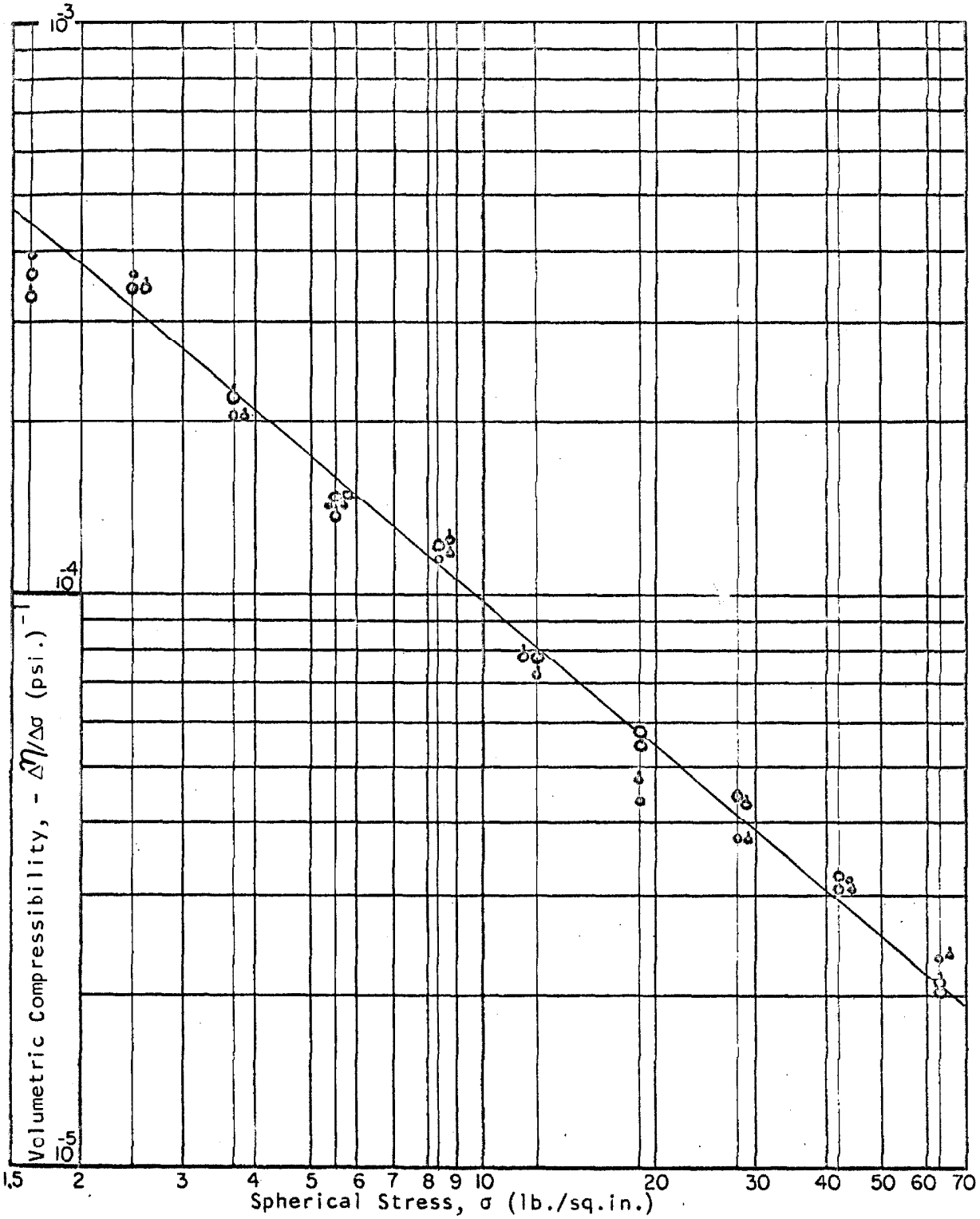

Figure 7.16 Volumetric Compressibility as a Function of Applied Spherical Stress.

Spherical Compression Test Nos. 6-1-16 through 6-1-18

7.3 STRESS-STRAIN EXPERIMENTS

THREE-DIMENSIONAL COMPRESSION APPARATUS

Fifteen three-dimensional compression experiments were attempted, two of which failed due to apparatus malfunctions. A brief resume of the entire program is followed by the presentation of experimental logs and test results for Experiment Nos. 2 through 6 and 8 through 15. Complete data and example calculations of test results for Experiment No. 13 are given in Appendixes A12 and A13 respectively.

In all experiments the volumetric compressibilities were corrected for the effects of rubber penetration, Appendix A8.1. Principal strains for all experiments, with exception of Experiment No. 2, were corrected for pressure-cell effects including rubber penetration, Appendix A8.2. The principal strains of Experiment No. 2 were corrected for pressure-cell effects, but rubber penetration was neglected.

7.31 RESUME OF LABORATORY PROGRAM

Experiment No. 1.--All pressure-cells leaked at the clamped valve-core-rubber connections under pressures as low as 5 psi. No useful data were obtained. New pressure-cells were constructed using valve-core joints bonded with epoxy adhesive.

Experiment No. 2.--The first deviatoric stress-strain data were obtained from this experiment. The apparatus was tested and experimental procedures were developed. The photographic measurement of strain proved to be impractical and erratic. An accurate measurement of strain was not obtained for initial test cycles and final test cycles were carried out on a sample with a considerable history of

stress and strain. Average compression stress paths I_{13*}(AC) were predominate, and these normally were immediately preceded and followed by spherical stress cycles. One circular compression stress path I_{12} was carried out.

Experiment No. 3.--Initial spherical stress cycles were performed for purposes of calibration. This experiment was designed primarily to carry out a circular compression stress path I_{12} at a relatively low deviatoric state of stress. The triaxial compression stress path I_{13*}(TC) was used to develop initial shear. Regulator no. 1 failed during the first circular compression cycle. The sample was seriously distorted and the test was completed prematurely.

Experiment No. 4.--This experiment was designed primarily to obtain yield in triaxial compression I_{13*}(TC) and to study the subsequent behavior in spherical compression (SC). Initial spherical stress cycles were performed for purposes of calibration and for comparison with final spherical stress cycles.

Experiment No. 5.--Initial spherical stress cycles were performed for purposes of calibration and comparison. This experiment was designed primarily to obtain yield in triaxial extension I_{13*}(TE) and to study subsequent behavior in spherical compression (SC). Following this, however, yield was obtained in average compression I_{13*}(AC) followed by spherical stress cycles, and finally a yield was obtained in triaxial compression I_{13*}(TC) followed by spherical stress cycles.

Experiment No. 6.--This experiment was designed primarily to carry out a circular compression I_{12} stress path at deviatoric stresses

slightly below yield. The triaxial compression I_{13*}(TC) stress path was utilized to develop initial shear, and the triaxial extension stress path I_{13*}(TE) was utilized for return to the spherical stress state. Spherical stress cycles were performed initially and finally.

Experiment Nos. 7-15.--These experiments were designed to obtain yield from a spherical state of stress using a variety of I_{13*} stress paths. In separate tests I_3* was varied from -0.8 to 0.8 in increments of 0.2, skipping the null value (average compression). Initial spherical stress cycles were carried out for purposes of calibration. Final spherical cycles were not performed. Experiment no. 7 failed during the process of saturation due to a block in the supply line caused by algae in the water supply reservoir. All pressure-volume tanks were cleaned and further difficulties were not encountered.

7.32 EXPERIMENTAL LOGS AND TEST RESULTS

The experimental logs, Tables 7.4 through 7.9, give the test series, stress history, and appropriate comments for each experiment. A new test series generally indicates a change in the loading program. The stress history is given in terms of the first stress invariant I_1 and the second and third modified and dimensionless stress invariants, I_2* and I_3* respectively.

The test results are given graphically for each test series, Figures 7.17 through 7.47. Results for deviatoric stress paths are generally followed by results for spherical compression cycles which were carried out prior to and following the corresponding deviatoric test.

Table 7.4 Log of Experiment No. 2

Test Series	Stress History	Comments
2-1-SC through 2-3-SC	$I_1 = 3 \leftrightarrow 30$ psi, I_2^*, $I_3^* = 0$	Dry sample used initially, behavior of pressure-cells observed, operation of photographic equipment checked.
2-4-I_{13^*}(AC) 2-4-I_{13^*}(AC_R)	$I_1 = 30$ psi, $I_2^* = 0 \rightarrow 0.14$, $I_3^* = 0$ $I_1 = 30$ psi, $I_2^* = 0.14 \rightarrow 0$, $I_3^* = 0$	Combination vac. (I_1=15 psi) and external pressure (I_1=15 psi) used. Vac. control found difficult and impractical. Photographic measurement of strain was erratic.
		Removed compression chamber from press frame, disassembled equip, repaired piston control, greased and centered sample, re-assembled equip with transparent photo grid adjacent sample, raised cell pressures to 8 psi and placed chamber in vertical position, saturated sample with 3.4 psi on drain. Rotated chamber to horiz position and placed in press frame.
2-5-SC through 2-8-SC	$I_1 = 15 \leftrightarrow 90$ psi, I_2^*, $I_3^* = 0$	Installed burette bank (10cc, 25cc, 50cc) in sample supply line. Made 10cc burette movable vertically to compensate for effect of air compressibility.
2-9-I_{13^*}(AC) 2-9-I_{13^*}(AC_R)	$I_1 = 45$ psi, $I_2^* = 0 \rightarrow 0.12$, $I_3^* = 0$ $I_1 = 45$ psi, $I_2^* = 0.12 \rightarrow 0$, $I_3^* = 0$	

Table 7.4 continued

Test Series	Stress History	Comments
		Performed 1st air vol test, V_A = 368 cc
2-10-SC through 2-13-SC	I_1 = 15 ↔ 90 psi, I_2*, I_3* = 0	
2-14-I_{13*}(AC)	I_1 = 54 psi, I_2* = 0 → 0.08, I_3* = 0	
2-15-I_{12}	I_1 = 54 psi, I_2* = 0.08, I_3* = 0 → 1	
2-15-I_{12R}	I_1 = 54 psi, I_2* = 0.08, I_3* = 1 → -1	
2-16-I_{12}	I_1 = 54 psi, I_2* = 0.08, I_3* = -1 → 0	
		Bur vol chg (volumetric strain burette) 1 cc over 3-day period.
2-17-I_{13}(AC_R)	I_1 = 54 psi, I_2* = 0.08 → 0, I_3* = 0	
2-18-SC through 2-21-SC	I_1 = 15 ↔ 90 psi, I_2*, I_3* = 0	
2-22-I_{13*}(AC)	I_1 = 75 psi, I_2* = 0 → 0.02, I_3* = 0	
2-22-I_{13*}(AC_R)	I_1 = 75 psi, I_2* = 0.02 → 0, I_3* = 0	
2-23-SC_R	I_1 = 75 → 60 psi, I_2*, I_3* = 0	

Table 7.4 continued

Test Series	Stress History	Comments
2-24-$I_{13*}(AC)$	I_1= 60 psi, I_2* = 0→ 0.03, I_3* = 0	
2-24-$I_{13*}(AC_R)$	I_1= 60 psi, I_2* = 0.03→ 0, I_3* = 0	
2-25-SC_R	I_1= 60→ 45 psi, I_2*, I_3* = 0	
2-26-$I_{13*}(AC)$	I_1= 45 psi, I_2* = 0→ 0.05, I_3* = 0	
2-26-$I_{13*}(AC_R)$	I_1= 45 psi, I_2* = 0.05→ 0, I_3* = 0	
2-27-SC_R	I_1= 45→ 30 psi, I_2*, I_3* = 0	
2-28-$I_{13*}(AC)$	I_1= 30 psi, I_2* = 0→ 0.07, I_3* = 0	
2-28-$I_{13*}(AC_R)$	I_1= 30 psi, I_2* = 0.07→ 0, I_3* = 0	
		Performed 2nd air vol test, V_A= 367 cc

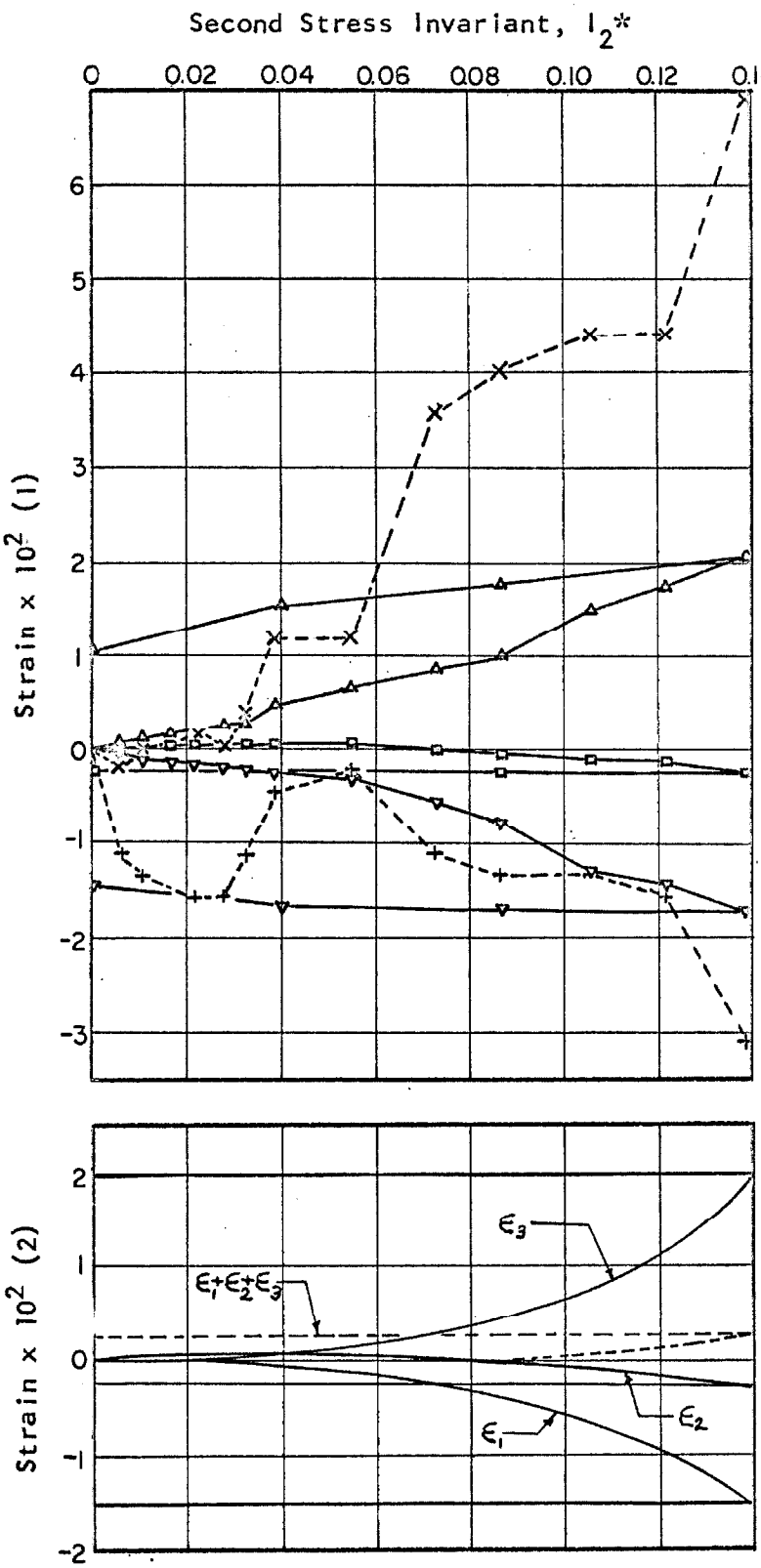

(1) Key:

▽ ϵ_1
⊡ ϵ_2
△ ϵ_3
} Volume Measurement

+ ϵ_1
x ϵ_3
} Photo Measurement

Solid lines--strains based on direct volume measurements with no correction for pressure cell or rubber penetration.

(2) Key:

ϵ_1, ϵ_2, ϵ_3 ——
$\epsilon_1+\epsilon_2+\epsilon_3$ ------

Estimate of strains ϵ_1 and ϵ_3 based on divergence of original rebound curves (1) from horizontal.

	Initial	Final (3)
η	0.361	0.364
$\epsilon_1 \times 10^2$	0	-1.5
$\epsilon_2 \times 10^2$	0	-0.2
$\epsilon_3 \times 10^2$	0	+2.0
$J_1 \times 10^2$	0	+0.3
$J_2 \times 10^3$	0	+0.63
$-J_3^*$		-0.4

(3) Based on estimated strains (2).

I_1 = 30 lb./sq. in.
I_2^* = 0 ↔ 0.14
I_3^* = 0

Figure 7.17 Strains as a Function of the Second Modified and Dimensionless Stress Invariant.

Average Compression Test Nos. 2-1-I_{13}(AC and AC_R)

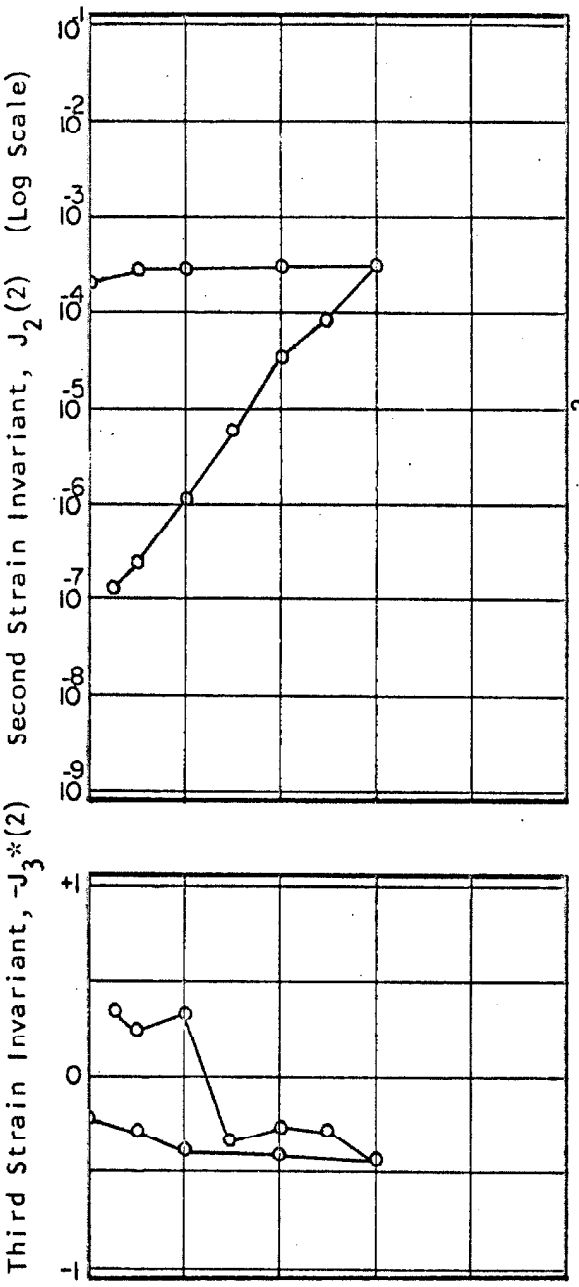

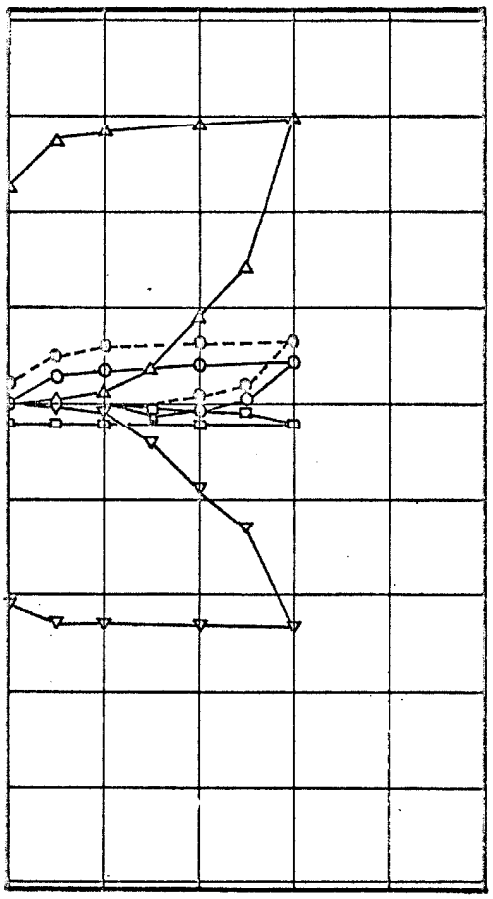

(1) Key: $\nabla\epsilon_1$ $\odot\epsilon_1+\epsilon_2+\epsilon_3$
$\boxdot\epsilon_2$ $\circ\epsilon_v$ (dotted line)
$\triangle\epsilon_3$

Strains based on volume measurements corrected for pressure cell effects. Zero strain I.P. this test.

	Initial	Yield(3)	Final(3)
η	0.363	None	0.363
$\epsilon_1 \times 10^2$	0		-0.92
$\epsilon_2 \times 10^2$	0		-0.10
$\epsilon_3 \times 10^2$	0		+1.13
$J_1 \times 10^2$	0		+0.11
$J_2 \times 10^4$	0		2.13
$-J_3^*$	-		-0.34

I_1 = 45 psi., I_2^*=0↔0.12, I_3^*= 0

(2) Basis of Calculation:
ϵ_v, ϵ_2, ϵ_3 with $\epsilon_1 = \epsilon_v - (\epsilon_2+\epsilon_3)$,
Zero strain I.P. this test.

(3) Based on: ϵ_v, ϵ_2, ϵ_3.

Figure 7.18 Strains and Strain Invariants as a Function of the Second Modified and Dimensionless Stress Invariant.
Average Compression Test Nos. 2-9-I_{13}* (AC & AC_R)

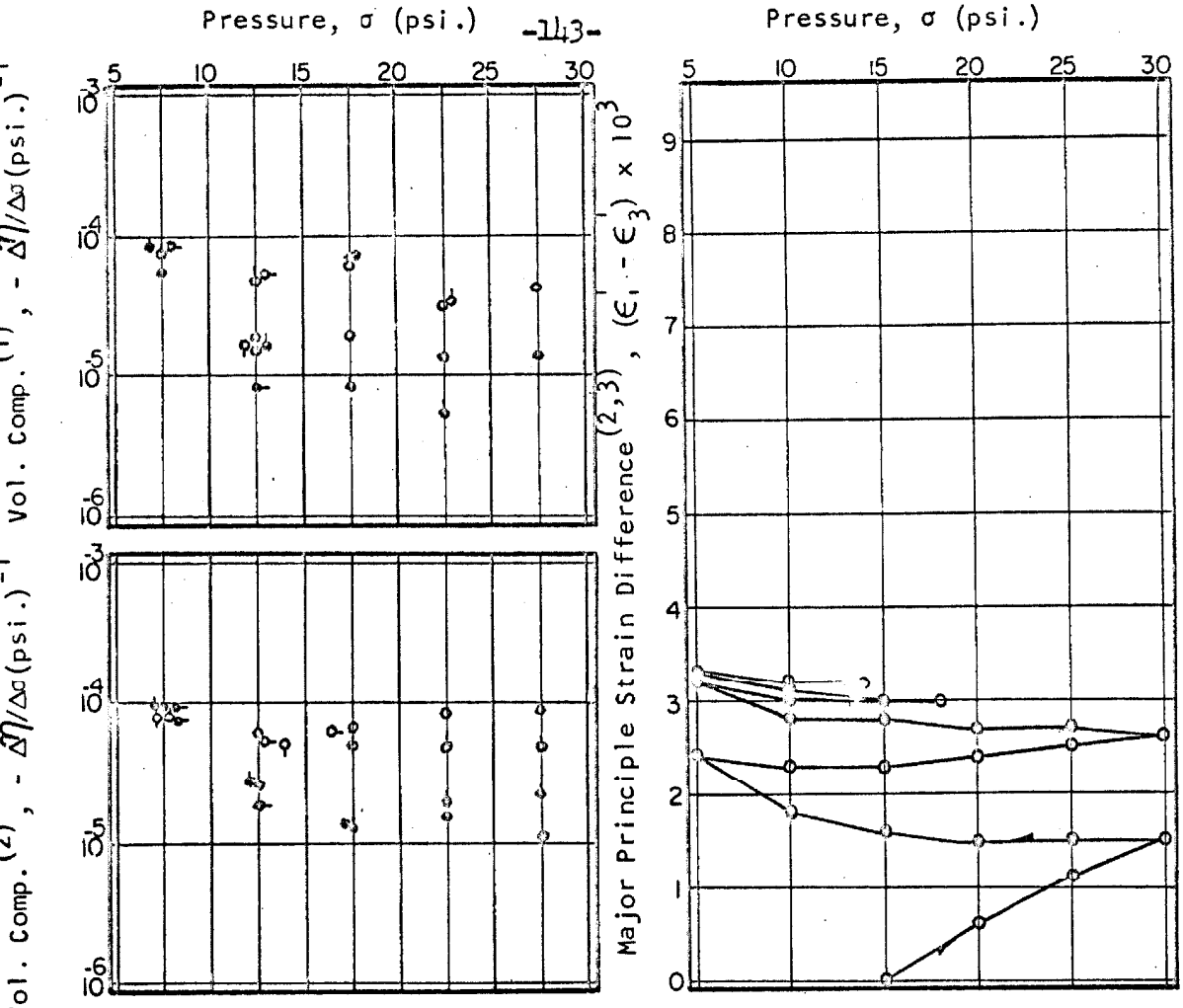

(1) Test Nos. 2-5-SC → 2-8-SC
Key: o 2-5 o- 2-7
ó 2-6 o 2-8

(2) Test Nos. 2-10-SC → 2-13-SC
Key: o 2-10 o- 2-12
ó 2-11 o 2-13

(3) Zero strain difference I.P. Test Series (2).

	Initial	Final (4)
η	0.363	0.362
$\epsilon_1 \times 10^2$	-0.92	-0.83
$\epsilon_2 \times 10^2$	-0.10	-0.16
$\epsilon_3 \times 10^2$	+1.13	+0.91
$J_1 \times 10^2$	+0.11	-0.08
$J_2 \times 10^4$	2.13	1.54
$-J_3$*	-0.34	-0.38

Zero Strain I.P. Test 2-9-I_{13}*(AC)

Compression - Clear Circles
Extension - Solid Circles

$\eta_{Initial} = 0.363$ $\eta_{Final} = 0.363$

Compressibility based on volume measurements corrected for rubber penetration.

(4) Basis of Calculation

$\epsilon_1 = \epsilon_{10} + \epsilon_v'/3 + (\epsilon_1' - \epsilon_3')/2$

$\epsilon_2 = \epsilon_{20} + \epsilon_v'/3$

$\epsilon_3 = \epsilon_{30} + \epsilon_v'/3 - (\epsilon_1' - \epsilon_3')/2$

Figure 7.19 Volumetric Compressibility and Apparent Major Principle Strain Difference as a Function of Applied Spherical Stress. Spherical Compression Test Nos. 2-5-SC through 2-8-SC and 2-10-SC through 2-13-SC

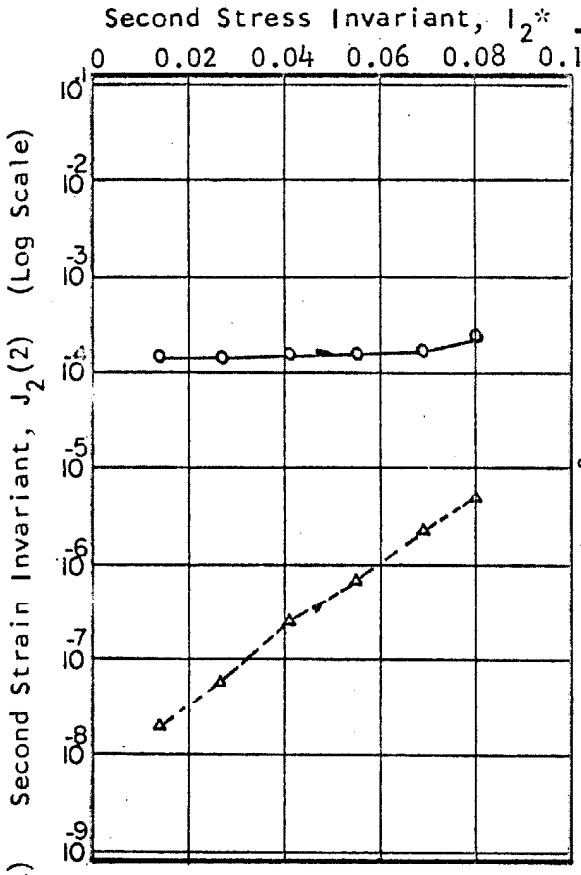

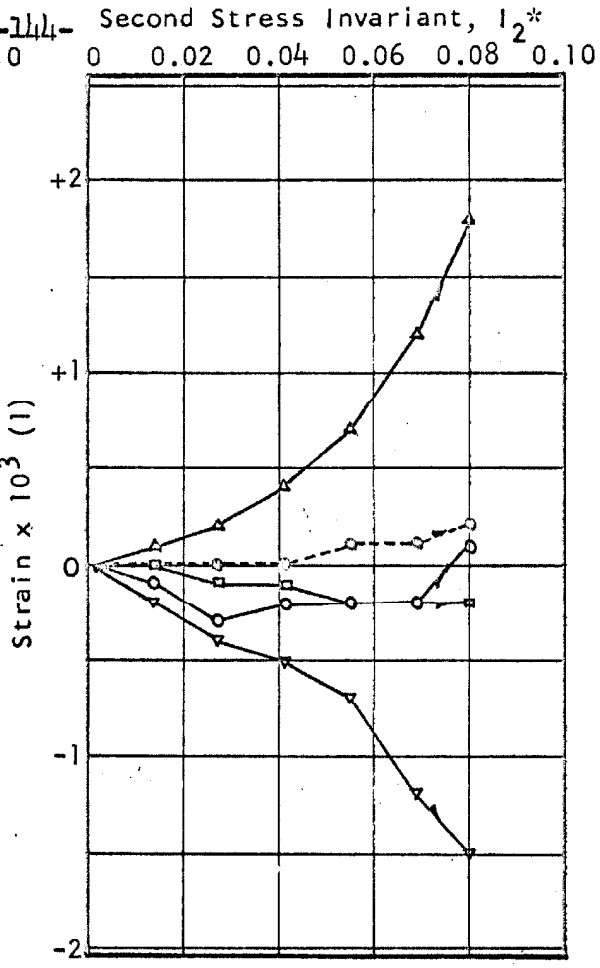

(1) Key: $\nabla\epsilon_1'$ $\odot\epsilon_1'+\epsilon_2'+\epsilon_3'$ $\boxdot\epsilon_2'$ $\circ\epsilon_v'$ (dotted line) $\triangle\epsilon_3'$

Strains based on volume measurements corrected for pressure cell effects. Zero strain I.P. this test.

	Initial	Yield(3)	Final(3)
η	0.362	None	0.362
$\epsilon_1 \times 10^2$	-0.83		-0.97
$\epsilon_2 \times 10^2$	-0.16		-0.18
$\epsilon_3 \times 10^2$	+0.91		+1.09
$J_1 \times 10^2$	-0.08		-0.06
$J_2 \times 10^4$	1.54		2.16
$-J_3^*$	-0.38		-0.39

I_1 = 54 psi., I_2^*=0→0.08, I_3^*= 0

(2) Basis of Calculation:

$\Delta\epsilon_v', \epsilon_2', \epsilon_3'$ with $\epsilon_1' = \epsilon_v' - (\epsilon_2' - \epsilon_3')$

$\circ\epsilon_v, \epsilon_2, \epsilon_3$ with $\epsilon_1 = \epsilon_v - (\epsilon_2 + \epsilon_3)$

Zero strain I.P. test 2-9-I_{13^*}(AC)

(3) Based on:

ϵ_v, ϵ_2, ϵ_3.

Figure 7.20 Strains and Strain Invariants as a Function of the Second Modified and Dimensionless Stress Invariant. Average Compression Test No. 2-14-I_{13^*}(AC)

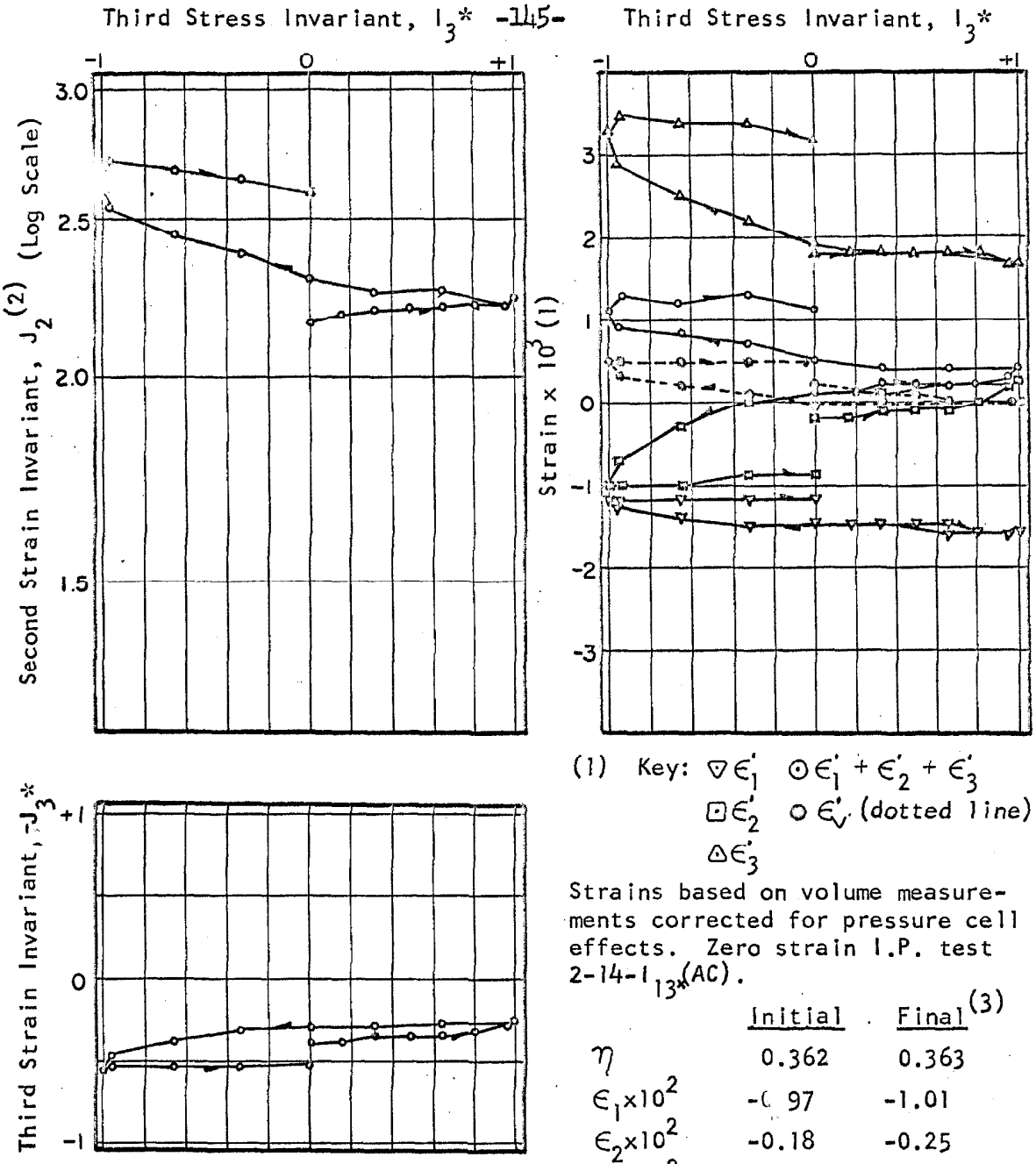

(1) Key: $\nabla\epsilon_1'$ $\odot\epsilon_1'+\epsilon_2'+\epsilon_3'$ $\boxdot\epsilon_2'$ $\circ\epsilon_v'$ (dotted line) $\triangle\epsilon_3'$

Strains based on volume measurements corrected for pressure cell effects. Zero strain I.P. test 2-14-I_{13}^*(AC).

	Initial	Final(3)
η	0.362	0.363
$\epsilon_1 \times 10^2$	-0.97	-1.01
$\epsilon_2 \times 10^2$	-0.18	-0.25
$\epsilon_3 \times 10^2$	+1.09	+1.23
$J_1 \times 10^2$	-0.06	-0.03
$J_2 \times 10^4$	2.16	2.60
$-J_3^*$	-0.39	-0.52

(2) Basis of Calculation:
$\ominus\epsilon_v, \epsilon_2, \epsilon_3$ with $\epsilon_1 = \epsilon_v - (\epsilon_2+\epsilon_3)$ and $\epsilon_j = \epsilon_{jo} + \epsilon_j'$.
Zero strain I.P. test 2-9-I_{13}^*(AC)

(3) Based on: ϵ_v, ϵ_2, ϵ_3. I_1=54 psi., I_2^*=0.08, I_3^*=0→+1→-1→0

Figure 7.21 Strains and Strain Invariants as a Function of the Third Modified and Dimensionless Stress Invariant.
Circular Compression Test Nos. 2-15-I_{12} & I_{12R} and 2-16-I_{12}

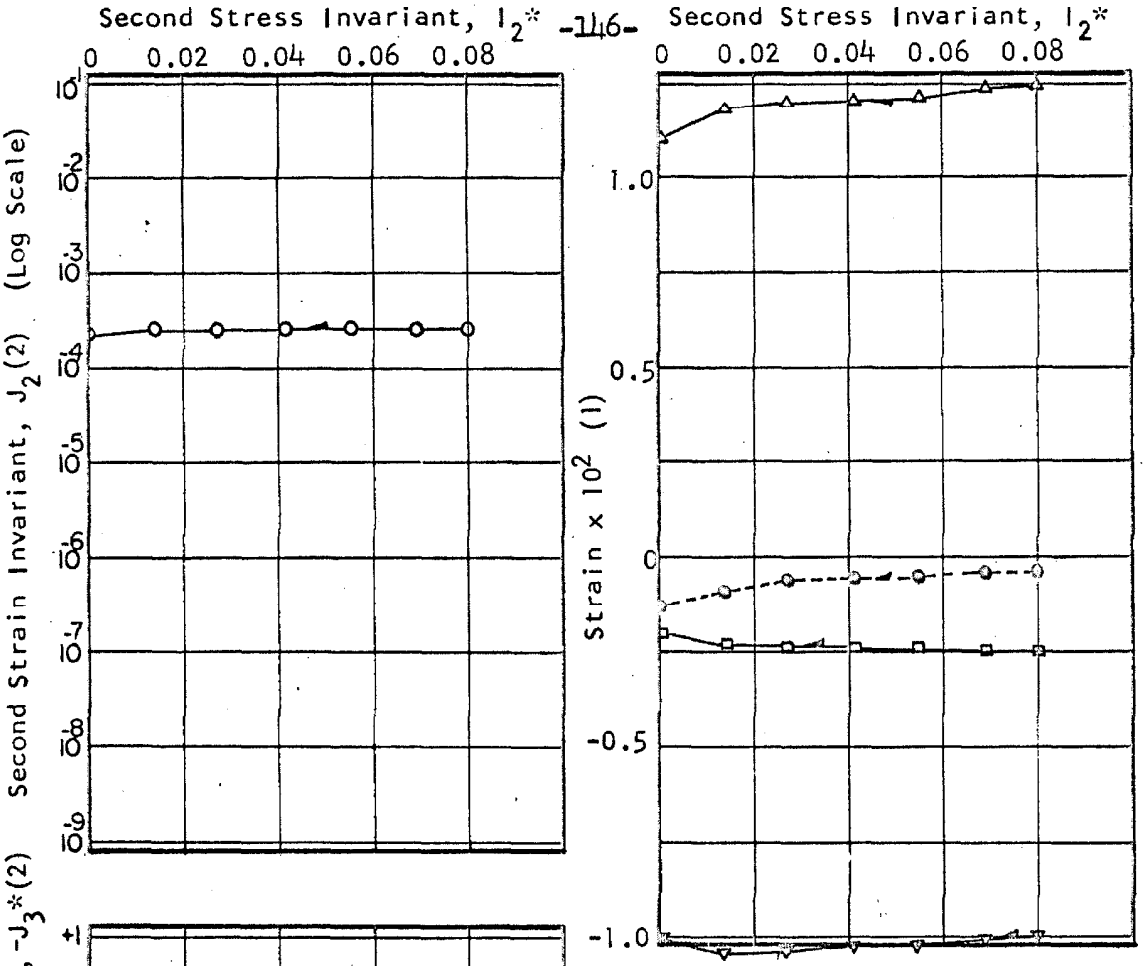

(1) Key: $\nabla\epsilon_1$ $\odot\epsilon_1$ $+\epsilon_2$ $+\epsilon_3$
$\boxdot\epsilon_2$ $\circ\epsilon_v$ (dotted line)
$\triangle\epsilon_3$

Strains based on volume measurements corrected for pressure cell effects.
Zero strain I.P. test 2-9-I_{13}* (AC)

	Initial	Yield(3)	Final(3)
η	0.363	None	0.362
$\epsilon_1 \times 10^2$	-1.01		-1.02
$\epsilon_2 \times 10^2$	-0.25		-0.21
$\epsilon_3 \times 10^2$	+1.23		+1.10
$J_1 \times 10^2$	-0.03		-0.13
$J_2 \times 10^4$	2.60		2.29
$-J_3^*$	-0.52		-0.39

I_1=54 psi., I_2^*=0.08 0, I_3^*= 0

(2) Basis of Calculation:
ϵ_v, ϵ_2, ϵ_3 with $\epsilon_1=\epsilon_v-(\epsilon_2+\epsilon_3)$
Zero strain I.P. test 2-9-I_{13}* (AC).

(3) Based on: ϵ_v, ϵ_2, ϵ_3

Figure 7.22 Strains and Strain Invariants as a Function of the Second Modified and Dimensionless Stress Invariant.
Average Compression Test No. 2-17-I_{13} (AC_R)

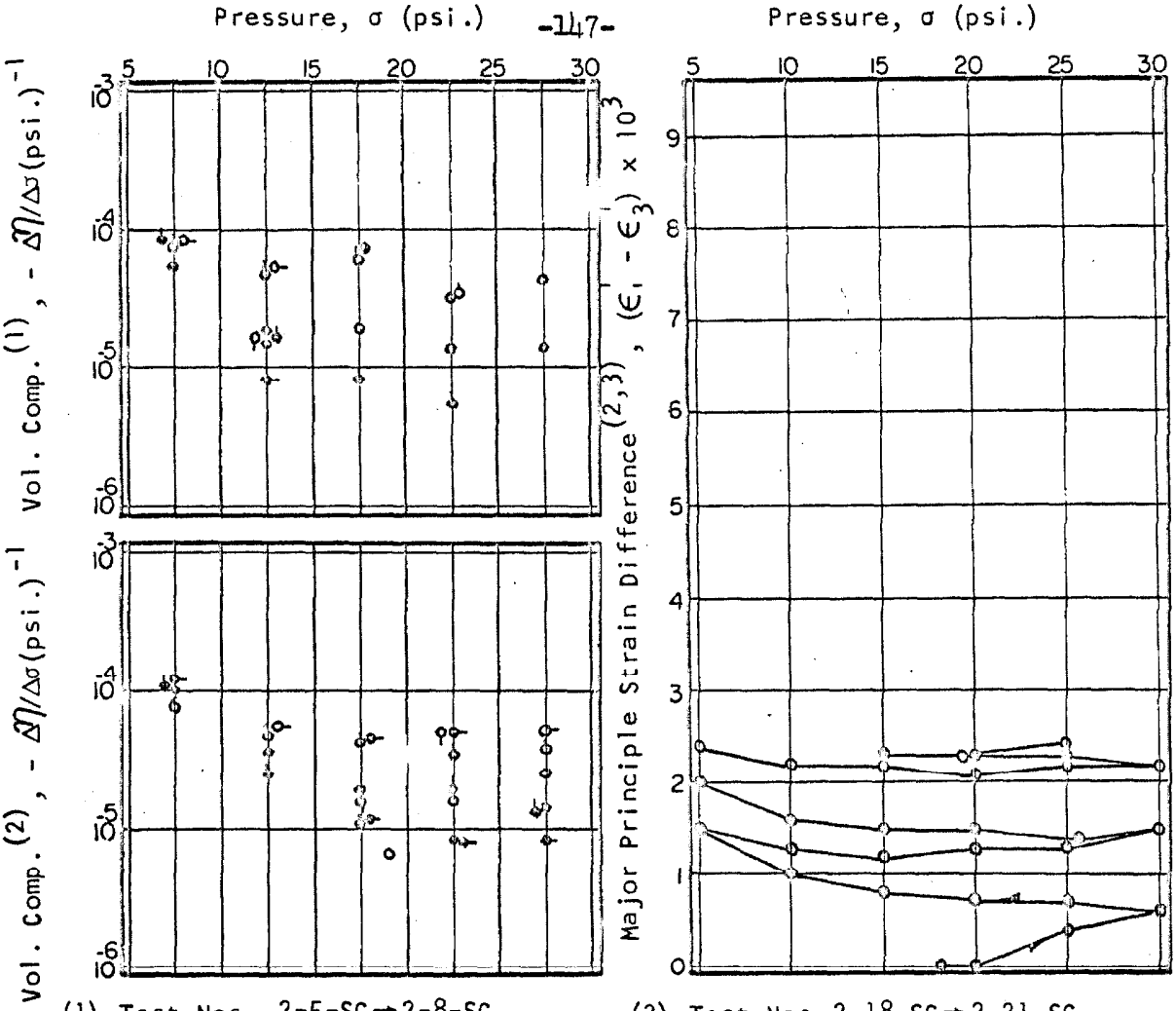

(1) Test Nos. 2-5-SC→2-8-SC
Key: o 2-5 o- 2-7
ó 2-6 ọ 2-8

(2) Test Nos. 2-18-SC→2-21-SC
Key: o 2-18 o- 2-20
ó 2-19 ọ 2-21

(3) Zero strain difference I.P. Test Series (2).

Compression - Clear Circles
Extension - Solid Circles

η Initial = 0.363 η Final = 0.363

Compressibility based on volume measurements corrected for rubber penetration.

	Initial	Final (4)
η	0.362	0.361
$\epsilon_1 \times 10^2$	-1.02	-0.94
$\epsilon_2 \times 10^2$	-0.21	-0.25
$\epsilon_3 \times 10^2$	+1.10	+0.94
$J_1 \times 10^2$	-0.13	-0.25
$J_2 \times 10^4$	2.29	1.81
$-J_3$*	-0.39	-0.44

Zero Strain I.P. Test 2-9-I_{13}* (AC)

(4) Basis of Calculation

$\epsilon_1 = \epsilon_{10} + \epsilon_v'/3 + (\epsilon_1' - \epsilon_3')/2$

$\epsilon_2 = \epsilon_{20} + \epsilon_v'/3$

$\epsilon_3 = \epsilon_{30} + \epsilon_v'/3 - (\epsilon_1' - \epsilon_3')/2$

Figure 7.23 Volumetric Compressibility and Apparent Major Principle Strain Difference as a Function of Applied Spherical Stress. Spherical Compression Test Nos. 2-5-SC through 2-8-SC and 2-18-SC through 2-21-SC

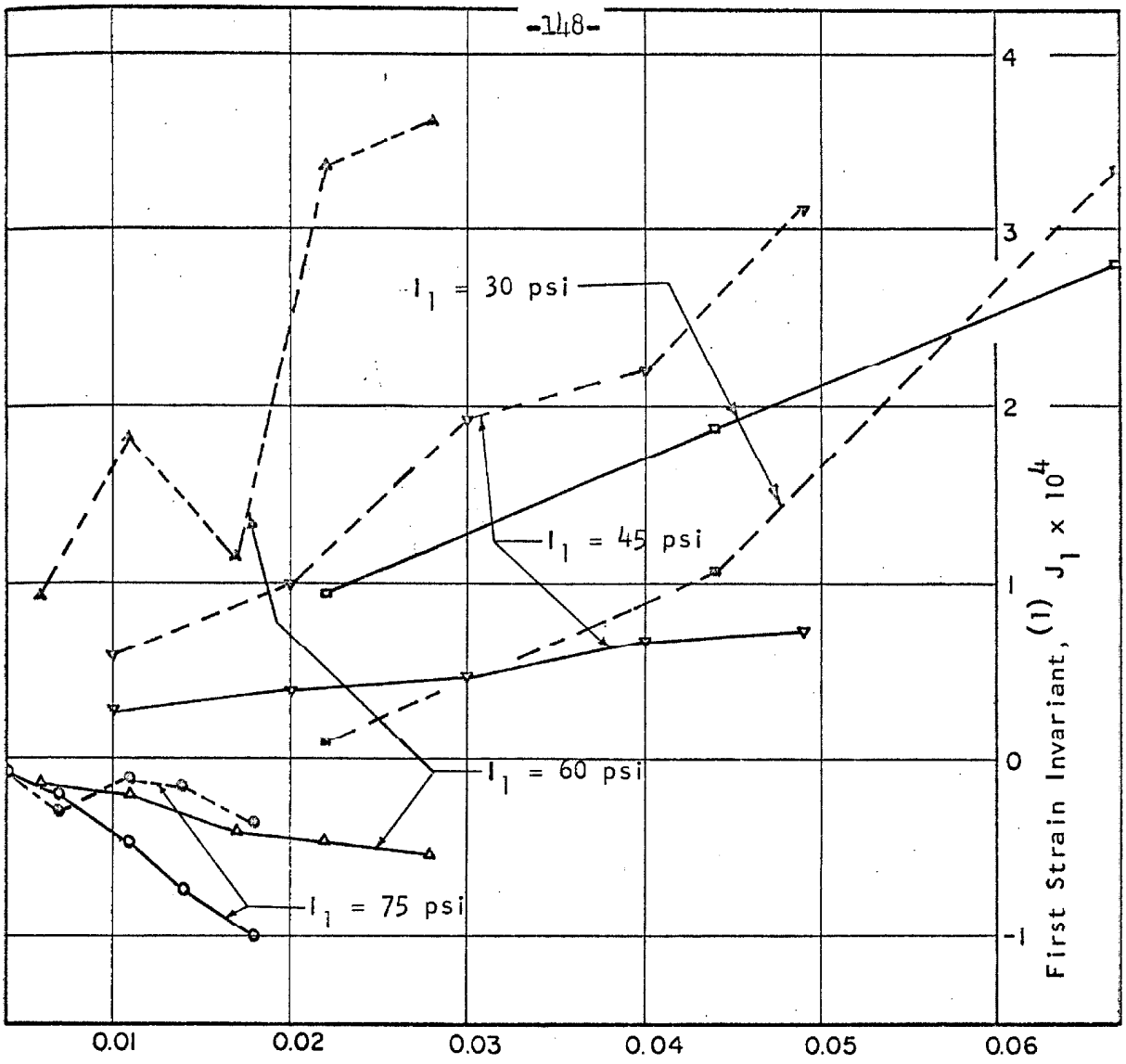

Key:
- ⊙ 2-22
- △ 2-24
- ▽ 2-26
- ⊡ 2-28
- ○ 2-22
- △ 2-24
- ▽ 2-26
- □ 2-28

$J_1 = \epsilon_v'$ ——

$J_1 = \epsilon_1' + \epsilon_2' + \epsilon_3'$ ---

Strains corrected for pressure cell effects. Zero strain taken I.P. each test.

State of strain prior to test No. 2-22-I_{13}(AC)

η = 0.361 $J_1 = -0.25 \times 10^{-2}$

$\epsilon_1 = -0.94 \times 10^{-2}$ $J_2 = 1.81 \times 10^{-4}$

$\epsilon_2 = -0.25 \times 10^{-2}$ $-J_3^* = -0.44$

$\epsilon_3 = +0.94 \times 10^{-2}$

Zero strain I.P. test No. 2-9-I_{13}(AC)

Figure 7.24 The First Strain Invariant as a Function of the Second Modified and Dimensionless Stress Invariant.

Average Compression Test Nos. 2-22-I_{13}(AC) through 2-28-I_{13}(AC)

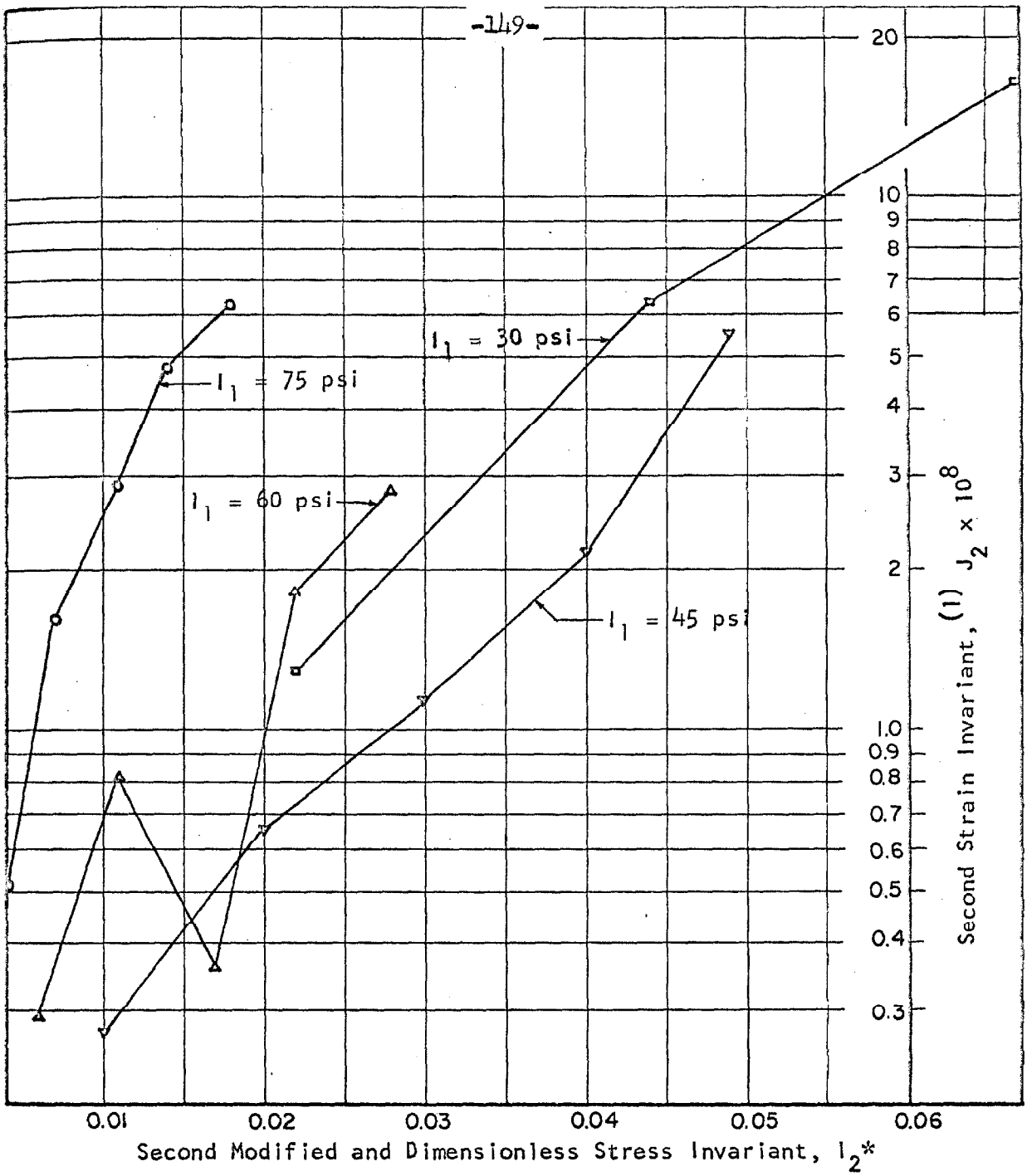

(1) Basis of calculation:
$\epsilon_1', \epsilon_2', \epsilon_3'$

Strains corrected for pressure cell effects. Zero Strain taken I.P. each test.

Key: ⊙ 2-22
△ 2-24
▽ 2-26
⊡ 2-28

Figure 7.25 The Second Strain Invariant as a Function of the Second Modified and Dimensionless Stress Invariant.
Average Compression Test Nos. 2-22-I_{13}(AC) through 2-28-I_{13}(AC)

Table 7.5 Log of Experiment No. 3

Test Series	Stress History	Comments
3-1-SC through 3-4-SC	$I_1 = 15 \leftrightarrow 90$ psi, I_2^*, $I_3^* = 0$	Bur vol chg, 1cc/16 hr. Performed air vol test, $V_A = 16$ cc.
3-5-I_{13^*}(TC)	$I_1 = 54$ psi, $I_2^* = 0 \rightarrow 0.02$, $I_3^* = 1$	Strains too small for accuracy.
3-6-I_{12R}	$I_1 = 54$ psi, $I_2^* = 0.02$, $I_3^* = 1 \rightarrow -1$	Strains too small for accuracy. At $I_3^* = -1$ Regulator No. 1 ruptured and σ_1 was reduced to 0.7 psi, flow valves subsequently closed.

Table 7.6 Log of Experiment No. 4

4-1-SC through 4-3-SC	$I_1 = 15 \leftrightarrow 105$ psi, I_2^*, $I_3^* = 0$	
4-4-I_{13^*}(TC)	$I_1 = 54$ psi, $I_2^* = 0 \rightarrow 0.18$, $I_3^* = 1$	First yield obtained when rate of deformation increased in time at $I_2^* = 0.18$. Closed flow valves, reduced loads, opened flow valves.
4-4-I_{13^*}(TC_R)	$I_1 = 54$ psi, $I_2^* = 0.18 \rightarrow 0$, $I_3^* = 1$	
4-5-SC through 4-10-SC_R	$I_1 = 15 \leftrightarrow 90$ psi, I_2^*, $I_3^* = 0$	Performed air vol test, $V_A = 16$ cc.

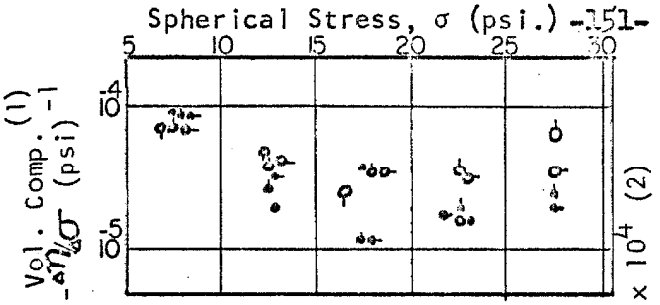

(1) Test Nos. 3-1-SC - 3-4-SC

Key: ⊙ 3-1 ⊙ 3-3
⊙ 3-2 ⊙ 3-4
Compression-Clear, Extension-Solid
Initial η = 0.329 Final η = 0.329

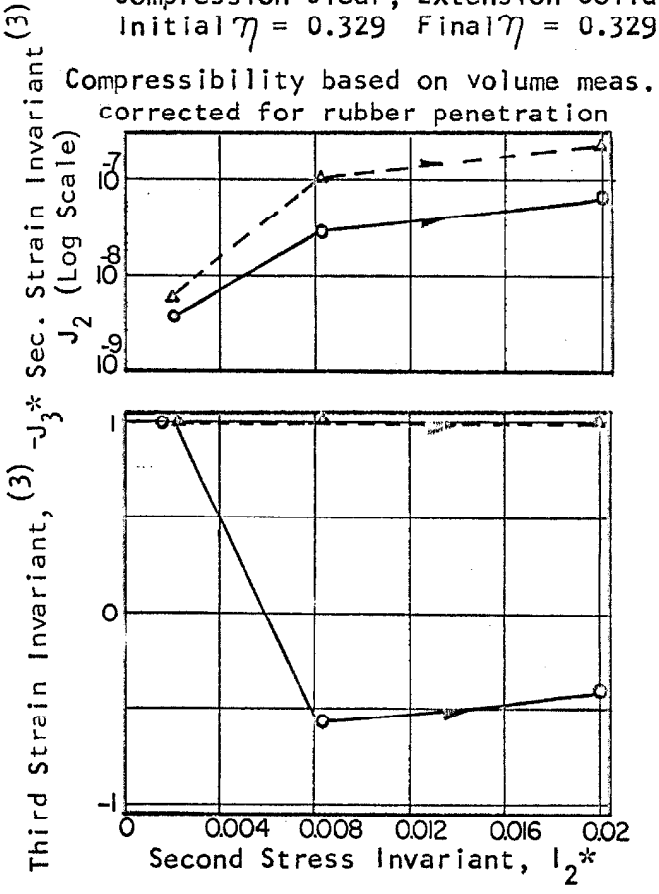

(3) Test No. 3-5-I_{13}* (TC), Basis of Calculation:
⊖ $\epsilon_v, \epsilon_2, \epsilon_3$ with $\epsilon_1 = \epsilon_v - (\epsilon_2 + \epsilon_3)$
⊿ ϵ_v, ϵ_3 with $\epsilon_2 = \epsilon_3$ and
$\epsilon_1 = \epsilon_v - (\epsilon_2 + \epsilon_3)$

(4) Based on: $\epsilon_v, \epsilon_2, \epsilon_3$.

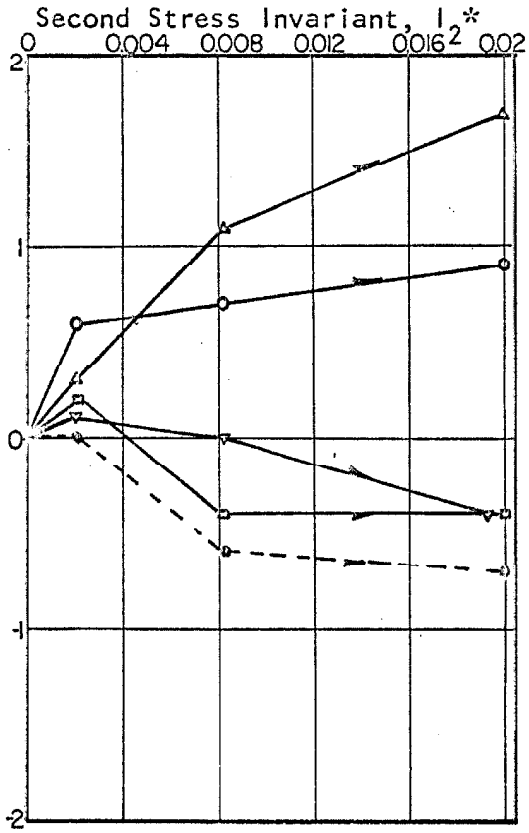

(2) Test No. 3-5-I_{13}*

Key: ▽ ϵ_1 ⊙ $\epsilon_1+\epsilon_2+\epsilon_3$
⊡ ϵ_2 ○ ϵ_v (dotted line)
△ ϵ_3

Strains based on vol. meas. corrected for pressure cell and rubber penetration. Zero strain I.P. this test.

	Initial	Final (4)
η	0.329	0.329
$\epsilon_1 \times 10^2$	0	-0.02
$\epsilon_2 \times 10^2$	0	0.00
$\epsilon_3 \times 10^2$	0	+0.02
$J_1 \times 10^2$	0	-0.01
$J_2 \times 10^8$	0	6.89
$-J_3^*$	—	-0.39

I_1=54 psi. I_2^*= 0→0.02 I_3^*=+ 1

Figure 7.26 Vol. Compressibility-Spherical Compression Test Nos. 3-1-SC, 3-4-SC, Strains and Strain Invariants as a Function of the Second Modified and Dimensionless Stress Invariant.

Triaxial Compression Test No. 3-[illegible]-SC)

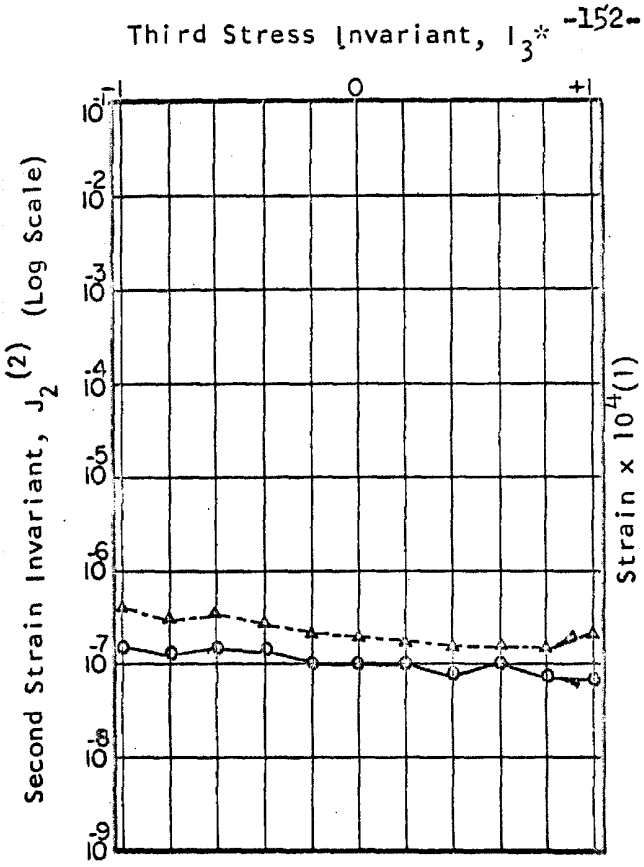

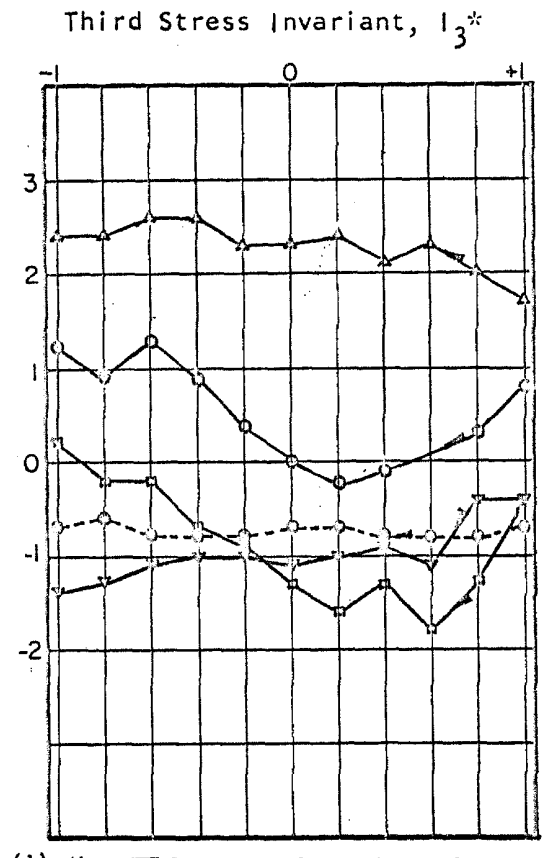

(1) Key: $\nabla\epsilon_1$ $\odot\epsilon_1+\epsilon_2+\epsilon_3$
$\square\epsilon_2$ $\circ\epsilon_v$ (dotted line)
$\triangle\epsilon_3$

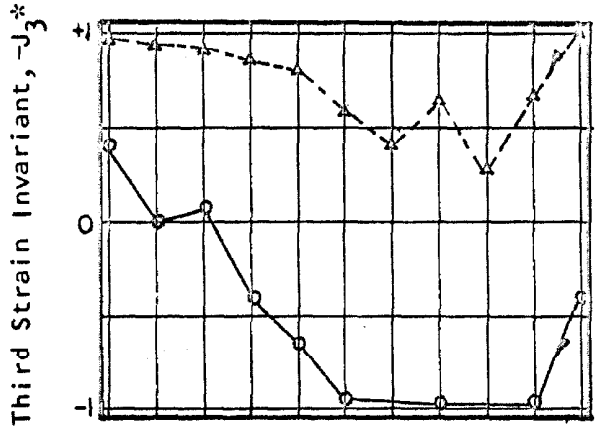

Strains based on volume measurements corrected for pressure cell and rubber penetration. Zero strain I.P. test 3-5-I_{13}^*(TC)

	Initial	Final (3)
η	0.329	0.329
$\epsilon_1 \times 10^2$	-0.02	-0.03
$\epsilon_2 \times 10^2$	0.00	0.00
$\epsilon_3 \times 10^2$	+0.02	+0.02
$J_1 \times 10^2$	-0.01	-0.01
$J_2 \times 10^8$	6.89	16.5
$-J_3^*$	-0.39	+0.38

I_1= 54 psi, I_2^*= 0.02 , I_3^*=+1→-1

(2) Basis of Calculation:
$\circ\epsilon_v$, ϵ_2, ϵ_3 with $\epsilon_1 = \epsilon_v-(\epsilon_2+\epsilon_3)$
$\triangle$ I.P. ϵ_{vo}, ϵ_{30}, with $\epsilon_{20} = \epsilon_{30}$ and and $\epsilon_{10} = \epsilon_{vo} - (\epsilon_{10}+\epsilon_{30})$ and rem. pts. using ϵ_v', ϵ_2', ϵ_3' this test.

(3) Based on: ϵ_v, ϵ_2, ϵ_3

Figure 7.27 Strains and Strain Invariants as a Function of the Third Modified and Dimensionless Stress Invariant.

Circular Compression Test Nos. 3-5-

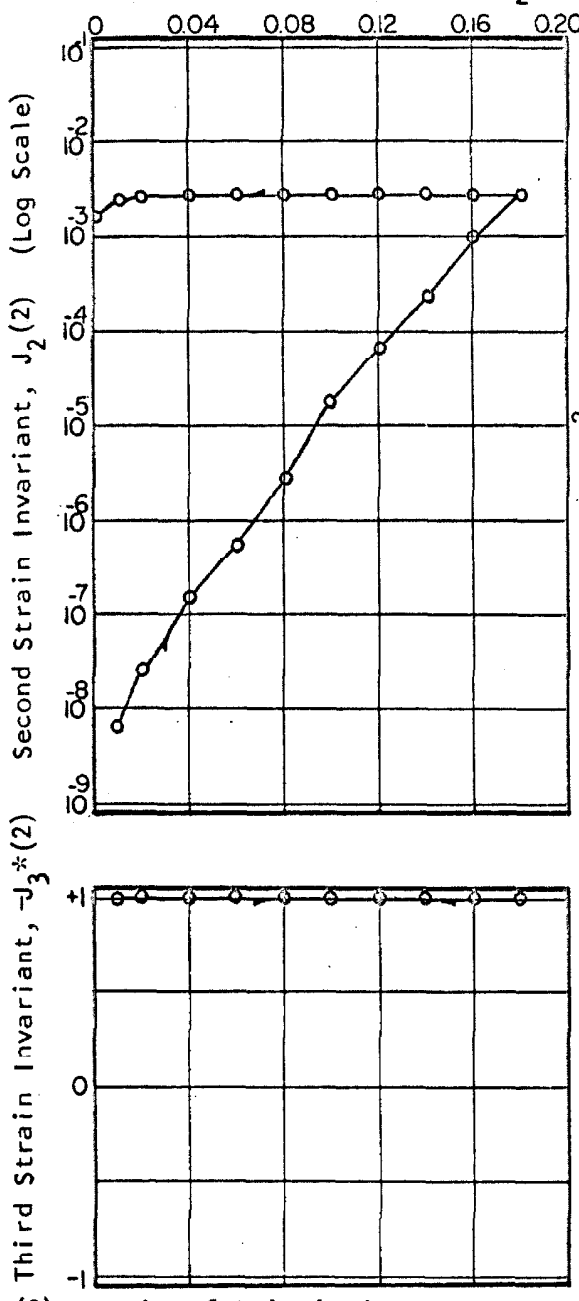

(2) Basis of Calculation:
$\bigcirc \epsilon_2$, ϵ_v with $\epsilon_3 = \epsilon_2$ and
$\epsilon_1 = \epsilon_v - (\epsilon_2 + \epsilon_3)$, $J_3^* = +1$

Zero strain I.P. this test.

(3) Based on: ϵ_2, ϵ_v.

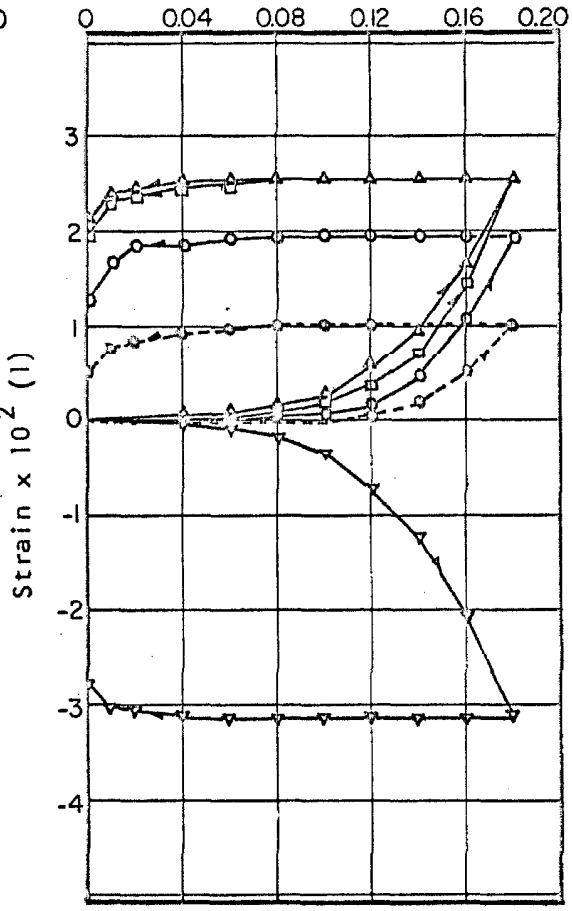

(1) Key: $\triangledown \epsilon_1$ $\odot \epsilon_1 + \epsilon_2 + \epsilon_3$
$\square \epsilon_2$ $\bigcirc \epsilon_v$ (dotted line)
$\triangle \epsilon_3$

Strains based on volume measurements corrected for pressure cell and rubber penetration. Zero strain I.P. this test.

	Initial	Yield(3)	Final(3)
η	0.340	0.343	0.343
$\epsilon_1 \times 10^2$	0	-2.38	-3.38
$\epsilon_2 \times 10^2$	0	+1.45	+1.94
$\epsilon_3 \times 10^2$	0	+1.45	+1.94
$J_1 \times 10^2$	0	+0.52	+0.50
$J_2 \times 10^3$	0	0.98	1.89
$-J_3^*$	-	+1	+1

$I_1 = 54$ psi., $I_2^* = 0 \leftrightarrow 0.18$, $I_3^* = +1$

Figure 7.28 Strains and Strain Invariants as a Function of the Second Modified and Dimensionless Stress Invariant.

Yield Test Nos. 4-4-I_{13}^* (TC & TC_R)

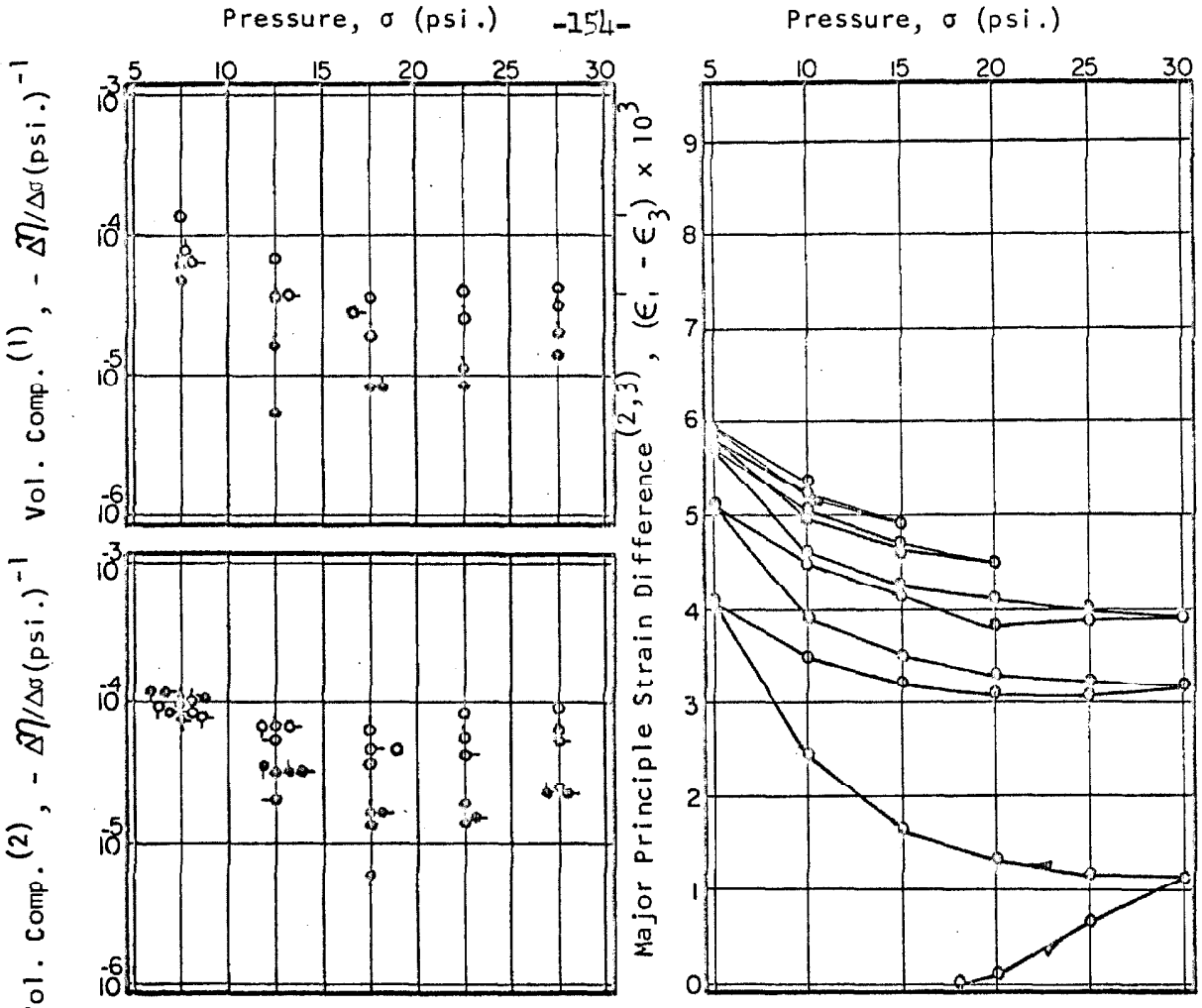

(1) Test Nos. 4-1-SC→4-3-SC

Key: ○ 4-1
◑ 4-2
◎ 4-3

Compression - Clear Circles
Extension - Solid Circles

η Initial = 0.341 η Final = 0.340

Compressibility based on volume measurements corrected for rubber penetration.

(2) Test Nos. 4-5-SC→4-10-SC

Key: ○ 4-5 ♀ 4-8
◑ 4-6 ◎ 4-9
♂ 4-7 ♀ 4-10

(3) Zero strain difference I.P. Test Series (2).

	Initial	Final (4)
η	0.343	0.342
$\epsilon_1 \times 10^2$	-3.38	-3.14
$\epsilon_2 \times 10^2$	+1.94	+1.74
$\epsilon_3 \times 10^2$	+1.94	+1.74
$J_1 \times 10^2$	+0.50	+0.34
$J_2 \times 10^3$	1.89	1.59
$-J_3$*	+1	+1

Zero Strain I.P. Test $4\text{-}4\text{-}I_{13}$* (TC)

(4) Basis of Calculation

$$\epsilon_1 = \epsilon_{10} + \epsilon_v'/3 + (\epsilon_1' - \epsilon_3')/2$$
$$\epsilon_2 = \epsilon_{20} + \epsilon_v'/3 - (\epsilon_1' - \epsilon_3')/4$$
$$\epsilon_3 = \epsilon_{30} + \epsilon_v'/3 - (\epsilon_1' - \epsilon_3')/4$$

Figure 7.29 Volumetric Compressibility and Apparent Major Principle Strain Difference as a Function of Applied Spherical Stress. Spherical Compression Test Nos. 4-1-SC through 4-3-SC and 4-5-SC through 4-10-SC

Table 7.7 Log of Experiment No. 5

Test Series	Stress History	Comments
5-1-SC through 5-5-SC	I_1 = 15 ↔ 90 psi, I_2*, I_3* = 0	Performed air vol test, V_A = 31 cc
5-6-I_{13}*(TE) 5-6-I_{13}*(TE_R)	I_1 = 54 psi, I_2* = 0→ 0.11, I_3* = -1 I_1 = 54 psi, I_2* = 0.11→0, I_3* = -1	Rate of strain increased in time at I_2* = 0.11. Flow valves closed, loads reduced, valves opened.
5-7-SC through 5-10-SC	I_1 = 15 ↔ 90 psi, I_2*, I_3* = 0	
5-11-I_{13}*(AC) 5-11-I_{13}*(AC_R)	I_1 = 54 psi, I_2* = 0→ 0.13, I_3* = 0 I_1 = 54 psi, I_2* = 0.13→ 0, I_3* = 0	Rate of strain increased in time at I_2* = 0.13. Flow valves closed, loads reduced, valves opened.
5-12-SC through 5-15-SC	I_1 = 15 ↔ 90 psi, I_2*, I_3* = 0	
5-16-I_{13}*(TC) 5-16-I_{13}*(TC_R)	I_1 = 54 psi, I_2* = 0→ 0.20, I_3* = 1 I_1 = 54 psi, I_2* = 0.20→ 0, I_3* = 1	Rate of strain increased in time at I_2* = 0.20. Flow valves closed, loads reduced, valves opened.
5-17-SC through 5-19-SC_R	I_1 = 15 ↔ 90 psi, I_2*, I_3* = 0	

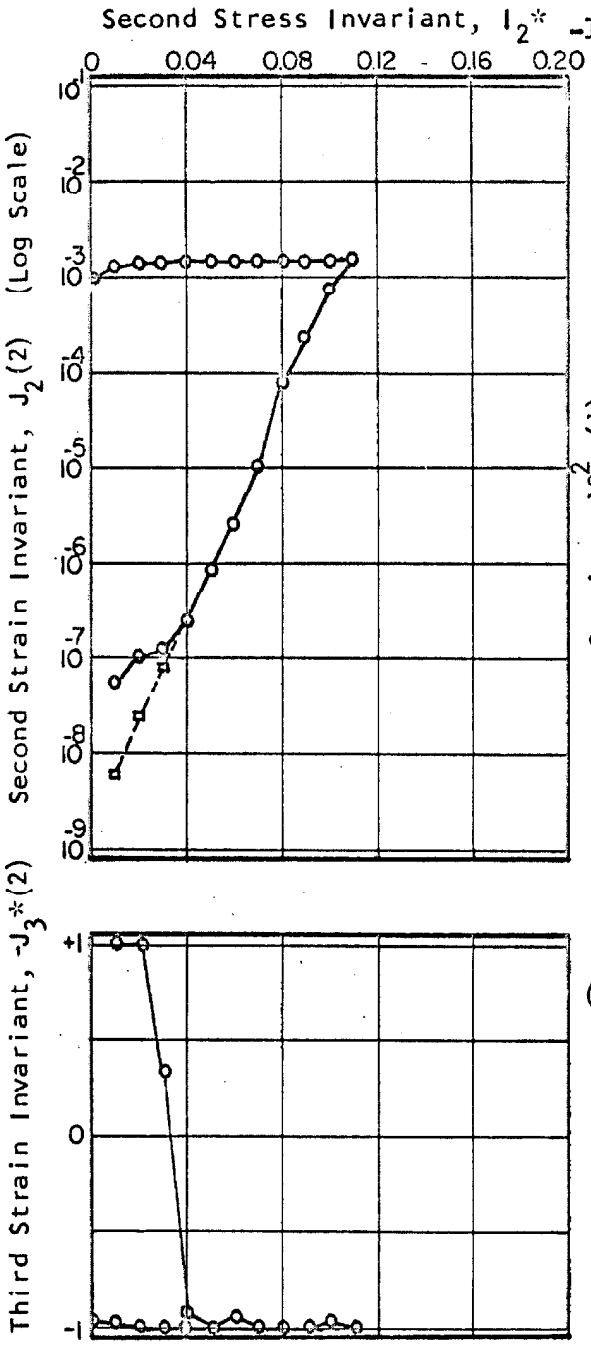

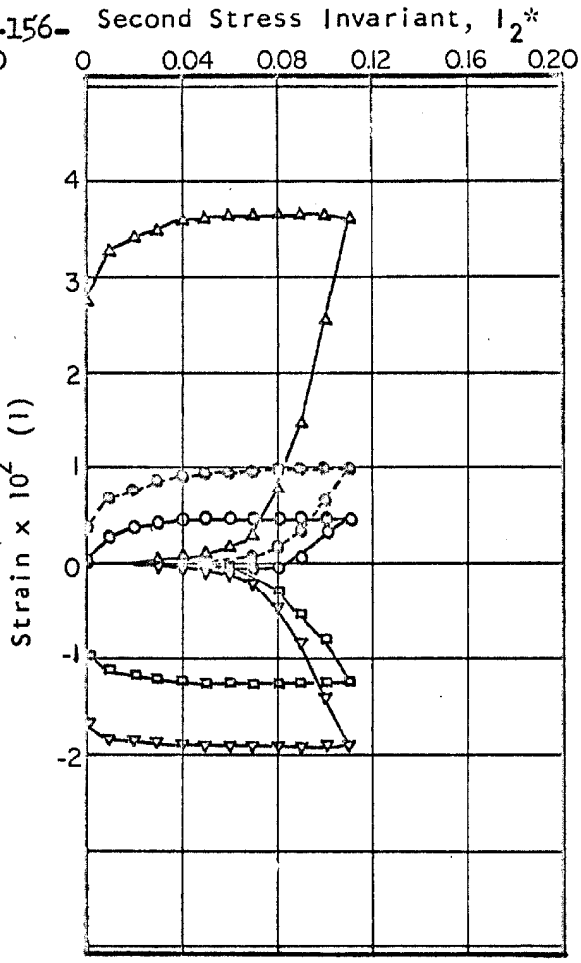

(1) Key: $\nabla\epsilon_1$ $\odot\epsilon_1+\epsilon_2+\epsilon_3$
$\boxdot\epsilon_2$ $\circ\epsilon_v$ (dotted line)
$\triangle\epsilon_3$

Strains based on volume measurements corrected for pressure cell and rubber penetration. Zero strain I.P. this test.

	Initial	Yield(3)	Final(3)
η	0.336	0.342	0.339
$\epsilon_1 \times 10^2$	0	-0.95	-1.15
$\epsilon_2 \times 10^2$	0	-0.95	-1.15
$\epsilon_3 \times 10^2$	0	+2.53	+2.67
$J_1 \times 10^2$	0	+0.63	+0.36
$J_2 \times 10^3$	0	0.81	0.98
$-J_3^*$	-	-1	-1

I_1= 54 psi., I_2^*=0→0.11, I_3^*= -1

(2) Basis of Calculation:
$\circ\epsilon_v$, ϵ_2, ϵ_3 with $\epsilon_1=\epsilon_v-(\epsilon_2+\epsilon_3)$
$\square\epsilon_v$, ϵ_3 with $\epsilon_1=\epsilon_2=(\epsilon_v-\epsilon_3)/2$

$J_3^* = -1$

(3) Based on: ϵ_v, ϵ_3

Figure 7.30 Strains and Strain Invariants as a Function of the Second Modified and Dimensionless Stress Invariant.
Yield Test No. 5-6-I_{13}* (TE & TE_R)

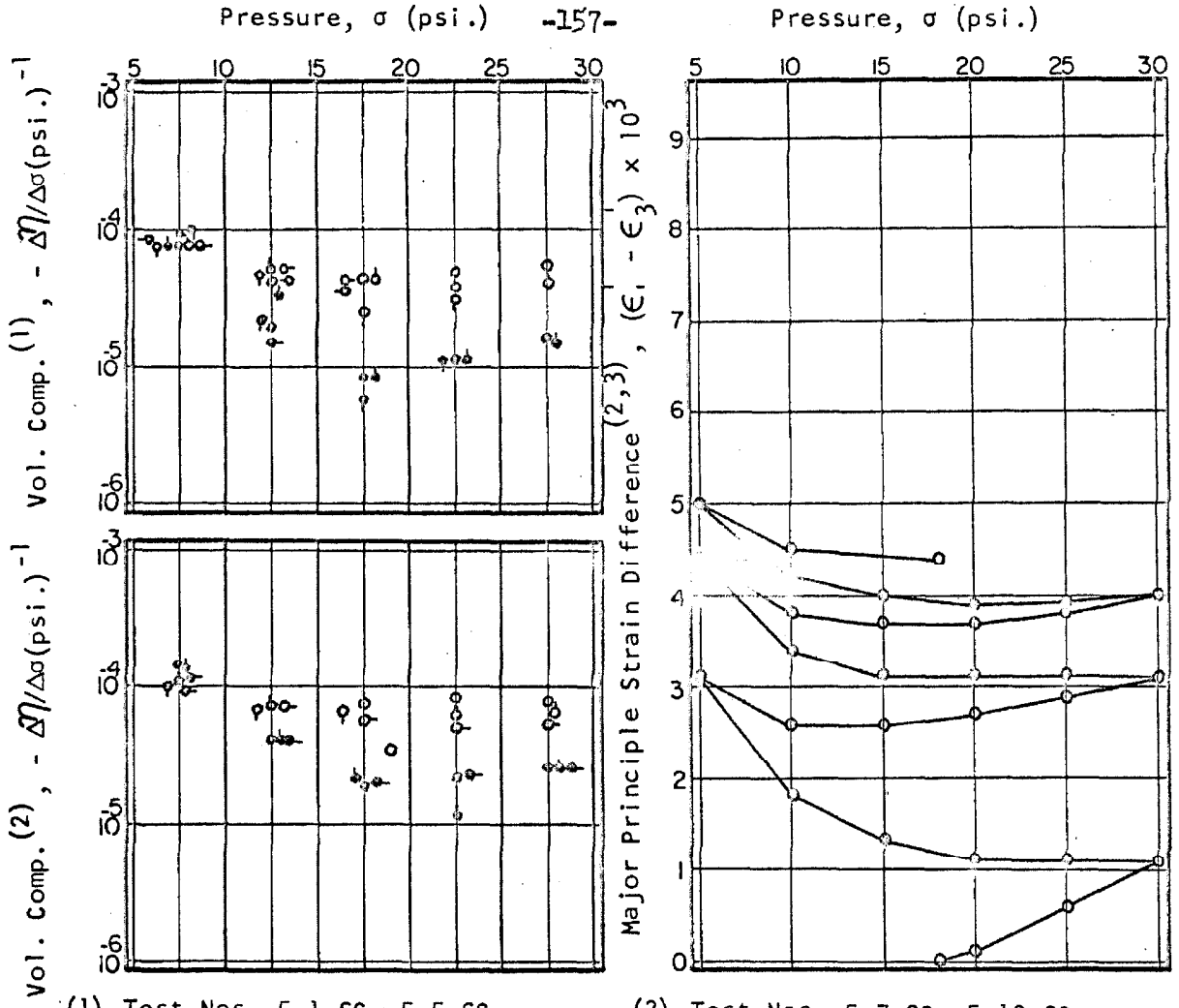

(1) Test Nos. 5-1-SC→5-5-SC
Key: ○ 5-1 ◐ 5-4
◑ 5-2 ◑ 5-5
○ 5-3

(2) Test Nos. 5-7-SC→5-10-SC
Key: ○ 5-7 ○ 5-9
◑ 5-8 ◐ 5-10

(3) Zero strain difference I.P. Test Series (2).

Compression - Clear Circles
Extension - Solid Circles

η Initial = 0.337 η Final = 0.336

Compressibility based on volume measurements corrected for rubber penetration.

	Initial	Final (4)
η	0.339	0.337
$\epsilon_1 \times 10^2$	-1.15	-7.51
$\epsilon_2 \times 10^2$	-1.15	-7.51
$\epsilon_3 \times 10^2$	+2.67	-4.02
$J_1 \times 10^2$	+0.36	-19.04
$J_2 \times 10^3$	0.98	0.81
$-J_3$*	-1	-1

Zero Strain I.P. Test 5-6-I_{13}* (TE)

(4) Basis of Calculation

$$\epsilon_1 = \epsilon_{10} + \epsilon_v'/3 + (\epsilon_1' - \epsilon_3')/4$$
$$\epsilon_2 = \epsilon_{20} + \epsilon_v'/3 + (\epsilon_1' - \epsilon_3')/4$$
$$\epsilon_3 = \epsilon_{30} + \epsilon_v'/3 - (\epsilon_1' - \epsilon_3')/2$$

Figure 7.31 Volumetric Compressibility and Apparent Major Principle Strain Difference as a Function of Applied Spherical Stress. Spherical Compression Test Nos. 5-1-SC through 5-5-SC and 5-7-SC through 5-10-SC

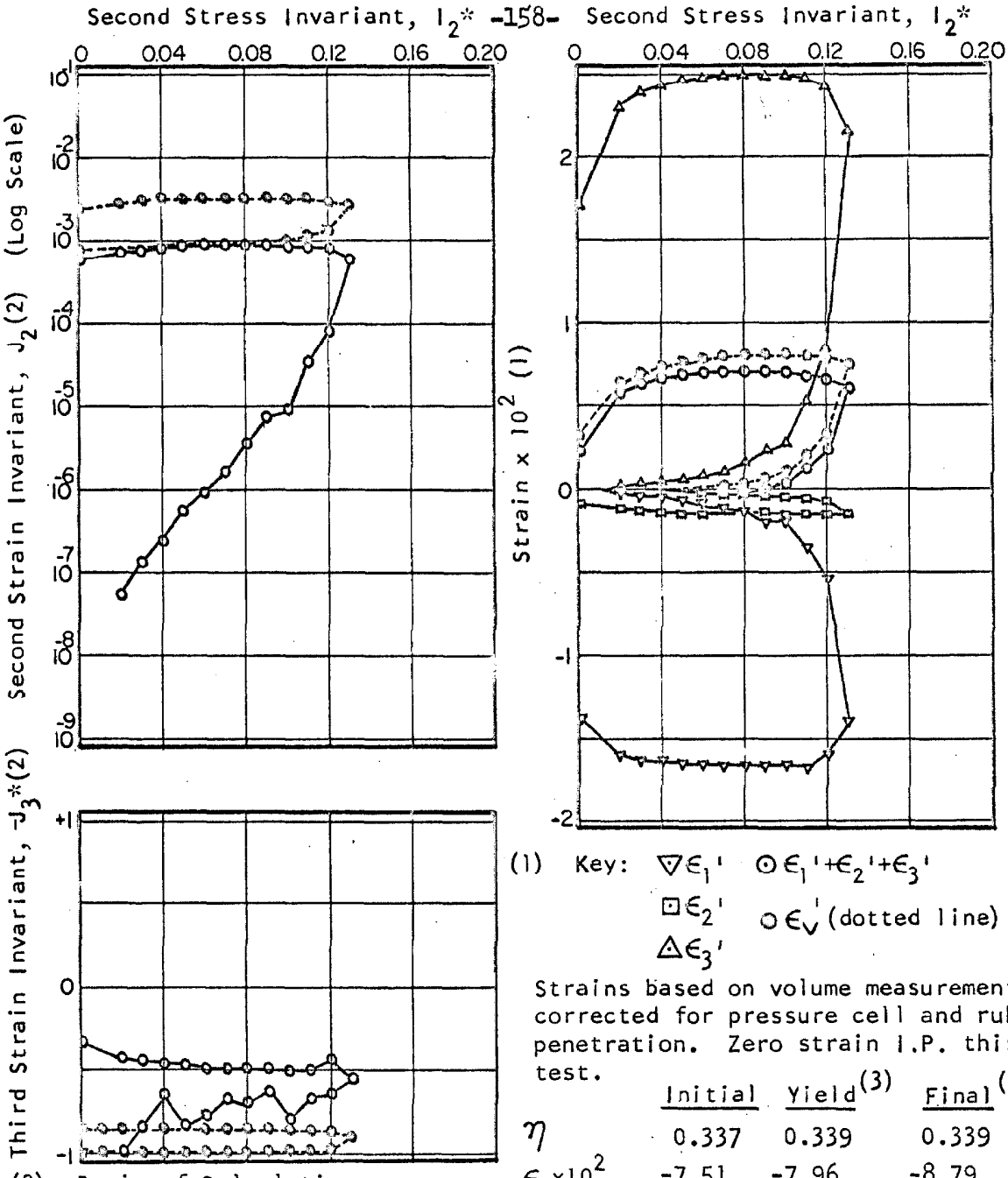

(1) Key: $\nabla\epsilon_1'$ $\odot\epsilon_1'+\epsilon_2'+\epsilon_3'$ $\square\epsilon_2'$ $\circ\epsilon_v'$ (dotted line) $\triangle\epsilon_3'$

Strains based on volume measurements corrected for pressure cell and rubber penetration. Zero strain I.P. this test.

	Initial	Yield(3)	Final(3)
η	0.337	0.339	0.339
$\epsilon_1 \times 10^2$	-7.51	-7.96	-8.79
$\epsilon_2 \times 10^2$	-7.51	-7.58	-7.60
$\epsilon_3 \times 10^2$	-4.02	-3.17	-2.33
$J_1 \times 10^2$	-19.04	-18.71	-18.72
$J_2 \times 10^3$	0.81	1.42	2.36
$-J_3^*$	-1	-0.98	-0.86

I_1 = 54 psi., I_2^*=0↔0.13, I_3^*= 0

(2) Basis of Calculation:
○ ϵ_v',ϵ_2',ϵ_3' with ϵ_1' = ϵ_v' - (ϵ_2'+ϵ_3'). Zero strain I.P. this test.
● ϵ_v,ϵ_2,ϵ_3 with $\epsilon_1=\epsilon_v-(\epsilon_2+\epsilon_3)$ Zero strain I.P. test 5-6-I_{13}^*(TE)

(3) Based on:
ϵ_v, ϵ_2, ϵ_3

Figure 7.32 Strains and Strain Invariants as a Function of the Second Modified and Dimensionless Stress Invariant.
Yield Test No. 5-11-I_{13}^* (AC &AC_R)

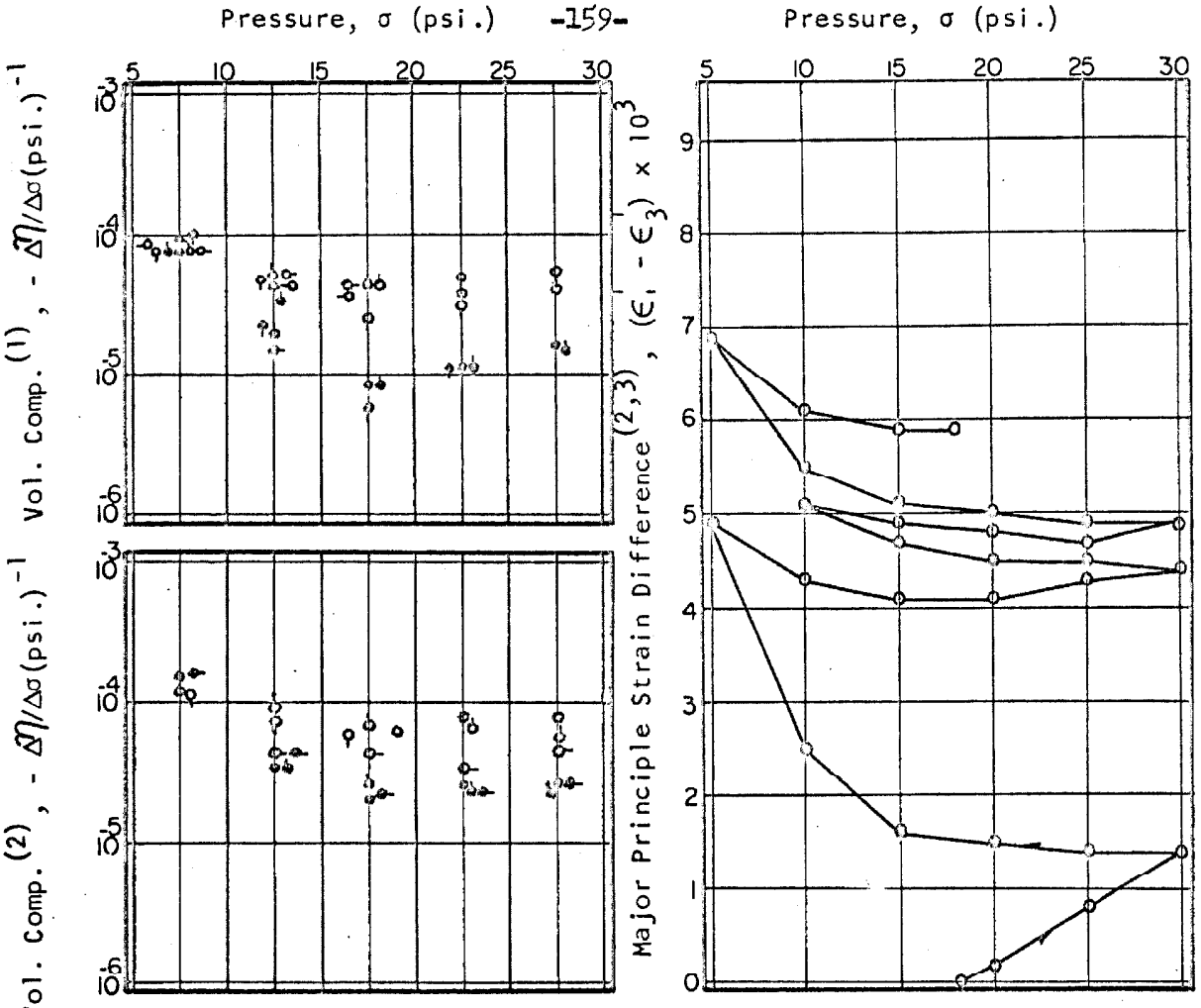

(1) Test Nos. 5-1-SC→5-5-SC
Key: ○ 5-1 ◐ 5-4
◑ 5-2 ◒ 5-5
◒ 5-3

(2) Test Nos. 5-12-SC→5-15-SC
Key: ○ 5-12 ◒ 5-14
◑ 5-13 ◐ 5-15

(3) Zero strain difference I.P. Test Series (2).

Compression - Clear Circles
Extension - Solid Circles

η Initial = 0.337 η Final = 0.336

Compressibility based on volume measurements corrected for rubber penetration.

	Initial	Final (4)
η	0.339	0.338
$\epsilon_1 \times 10^2$	-8.79	-14.40
$\epsilon_2 \times 10^2$	-7.60	-13.51
$\epsilon_3 \times 10^2$	-2.33	-8.54
$J_1 \times 10^2$	-18.72	-36.45
$J_2 \times 10^3$	2.36	1.99
$-J_3$*	-0.86	-0.91

Zero Strain I.P. Test 5-6-I_{13}* (TE)

(4) Basis of Calculation

$$\epsilon_1 = \epsilon_{10} + \epsilon_v'/3 + (\epsilon_1' - \epsilon_3')/2$$
$$\epsilon_2 = \epsilon_{20} + \epsilon_v'/3$$
$$\epsilon_3 = \epsilon_{30} + \epsilon_v'/3 - (\epsilon_1' - \epsilon_3')/2$$

Figure 7.33 Volumetric Compressibility and Apparent Major Principle Strain Difference as a Function of Applied Spherical Stress. Spherical Compression Test Nos. 5-1-SC through 5-5-SC and 5-12-SC through 5-15-SC

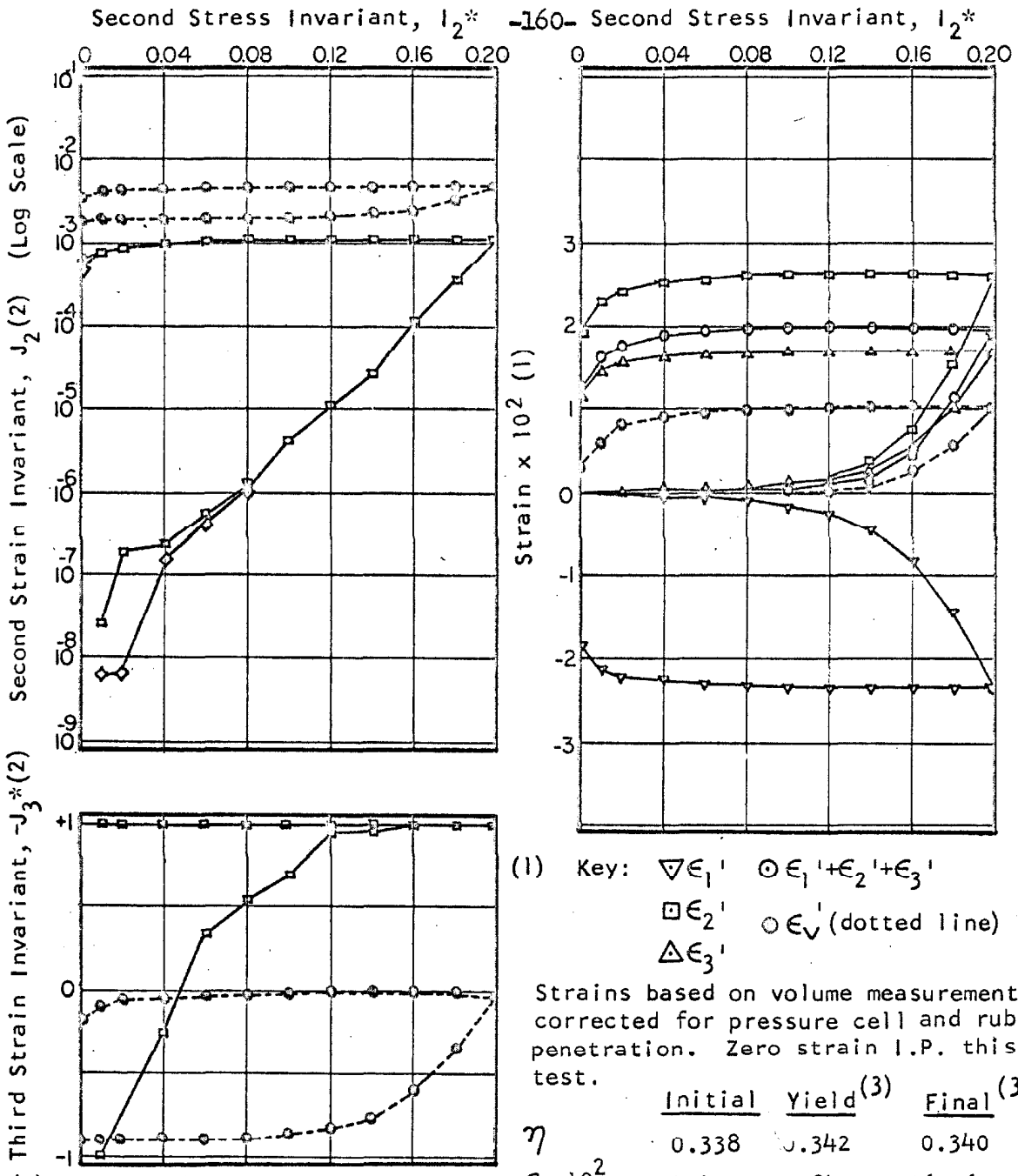

(1) Key: $\nabla\epsilon_1'$ $\odot\epsilon_1'+\epsilon_2'+\epsilon_3'$ $\square\epsilon_2'$ $\circ\epsilon_v'$ (dotted line) $\triangle\epsilon_3'$

Strains based on volume measurements corrected for pressure cell and rubber penetration. Zero strain I.P. this test.

	Initial	Yield(3)	Final(3)
η	0.338	0.342	0.340
$\epsilon_1 \times 10^2$	-14.40	-15.84	-16.26
$\epsilon_2 \times 10^2$	-13.51	-12.52	-12.43
$\epsilon_3 \times 10^2$	-8.54	-7.55	-7.46
$J_1 \times 10^2$	-36.45	-35.92	-36.15
$J_2 \times 10^3$	1.99	3.48	3.89
$-J_3^*$	-0.91	-0.34	-0.19

I_1 = 54 psi., I_2^*=0↔0.20, I_3^*= +1

(2) Basis of Calculation:

$\Diamond\epsilon_v', \epsilon_1'$ with $\epsilon_2'=\epsilon_3'=(\epsilon_v'-\epsilon_1')/2$

$\square\epsilon_v, \epsilon_1', \epsilon_3'$ with $\epsilon_2'=\epsilon_v'-(\epsilon_1'+\epsilon_3')$

$\circ\epsilon_v, \epsilon_1$ with $\epsilon_2=\epsilon_3=(\epsilon_v-\epsilon_1)/2$

(3) Based on: ϵ_v, ϵ_1. Zero strain I.P. test 5-6-I_{13}^*(TE)

Figure 7.34 Strains and Strain Invariants as a Function of the Second Modified and Dimensionless Stress Invariant.

Yield Test No. 5-16-I_{13}^* (TC & TC_R)

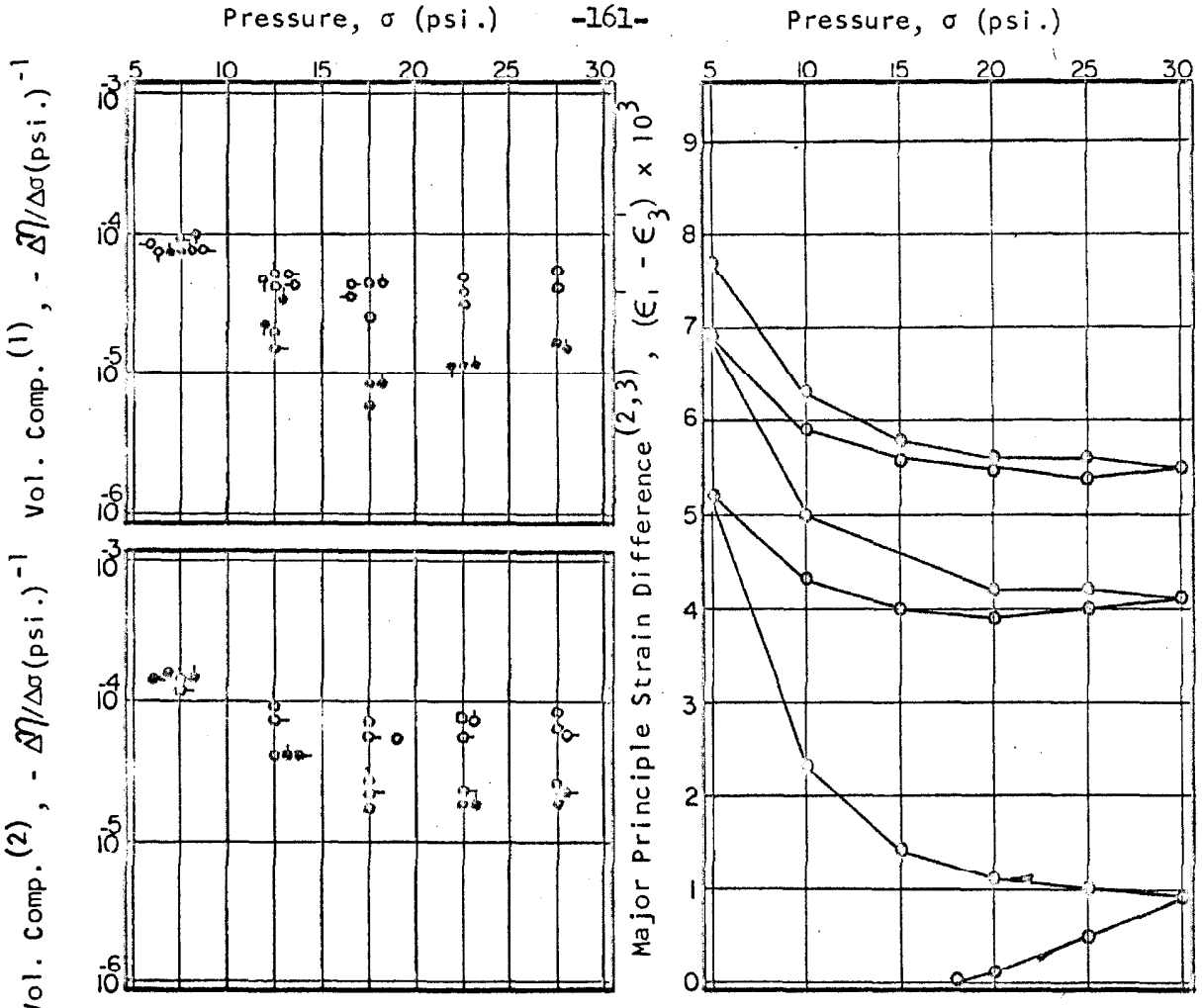

(1) Test Nos. 5-1-SC→5-5-SC
Key: o 5-1 ϙ 5-4
ȯ 5-2 -o 5-5
o- 5-3

Compression - Clear Circles
Extension - Solid Circles

η Initial =0.337 η Final =0.336

Compressibility based on volume measurements corrected for rubber penetration.

(2) Test Nos. 5-17-SC→5-19-SC
Key: o 5-17 o- 5-19
ȯ 5-18

(3) Zero strain difference I.P. Test Series (2).

	Initial	Final (4)
η	0.340	0.339
$\epsilon_1 \times 10^2$	-16.26	-19.56
$\epsilon_2 \times 10^2$	-12.43	-16.30
$\epsilon_3 \times 10^2$	-7.46	-11.33
$J_1 \times 10^2$	-36.15	-47.19
$J_2 \times 10^3$	3.89	3.44
$-J_3$*	-0.19	-0.35

Zero Strain I.P. Test 5-6-I_{13}* (TE)

(4) Basis of Calculation

$$\epsilon_1 = \epsilon_{10} + \epsilon_v'/3 + (\epsilon_1' - \epsilon_3')/2$$
$$\epsilon_2 = \epsilon_{20} + \epsilon_v'/3 - (\epsilon_1' - \epsilon_3')/4$$
$$\epsilon_3 = \epsilon_{30} + \epsilon_v'/3 - (\epsilon_1' - \epsilon_3')/4$$

Figure 7.35 Volumetric Compressibility and Apparent Major Principle Strain Difference as a Function of Applied Spherical Stress. Spherical Compression Test Nos. 5-1-SC through 5-5-SC and 5-17-SC through 5-19-SC

Table 7.8 Log of Experiment No. 6

Test Series	Stress History	Comments
6-1-SC through 6-5-SC	I_1 = 15 – 90 psi, I_2*, I_3* = 0	Performed air vol test, V_A = 94 cc
6-6-I_{13*}(TC)	I_1 = 54 psi, I_2* = 0 → 0.10, I_3* = 1	
6-7-I_{12R}	I_1 = 54 psi, I_2* = 0.10, I_3* = 1 → -1	
6-8-I_{13*}(TE_R)	I_1 = 54 psi, I_2* = 0.10 → 0, I_3* = -1	
6-9-SC through 6-11-SC_R	I_1 = 15 – 90 psi, I_2*, I_3* = 0	

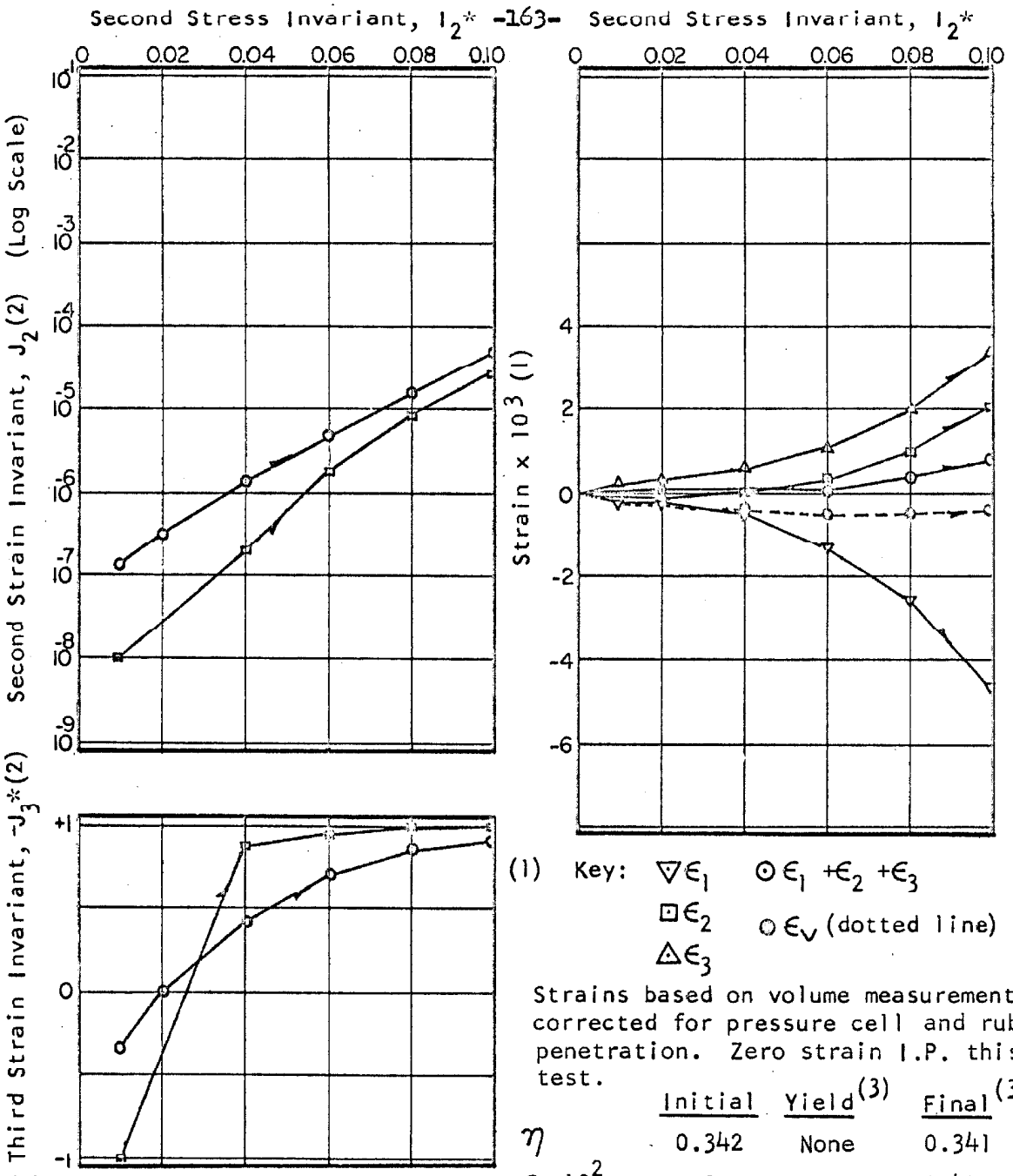

(1) Key: $\nabla\epsilon_1$ $\odot\epsilon_1+\epsilon_2+\epsilon_3$ $\square\epsilon_2$ $\circ\epsilon_v$ (dotted line) $\triangle\epsilon_3$

Strains based on volume measurements corrected for pressure cell and rubber penetration. Zero strain I.P. this test.

	Initial	Yield(3)	Final(3)
η	0.342	None	0.341
$\epsilon_1 \times 10^2$	0		-0.47
$\epsilon_2 \times 10^2$	0		+0.21
$\epsilon_3 \times 10^2$	0		+0.22
$J_1 \times 10^2$	0		-0.04
$J_2 \times 10^5$	0		3.13
$-J_3^*$	-		+1

(2) Basis of Calculation:

$\circ\ \epsilon_v, \epsilon_2, \epsilon_3$ with $\epsilon_1 = \epsilon_v - (\epsilon_2+\epsilon_3)$

$\square\ \epsilon_v, \epsilon_1, \epsilon_2$ with $\epsilon_3 = \epsilon_v - (\epsilon_1+\epsilon_2)$

(3) Based on: $\epsilon_v, \epsilon_1, \epsilon_2$.

$I_1 = 54$ psi., $I_2^* = 0 \rightarrow 0.10$, $I_3^* = +1$

Figure 7.36 Strains and Strain Invariants as a Function of the Second Modified and Dimensionless Stress Invariant.

Triaxial Compression Test No. 6-6-I_{13} (TC)

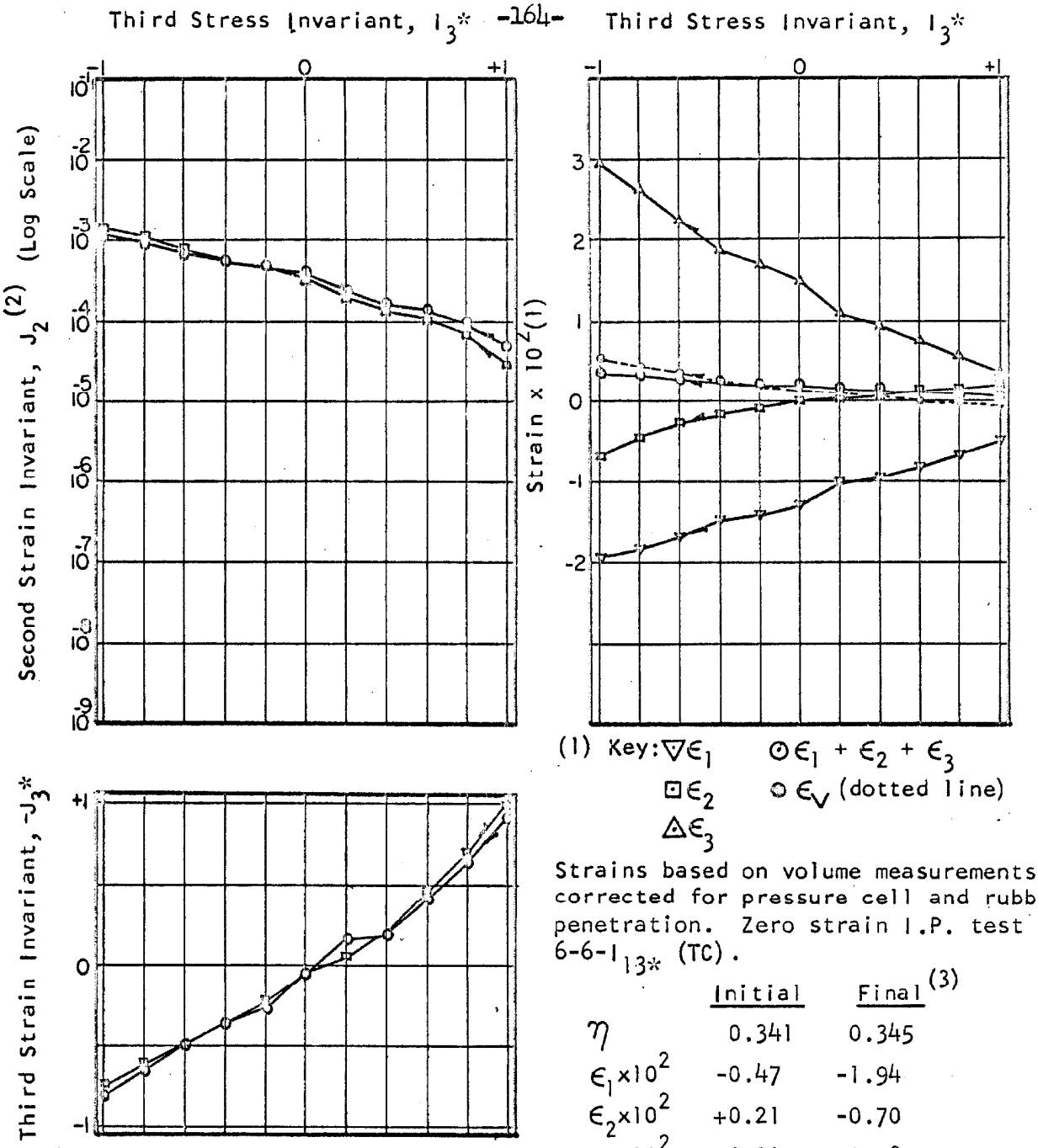

Strains based on volume measurements corrected for pressure cell and rubber penetration. Zero strain I.P. test 6-6-I_{13}* (TC).

	Initial	Final (3)
η	0.341	0.345
$\epsilon_1 \times 10^2$	-0.47	-1.94
$\epsilon_2 \times 10^2$	+0.21	-0.70
$\epsilon_3 \times 10^2$	+0.22	+3.18
$J_1 \times 10^2$	-0.04	+0.54
$J_2 \times 10^5$	3.13	143
$-J_3^*$	+1	-0.76

I_1=54 psi, I_2^*= 0.10 , I_3^*=+1→ -1

Figure 7.37 Strains and Strain Invariants as a Function of the Third Modified and Dimensionless Stress Invariant.

Circular Compression Test Nos. 6-7-I_{12R}

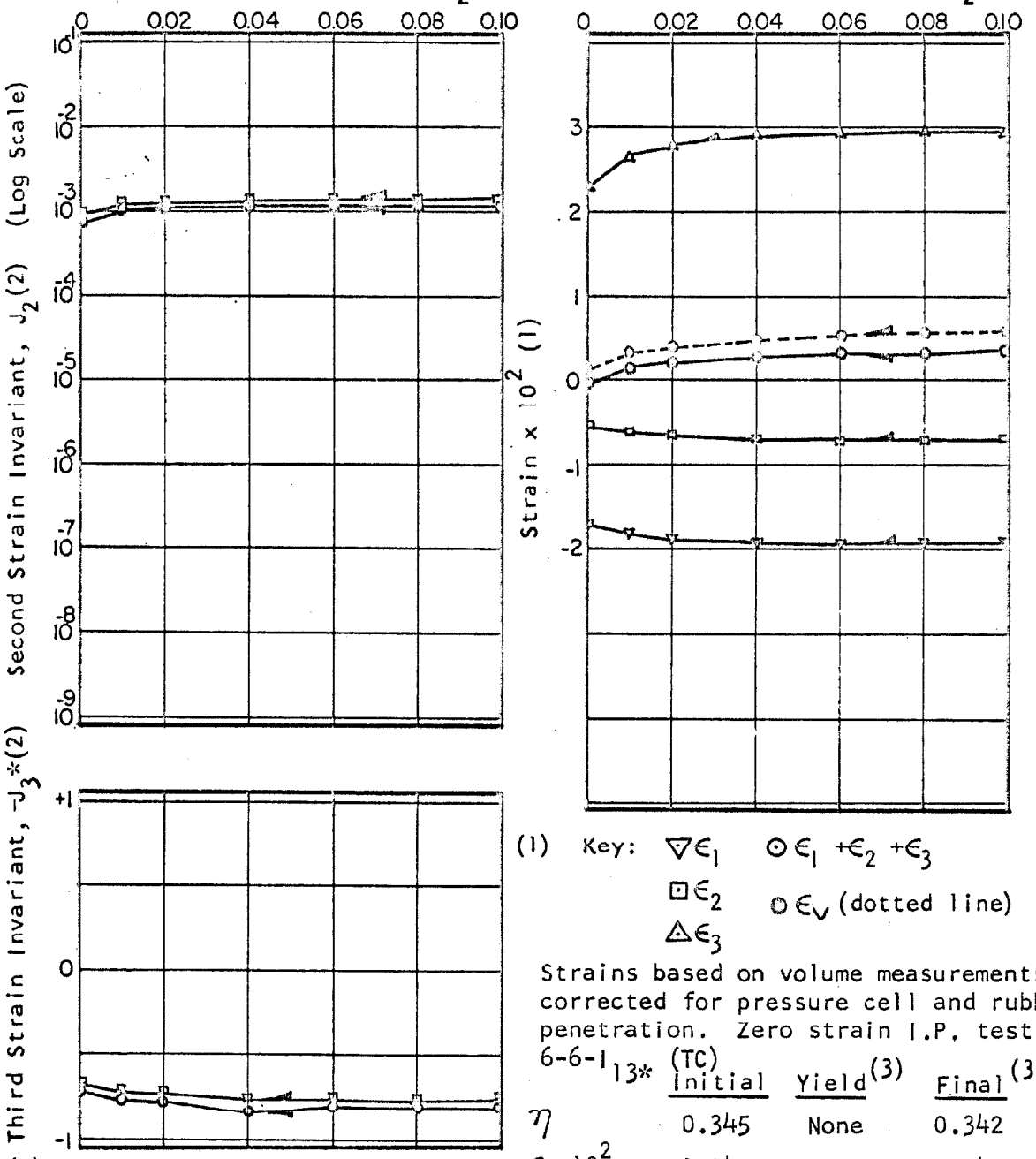

(1) Key: $\nabla\epsilon_1$ $\odot\epsilon_1+\epsilon_2+\epsilon_3$ $\boxdot\epsilon_2$ $\circ\epsilon_v$ (dotted line) $\triangle\epsilon_3$

Strains based on volume measurements corrected for pressure cell and rubber penetration. Zero strain I.P. test

$6\text{-}6\text{-}I_{13}^*$ (TC)	Initial	Yield(3)	Final(3)
η	0.345	None	0.342
$\epsilon_1 \times 10^2$	-1.94		-1.74
$\epsilon_2 \times 10^2$	-0.70		-0.58
$\epsilon_3 \times 10^2$	+3.18		+2.39
$J_1 \times 10^2$	+0.54		+0.07
$J_2 \times 10^3$	1.43		0.91
$-J_3^*$	-0.76		-0.67

I_1= 54 psi., I_2^*=0.10→0, I_3^*= -1

(2) Basis of Calculation:

$\odot\epsilon_v$, ϵ_2, ϵ_3 with $\epsilon_1 = \epsilon_v - (\epsilon_2+\epsilon_3)$

$\square\epsilon_v$, ϵ_1, ϵ_2 with $\epsilon_3 = \epsilon_v - (\epsilon_1+\epsilon_2)$

(3) Based on: ϵ_v, ϵ_1, ϵ_2.

Figure 7.38 Strains and Strain Invariants as a Function of the Second Modified and Dimensionless Stress Invariant.

Triaxial Extension Test No. $6\text{-}8\text{-}I_{13}^*$ (TE_R)

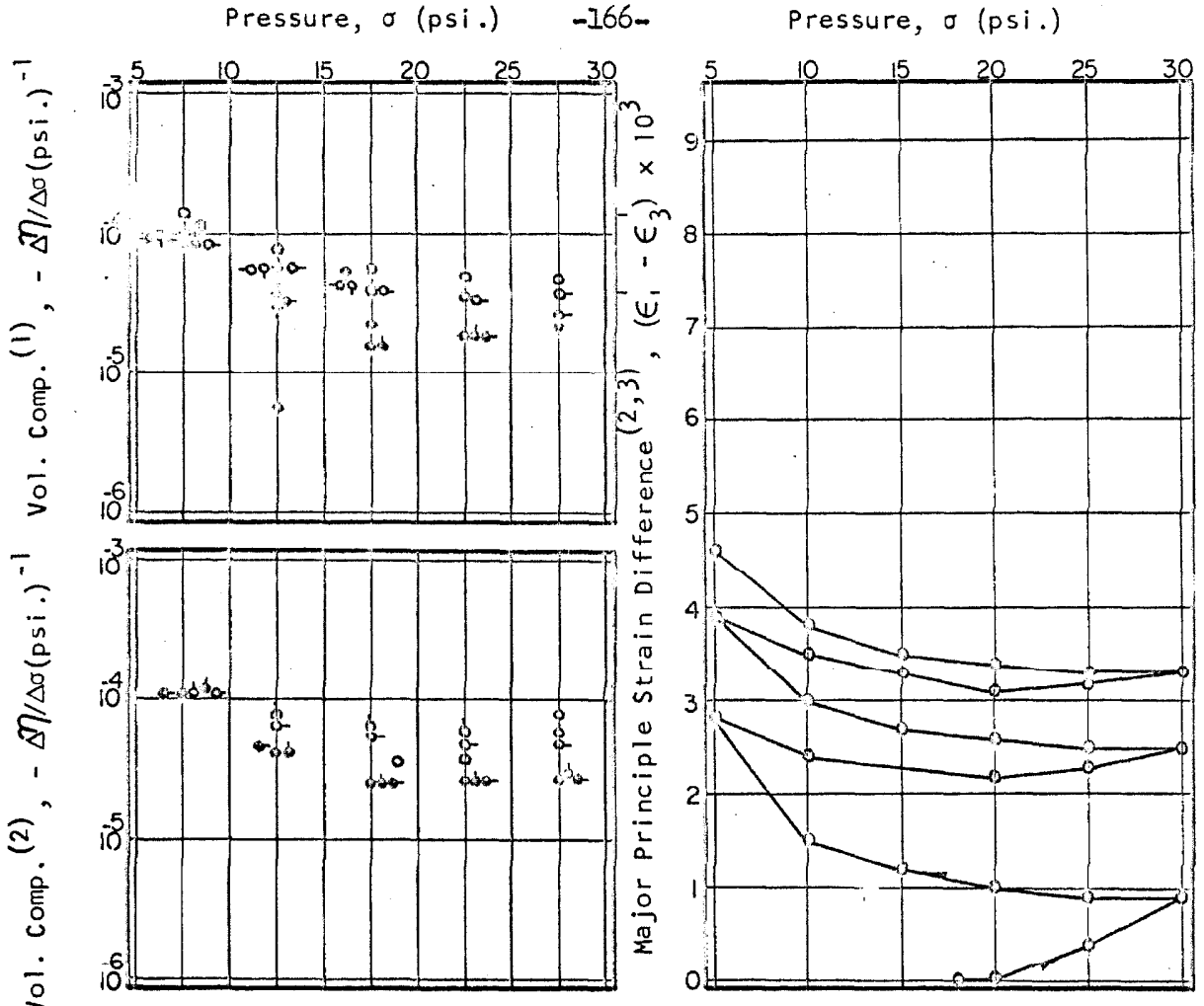

(1) Test Nos. 6-1-SC→ 6-5-SC
Key: o 6-1 ♀ 6-4
♁ 6-2 -o 6-5
o- 6-3

(2) Test Nos. 6-9-SC→6-11-SC
Key: o 6-9 o-6-11
♁ 6-10

(3) Zero strain difference I.P. Test Series (2).

Compression - Clear Circles
Extension - Solid Circles

η Initial = 0.343 η Final = 0.342

Compressibility based on volume measurements corrected for rubber penetration.

	Initial	Final (4)
η	0.342	0.342
$\epsilon_1 \times 10^2$	-1.74	-1.53
$\epsilon_2 \times 10^2$	-0.58	-0.60
$\epsilon_3 \times 10^2$	+2.39	+2.13
$J_1 \times 10^2$	+0.07	0.00
$J_2 \times 10^3$	0.91	0.72
$-J_3$*	-0.67	-0.73

Zero Strain I.P. Test 6-6-I_{13}* (TC)

(4) Basis of Calculation

$$\epsilon_1 = \epsilon_{10} + \epsilon_v'/3 + (\epsilon_1' - \epsilon_3')/2$$
$$\epsilon_2 = \epsilon_{20} + \epsilon_v'/3$$
$$\epsilon_3 = \epsilon_{30} + \epsilon_v'/3 - (\epsilon_1' - \epsilon_3')/2$$

Figure 7.39 Volumetric Compressibility and Apparent Major Principle Strain Difference as a Function of Applied Spherical Stress. Spherical Compression Test Nos. 6-1-SC through 6-5-SC and 6-9-SC through 6-11-SC

Table 7.9 Log of Experiment Nos. 8 through 15

Test Series	Stress History	Comments
9-4-I_{13*}, I_{13*R}	I_1 = 54 psi, I_2^* = 0 ↔ 0.12, I_3^* = -0.8	
14-5-I_{13*}, I_{13*R}	I_1 = 54 psi, I_2^* = 0 ↔ 0.12, I_3^* = -0.6	
15-5-I_{13*}, I_{13*R}	I_1 = 54 psi, I_2^* = 0 ↔ 0.12, I_3^* = -0.4	
10-4-I_{13*}, I_{13*R}	I_1 = 54 psi, I_2^* = 0 ↔ 0.13, I_3^* = -0.2	Local yield
11-5-I_{13*}, I_{13*R}	I_1 = 54 psi, I_2^* = 0 ↔ 0.14, I_3^* = 0.2	
12-5-I_{13*}, I_{13*R}	I_1 = 54 psi, I_2^* = 0 ↔ 0.15, I_3^* = 0.4	
13-5-I_{13*}, I_{13*R}	I_1 = 54 psi, I_2^* = 0 ↔ 0.16, I_3^* = 0.6	
8-5-I_{13*}, I_{13*R}	I_1 = 54 psi, I_2^* = 0 ↔ 0.18, I_3^* = 0.8	

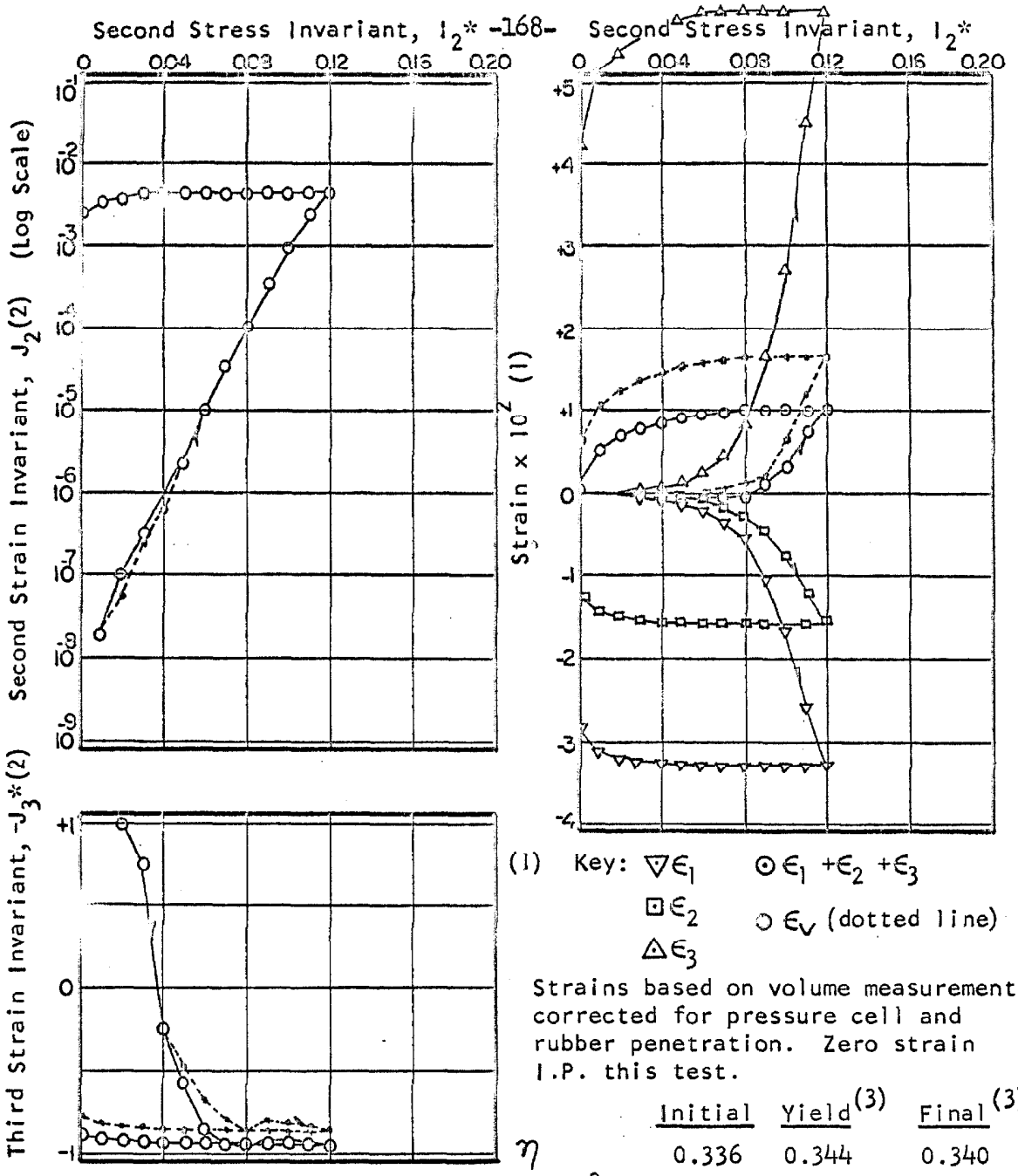

(1) Key: $\nabla\epsilon_1$ $\odot\epsilon_1+\epsilon_2+\epsilon_3$ $\boxdot\epsilon_2$ $\circ\epsilon_v$ (dotted line) $\triangle\epsilon_3$

Strains based on volume measurements corrected for pressure cell and rubber penetration. Zero strain I.P. this test.

(2) Basis of Calculation:

$\epsilon_1, \epsilon_2, \epsilon_3$.

$\epsilon_v, \epsilon_2, \epsilon_3$ with $\epsilon_1 = \epsilon_v - (\epsilon_2 + \epsilon_3)$

Zero strain I.P. this test.

(3) Based on ϵ_v, ϵ_2, ϵ_3

	Initial	Yield(3)	Final(3)
η	0.336	0.344	0.340
$\epsilon_1 \times 10^2$	0	-2.10	-2.33
$\epsilon_2 \times 10^2$	0	-1.20	-1.24
$\epsilon_3 \times 10^2$	0	+4.50	+4.18
$J_1 \times 10^2$	0	+1.20	+0.61
$J_2 \times 10^3$	0	2.56	2.43
$-J_3^*$		-0.93	-0.89

$I_1 = 54$ psi, $I_2^* = 0 \rightarrow 0.12$, $I_3^* = -0.8$

Figure 7.40 Strains and Strain Invariants as a Function of the Second Modified and Dimensionless Stress Invariant. Yield Test Nos. 9-4-1 13* & 13*R

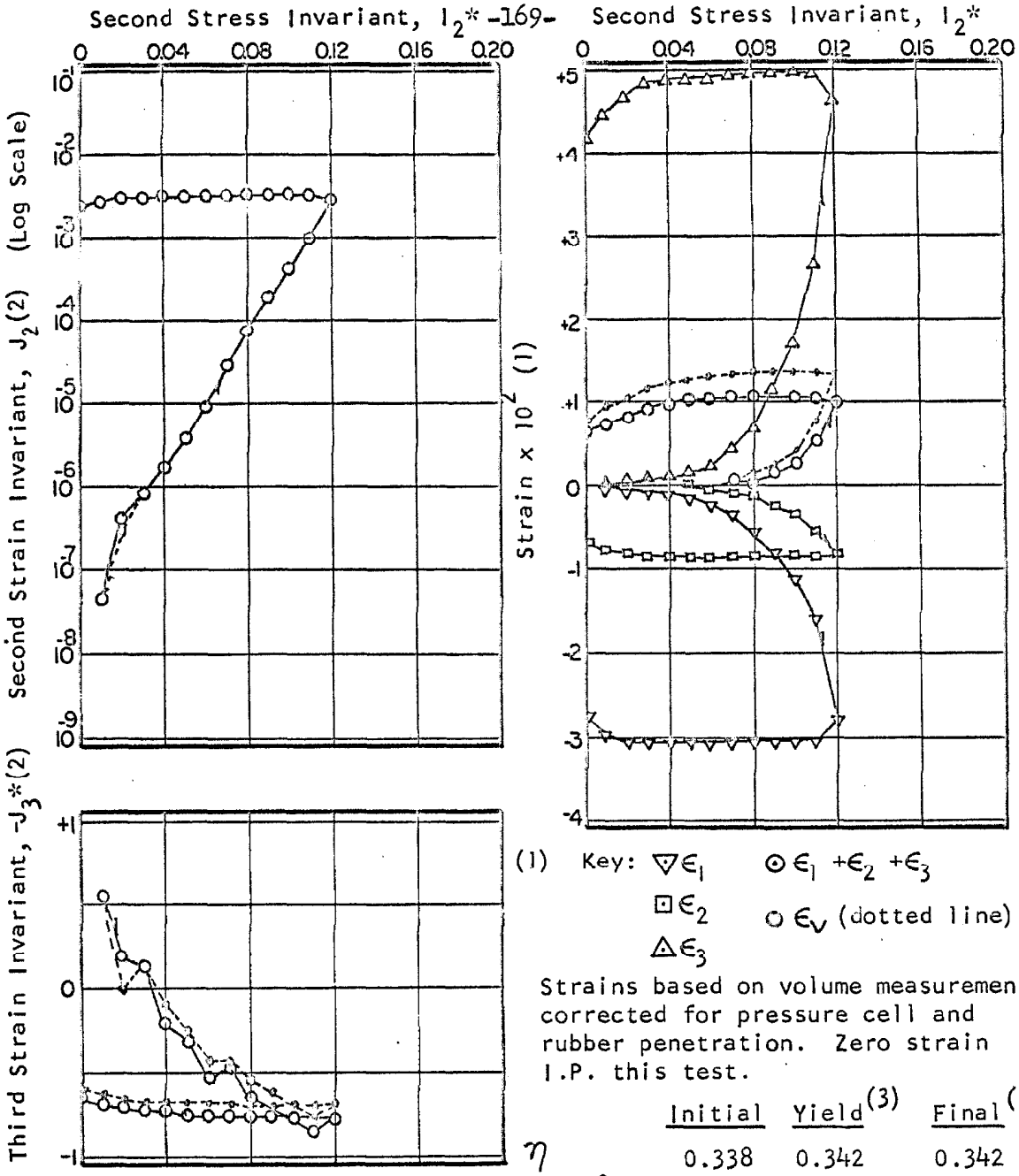

(1) Key: $\nabla\epsilon_1$ $\odot\epsilon_1+\epsilon_2+\epsilon_3$
$\boxdot\epsilon_2$ $\circ\epsilon_v$ (dotted line)
$\triangle\epsilon_3$

Strains based on volume measurements corrected for pressure cell and rubber penetration. Zero strain I.P. this test.

(2) Basis of Calculation:

$\cdot\!\circ\!\cdot\ \epsilon_1, \epsilon_2, \epsilon_3$.

$\circ\ \epsilon_v, \epsilon_2, \epsilon_3$ with $\epsilon_1 = \epsilon_v - (\epsilon_2 + \epsilon_3)$

Zero strain I.P. this test.

(3) Based on ϵ_v, ϵ_2, ϵ_3

	Initial	Yield(3)	Final(3)
η	0.338	0.342	0.342
$\epsilon_1 \times 10^2$	0	-1.38	-2.66
$\epsilon_2 \times 10^2$	0	-0.56	-0.68
$\epsilon_3 \times 10^2$	0	+2.67	+4.07
$J_1 \times 10^2$	0	+0.73	+0.73
$J_2 \times 10^3$	0	0.92	2.39
$-J_3^*$		-0.84	-0.65

I_1 = 54 psi, I_2^*=0 to 0.12, I_3^* = -0.6

Figure 7.41 Strains and Strain Invariants as a Function of the Second Modified and Dimensionless Stress Invariant. Yield Test Nos. 14-5-I_{13^*} & 13*R

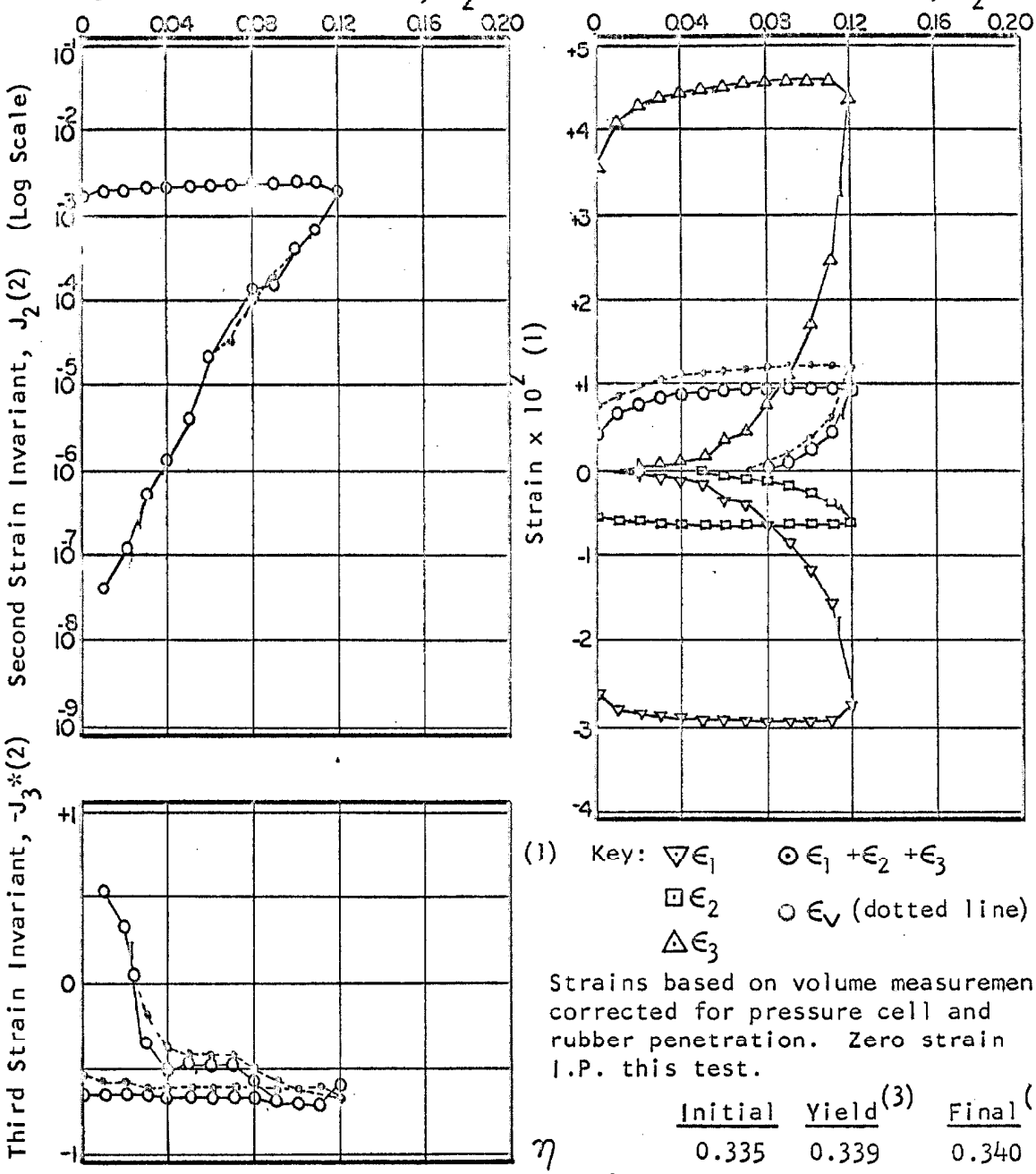

(1) Key: $\nabla\epsilon_1$ $\odot\epsilon_1+\epsilon_2+\epsilon_3$
$\square\epsilon_2$ $\circ\epsilon_v$ (dotted line)
$\triangle\epsilon_3$

Strains based on volume measurements corrected for pressure cell and rubber penetration. Zero strain I.P. this test.

(2) Basis of Calculation:

$\epsilon_1, \epsilon_2, \epsilon_3$.

$\epsilon_v, \epsilon_2, \epsilon_3$ with $\epsilon_1 = \epsilon_v - (\epsilon_2 + \epsilon_3)$

Zero strain I.P. this test.

(3) Based on ϵ_v, ϵ_2, ϵ_3

	Initial	Yield(3)	Final(3)
η	0.335	0.339	0.340
$\epsilon_1 \times 10^2$	0	-1.42	-2.26
$\epsilon_2 \times 10^2$	0	-0.40	-0.52
$\epsilon_3 \times 10^2$	0	+2.42	+3.54
$J_1 \times 10^2$	0	+0.60	+0.76
$J_2 \times 10^3$	0	0.79	1.77
$-J_3^*$		-0.70	-0.63

$I_1 = 54$ psi, $I_2^* = 0 \leftrightarrow 0.12$, $I_3^* = -0.4$

Figure 7.42 Strains and Strain Invariants as a Function of the Second Modified and Dimensionless Stress Invariant. Yield Test Nos. 15-5-I_{13*} & 13*R

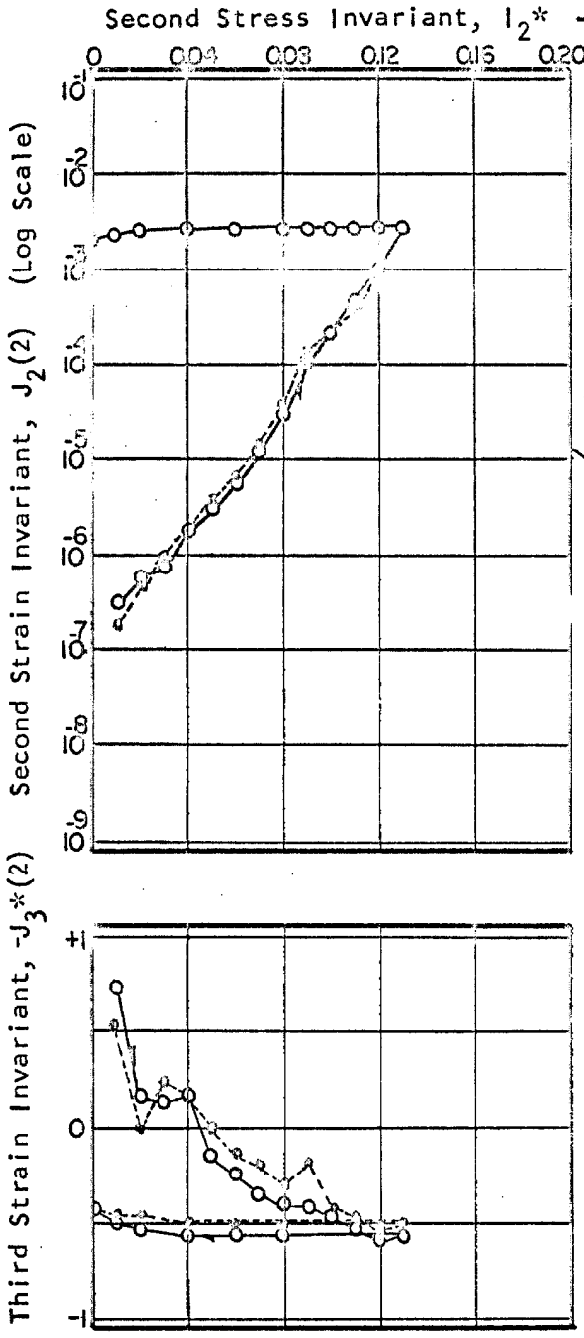

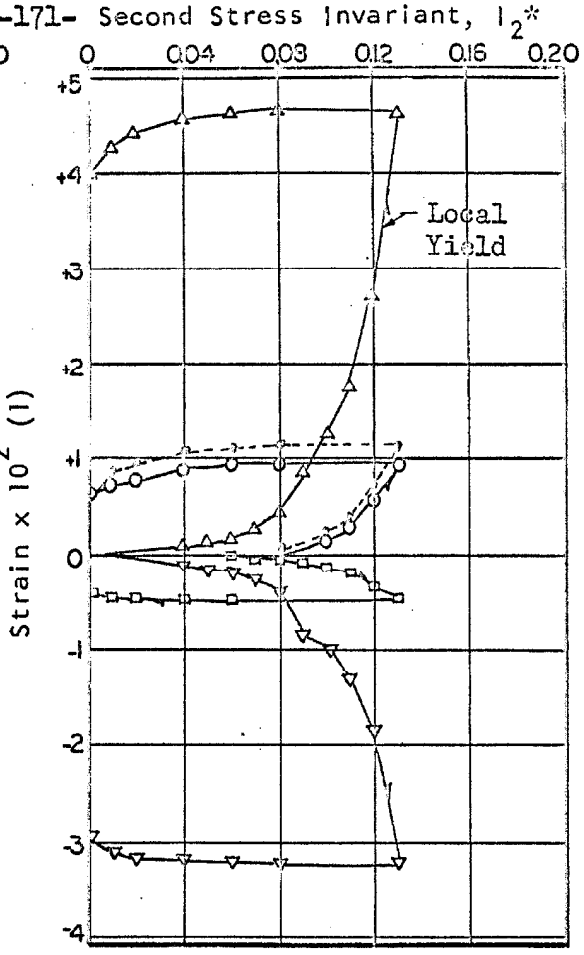

(1) Key: $\nabla\epsilon_1$ $\odot\epsilon_1+\epsilon_2+\epsilon_3$
$\square\epsilon_2$ $\circ\epsilon_v$ (dotted line)
$\triangle\epsilon_3$

Strains based on volume measurements corrected for pressure cell and rubber penetration. Zero strain I.P. this test.

	Initial	Yield(3)	Final(3)
η	0.339	0.343	0.343
$\epsilon_1 \times 10^2$	0	-1.73	-3.00
$\epsilon_2 \times 10^2$	0	-0.31	-0.40
$\epsilon_3 \times 10^2$	0	+2.76	+3.99
$J_1 \times 10^2$	0	+0.72	+0.59
$J_2 \times 10^3$	0	1.05	2.50
$-J_3^*$		-0.57	-0.43

(2) Basis of Calculation:

--o-- ϵ_1, ϵ_2, ϵ_3.

—o— $\epsilon_v, \epsilon_2, \epsilon_3$ with $\epsilon_1 = \epsilon_v - (\epsilon_2 + \epsilon_3)$

Zero strain I.P. this test.

(3) Based on ϵ_v, ϵ_2, ϵ_3

I_1 = 54 psi, I_2^* = 0 ↔ 0.13, I_3^* = -0.2

Figure 7.43 Strains and Strain Invariants as a Function of the Second Modified and Dimensionless Stress Invariant. Yield Test Nos. 10-4-1 13* & 13*R

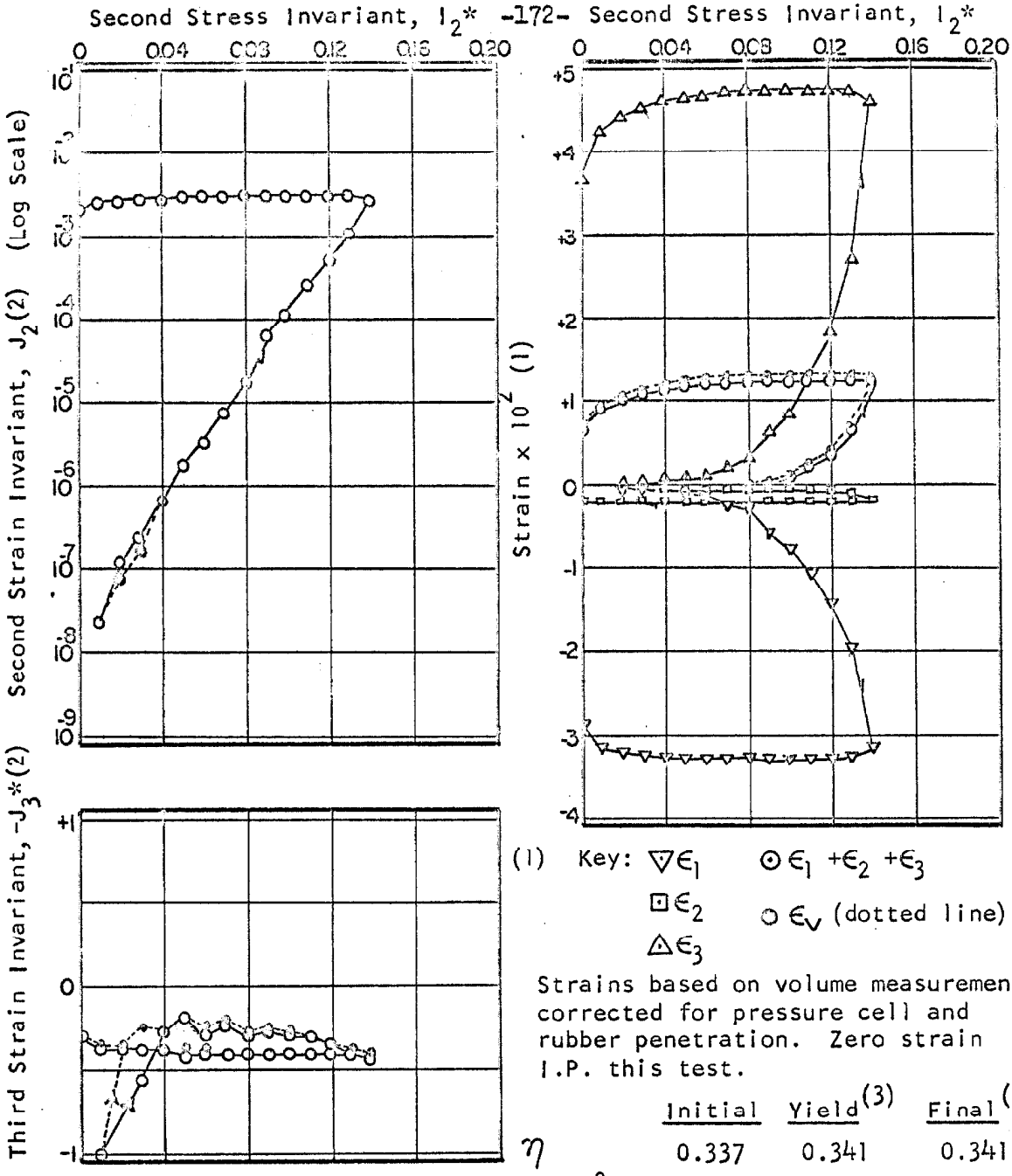

(1) Key: $\nabla\epsilon_1$ $\odot\epsilon_1+\epsilon_2+\epsilon_3$
$\boxdot\epsilon_2$ $\circ\epsilon_v$ (dotted line)
$\triangle\epsilon_3$

Strains based on volume measurements corrected for pressure cell and rubber penetration. Zero strain I.P. this test.

(2) Basis of Calculation:

$\cdots\circ\epsilon_1, \epsilon_2, \epsilon_3$.

$-\circ\epsilon_v, \epsilon_2, \epsilon_3$ with $\epsilon_1=\epsilon_v-(\epsilon_2+\epsilon_3)$

Zero strain I.P. this test.

(3) Based on ϵ_v, ϵ_2, ϵ_3

	Initial	Yield(3)	Final(3)
η	0.337	0.341	0.341
$\epsilon_1 \times 10^2$	0	-1.87	-2.86
$\epsilon_2 \times 10^2$	0	-0.12	-0.17
$\epsilon_3 \times 10^2$	0	+2.70	+3.70
$J_1 \times 10^2$	0	+0.71	+0.67
$J_2 \times 10^3$	0	1.06	2.17
$-J_3^*$		-0.40	-0.30

I_1= 54 psi, I_2^*=0↔0.14, I_3^*= +0.2

Figure 7.44 Strains and Strain Invariants as a Function of the Second Modified and Dimensionless Stress Invariant. Yield Test Nos. 11-5-I_{13}* & 13*R

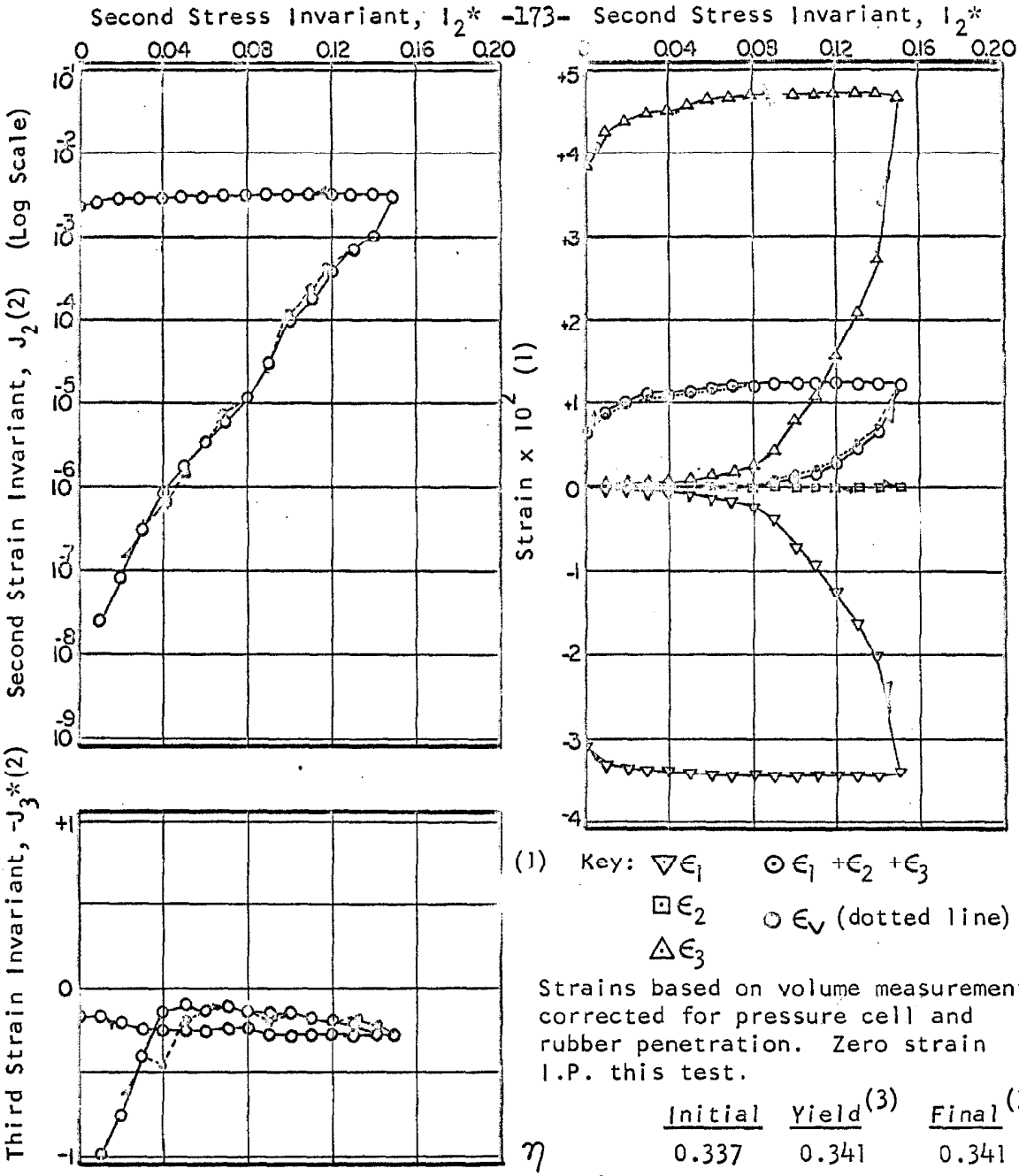

(1) Key: $\nabla\epsilon_1$ $\odot\epsilon_1+\epsilon_2+\epsilon_3$ $\boxdot\epsilon_2$ $\circ\epsilon_v$ (dotted line) $\triangle\epsilon_3$

Strains based on volume measurements corrected for pressure cell and rubber penetration. Zero strain I.P. this test.

(2) Basis of Calculation:

---o--- $\epsilon_1, \epsilon_2, \epsilon_3$.

—o— $\epsilon_v, \epsilon_2, \epsilon_3$ with $\epsilon_1=\epsilon_v-(\epsilon_2+\epsilon_3)$

Zero strain I.P. this test.

(3) Based on ϵ_v, ϵ_2, ϵ_3

	Initial	Yield(3)	Final(3)
η	0.337	0.341	0.341
$\epsilon_1 \times 10^2$	0	-1.99	-3.14
$\epsilon_2 \times 10^2$	0	.0	0
$\epsilon_3 \times 10^2$	0	+2.70	+3.77
$J_1 \times 10^2$	0	+0.71	+0.63
$J_2 \times 10^3$	0	1.11	2.39
$-J_3^*$		-0.27	-0.17

I_1= 54 psi, I_2^*=0→0.15, I_3^*= +0.4

Figure 7.45 Strains and Strain Invariants as a Function of the Second Modified and Dimensionless Stress Invariant. Yield Test Nos. 12-5-I_{13}* & 13*R

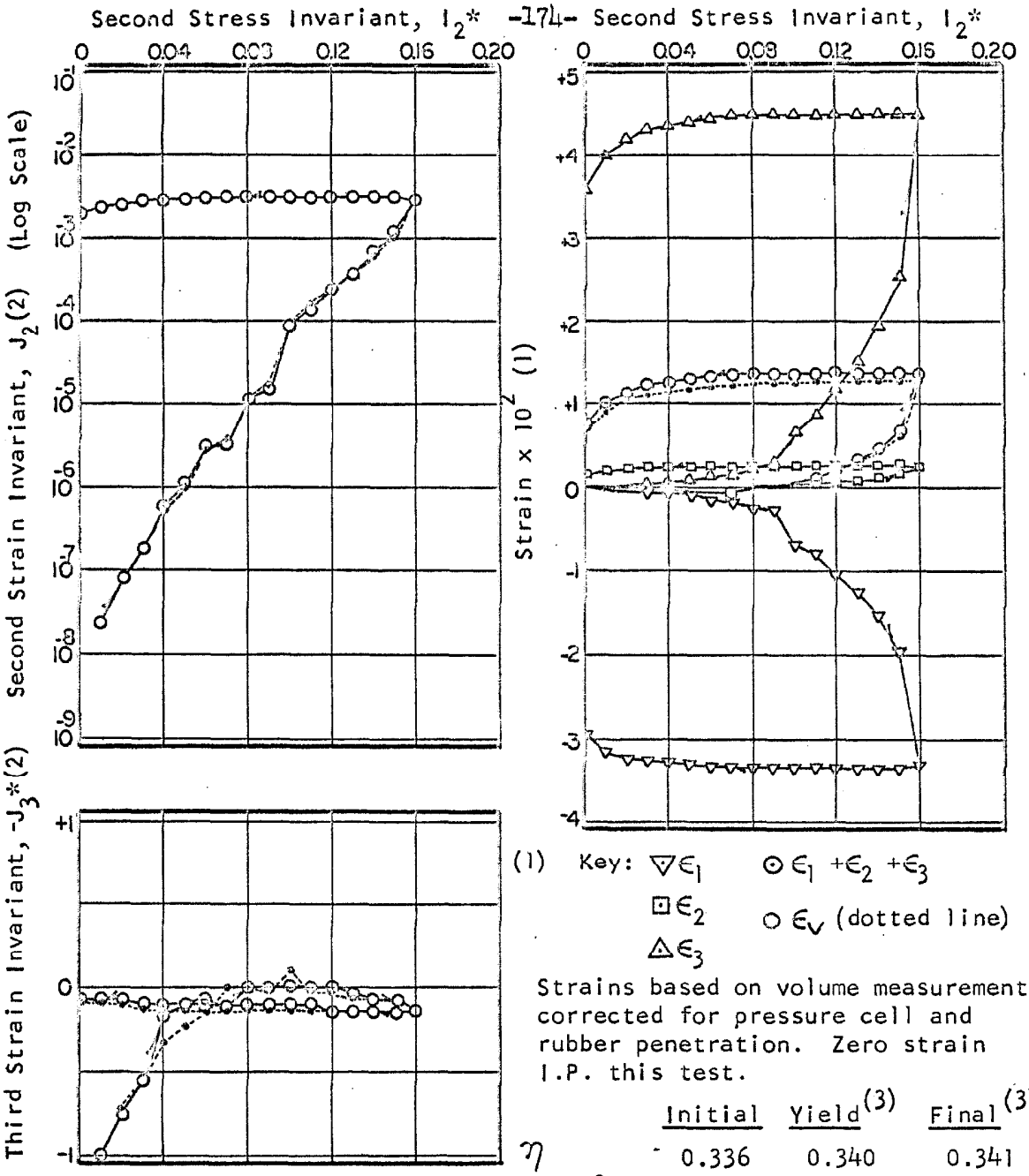

(1) Key: $\nabla\epsilon_1$ $\odot\epsilon_1+\epsilon_2+\epsilon_3$
$\boxdot\epsilon_2$ $\circ\epsilon_v$ (dotted line)
$\triangle\epsilon_3$

Strains based on volume measurements corrected for pressure cell and rubber penetration. Zero strain I.P. this test.

(2) Basis of Calculation:
--O-- ϵ_1, ϵ_2, ϵ_3.
—O— $\epsilon_v, \epsilon_2, \epsilon_3$ with $\epsilon_1 = \epsilon_v - (\epsilon_2+\epsilon_3)$
Zero strain I.P. this test.

(3) Based on ϵ_v, ϵ_2, ϵ_3

	Initial	Yield(3)	Final(3)
η	0.336	0.340	0.341
$\epsilon_1 \times 10^2$	0	-2.03	-3.01
$\epsilon_2 \times 10^2$	0	+0.14	+0.13
$\epsilon_3 \times 10^2$	0	+2.50	+3.53
$J_1 \times 10^2$	0	+0.61	+0.65
$J_2 \times 10^3$	0	1.03	2.14
$-J_3^*$		-0.07	-0.07

$I_1 = 54$ psi, $I_2^* = 0$ to 0.16, $I_3^* = +0.6$

Figure 7.46 Strains and Strain Invariants as a Function of the Second Modified and Dimensionless Stress Invariant. Yield Test Nos. 13-5-I_{13^*} & 13*R

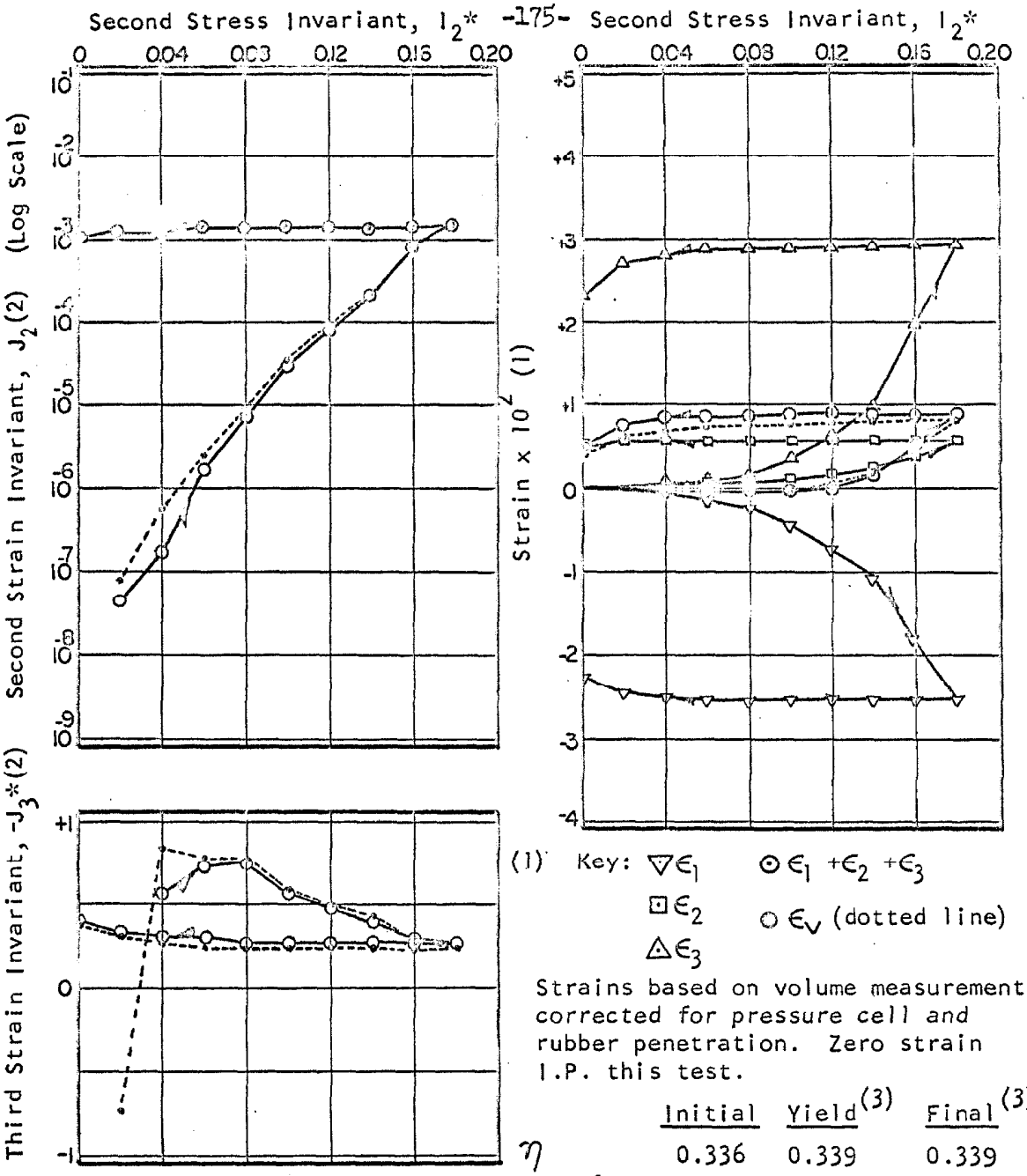

(1) Key: $\nabla\epsilon_1$ $\odot\epsilon_1 + \epsilon_2 + \epsilon_3$
$\square\epsilon_2$ $\circ\epsilon_v$ (dotted line)
$\triangle\epsilon_3$

Strains based on volume measurements corrected for pressure cell and rubber penetration. Zero strain I.P. this test.

	Initial	Yield(3)	Final(3)
η	0.336	0.339	0.339
$\epsilon_1 \times 10^2$	0	-1.85	-2.37
$\epsilon_2 \times 10^2$	0	+0.37	+0.49
$\epsilon_3 \times 10^2$	0	+1.94	+2.28
$J_1 \times 10^2$	0	+0.46	+0.40
$J_2 \times 10^3$	0	0.73	1.10
$-J_3^*$		+0.30	+0.40

(2) Basis of Calculation:

—o— ϵ_1, ϵ_2, ϵ_3.

—o— $\epsilon_v, \epsilon_2, \epsilon_3$ with $\epsilon_1 = \epsilon_v - (\epsilon_2 + \epsilon_3)$

Zero strain I.P. this test.

(3) Based on ϵ_v, ϵ_2, ϵ_3

I_1 = 54 psi, I_2^* = 0 → 0.18, I_3^* = +0.8

Figure 7.47 Strains and Strain Invariants as a Function of the Second Modified and Dimensionless Stress Invariant. Yield Test Nos. 8-5-I$_{13*}$ & 13*R

8. ANALYSIS OF TEST RESULTS

8.1 SPHERICAL COMPRESSION EXPERIMENTS

8.11 EXPERIMENT NO. 4 (Median Porosity)

Erratic results, Figure 7.4, reported for tests 4-1 through 4-6 were not considered reliable. Improvements were subsequently made in the apparatus and in the test procedures, and the results for tests 4-7 and 4-8 were considered valid. Figures 7.5, 7.6 and 7.7 indicate that the strain response was nearly elastic at porosities of 0.365–0.368, and that with exception of test cycle 4-8-6 approximately 96–98% of the maximum volumetric deformations were returnable in a full cycle of stress from 1.3 to 77 psi.

Plots of volumetric compressibility versus pressure, Figure 7.8 (log-log scale), for the final three cycles of stress are closely fit by the relationship

$$-\frac{\Delta n}{\Delta \sigma} = 7.60 \times 10^{-4}\ \sigma^{-0.852} \qquad (8.1)$$

$$n(\sigma = 18 \text{ psi}) \doteq 0.366$$

Based upon plotted results, the volumetric compressibility in extension was less than the above relationship would indicate with the major deviations occurring at intermediate loads. Unfortunately, rubber penetration leads to the same sort of deviation, Figure A2.8, and it is possible that the differences given by Figure 7.8 are in part due to errors in rubber penetration corrections.

8.12 EXPERIMENT NO. 5 (Highest Porosity)

Figure 7.9 indicates that strain response was for the most part elastic for each of the first five complete cycles of stress, and that at porosities of 0.388–0.393 approximately 89–90% of the maximum volumetric deformations were returnable in a single stress cycle. The degree of elasticity for these initial stress reversals was essentially unchanged for a constant minor stress of 1.3 psi and increasing values of maximum stress from 10.1 to 51.3 psi.

Figure 7.10 indicates that under three consecutive and relatively small stress reversals from 15.2 to 22.8 psi the strain response was measurably elastic.

Figure 7.11 shows that for a maximum stress of 76.9 psi the degree of elasticity increased gradually with a decreasing range in stress variation, and that at porosities of 0.386–0.390 approximately 95% of volumetric strain was returnable for a full cycle of stress.

Figure 7.12 illustrates strain response under various stress reversals, and shows that under a full stress cycle the returnable deformation was approximately 97% at porosities of 0.386–0.389. On the average, the degree of elasticity advanced steadily (from 89 to 97%) with the number of stress cycles and with a relatively small decrease in porosity.

Plots of volumetric compressibility versus pressure, Figure 7.13 (log-log scale), for the final two cycles of stress are closely fit by the relationship

$$-\frac{\Delta n}{\Delta \sigma} = 1.20 \times 10^{-3}\ \sigma^{-0.867} \qquad (8.2)$$

$$n(\sigma = 18 \text{ psi}) \doteq 0.387$$

Based upon plotted results, volumetric compressibility in extension was less than the above relationship would indicate with the major deviations occurring at intermediate loads (same as previous experiment).

8.13 EXPERIMENT NO. 6 (Lowest Porosity)

Figure 7.14 indicates that the strain response under short reversals of stress was essentially elastic at porosities of 0.341-0.343.

Figure 7.15 shows that under a full cycle of stress approximately 97% of the maximum volumetric deformation was returnable.

Plots of volumetric compressibility versus pressure, Figure 7.16 (log-log scale) for the final three cycles of stress are closely fit by the relationship

$$-\frac{\Delta n}{\Delta \sigma} = 6.70 \times 10^{-4}\ \sigma^{-0.837} \qquad (8.3)$$

$$n(\sigma = 18 \text{ psi}) \doteq 0.342$$

Again the volumetric compressibility in expansion was somewhat less than the above relationship would indicate at median loads.

8.14 COMBINED ANALYSIS--EXPERIMENTS 4, 5 and 6, ASSUMING ELASTIC STRAIN RESPONSE

Based upon Figures 7.8, 7.13 and 7.16 and assuming volumetric compressibility in extension equivalent to that in compression, the following relationship between volumetric compressibility and spherical stress is proposed

$$-\frac{dn}{d\sigma} = C_1(n)\ \sigma^{C_2(n)} \qquad (8.4)$$

The porosity for a single cycle of stress varied slightly. Figure 8.1 gives a plot of C_1 and C_2 from Equations 8.1, 8.2 and 8.3 versus the

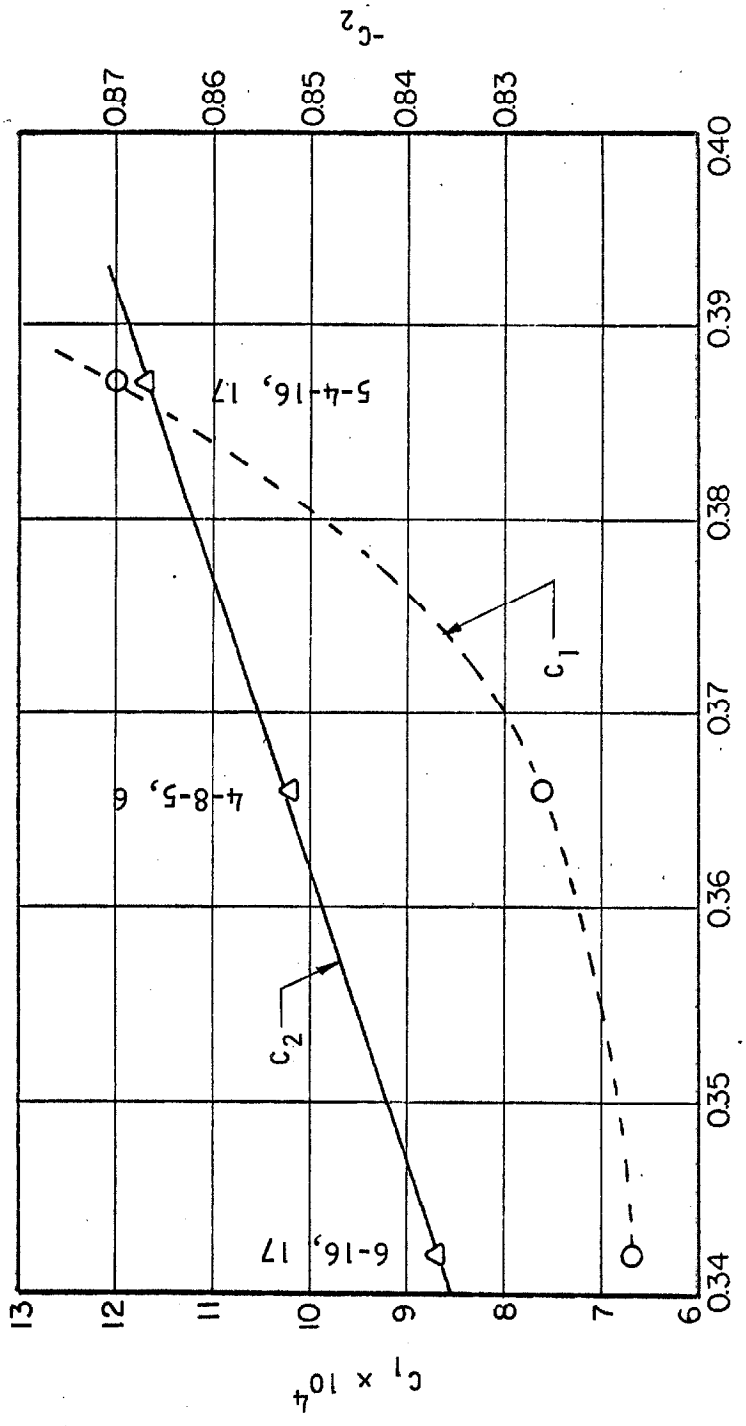

$$-\frac{dn}{d\sigma} = c_1(n)\sigma^{c_2(n)} \quad \text{where } \sigma \text{ is measured in psi units}$$

Figure 8.1 Empirical Fit, Volumetric Compressibility as a Function of Spherical Stress, Final Stress Cycles--Spherical Compression Experiments 4, 5 and 6.

porosity obtained at σ = 18 psi. For the range of porosities represented, n = 0.34–0.39, the relationship between C_2 and n is closely fit by the linear relationship $C_2 = -0.609 - 2/3\ n$. The relationship between C_2 and n might be fit by a third degree polynomial function; however, insufficient data were obtained to justify such an assumption.

The estimation of porosity for a particular stress-strain interval is given by integration of Equation 8.4

$$-\int_{n_0}^{n} dn = \int_{\sigma_0}^{\sigma} C_1(n)\, \sigma^{C_2(n)}\, d\sigma \tag{8.5}$$

where n_0 and σ_0 represent initial values of porosity and stress respectively. If $C_1(n)$ and $C_2(n)$ are assumed constant for a particular stress-strain interval then Equation 8.5 is approximated by

$$n = n_0 - \frac{C_1(n_0)}{C_2(n_0)+1}\left[\sigma^{C_2(n_0)+1} - \sigma_0^{C_2(n_0)+1}\right] \tag{8.6}$$

For the particular sand of this study the values $C_1(n_0)$ and $C_2(n_0)$ might be obtained from Figure 8.1 for lack of more complete evidence.

Equation 8.4 may be converted to the form of equations given in Section 3.43 as follows: Porosity is defined by $n = V_V/V$ and by differentiating one obtains

$$dn = d\left(\frac{V_V}{V}\right)$$

Since the change in solid volume was assumed at the outset to be negligible and the strains small then it follows that

$$dn \doteq \frac{dV_V}{V} = \frac{dV}{V} = dJ_1 \tag{8.7}$$

Also, for spherical stress states where $\sigma_1 = \sigma_2 = \sigma_3$ it follows that

$$I_1 = \sigma_1 + \sigma_2 + \sigma_3 = 3\sigma, \quad \sigma = \frac{I_1}{3} \tag{8.8}$$

and by differentiation then

$$d\sigma = \frac{1}{3} dI_1 \tag{8.9}$$

Upon substituting Equations 8.7, 8.8 and 8.9 into Equation 8.4 then

$$dJ_1 = - \frac{C_1(n)}{3[1+C_2(n)]} I_1^{C_2(n)} dI_1 \tag{8.10}$$

Assuming elastic and isotropic strain response and upon comparison with the general stress-strain relationships given by Equations 3.61, 3.62, 3.63, 3.66 and 3.67, it follows that for spherical stress states

$$dJ_1 = C_{11} dI_1 + C_{13} dI_3^* \tag{8.11}$$

$$dJ_2 = C_{21} dI_1 + C_{23} dI_3^* \tag{8.12}$$

$$dJ_3 = C_{31} dI_1 + C_{33} dI_3^* \tag{8.13}$$

and $C_{ijC} = C_{ijR} = C_{ij}(n, I_1, I_2^*, I_3^*) = C_{ij}(n, I_1, 0, I_3^*)$

where

$$C_{11} = - \frac{C_1(n)}{3[1+C_2(n)]} I_1^{C_2(n)} \tag{8.14}$$

and

$$C_{21} = C_{31} = C_{13} = C_{23} = 0 \tag{8.15}$$

For the spherical state of stress, C_{33} at this stage is arbitrary.

For the three-dimensional compression experiments, the porosity n was on the order of 0.34 and the initial strain response under spherical stress cycles might be approximated by Equation 8.3, which when converted into the form of Equation 8.10 reads

$$dJ_1 = -5.60 \times 10^{-4} I_1^{-0.837} dI_1 \tag{8.16}$$

and in this case

$$C_{11} = C_{11}(0.34,\ I_1,\ 0,\ I_3{}^*) = -5.60 \times 10^{-4}\ I_1^{-0.837} \qquad (8.17)$$

8.15 COMBINED ANALYSIS--EXPERIMENTS 4, 5 and 6, CONSIDERATION OF NON-ELASTIC STRAIN RESPONSE

The returnable volumetric strain expressed as a per cent of the maximum which occurs for a complete cycle of stress is here defined as the degree of elasticity D_v

$$D_v = \frac{n_2 - n_1}{n_0 - n_1} \qquad (8.18)$$

where n_0 = initial porosity at initial stress σ_0

n_1 = porosity at maximum stress σ_1

n_2 = final porosity at initial stress σ_0

A plot of the degree of elasticity for fixed range stress cycles from 1.3 to 76.9 psi versus porosity is given by Figure 8.2 for the combined experiments. The effect of stress history becomes more significant with increasing porosity. It is suggested that $D_v = 100\%$ represents an upper limit which the various curves would approach asymptotically with increasing stress history and decreasing porosity.

The degree of elasticity normally increases as the range of stress decreases, and varies little with the magnitude or level of stress.

In summary, the stress-strain behavior reported here was for the most part elastic. The stress levels were limited from 1.3 to 76.9 psi and the porosities ranged from 0.34 to 0.39.

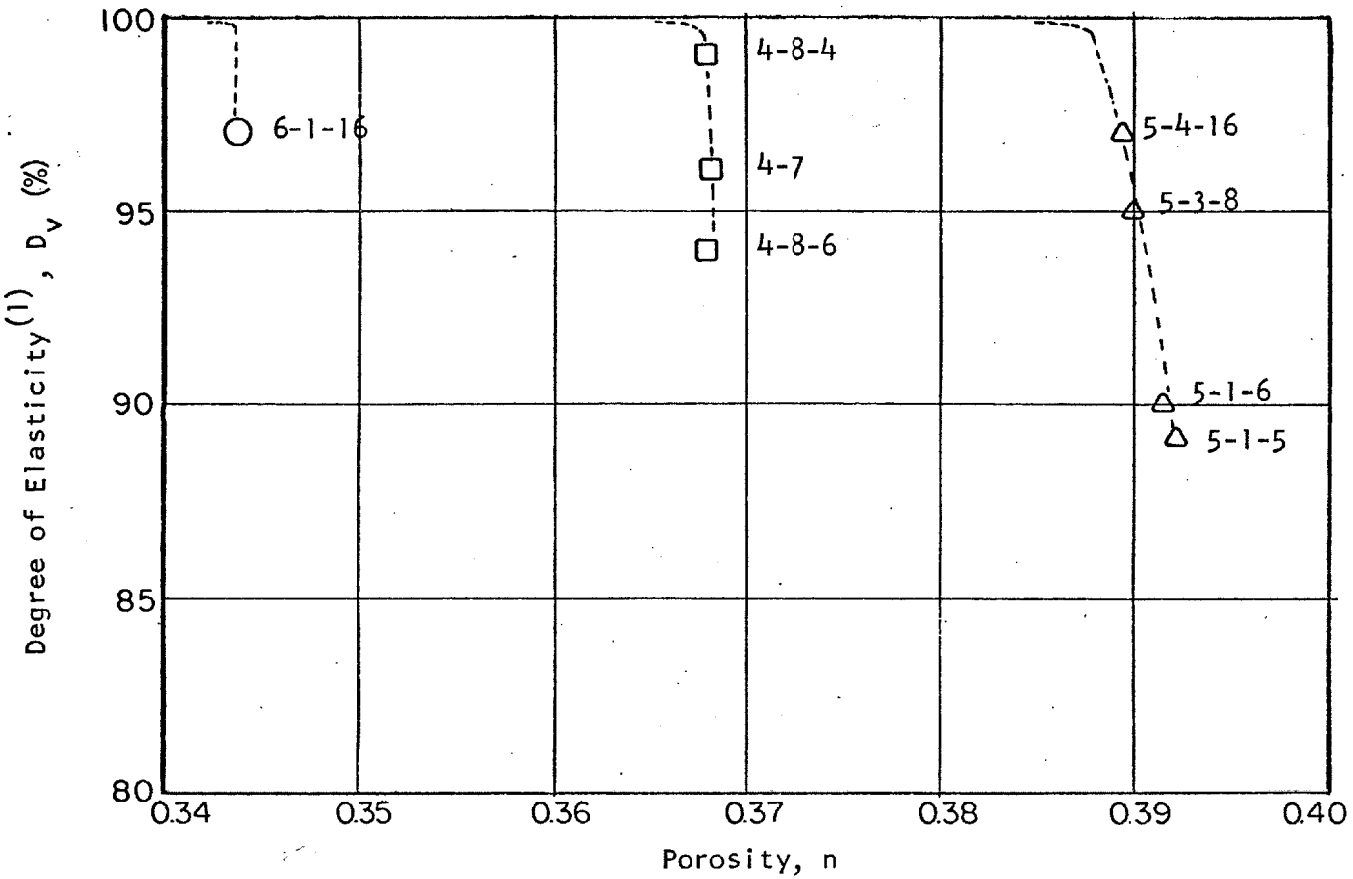

(1) Based on returnable volumetric strain for full cycles of spherical stress σ from 1.3 to 76.9 to 1.3 psi.

$$D_v = \frac{n_2 - n_1}{n_0 - n_1}$$

Figure 8.2 Degree of Elasticity as a Function of Stress History and Porosity, Spherical Compression Experiments 4, 5 and 6.

8.2 THREE-DIMENSIONAL COMPRESSION EXPERIMENTS

8.21 SPHERICAL COMPRESSION STRESS PATHS

Spherical compression stress paths, denoted SC for increasing I_1 (compression) and SC_R for decreasing I_1 (extension), were carried out both prior to and following certain deviatoric stress cycles, Figures 7.19, 7.23, 7.29, 7.31, 7.33, 7.35 and 7.39. The initial tests indicate lower compressibilities, i.e. Figure 7.39, than would be predicted from spherical apparatus results obtained at the same porosity, Figure 7.16. This may be explained by the fact that the base cell in the three-dimensional apparatus did not apply normal stress over the entire base of the test specimen. (This was neglected in computing the compressibility $-\Delta n/\Delta\sigma$.) The major deviations normally occurred at low to intermediate loads (5–20 psi), while the compressibilities at 25–30 psi were practically equivalent. This may be explained by the introduction of shear through slightly non-homogeneous loading at higher pressures. Extension compressibilities were noticeably lower, supporting the previous statement. Errors in the rubber penetration corrections may also have contributed to the foregoing deviations. The spherical apparatus was considered nearly ideal and produced a more accurate stress-strain relationship for the initial states of spherical stress.

8.22 CIRCULAR COMPRESSION (DEVIATORIC) STRESS PATHS, NOT CARRIED TO YIELD

Circular compression stress paths, denoted I_{12} for increasing I_3^*, and I_{12R} for decreasing I_3^*, were carried out with I_1 and I_2^* held constant.

Figure 7.21 represents results from three circular compression stress paths, the first of which was carried out from an initial state of deviatoric stress well below yield, which in turn was developed from a spherical stress state by way of an average compression test ($I_3^* = 0$). The circular test for I_3^* increasing from 0 to 1 indicated that $\epsilon_v(J_1)$ decreased slightly, J_2 increased slightly and $-J_3^*$ increased slightly. Upon decreasing I_3^* then from 1 to -1, J_1 increased, J_2 increased and $-J_3^*$ decreased. Finally, upon increasing I_3^* from -1 to 0, J_1 remained essentially fixed, J_2 decreased and $-J_3^*$ remained essentially constant. Assuming that progress toward yield and the resulting decreased stability are associated with volume expansion and increasing J_2 results in the conclusion that the I_{12R} stress path (I_3^* decreasing) leads toward yield, and that the I_{12} stress path (I_3^* increasing) leads toward increased stability. The I_{12R} stress path might be considered for use as a yield test if I_2^* were initially greater than some indeterminate critical value.

Figure 7.27 represents results of one circular compression stress path carried out from a relatively small initial state of deviatoric stress, which in turn was developed from the spherical stress state by way of a triaxial compression test ($I_3^* = 1$). The results are considered inconclusive as the strains were of the same order of magnitude as the pressure-cell corrections. It appears that $\epsilon_v(J_1)$ remained essentially constant as I_3^* was reduced from 1 to -1. This was believed to be the most reliable measurement since it was not affected by pressure-cell compressibility to the same degree as was

the measurement of principal strains. On the basis of physical reasoning it was hoped that it might be shown that stress-strain behavior for I_2^* approaching zero would be comparable with that of the linearly elastic and isotropic solid for which $J_1 = 0$, $J_2 = 0$ and $-J_3^* = I_3^*$ (see Equations 3.45, 3.46 and 3.51).

Figure 7.37 represents the results of a circular compression stress path carried out from an initial state of deviatoric stress near yield, which was in turn developed from the spherical stress state by way of a triaxial compression test ($I_3^* = 1$). The test indicated that for I_3^* decreasing from 1 to -1, $\epsilon_v(J_1)$ increased, J_2 increased, and $-J_3^*$ decreased approximately according to the relationship $-J_3^* \cong I_3^*$. The first two results substantiated earlier statements regarding the unstable characteristic of the I_{12R} stress path, and it is likely that yield was nearly obtained for $I_3^* = -1$. The latter result was most interesting; however, Figure 7.19 would not substantiate the hypothesis that $-J_3^* = I_3^*$ for either the I_{12} or the I_{12R} stress paths. The results of Experiment 2 were in general considered less reliable than those of subsequent experiments.

It is difficult, on the basis of the limited number of I_{12} tests performed, to arrive at a meaningful mathematical expression for the stress-strain relationship in the form of Equations 3.61, 3.62, 3.63, 3.66 and 3.67. For circular compression these expressions reduce to

$$dJ_1 = C_{13}dI_3^* \tag{8.19}$$

$$dJ_2 = C_{23}dI_3^* \tag{8.20}$$

$$dJ_3^* = C_{33}dI_3^* \tag{8.21}$$

and

$$C_{ij} = C_{ij}(n, I_1, I_2^*, I_3^*) \tag{8.22}$$

Since the strain response is dependent upon the direction of loading then $C_{ijC} \neq C_{ijR}$. The strain response was slight for the I_{12} stress path where $dI_3^* > 0$, thus it might be assumed that

$$C_{13C} = 0, \quad C_{23C} = 0, \quad C_{33C} = -1 \quad \text{(i.e. linear elasticity)} \tag{8.23}$$

Based upon Figure 7.37 a straight line fit to the volumetric strain data gives

$$J_1 \doteq 2.5 \times 10^{-3} - 2.9 \times 10^{-3}\, I_3^* \tag{8.24}$$

and since $C_{13} = \dfrac{\partial J_1}{\partial I_3^*}$ it follows that

$$C_{13R}(0.32, 54 \text{ psi}, 0.10, I_3^*) = -2.9 \times 10^{-3} \tag{8.25}$$

A straight line fit to the J_2 response curve gives

$$\log_{10} J_2 = -3.56 - 0.725\, I_3^* \tag{8.26}$$

or in exponential form

$$J_2 = e^{-(8.18 + 1.67\, I_3^*)} \tag{8.27}$$

and since $C_{23} = \dfrac{\partial J_2}{\partial I_3^*}$ it follows that

$$C_{23R}(0.34, 54 \text{ psi}, 0.10, I_3^*) = -1.67\, e^{-(8.18+1.67\, I_3^*)} \tag{8.28}$$

The relationship between $-J_3^*$ and I_3^* is approximately given by

$$-J_3^* = I_3^* \tag{8.29}$$

and since $C_{33} = \dfrac{\partial J_3^*}{\partial I_3^*}$ it follows that

$$C_{33R}(0.34, 54 \text{ psi}, 0.10, I_3^*) = -1 \tag{8.30}$$

The coefficient functions given by Equations 8.23, 8.25, 8.28 and 8.30 strictly include only the effect of the variable I_3^* as they were derived from a single test with n = 0.34, I_1 = 54 psi and I_2^* = 0.10. It is suggested that I_1 is of minor importance in the deviatoric tests except as included in $I_2^* = I_2/I_1^2$. A major question still remains as to the effect of I_2^*. Equation 8.15 requires that C_{13R} and C_{23R} approach zero at $I_2^* = 0$. A possible set of coefficient functions which satisfies the latter requirement and agrees with Equations 8.25 and 8.28 is

$$C_{13R}(0.32,\ 54 \text{ psi},\ I_2^*,\ I_3^*) = -2.9 \times 10^{-3} \left(\frac{I_2^*}{0.10}\right)^p \qquad (8.31)$$

and

$$C_{23R}(0.34, 54 \text{ psi}, I_2^*, I_3^*) = -1.67\left(\frac{I_2^*}{0.10}\right)^m e^{-(8.18+1.67\ I_3^*)} \qquad (8.32)$$

where p and m are arbitrary constants. Further discussion will follow analysis of radial compression tests carried to yield, Section 8.244, where the values p = 2 and m = 1 are suggested.

8.23 RADIAL COMPRESSION (DEVIATORIC) STRESS PATHS, NOT CARRIED TO YIELD

Radial compression stress paths, denoted I_{13*} for increasing I_2^* and I_{13*R} for decreasing I_2^* were carried out with I_1 and I_3^* held constant. Figures 7.17, 7.18, 7.20, 7.22, 7.24, 7.25, 7.26, 7.36 and 7.38 illustrate results from such tests not carried to yield.

8.231 Experiment No. 2. Results of the first deviatoric stress cycle, Figure 7.17, are not considered reliable. The data was not corrected for the effect of pressure-cell compression nor was internal volume change measured.

Results of the second average compression stress cycle, Figure 7.18, indicate that volumetric strain $\epsilon_v(J_1)$ initially decreased then increased, becoming positive for I_2^* exceeding 0.06. The relationship between J_2 and I_2^* for increasing values of I_2^* was nearly of the form $\log_{10} J_2 = a_3 + a_4 I_2^*$, where a_3 and a_4 were constants with $I_3^* = 0$. The function $-J_3^*$ decreased, becoming negative with increasing I_2^*. The degree of volumetric strain return upon rebound exceeded that of the principal strains by a factor of 2 to 3.

The form of results obtained from the third average compression stress path (increasing I_2^*), Figure 7.20, essentially substantiates earlier work. The next average compression stress path, Figure 7.22, which followed a circular test series, indicates relatively small strain response in return to the spherical stress state.

A series of four average compression stress cycles, Figures 7.24 and 7.25, were carried out to obtain a measure of the influence of I_1 on the strain response. Deviatoric stresses were relatively small, and the results are inaccurate at corresponding strains. The interpretation of results is questionable; however, it appears from Figure 7.24 that J_1 (volumetric strain) is initially negative for $I_1 > 45$ psi and positive for $I_1 < 45$ psi. From Figure 7.25 it seems evident that I_1 has no marked effect upon J_2 (except as included in I_2^*). The function $-J_3^*$ is so sensitive to errors in strain measurement that nothing would be gained by its presentation. Additional deviatoric tests were carried out at $I_1 = 54$ psi, thus some initial negative volumetric strain

was to be expected. The effects of the variable I_1 were neglected in planning further experiments in favor of the variable $I_2^* = I_2/I_1^2$.

In general, the results of Experiment No. 2 are not considered so reliable as those of subsequent experiments, but this experiment clearly pointed the way and indicated the form of results to be expected.

8.232 Other Experiments. An average compression stress path was used to develop initial shear for a circular test series, Figure 7.26; however, the strains were so small that the results are considered unreliable. The results of a triaxial compression stress path, Figure 7.36, indicate that as I_2^* was increased J_1 initially decreased then increased; J_2 increased nearly in accordance with the relationship $\log_{10} J_2 = a_3 + a_4 I_2^*$, where a_3 and a_4 are constants; and $-J_3^*$ increased, nearly reaching 1 at $I_2^* = 0.10$. The latter result depended somewhat on the method of calculation, and was of interest because it was expected that $-J_3^* = 1$ throughout (assuming an initially isotropic sample). The unexpected deviation was attributed to errors in strain measurement below $I_2^* = 0.08$. It is considered that the numerical values of strain and functions thereof obtained where $J_1 < 0$ are most likely unreliable and not deserving of detailed numerical analysis.

8.24 RADIAL COMPRESSION (DEVIATORIC) STRESS PATHS, CARRIED TO YIELD FROM AN INITIALLY SPHERICAL STATE OF STRESS

A number of tests were carried to first yield, as defined in Section 2.3, from a spherical state of stress by way of radial compression. Figure 7.28 gives the results of a triaxial compression test

($I_3^* = 1$); Figure 7.30 gives the results of a triaxial extension test ($I_3^* = -1$); and Figures 7.40 through 7.47 give the results of radial tests for which $I_3^* = -0.8, -0.6, -0.4, -0.2, 0.2, 0.4, 0.6$ and 0.8 respectively.

8.241 The First Strain Invariant as a Function of the Second and Third Modified and Dimensionless Strain Invariants. Figure 8.3 gives J_1 plotted against I_2^* and I_3^* for ten I_{13}^* yield tests. In each case J_1 was calculated by summation of the principal strains and the J_1 surface is erratic. Figure 8.4 gives a similar plot; but here J_1 was taken directly as the corrected volumetric strain measurement. The J_1 surface of Figure 8.4 is relatively smooth and is considered superior to that of Figure 8.3. Justification for the calculation of the principal strain $\epsilon_1 = \epsilon_v - (\epsilon_2 + \epsilon_3)$ is given by comparison of the two plots, and by the probability that the σ_1 pressure-cell lags the test specimen movement to a greater degree than in the spherical calibration tests. Various comparisons of this nature were given in the presentation of test results, Chapter 7. Further analysis is thus primarily based upon the corrected strain measurements ϵ_v, ϵ_2 and ϵ_3, with ϵ_1 calculated. Figure 8.5 gives the J_1 surface from Figure 8.4 transformed to an octahedral plane in principal stress space. A substantial break in the J_1 surface occurs for $I_3^* = 0.8$–1.0. A triaxial compression test performed on an initially anisotropic sample, Figure 7.34, reached yield at $I_2^* = 0.18$–0.20, suggesting that the foregoing break may be too sharp but nevertheless represents a true characteristic of the material and is not just the result of a single test error. Further

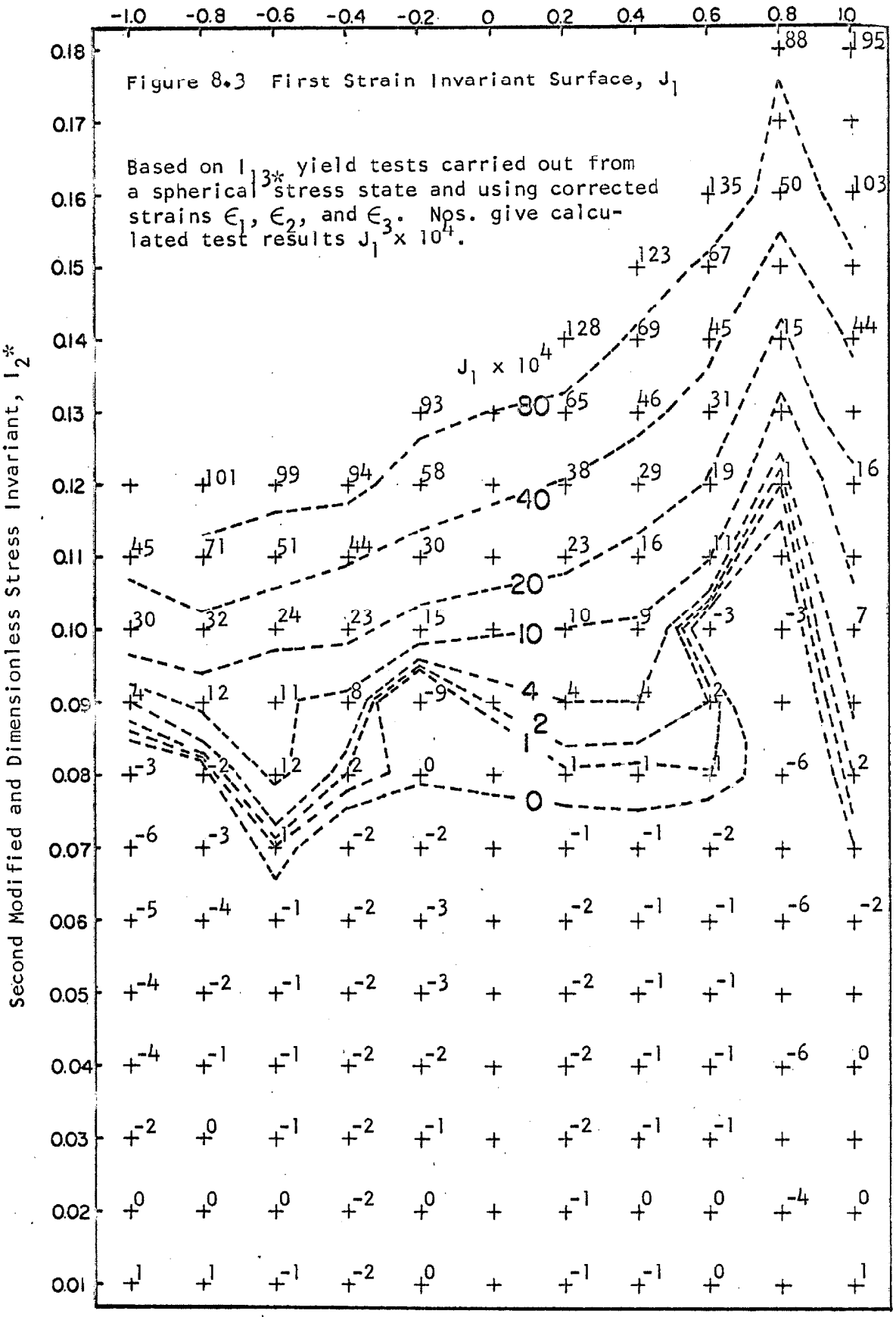

Figure 8.3 First Strain Invariant Surface, J_1

Based on I_{13}^* yield tests carried out from a spherical stress state and using corrected strains ϵ_1, ϵ_2, and ϵ_3. Nos. give calculated test results $J_1 \times 10^4$.

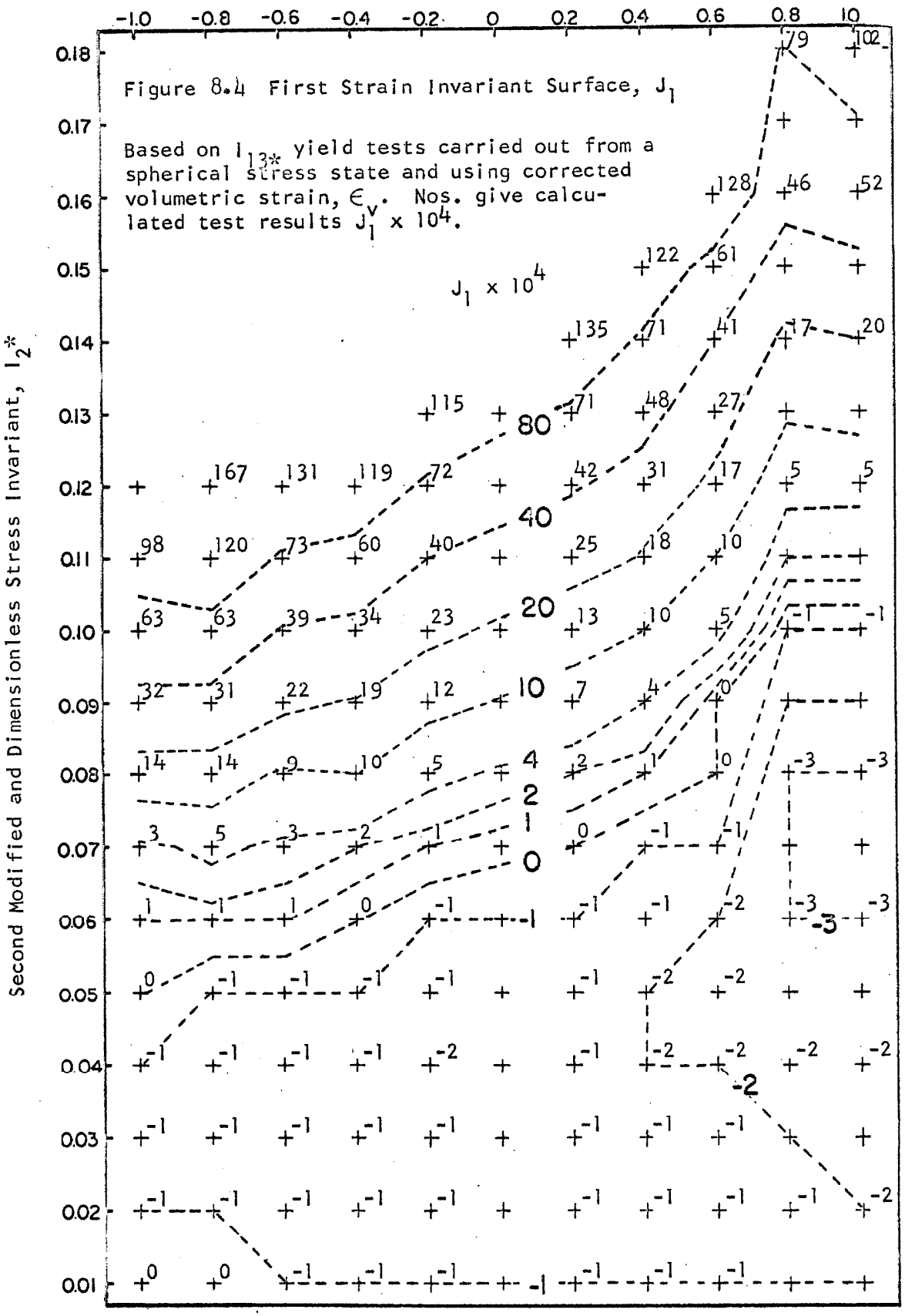

Figure 8.4 First Strain Invariant Surface, J_1

Based on I_{13}^* yield tests carried out from a spherical stress state and using corrected volumetric strain, ϵ_v. Nos. give calculated test results $J_1 \times 10^4$.

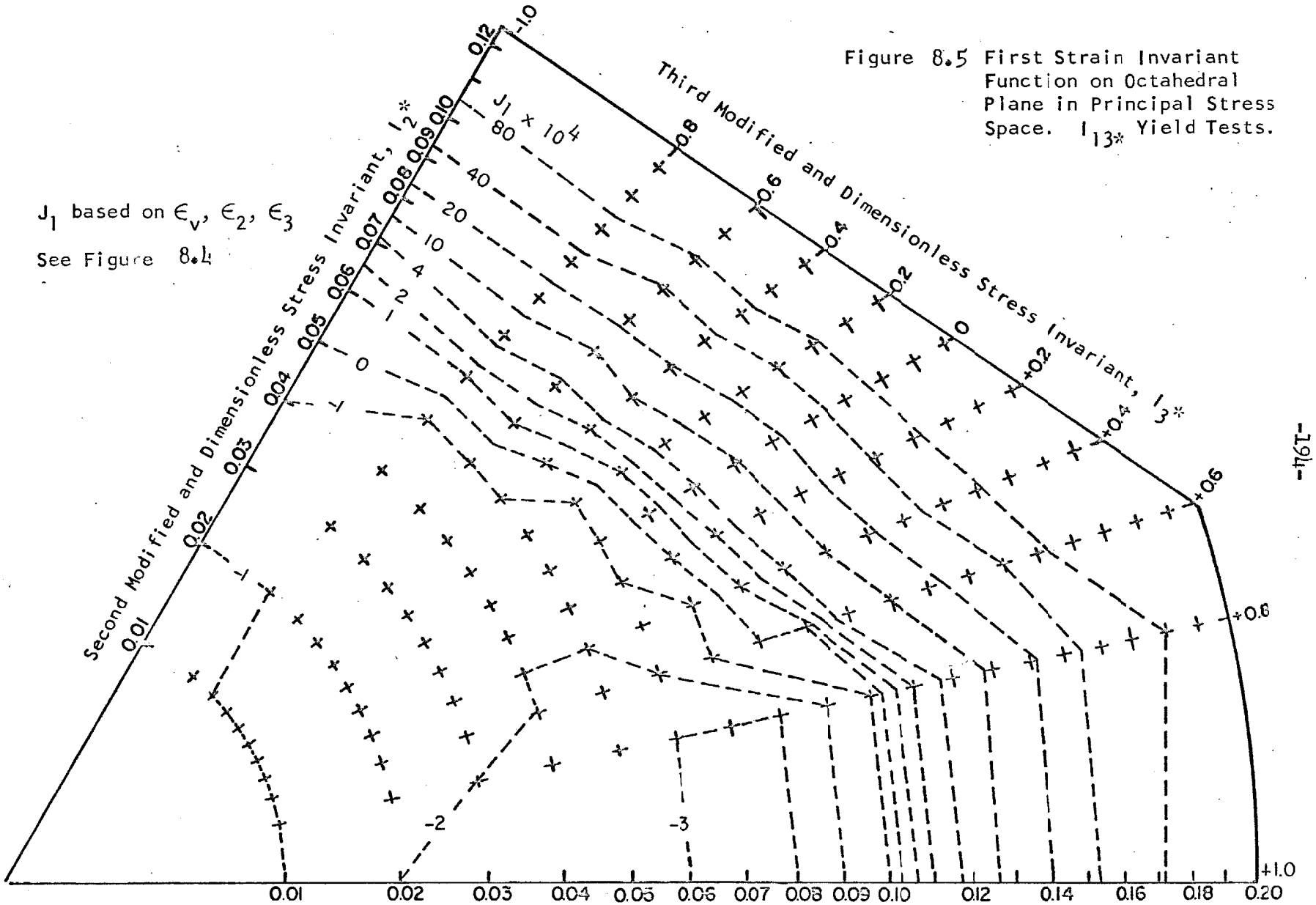

J_1 based on ϵ_v, ϵ_2, ϵ_3

See Figure 8.4

Figure 8.5 First Strain Invariant Function on Octahedral Plane in Principal Stress Space. I_{13}^* Yield Tests.

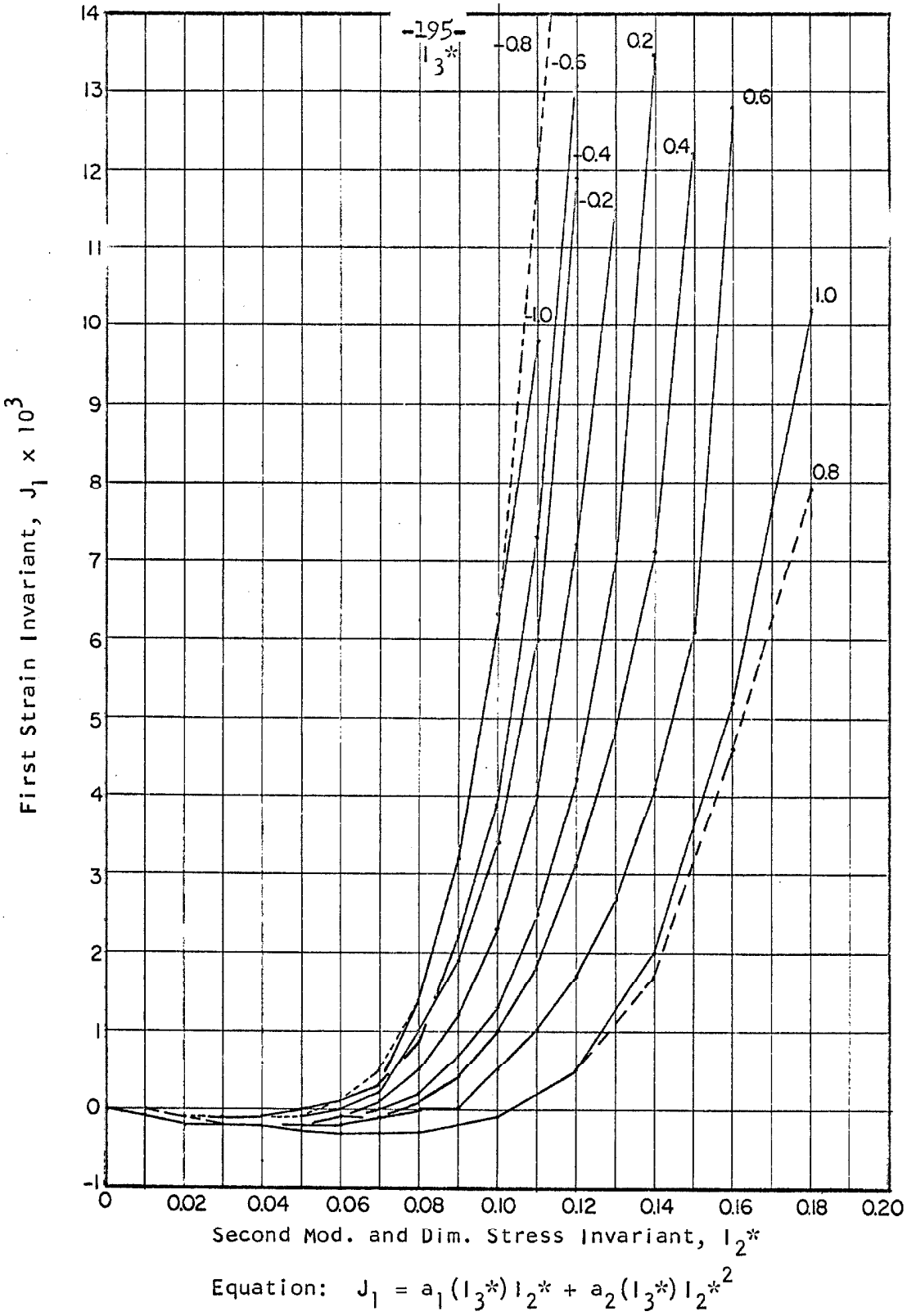

Figure 8.6 First Strain Invariant as a Function of the Second and Third Modified and Dimensionless Stress Invariants. I_{13}* Yield Tests.

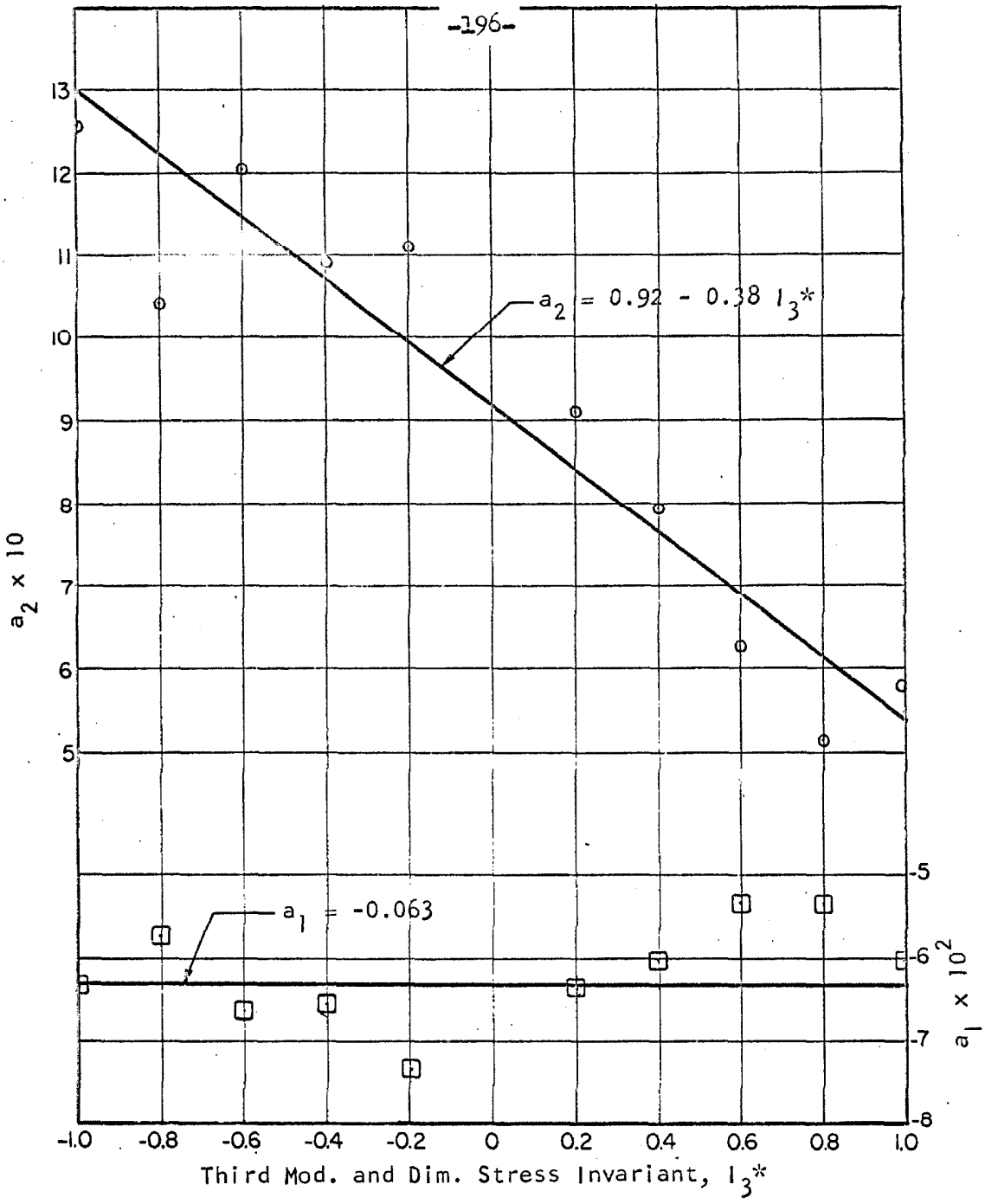

Equation: $J_1 = a_1 I_2^* + a_2 I_2^{*2}$ (Second order polynomial)

Based on: I_{13*} yield tests carried out from a spherical compression stress state.

Figure 8.7 Empirical Fit - The First Strain Invariant as a Function of the Second and Third Modified and Dimensionless Stress Invariants.

indications of unusual behavior occurring near the triaxial compression stress state are given by the J_1 surface depression (volumetric compression) occurring for $I_3^* \geq 0.4$ and $0.02 \leq I_2^* \leq 0.09$.

Detailed consideration of first yield is deferred to Section 8.4 where the state of stress prior to and following yield will be corrected for the effect of the rubber membrane.

Figure 8.6 gives a combined plot showing J_1 as a function of I_2^* for ten tests at fixed values of I_3^*. The simplest expression giving negative initial and positive final values of J_1 was selected to fit this data--a second order polynomial in I_2^* with coefficients in I_3^*

$$J_1 = a_0(I_3^*) + a_1(I_3^*)\, I_2^* + a_2(I_3^*)\, I_2^{*2} \tag{8.33}$$

Three points were chosen for curve fitting at fixed values of I_3^*: $J_1 = 0$ at $I_2 = 0$, I_2^* at $J_1 = 0$, and J_1 at I_2^* immediately before yield. The first condition requires that $a_0(I_3^*) = 0$. Values of a_1 and a_2 were determined for each test and plotted against I_3^* as shown in Figure 8.7, resulting in the following approximations

$$a_1 = -0.063 \tag{8.34}$$

$$a_2 = 0.92 - 0.38\, I_3^* \tag{8.35}$$

Substitution of Equations 8.34 and 8.35 into Equation 8.33 results in

$$J_1 = -0.063\, I_2^* + (0.92 - 0.38\, I_3^*)\, I_2^{*2} \tag{8.36}$$

In the form of Equations 3.61 and 3.66 for this case with I_1 and I_3^* constant

$$dJ_1 = C_{12}\, dI_2^* \tag{8.37}$$

where

$$C_{ijC}(n,\ I_1,\ I_2^*,\ I_3^*) = C_{12C}(0.34,\ 54\ \text{psi},\ I_2^*,\ I_3^*) \tag{8.38}$$

and since $C_{12} = \frac{\partial J_1}{\partial I_2^*}$ it follows from Equation 8.36 that

$$C_{12C} = -0.063 + (1.84 - 0.76\ I_3^*)\ I_2^* \tag{8.39}$$

Equation 8.39 is considered most reliable where J_1 0, or from Equation 8.39

$$I_2^* \geq \frac{0.063}{0.92 - 0.38\ I_3^*} \tag{8.40}$$

For $J_1 < 0$ it is suggested that a better approximation is perhaps given by

$$C_{12C} \doteq 0 \tag{8.41}$$

Neglecting elastic rebound for decreasing I_2^* (i.e. Figure 7.46) results in

$$C_{12R} \doteq 0 \tag{8.42}$$

8.242 Second Strain Invariant as a Function of the Second and Third Modified and Dimensionless Stress Invariants. Figure 8.8 gives J_2 plotted against I_2^* and I_3^* for ten I_{13^*} yield tests. Figure 8.9 gives the J_2 surface from Figure 8.8 transformed to an octahedral plane in principal stress space. Again, a noticeable break occurs in the J_2 surface for $I_3^* = 0.8$–1.0 and $I_2^* \geq 0.12$.

Figures 8.10 and 8.11 give combined plots showing J_2 as a function of I_2^* for ten tests at fixed values of I_3^*. The expression given to represent these results is

$$\log_{10} J_2 = a_3(I_3^*) + a_4(I_3^*)\ I_2^* \tag{8.43}$$

Curve fitting was based primarily upon results where $I_2^* \geq 0.06$. Values of a_3 and a_4 were determined for each test and plotted against I_3^* as shown in Figure 8.12, resulting in the following approximations

$$a_3 = -7.5 \tag{8.44}$$

$$a_4 = 36 - 10.2\ I_3^* \tag{8.45}$$

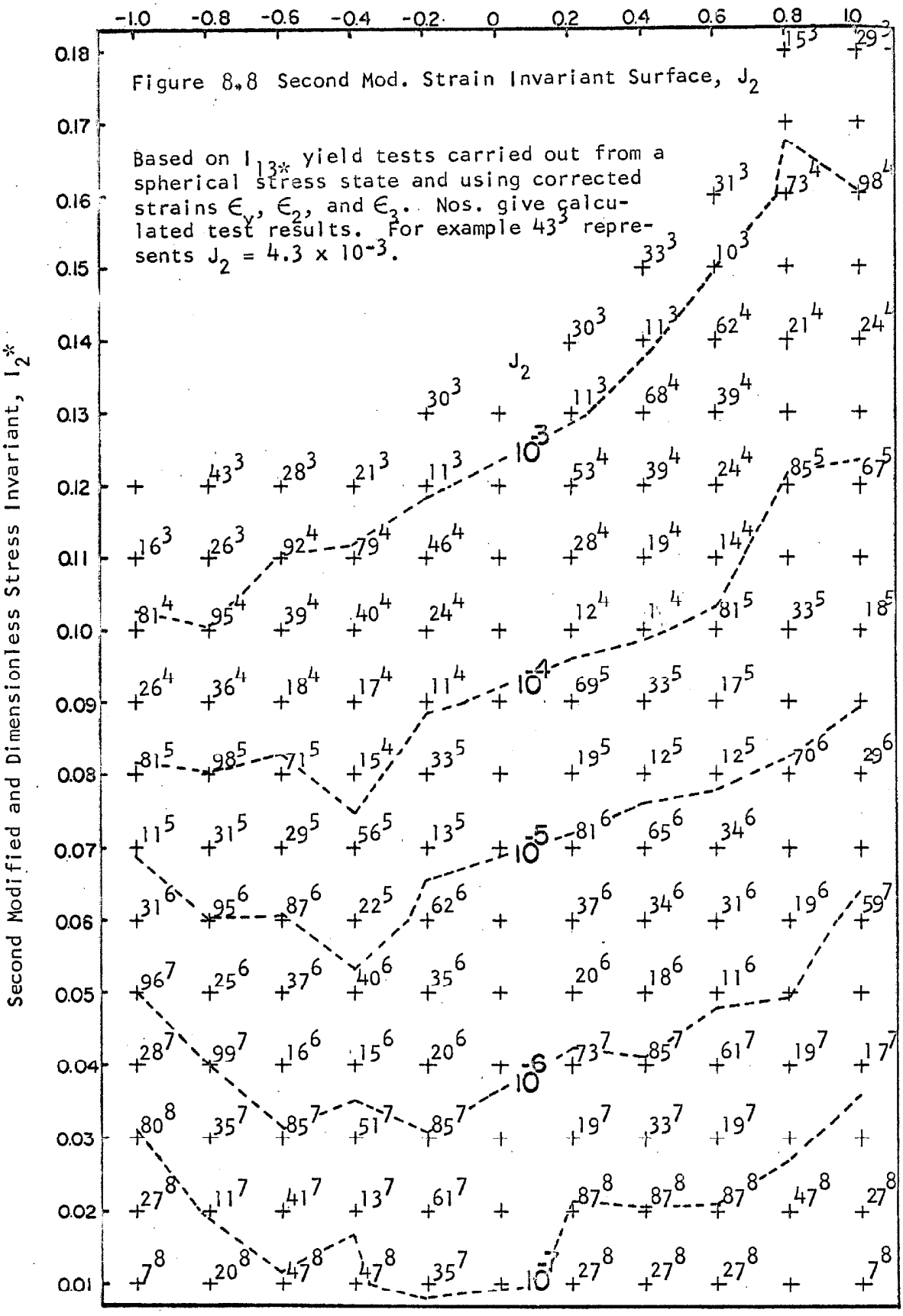

Figure 8.8 Second Mod. Strain Invariant Surface, J_2

Based on I_{13}^* yield tests carried out from a spherical stress state and using corrected strains ϵ_1, ϵ_2, and ϵ_3. Nos. give calculated test results. For example 43^3 represents $J_2 = 4.3 \times 10^{-3}$.

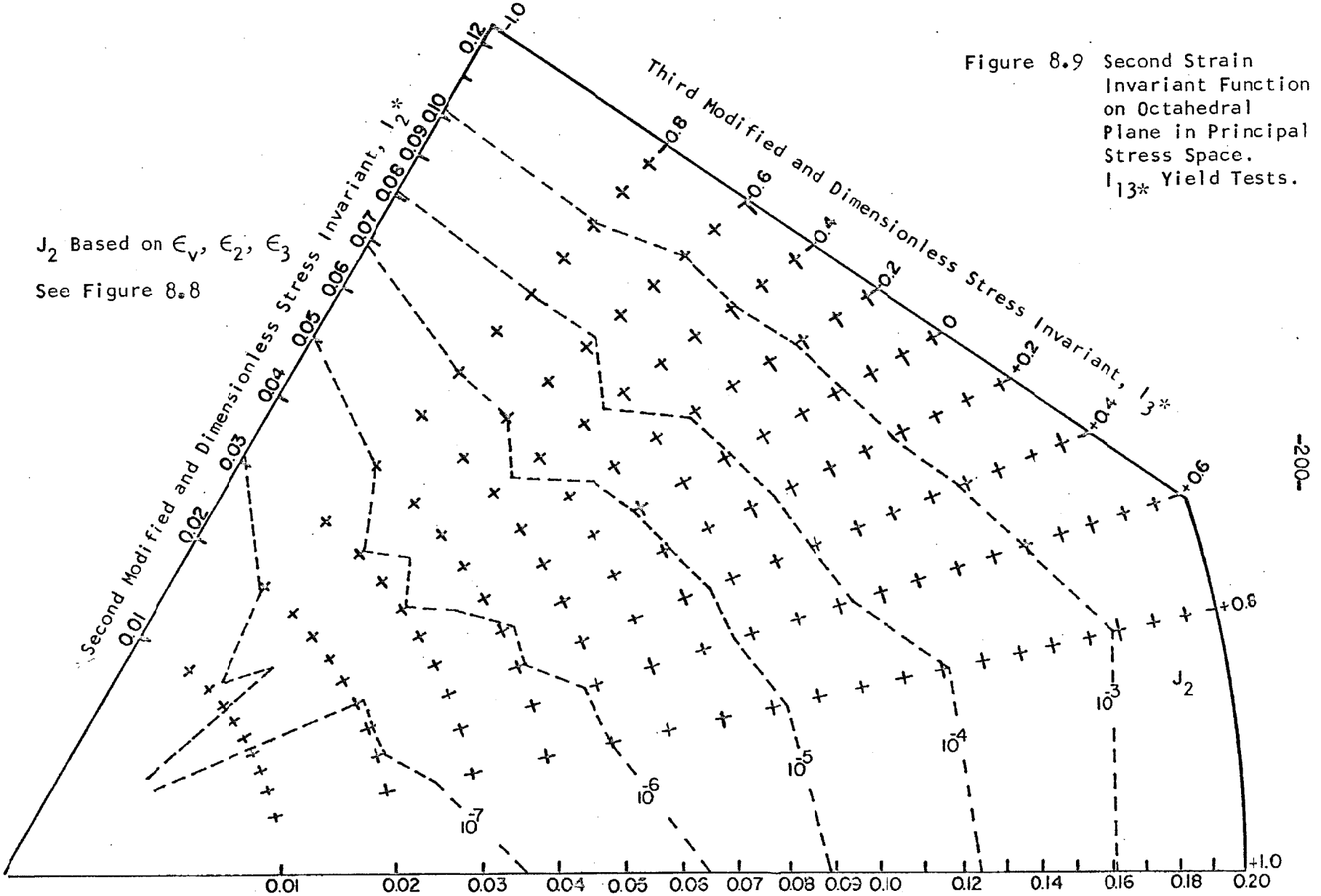

Figure 8.9 Second Strain Invariant Function on Octahedral Plane in Principal Stress Space. I_{13}* Yield Tests.

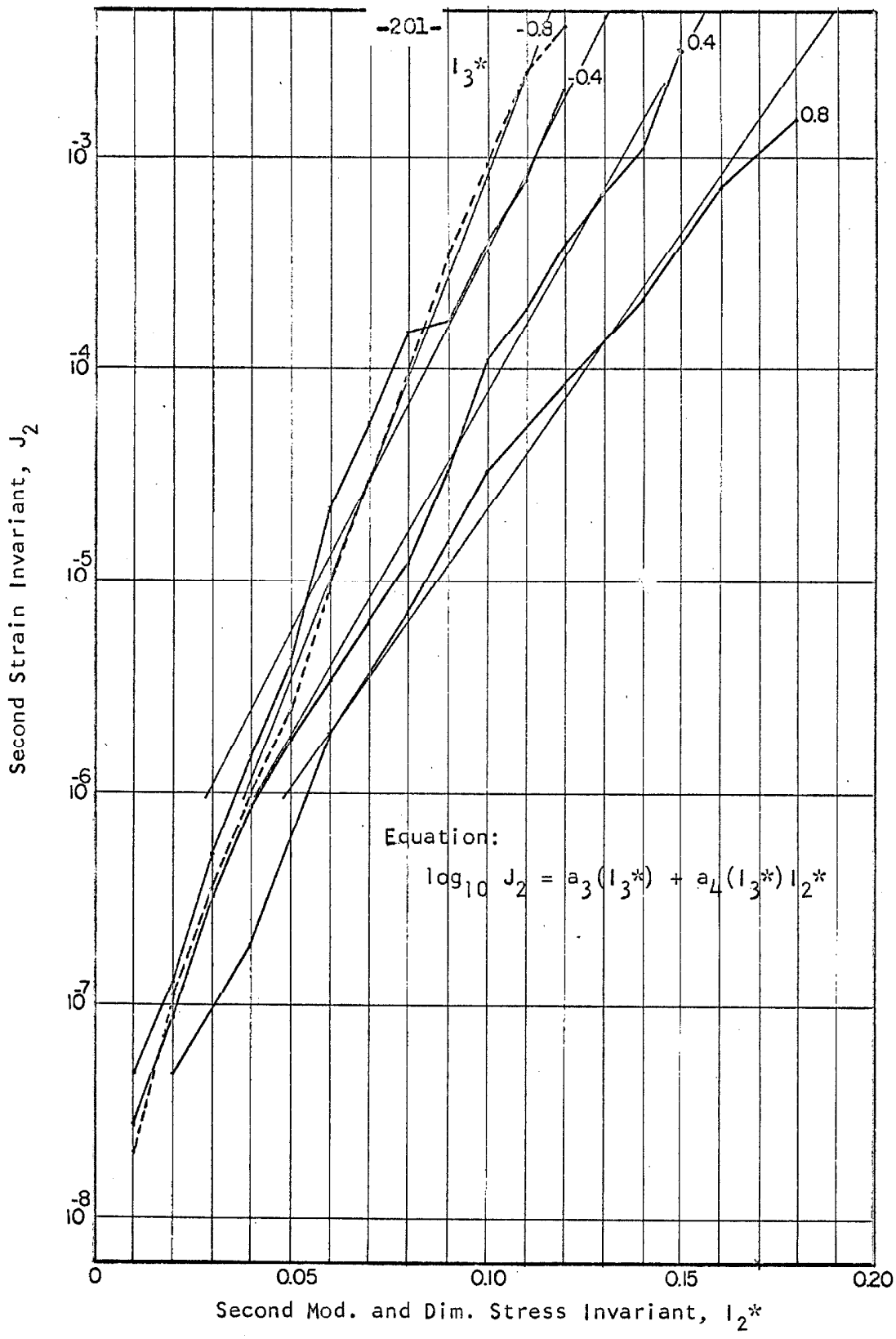

Figure 8.10 Second Strain Invariant as a Function of the Second Modified and Dimensionless Stress Invariant, I_{13}^* Yield Tests, $I_3^* = -0.8, -0.4, +0.4, +0.8$.

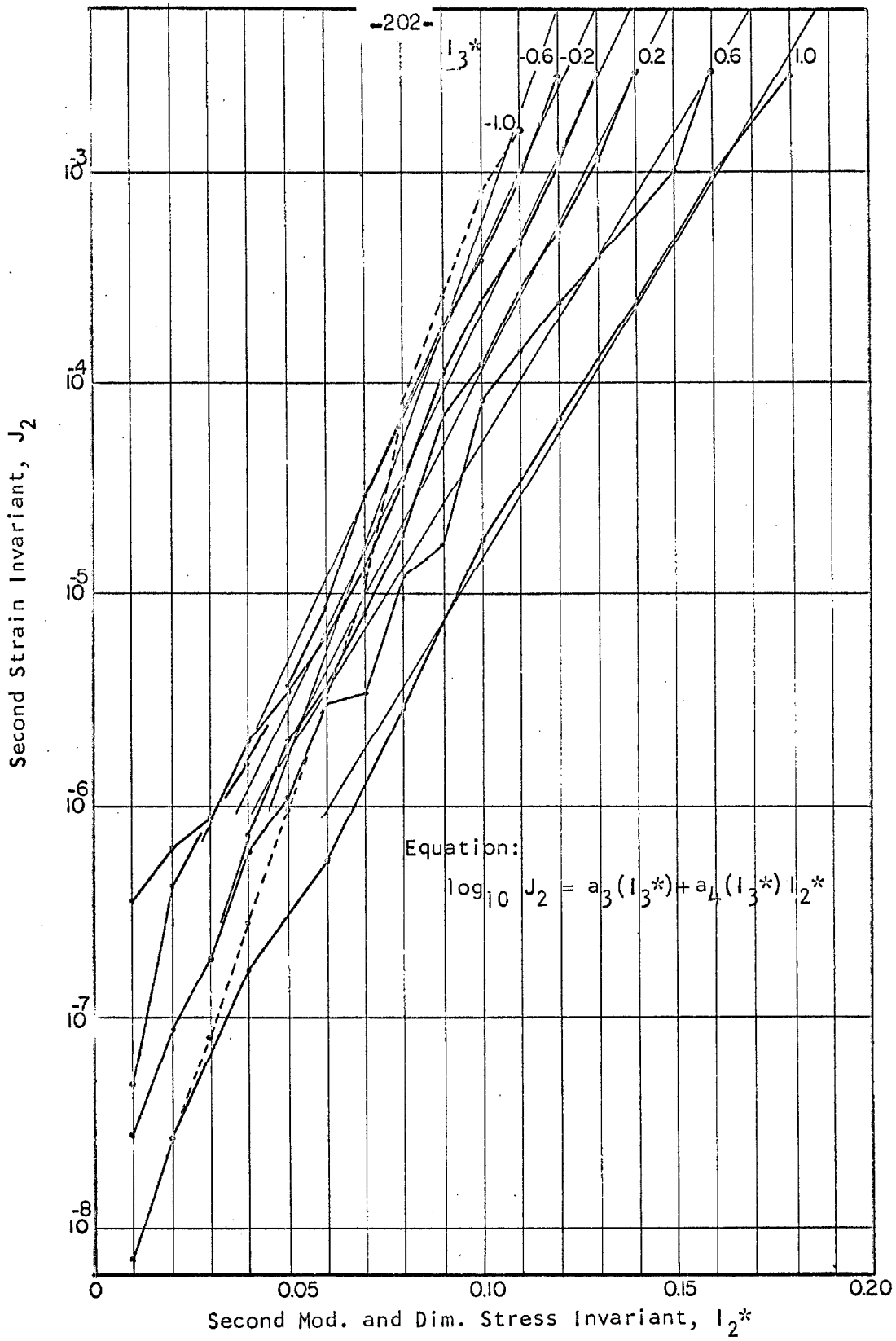

Figure 8.11 Second Strain Invariant as a Function of the Second Modified and Dimensionless Stress Invariant, I_{13}^* Yield Tests, I_3^* = -1, -0.6, -0.2, +0.2, +0.6, +1.

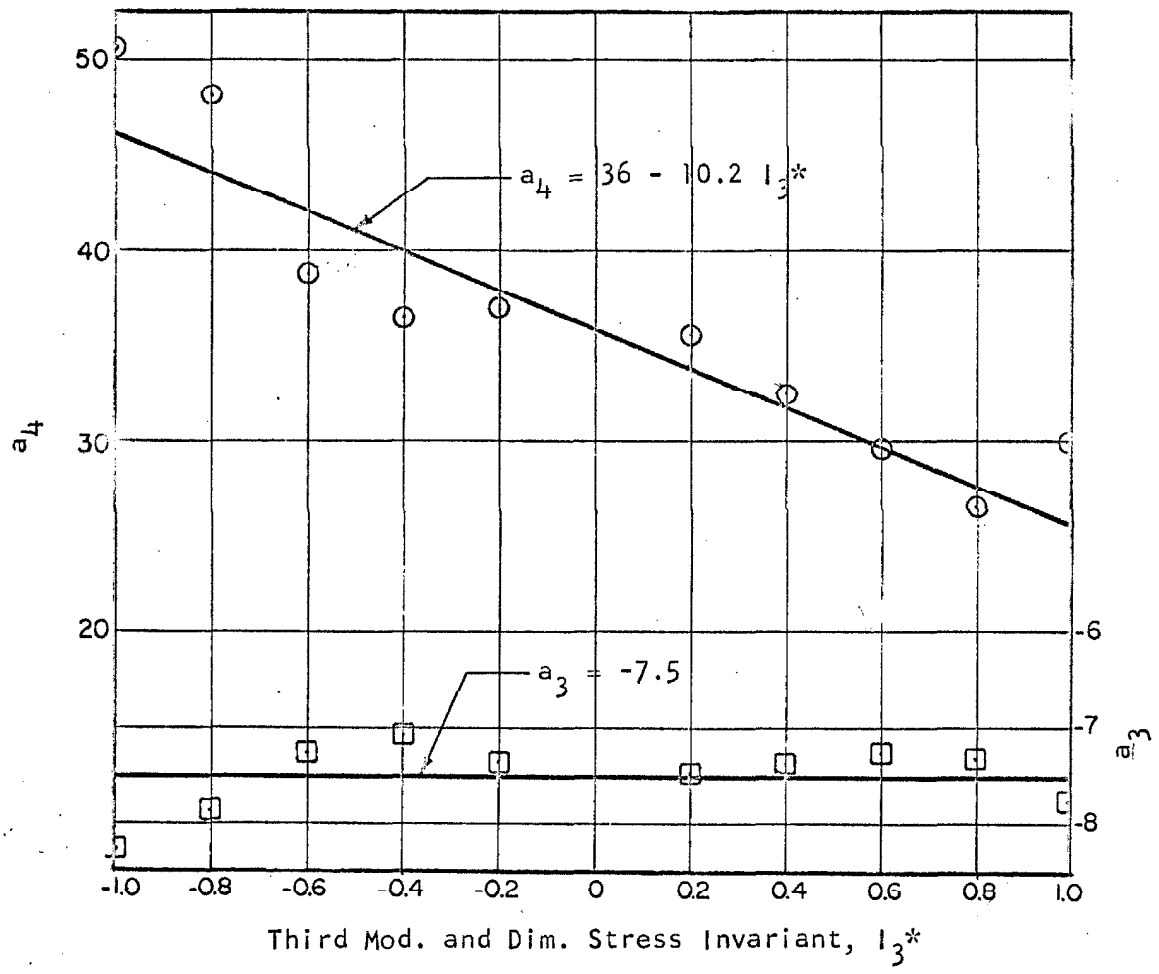

Equation: $\log_{10} J_2 = a_3 + a_4 I_2^*$

$J_2 = e^{2.30(a_3 + a_4 I_2^*)}$ (exponential)

Based on: I_{13^*} yield tests carried out from a spherical compression stress state.

Figure 8.12 Empirical Fit - The Second Modified Strain Invariant as a Function of the Second and Third Modified and Dimensionless Stress Invariants.

Equation 8.43 is given in exponential form by

$$J_2 = e^{2.30(a_3 + a_4 I_2^*)} \tag{8.46}$$

and upon substitution of Equations 8.44 and 8.45 may be written

$$J_2 = e^{82.9 I_2^*(1-0.283 I_3^*)-17.27} \tag{8.47}$$

In the form of Equations 3.62 and 3.66 for this case with I_1 and I_3^* constant

$$dJ_2 = C_{22} dI_2^* \tag{8.48}$$

where

$$C_{ijC}(n, I_1, I_2^*, I_3^*) = C_{22C}(0.34, 54 \text{ psi}, I_2^*, I_3^*) \tag{8.49}$$

and since $C_{22} = \frac{\partial J_2}{\partial I_3^*}$ it follows from Equation 8.47 that

$$C_{22C} = 82.9 (1-0.283 I_3^*) e^{82.9 I_2^*(1-0.283 I_3^*)-17.27} \tag{8.50}$$

Neglecting elastic rebound for decreasing I_2^* (i.e. Figure 7.46) results in

$$C_{22R} \doteq 0 \tag{8.51}$$

8.243 The Third Modified and Dimensionless Strain Invariant as a Function of the Second and Third Modified and Dimensionless Stress Invariants. Figure 8.13 gives $-J_3$ results plotted against I_2^* and I_3^* for eight yield tests. The vertical boundaries of this plot were assumed such that $I_3^*, -J_3^* = 1$ and $I_3^*, -J_3^* = -1$. Errors in strain measurement are particularly noticeable in the calculation of $-J_3^*$ and the results are not smooth. Lines of constant $-J_3^*$ for the linearly elastic solid would be vertical such that $-J_3^* = I_3^*$. Figure 8.14 gives the $-J_3^*$ surface from Figure 8.13 transformed to an octahedral plane in principal stress space.

Figure 8.15 gives combined plots showing $-J_3^*$ as a function of I_2^* for eight tests at fixed values of I_3^*. Curve fitting was primarily based upon those results for $I_2^* \geq 0.06$, corresponding with the previous case. The erratic nature of the data for $I_2^* \leq 0.04$ is attributed to errors in strain measurement. A linear expression in I_2^* was selected to fit these results with the coefficients in I_3^*

$$-J_3^* = a_5(I_3^*) + a_6(I_3^*)\, I_2^* \tag{8.52}$$

Values of a_5 and a_6 were determined for each test and plotted against I_3^* as shown in Figure 8.16 resulting in the following approximations

$$a_5 = -0.10 + 0.70\, I_3^* \tag{8.53}$$

$$a_6 = -3.00\,(1 - I_3^{*2}) \tag{8.54}$$

Substitution of Equations 8.53 and 8.54 into Equation 8.52 results in

$$-J_3^* = -0.10 + 0.70\, I_3^* - 3(1 - I_3^{*2})\, I_2^* \tag{8.55}$$

In the form of Equations 3.63 and 3.66 for this case with I_1 and I_3^* constant

$$dJ_3 = C_{32}\, dI_2^* \tag{8.56}$$

where

$$C_{ijC}(n,\, I_1,\, I_2^*,\, I_3^*) = C_{32C}(0.34,\, 54 \text{ psi}, I_2^*, I_3^*) \tag{8.57}$$

and since $C_{32} = \dfrac{\partial J_3^*}{\partial I_2^*}$ it follows from Equation 8.55 that

$$C_{32C} = 3(1 - I_3^{*2}) \tag{8.58}$$

Neglecting elastic rebound for decreasing I_2^* (i.e. Figure 7.46) results in

$$C_{32R} \doteq 0 \tag{8.59}$$

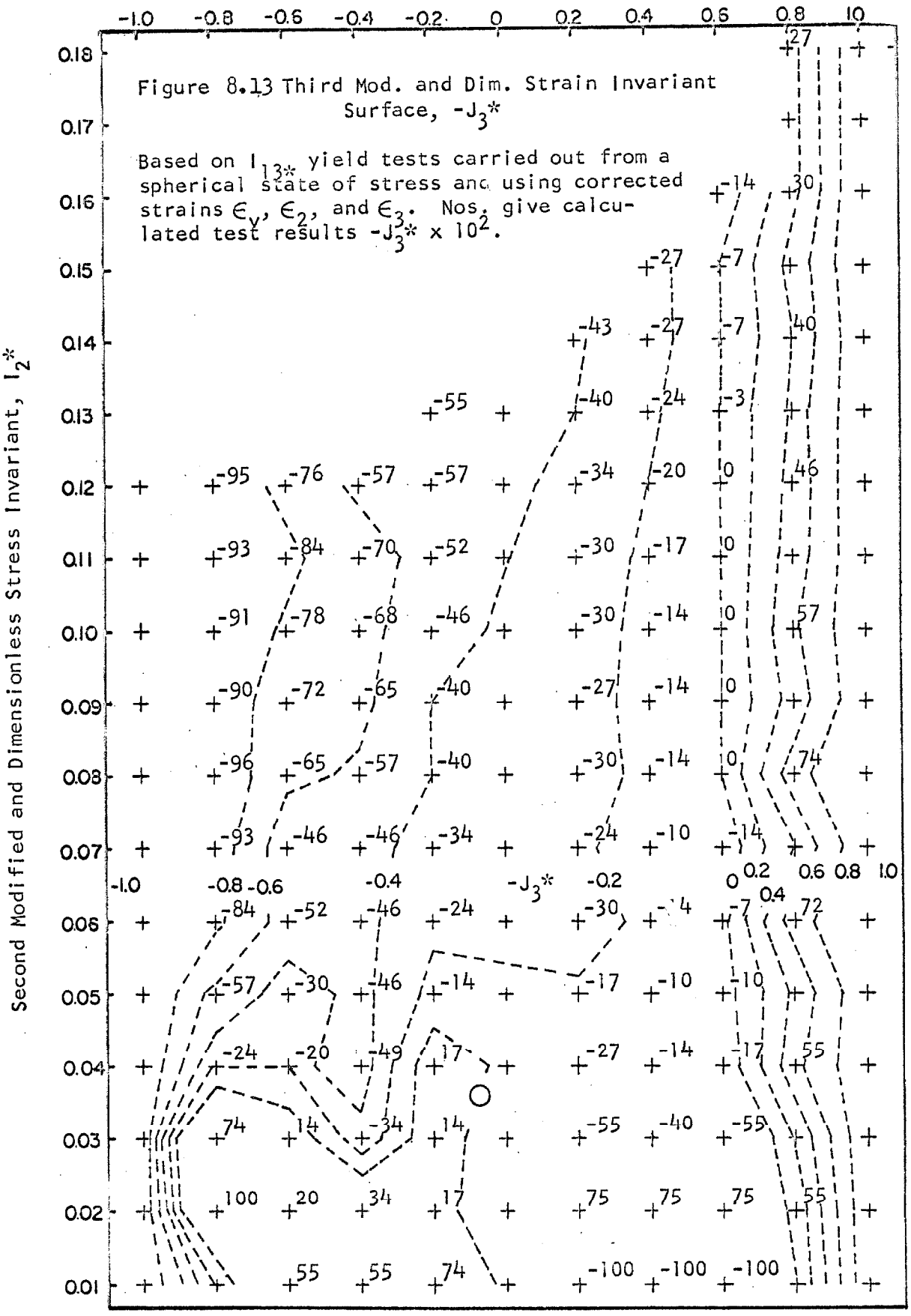
Third Modified and Dimensionless Stress Invariant, I_3^*
Second Modified and Dimensionless Stress Invariant, I_2^*
$-J_3^*$
-1.0 -0.8 -0.6 -0.4 -0.2 0 0.2 0.4 0.6 0.8 1.0
0.18 0.17 0.16 0.15 0.14 0.13 0.12 0.11 0.10 0.09 0.08 0.07 0.06 0.05 0.04 0.03 0.02 0.01
Figure 8.13 Third Mod. and Dim. Strain Invariant Surface, $-J_3^*$
Based on I_{13^*} yield tests carried out from a spherical state of stress and using corrected strains ϵ_v, ϵ_2, and ϵ_3. Nos. give calculated test results $-J_3^* \times 10^2$.

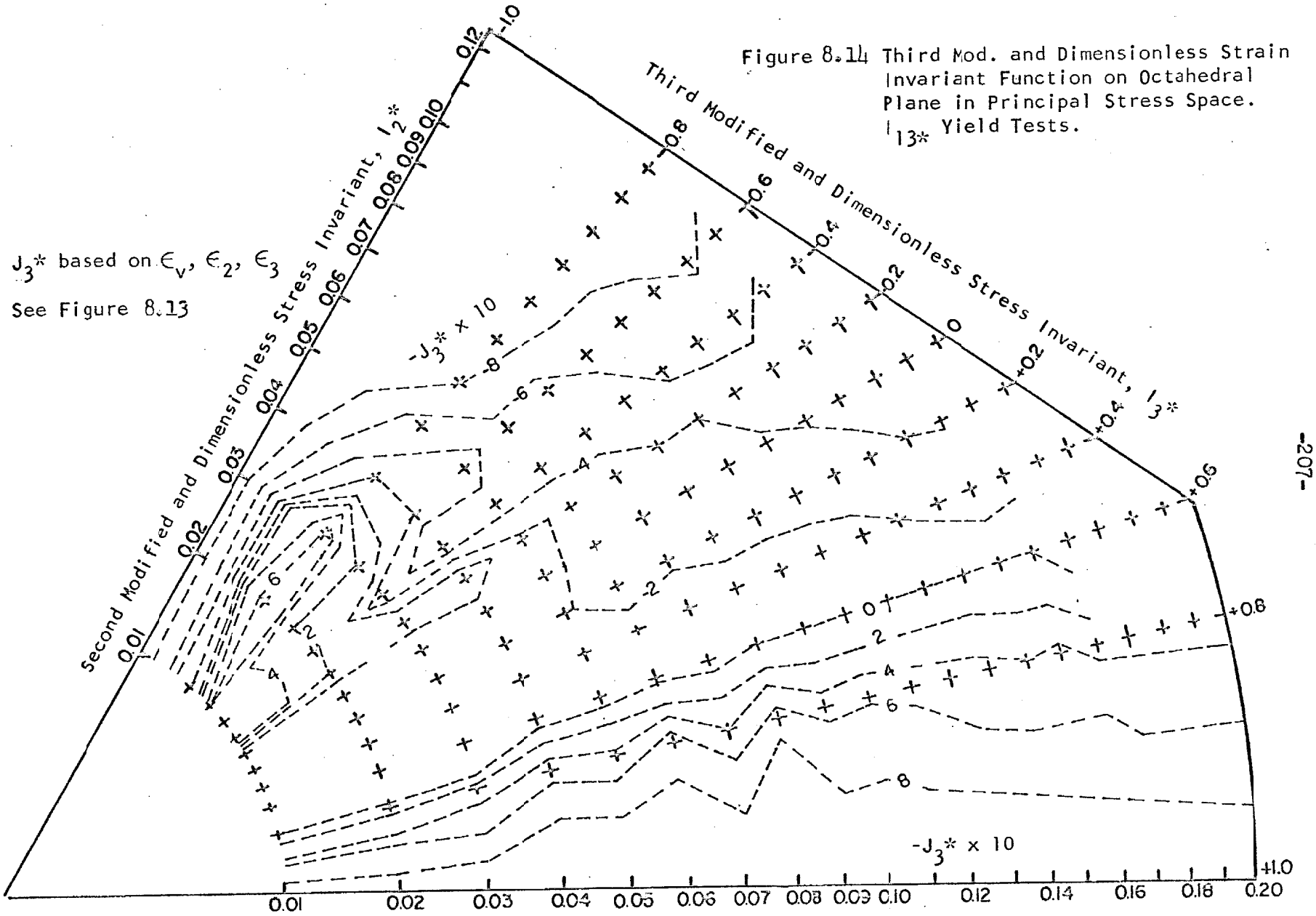

Figure 8.14 Third Mod. and Dimensionless Strain Invariant Function on Octahedral Plane in Principal Stress Space. I_{13}^* Yield Tests.

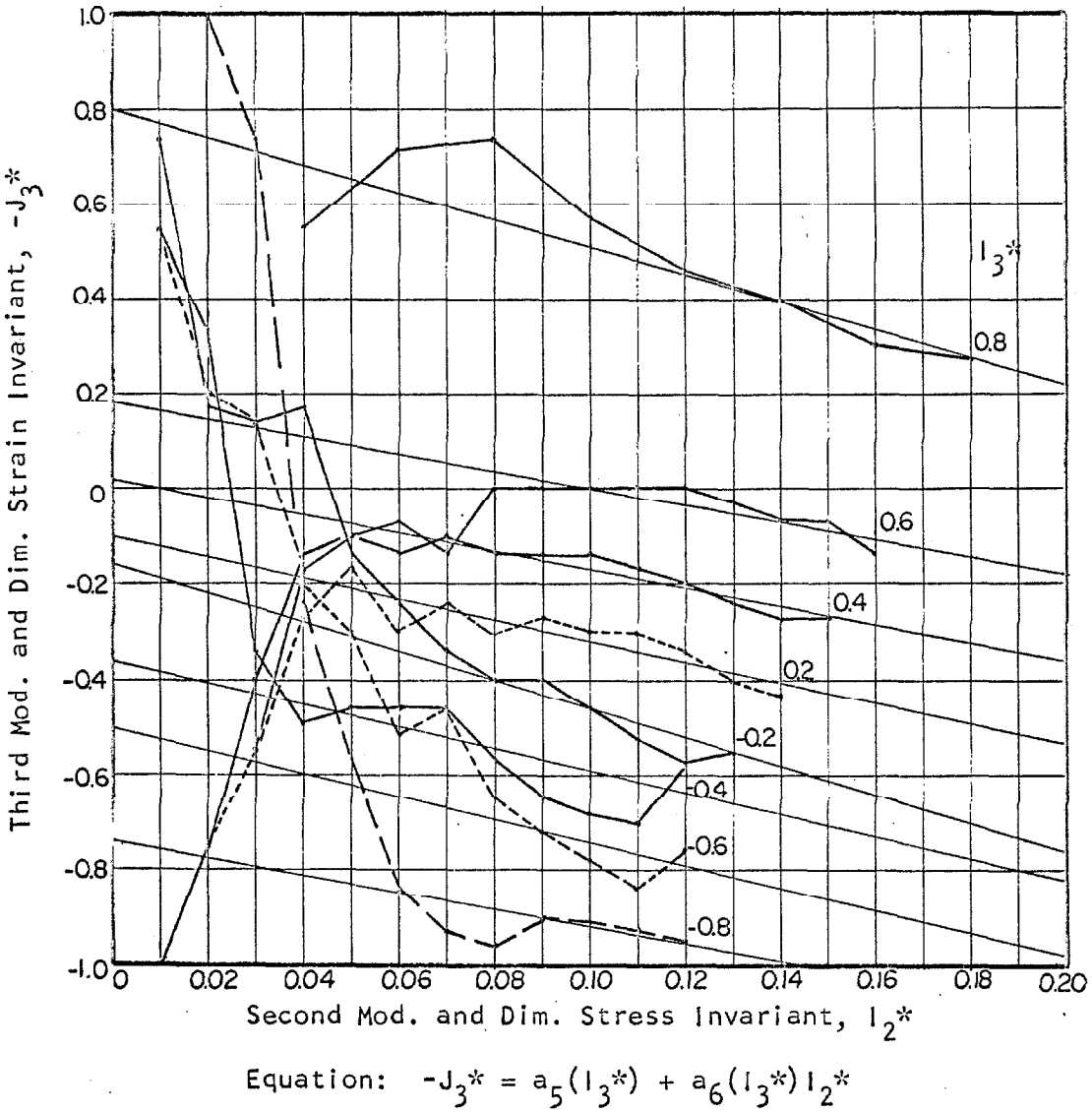

Figure 8.15 Third Modified and Dimensionless Strain Invariant as a Function of the Second and Third Modified Stress Invariants. I_{13}* Yield Tests.

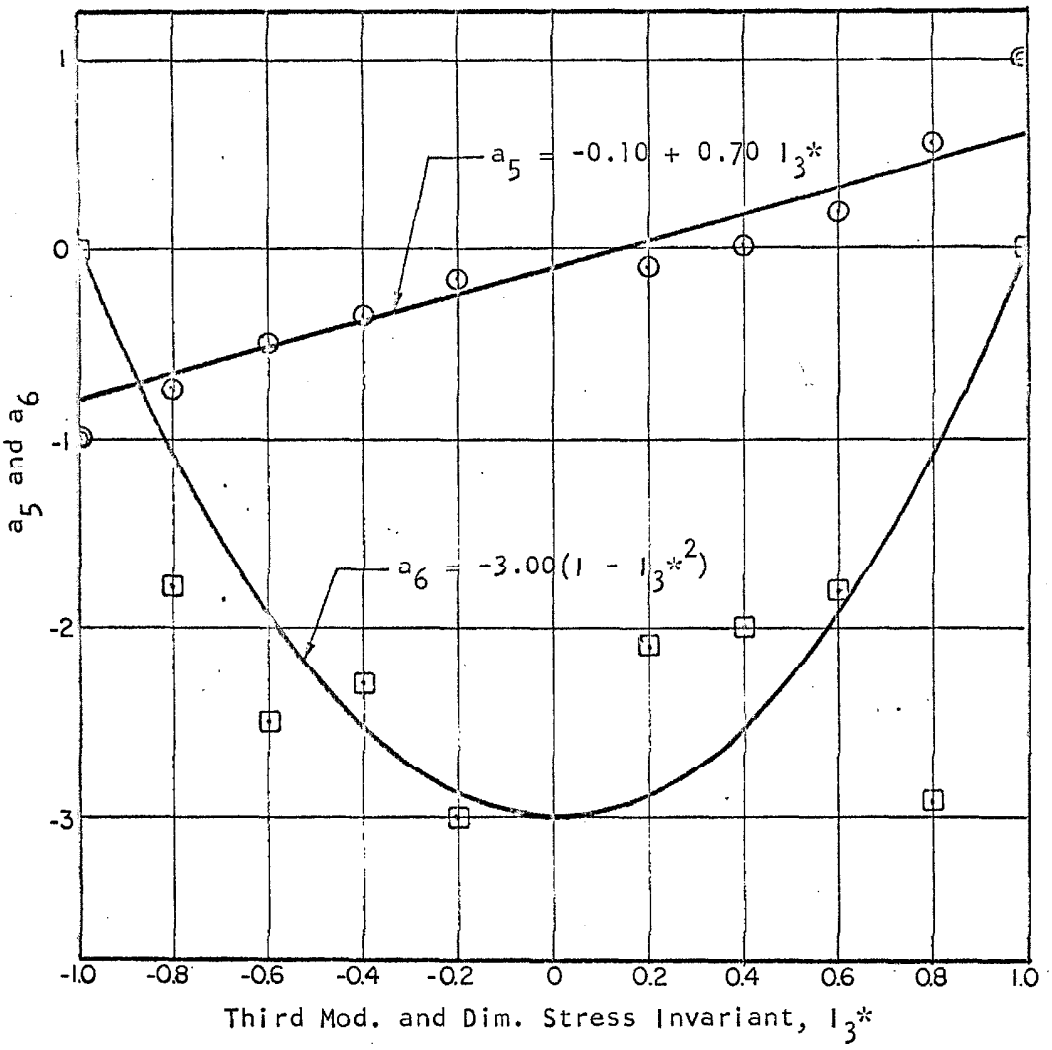

Equation: $-J_3^* = a_5 + a_6 I_2^*$ (First order polynomial)

Based on: I_{13^*} yield tests carried out from a spherical compression stress state.

Figure 8.16 Empirical Fit - The Third Modified and Dimensionless Strain Invariant as a Function of the Second and Third Modified and Dimensionless Stress Invariants.

8.244 Application to Circular Compression. Equations 8.25 and 8.28 were derived from a single test and do not include the effect of the variable I_2^*. Equations 8.31 and 8.32 were proposed to include the effect of I_2^*; however, the constants p and m were arbitrary. One would not expect to obtain an accurate measure of circular response from equations derived from radial stress paths because of differences in stress-strain history and the direction of loading. For lack of a better method, however, partial differentiation of Equations 8.36 and 8.50 with respect to I_3^* results in

$$\frac{\partial J_1}{\partial I_3^*} = -0.38\ I_2^{*2} \tag{8.60}$$

and

$$\frac{\partial J_2}{\partial I_3^*} = -23.5\ I_2^*\ e^{82.9\ I_2^*(1-0.283\ I_3^*)-17.27} \tag{8.61}$$

For $I_2^* = 0.10$ these expressions reduce to

$$\frac{\partial J_1}{\partial I_3^*} = -3.8 \times 10^{-3} \tag{8.62}$$

and

$$\frac{\partial J_2}{\partial I_3^*} = -2.35\ e^{-(8.98\ +\ 2.34\ I_3^*)} \tag{8.63}$$

which indicate strain response which is of the same order of magnitude, but high as compared with that from circular compression Equations 8.25 and 8.28 respectively. There is little reason to believe the response should be equivalent; however, it was considered that the general form of the relationship might be similar, and thus give some indication as to suitable constants p and m for use in Equations 8.31 and 8.32. Equation 8.60 suggests the value $p = 2$, and Equation 8.61 suggests the value $m = 1$.

8.3 A GENERAL STRESS-STRAIN RELATIONSHIP IN INVARIANT FORM

The following stress-strain relationships from Chapter 3 were adopted for purposes of analysis

$$dJ_1 = C_{11}dI_1 + C_{12}dI_2^* + C_{13}dI_3^* \quad [3.61]$$

$$dJ_2 = C_{21}dI_1 + C_{22}dI_2^* + C_{23}dI_3^* \quad [3.62]$$

$$dJ_3^* = C_{31}dI_1 + C_{32}dI_2^* + C_{33}dI_3^* \quad [3.63]$$

where

$$C_{ij} = C_{ijC}(n, I_1, I_2^*, I_3^*), \quad dI_j > 0 \quad [3.66]$$

$$= C_{ijR}(n, I_1, I_2^*, I_3^*), \quad dI_j < 0 \quad [3.67]$$

The coefficient functions obtained by preceding analyses are summarized as follows for the particular sand of this study at $n \doteq 0.34$.

Spherical Compression

$$C_{11C} = C_{11R} = -5.60 \times 10^{-4}\, I_1^{-0.837} \qquad (I_1 \text{ in psi}) \quad [8.16]$$

$$C_{21C} = C_{21R} = 0 \quad [8.15]$$

$$C_{31C} = C_{31R} = 0 \quad [8.15]$$

Radial Compression

$$C_{12C} = -0.063 + (1.84 - 0.76\, I_3^*)\, I_2^*, \quad I_2^* \geq 0.6 \quad [8.39]$$

$$= 0, \quad I_2^* < 0.6 \quad [8.41]$$

$$C_{12R} = 0 \quad [8.42]$$

$$C_{22C} = 82.9\,(1-0.283\, I_3^*)e^{82.9\, I_2^*(1-0.283\, I_3^*)-17.27} \quad [8.50]$$

$$C_{22R} = 0 \quad [8.51]$$

$$C_{32C} = 3(1 - I_3^{*2}) \quad [8.58]$$

$$C_{32R} = 0 \quad [8.59]$$

Circular Compression

$$C_{13C} = 0 \qquad [8.23]$$

$$C_{13R} = -0.29\ I_2^{*2} \qquad [8.31]$$

$$C_{23C} = 0 \qquad [8.23]$$

$$C_{23R} = -16.7\ I_2^*\ e^{-(8.18+1.67\ I_3^*)} \qquad [8.32]$$

$$C_{33C} = C_{33R} = -1 \qquad [8.23,\ 8.30]$$

The foregoing incremental stress-strain equations do not include the yield condition, and are best applied to stress histories obtained in this investigation. In the general form presented, however, predictions may be made for an arbitrary stress increment.

8.4 A FIRST YIELD CRITERION BASED ON RADIAL COMPRESSION STRESS PATHS PROCEEDING FROM AN INITIAL SPHERICAL STATE OF STRESS

Analyses of previous sections were based upon test results corrected for the strain effects of membrane penetration and pressure-cell behavior; applied stresses were used throughout. Since the major and minor principal strains at yield were on the order of 2-5%, the stress effect, Appendix A9, was measurable and will be taken into account here. Corrected principal stresses and stress invariant functions, Table 8.1, were calculated from the corrected principal strains immediately prior to and following first yield for the ten radial tests of Section 8.24. Figure 8.17 gives I_2^* plotted as a function of I_3^*, and a first yield range is established. Figure 8.18 gives results from Figure 8.17 transformed to an octahedral plane in principal stress space for comparison with the Mohr-Coulomb theory of failure.

The first yield stress relationship in general form as given by Equation 3.71 was

$$C_{1y}(n, I_1, I_2^*, I_3^*) = 0$$

and since n and I_1 were essentially fixed for the ten radial tests considered here, the relationship is given by

$$C_{1y}(0.34, 54 \text{ psi}, I_2^*, I_3^*) = 0$$

This may be written in the form

$$I_2^* = \bar{\Phi}(I_3^*) \tag{8.64}$$

The simplest expression in invariant form which was found to fit the first yield range was

$$I_2^* = 0.116 + 0.016\,(1 + I_3^*)^2 \tag{8.65}$$

This expression is plotted as a solid continuous curve on Figures 8.17 and 8.18.

It is suggested for the stress history represented that a first yield criterion which accounts for variations in porosity might be approximated by the generalization of Equation 8.65 such that

$$I_2^* = b_1(n) + b_2(n)[1 + I_3^*]^2 \tag{8.66}$$

Table 8.1 Calculation of Stress-Corrected First Yield Criterion

Test	Applied Values (I_1 = 54 psi)				Principal Strains (1)			Stress-Corrected Values (2)				
	I_3^*	σ_1 psi	σ_2 psi	σ_3 psi	$-\epsilon_1$ x 10^{-4}	ϵ_2 x 10^{-4}	ϵ_3 x 10^{-4}	σ_1 psi	σ_3 psi	I_1 psi	I_2^* x 10^3	I_3^* x 10^3
					Before Yield							
4-4	1.0	35.64	9.18	9.18	238	145	145	34.77	8.70	52.65	161	1000
8-5	0.8	35.23	12.63	6.13	185	37	194	34.32	5.60	52.55	162	755
13-5	0.6	34.27	14.37	5.37	203	14	250	33.28	4.84	52.49	152	534
12-5	0.4	33.28	15.74	4.98	199	0	270	32.24	4.41	52.39	143	314
11-5	0.2	32.27	16.93	4.80	187	-12	270	31.18	4.18	52.29	133	97
10-4	-0.2	30.68	19.02	4.29	173	-31	276	29.51	3.57	52.10	125	-320
15-5	-0.4	29.55	20.00	4.45	142	-40	242	28.35	3.64	51.99	117	-523
14-5	-0.6	28.82	21.11	4.07	138	-56	267	27.59	3.25	51.95	118	-710
9-4	-0.8	27.84	22.45	3.71	210	-120	450	26.57	3.11	52.13	118	-878
5-6	-1.0	24.97	24.97	4.06	95	-95	253	23.59	3.03	51.59	113	-985
					After Yield							
4-4	1.0	36.71	8.65	8.65	408	255	255	35.64	8.25	52.54	178	999
8-5	0.8	36.28	12.31	5.41	264	54	289	35.32	5.02	52.65	180	761
13-5	0.6	34.80	14.25	4.95	341	23	446	33.74	4.68	52.67	158	550
12-5	0.4	33.82	15.66	4.52	341	0	463	32.69	4.21	52.56	149	330
11-5	0.2	32.81	16.89	4.30	306	-19	460	31.68	3.95	52.52	140	115
10-4	-0.2	31.20	19.07	3.73	299	-47	461	29.96	3.26	52.29	132	-310
15-5	-0.4	30.06	20.09	3.85	250	-62	431	28.83	3.31	52.23	123	-513
14-5	-0.6	29.30	21.25	3.45	249	-81	461	28.03	2.90	52.18	124	-700
9-4	-0.8	28.28	22.65	3.08	263	-157	587	27.03	2.69	52.37	123	-872
5-6	-1.0	25.31	24.31	3.38	130	-130	358	23.94	2.51	51.76	122	-987

(1) Strains corrected for pressure-cell effects and rubber penetration.

(2) Stress-corrected σ_2 = applied σ_2, stress-corrected values of σ_1 and σ_3 calculated from Equations A9.9 and A9.10.

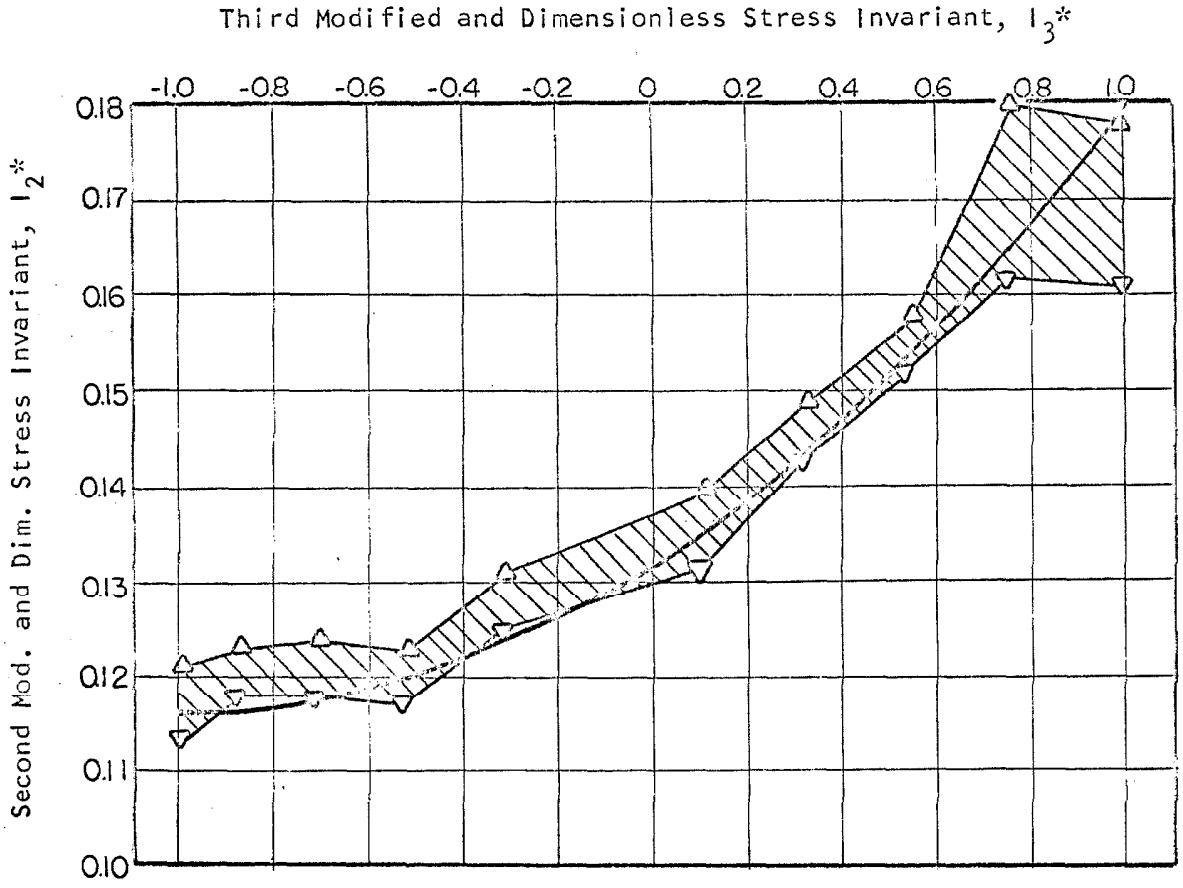

First yield range based on I_{13}^* test results corrected for stress and strain effects attributed to rubber characteristics.

Figure 8.17 Stress-Strain Corrected First Yield Zone, Second Modified and Dimensionless Stress Invariant as a Function of the Third Modified and Dimensionless Stress Invariant.

Figure 8.18

Stress-Strain Corrected First Yield Zone on an Octahedral Plane in Principal Stress Space

(See Figure 8.17)

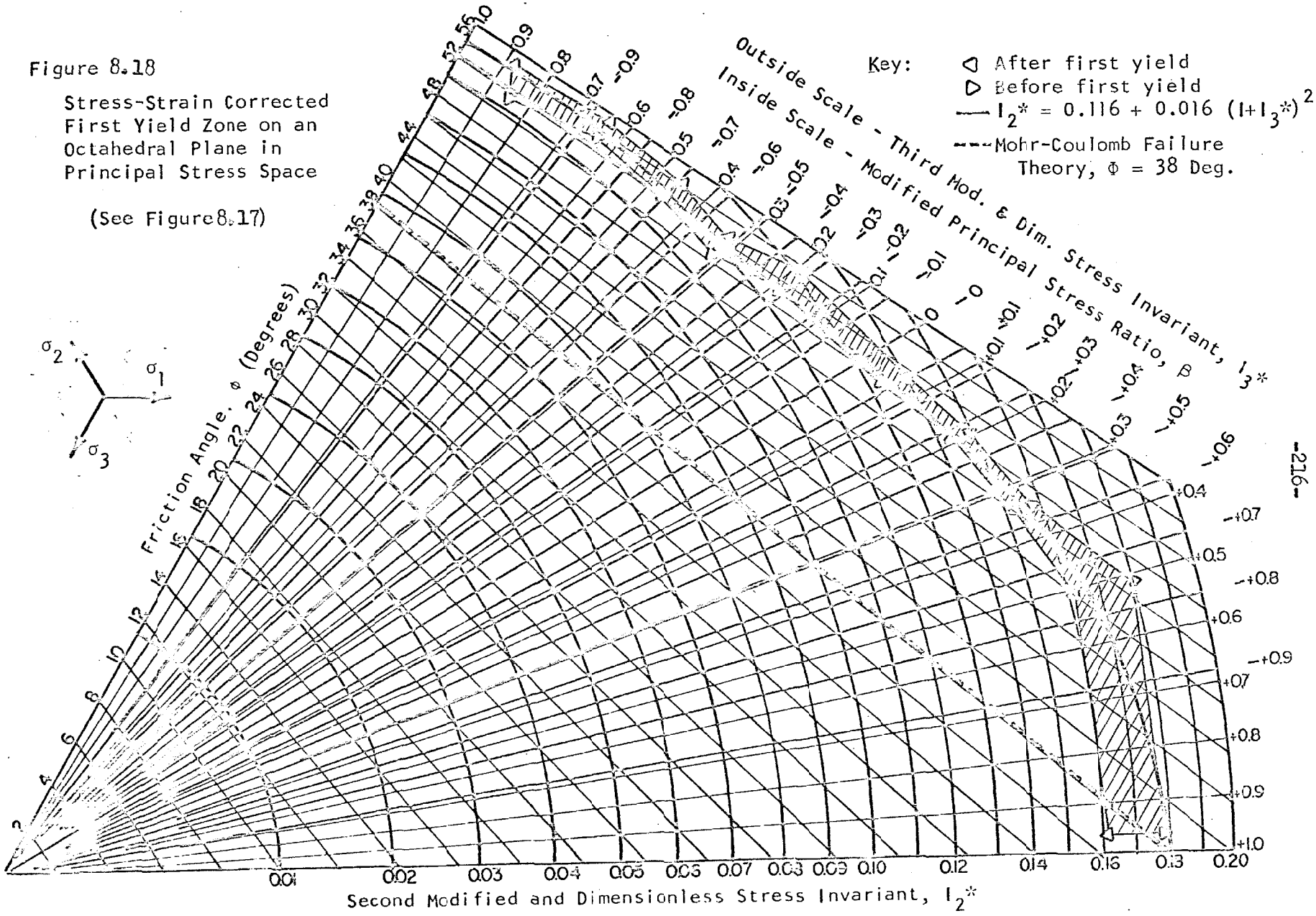

9. DISCUSSION

9.1 ISOTROPY

The question of isotropy is important in the interpretation of experimental results obtained in this investigation. The stress-strain relationship for sand subjected to general stress states is in part dependent upon stress-strain history or induced anisotropy. After forming and upon application of spherical stress, test specimens in both apparatus were believed isotropic. Three-dimensional compression samples were believed to become increasingly anisotropic with application of deviatoric stress.

9.11 SPHERICAL COMPRESSION

No attempt was made to measure linear strains in the spherical apparatus. Volumetric strains were sufficient upon the assumption that the material was isotropic. Specimens were formed by pouring sand into a cylindrical mold--lower porosities being obtained by compaction with a small-diameter rod. The high degree of elasticity (later discussed) obtained in the spherical apparatus was believed indicative of isotropic deformations. Anisotropic sand subjected to spherical stress undergoes shearing distortion which leads to higher and less elastic volumetric strains in comparison with isotropic material at the same porosity.

9.12 THREE-DIMENSIONAL COMPRESSION

Were the three-dimensional compression samples isotropic prior to deviatoric tests? It is possible that the sample forming procedure,

Figures 6.12 and 6.13, may have led to some diagonal stratification and anisotropy. Upon being subjected to spherical stress the deformations recorded by the volume change in the side cells were practically equivalent and it may be assumed that the material properties in the directions of minor and major principal stress were the same. Unequal compressibility of the base cell precluded a direct comparison with the intermediate principal strain under spherical compression.

If the specimens were initially stratified, angular distortion should have been evident near yield. The method of sample preparation and stress application were related and consistant as indicated by Figure 9.1. All samples remained visibly rectangular in shape with exception of Specimen No. 10, Figure 6.23, which yielded locally, and this may be attributed to a non-homogenity either in the material or in the stress application. Several indications thus substantiate the view that the samples were initially isotropic.

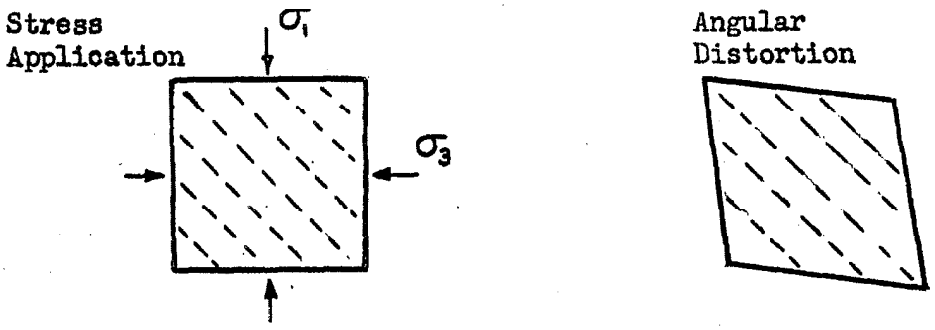

Figure 9.1 Anisotropic Three-Dimensional Test Specimen Subjected to Fixed Stress System

Were three-dimensional compression samples isotropic moving from spherical compression at low states of deviatoric stress?

Adopting the simplified assumption that the material is linearly elastic it follows that

$$-d\epsilon_1 = g_{11}d\sigma_1 + g_{12}d\sigma_2 + g_{13}d\sigma_3$$

$$-d\epsilon_2 = g_{21}d\sigma_1 + g_{22}d\sigma_2 + g_{23}d\sigma_3$$

$$-d\epsilon_3 = g_{31}d\sigma_1 + g_{32}d\sigma_2 + g_{33}d\sigma_3$$

where g_{ij} are elastic constants possibly dependent upon orientation. If the test specimens were diagonally stratified, then it follows by transformation of axes 1 and 3 that $g_{33} = g_{11}$, $g_{31} = g_{13}$, $g_{32} = g_{12}$ and $g_{23} = g_{21}$, and thus the first strain invariant may be written

$$-dJ_1 = -d\epsilon_1 - d\epsilon_2 - d\epsilon_3 = adI_1 + (b-a)d\sigma_2$$

where

$$a = g_{11} + g_{21} + g_{13}$$

$$b = 2g_{12} + g_{22}$$

For the deviatoric experiments $dI_1 = 0$ so that

$$dJ_1 = (a-b)d\sigma_2$$

If the material is isotropic then $b = a$ and $dJ_1 = 0$ (seeEquation 3.45).

Results obtained from deviatoric tests (i.e. Figures 7.40 through 7.47) best agree with the isotropic assumption or $dJ_1 = 0$. Generally the initial sign of dJ_1 was negative and then positive with increasing I_2* irrespective of the sign of $d\sigma_2$ in the various tests.

At low states of deviatoric stress the measured principal strains were of the same order of magnitude as the pressure-cell corrections and thus the volumetric strain measurements corrected for rubber penetration were believed the only reliable results. The

consistent however slight consolidation indicated initially is thought to represent a true mechanical characteristic of the material even though the accuracy of data obtained is questionable.

Anisotropic behavior was particularly noticeable where samples had yielded under relatively high states of deviatoric stress. Spherical compression stress cycles performed following deviatoric tests carried to yield (Figures 7.29, 7.31, 7.33 and 7.35), and following deviatoric tests not carried to yield (Figures 7.19, 7.23 and 7.39) indicate higher compressibilities in comparison with initial isotropic values. Anisotropic strain response is indicated by the variation of the major principal strain difference with spherical stress. Following a deviatoric test, volumetric compressibilities decreased with cycles of spherical stress--approaching former isotropic values-- and the rate of change of major principal strain difference decreased. Increasing cycles of spherical stress reduced anisotropy; however, it seems doubtful that the isotropic case would ultimately be obtained in this fashion.

9.2 ELASTICITY

The behavior of initially isotropic sand subjected to spherical stress was essentially elastic while the behavior of initially isotropic sand subjected to deviatoric stress was essentially inelastic. Isotropy and elasticity are evidently related with reference to the stress-strain behavior of sand. The hypothesis is advanced that elastic sand must be isotropic.

9.21 SPHERICAL COMPRESSION

The degree of elastic deformation obtained from tests performed in the spherical apparatus (see Figure 8.2) is dependent upon porosity and stress history. Higher degrees of elastic return were obtained with decreasing porosity while the effect of increasing cycles of stress was more noticeable with increasing porosity. The degree of elasticity was generally 90-100%, thus the sand of this study may be considered essentially elastic under spherical stress.

Higher elasticity recorded for denser samples is likely related to the decreased load carried by individual contacts while increases in elasticity with cycles of stress may be due to strain hardening of individual contacts.

9.22 THREE-DIMENSIONAL COMPRESSION

The degree of elastic return based upon radial stress cycles carried to yield from spherical compression (Figures 7.28, 7.30 and 7.40 through 7.47) was approximately 20% for minor principal strains, 15% for major principal strains, 15-20% for intermediate principal strains, and 40% for volumetric strains. Similar results were recorded from deviatoric tests not reaching yield (Figures 7.18, 7.22 and 7.38). On this basis it is concluded that the behavior of sand subjected to deviatoric stress is relatively inelastic. The manner in which elasticity varies as radial stress cycles are increased in span from spherical stress to yield was not studied in detail because of inaccurate measurement of small (i.e. less than 0.2%) principal strains. It is considered likely that the degree of elasticity varies from

90-100% at spherical compression to values indicated in the foregoing at yield.

Few circular compression stress cycles were carried out; however, Figures 7.21, 7.29 and 7.37 indicate that for constant I_1 and I_2*, decreasing I_3* is associated with strain response toward yield and increasing I_3* is associated with relatively inelastic strain response.

The degree of elastic return for initial cycles of spherical stress was generally on the order of 70-90%. This was lower than obtained in the spherical compression apparatus, and is thought to represent the result of less homogeneous loading. Compressibilities obtained were generally higher in compression and lower in extension, Figure 7.31. In comparison, Figure 7.16 indicates superiority of the spherical compression apparatus for the determination of spherical stress-strain relationships.

9.3 EFFECTS OF VIBRATION

A detailed study of vibration was not performed as a part of this study; however, the effects of vibration on experimental results were considered important and measures were taken to reduce these effects.

The apparatus was housed in the first basement story below ground of Thomas Engineering Building and the normal level of vibration was slight, there being no heavy traffic about the structure.

During the initial stages of experimental work (Spherical Compression Test 4-1) the starting of a vibration machine one floor above the apparatus produced a noticeable increase in the rate of volumetric

strain. Measurements of acceleration produced by various building equipment were subsequently made at the apparatus and it was discovered that the forementioned machine produced accelerations of 2×10^{-4} g when operated at relatively low frequencies from 10 to 30 cycles per second. Attempts to cushion the spherical apparatus with fibrous mats were not successful.

Steps immediately taken to reduce the possible adverse effects of vibration on spherical experiments included not operating the vibration machine during tests subsequent to 4-2 and reducing the time interval between successive load increments to 2 minutes. In preparation for three-dimensional experiments the compression chamber was mounted on vibration isolators, Figure A7.4, as was the vibration equipment on the floor above.

9.4 REPRODUCIBILITY OF TEST RESULTS

Where spherical specimens were most elastic, i.e. Figure 7.16, repeated cycles of stress gave reproducible results. Different samples were not formed to the same initial porosity, thus reproducibility of entire experiments cannot be guaranteed.

Nearly equal initial porosities were obtained in three-dimensional compression experiments and initial cycles of spherical stress yielded comparable results, Figures 7.26, 7.29, 7.31 and 7.39. Each three-dimensional specimen was then subjected to a different stress program such that identical experiments were not available for comparison. Results from similar stress paths, Figures 7.28 and 7.34, were not strictly comparable because the stress history was different.

9.5 SPHERICAL STRESS-STRAIN RELATIONSHIP

If the expression derived from spherical apparatus tests and given by Equation 8.4

$$\frac{dn}{d\sigma} = -C_1(n)\sigma^{C_2(n)}$$

or Equation 8.6

$$dJ_1 = -\frac{C_1(n)}{3[1+C_2(n)]} I_1^{C_2(n)} dI_1$$

is taken to describe the stress-strain relationship for a particular sand then stress-strain history and the direction of loading have been neglected, and it must be assumed that the material is isotropic and elastic. For the sand of this study the values C_1 and C_2 as functions of porosity are given for final stress cycles by Figure 8.1.

Wilson and Sutton (9) derived a relationship of the form $\epsilon = C\sigma^{2/3}$ where ϵ is linear strain and C a constant on the simplified assumptions that sand consists of spheres in the loosest (cubic) state of packing, and that the Hertz contact theory (38) is valid. Equations 8.4 and 8.6 satisfy this theory only if $C_1(n) = 2C$ and $C_2(n) = -1/3$. The questionable projection of triaxial compression test results reported by Wilson and Sutton to spherical compression (zero shear stress), Figures 7 through 10, generally does not satisfy the relationship $\epsilon = C\sigma^{2/3}$.

Kjellman (8), using three-dimensional apparatus, presented data for a spherical test on sand, Figure 5, from which the author obtained $C_1 = 1.21 \times 10^{-4}$ and $C_2 = -0.403$. For a stress cycle from 0 to 170 psi, the degree of elastic return was 78%. Jakobson (12), using the same apparatus, reported a spherical stress-strain relationship for sand in the form $\epsilon = C\sigma^a$. Jakobson implied the foregoing relationship was

derived to account for inelastic behavior--which it does not. No data was included on elastic return. For a single compression path, Figure 5, the author obtained $C_1 = 1.52 \times 10^{-2}$ and $C_2 = -0.388$.

Chaplin (17) indicates that non-spherical grain-to-grain contacts may account for variations from Hertzian theories and suggests values of a in the Jakobson formulation of $1/2(C_2 = -1/2)$. Triaxial compression results reported by Chaplin indicate that about 0.025% axial strain is required to obtain the factor 1/2 in one-dimensional consolidation. As with the Wilson and Sutton investigation, the projection of this result to spherical compression is questionable.

The author's work indicates a degree of elastic return of 90-100% which depends upon porosity and stress history. With the exception of Kjellman's data, none of the forementioned investigators have considered extension or elasticity. The results of numerous one-dimensional consolidation tests which are associated with appreciable shear have perhaps led to the erroneous impression that sand is relatively inelastic in spherical compression.

For a particular sand it is suggested that $C_1(n)$ be considered primarily as a measure of grain contacts per unit volume. Considerable variation from the author's values (which were on the order of 10^{-3}) are thus extected in different sands.

For a particular sand it is suggested that $C_2(n)$ be considered as a measure of the increase in grain contact area with load. The variation of $C_2(n)$ from the value -1/3 is attributed to two effects: the increase in the number of grain contacts with load, and the

non-spherical shape of certain grains at contact. The latter effect, originally suggested by Chaplin, is considered minor because the overall recorded behavior was essentially elastic.

The author's study indicates values of $C_2(n)$ on the order of -0.85, which are much less than those indicated by previous investigations. Large deviations do not seem physically reasonable and it is thought that shearing stress associated with test equipment has generally led to higher values of C_2. Also, it is not clear whether account was taken of membrane penetration by former investigators, i.e. Kjellman and Jakobson. The author's data uncorrected for rubber penetration would lead to higher values for $C_2(n)$ of about -0.67.

The spherical compression apparatus used in this investigation was thought superior to those used by previous investigators mainly because particular care was taken to eliminate boundary friction, and stress application was considered essentially homogeneous.

9.6 DEVIATORIC STRESS-STRAIN RELATIONSHIPS

Two basically different stress path families were used to develop relationships between applied deviatoric stress and strain response. Little data was obtained in circular compression, while a relatively large amount of data was obtained in radial compression. The measurement of principal strains at low deviatoric stress was considered unreliable and relationships obtained were not expected to represent material behavior near spherical compression.

Invariant functions were used throughout in planning and analysis of experimental work and thus the results obtained include the

effect of stress-strain history or induced anisotropy specifically for the stress paths carried out. Deviatoric stress-strain relationships do not account for variations in porosity as the initial porosity was essentially constant at 0.34 for all three-dimensional test specimens.

9.61 CIRCULAR COMPRESSION

Circular compression tests were carried out with $I_1 = 54$ psi and I_2^* fixed. Coefficient functions C_{13}, C_{23} and C_{33} were estimated (see Section 8.22) to fit the relationships given by Equations 8.19 through 8.22

$$dJ_1 = C_{13} dI_3^*, \quad dJ_2 = C_{23} dI_3^*, \quad dJ_3 = C_{33} dI_3^*$$

in terms of the second and third modified invariant stress functions. The results are summarized in Section 8.3.

The author's use of the circular compression stress path involving variation of the third stress invariant function is original and no data is available for comparison.

9.62 RADIAL COMPRESSION

Radial compression tests were carried out with $I_1 = 54$ psi and I_3^* fixed. Coefficient functions C_{12}, C_{22} and C_{33} were estimated (see Sections 8.23 and 8.24) to fit the relationships given by Equations 8.37, 8.48 and 8.56

$$dJ_1 = C_{12} dI_2^*, \quad dJ_2 = C_{22} dI_2^*, \quad dJ_3 = C_{32} dI_2^*$$

in terms of the second and third modified invariant stress functions. The results are summarized in Section 8.3.

Previous investigations which have included deviatoric stress paths of the radial compression type are rare. Standard triaxial

compression and extension tests (Sections 4.22 and 4.23) are performed with variations in spherical as well as deviatoric stress and are associated with non-homogeneous loading. Standard triaxial compression test results for the sand of this study are given by Figure 7.3.

Kjellman (8), using three-dimensional compression apparatus, presented test data for deviatoric radial compression tests comparable with those of this study; however, no attempt was made to obtain a stress-strain relationship. Kjellman's Figures 8 and 9 for average and triaxial compression tests may be compared with Figures 7.32 and 7.28 respectively from this investigation. The major difference noted in this comparison involves volumetric strain. Kjellman indicates higher initial consolidation and less expansion prior to yield. The spherical state of stress was approximately three times higher in Kjellman's tests. Of course, the sands tested were not identical. No provision was made for the independent measurement of volumetric strain in the Kjellman apparatus, the results relying entirely on addition of the principal strains.

Jakobson (12), using the Kjellman apparatus, performed triaxial compression and extension tests and analyzed data to obtain the modulus of elasticity and Poisson's ratio as functions of the friction angle below yield. Stress paths were carried out in standard fashion such that spherical stress varied during an experiment. Jakobson illustrated how both Poisson's ratio and the modulus of elasticity vary with shearing stress; however, the use of these terms in application to the complex behavior of sand is questionable. Both the modulus of

elasticity and Poisson's ratio are simply defined for initially isotropic material which is subjected to triaxial compression or extension; however, it is not apparent how these terms can be extended to the general case.

9.7 GENERAL STRESS-STRAIN RELATIONSHIPS

The superposition of strain response in incremental form for one spherical and two deviatoric stress paths as summarized in Section 8.3 represents the first attempt to obtain a general stress-strain relationship for sand based on experimental evidence. The incremental form of the relationships accounts for non-linearity, and the double definition of each coefficient function accounts for the direction of loading. The three stress paths of this investigation were orthogonal at a point in principal stress space.

The proposed stress-strain relationships in invariant form do not completely account for stress-strain history or induced anisotropy. In application, principal strains must be assumed coincident with principal stresses. Direct application of relationships proposed for a single stress increment first requires transformation of stress components to invariant stress functions. The selection of the proper coefficient functions C_{ij} requires definition of the sign of corresponding invariant stress increments. Application of the stress-strain relationship in invariant form results in obtaining invariant strain functions which then must be transformed to strain components.

For a significant change in the state of stress, the foregoing procedure for a single stress increment may be utilized in obtaining a

step-wise integration of the invariant relationships. The manner of stressing must be completely specified over the history considered as the coefficient functions are in general dependent both upon the state of stress and the direction of loading. Depending upon the individual case considered, certain terms may be integrated in closed form.

9.8 FIRST YIELD CRITERIA

The yield relationship derived from experimental data, Figure 8.17, and expressed by Equation 8.65 in invariant form was

$$I_2^* = 0.116 + 0.016\ (1+I_3^*)^2$$

The initial porosity for all deviatoric tests was 0.34 and thus the relationship does not account for variations in porosity. The stress history for the related tests, Figures 7.28, 7.30 and 7.40 through 7.47, was limited and the foregoing relationship is associated with a particular family of stress paths as follows: each sample was first subjected to several cycles of spherical stress where it was assumed the material was isotropic, and then deviatoric stress was applied to first yield such that $I_1 = 54$ psi and $I_3^* =$ constant. Values of I_3^* were varied from -1 to 1 in ten experiments.

It was suggested that generalization of Equation 8.65, obtained from this investigation, into the form of Equation 8.66

$$I_2^* = b_1(n) + b_2(n)[1+I_3^*]^2$$

might be developed to account for variations in porosity.

Anisotropic behavior of sand subjected to deviatoric stress suggests that a first yield criterion might better include, in more detail, the effect of stress-strain history, Section 2.43. A detailed

study of the effect of stress-strain history on first yield was not performed. A single triaxial compression test carried to yield on an initially anisotropic specimen, Figure 7.34, indicates failure at $I_2^* = 0.18–0.20$ while a similar test on an initially isotropic sample, Figure 7.28, indicates failure at $I_2^* = 0.16–0.18$. The latter result was, however, believed low in comparison with similar tests. (See the projection of test data, Figure 8.17, to $I_3^* = 1$ where first yield is estimated at $I_2^* = 0.18$.) A single average compression test on an initially anisotropic sample, Figure 7.32, indicated yield at $I_2^* = 0.12–0.13$ which is comparable with interpolated data for initially isotropic tests, Figure 8.17, where at $I_3^* = 0$, $I_2^* = 0.13$. The amount of such data obtained does not justify a conclusive statement on the effect of stress-strain history on first yield.

The results of past investigations on the form of the yield surface for sands were summarized in Table 3.1. Conventionally such studies are compared with the Mohr-Coulomb failure law, and a similar comparison for this study is given by Figure 8.18. This investigation indicates major divergence from the Mohr-Coulomb theory where the friction angle is independent of the state of stress. As the state of stress advances from triaxial extension to average compression, the friction angle remains essentially constant at 52°; while in moving to triaxial compression, the friction angle is reduced to 38°.

On the basis of standard triaxial compression tests, Figure 7.3, the peak point friction angle was 37.5° at an initial porosity of 0.34, 4% axial strain and 2% volumetric strain. The corresponding

three-dimensional compression test, Figure 7.28, required 2–3% axial strain, 1-1/2–2-1/2% lateral strain, and 1/2–1% volumetric strain to reach first yield. The generally higher strains recorded in the standard triaxial equipment are attributed to the relatively non-homogeneous application of stress, Section 4.12.

Of previous investigations reported in Table 3.1, the author's work best agrees with the works of Kjellman and Jakobson. It is unfortunate that Kjellman did not give data for triaxial extension; however, an 8° higher friction angle was recorded for average compression in comparison with triaxial compression. With some imagination Jakobson's work, which generally did not reach yield, can be extended to indicate a 9–17° higher friction angle for triaxial extension as compared with triaxial compression. The agreement of this study, which indicates a 14° higher angle of friction in both triaxial extension and average compression as compared with triaxial compression, with the works of Kjellman and Jakobson is attributed to a relatively homogeneous application of stress in both apparatuses.

The author's apparatus possesses one significant advantage over Kjellman's with reference to yield studies in that considerable strains (i.e. 10%) may be obtained without development of mechanical interference at corners of the test specimen. The apparatus of this study is capable of developing yield in a variety of materials and the questionable projection of test results to yield is thus avoided.

Experimental works reporting equivalent or lower friction angles in triaxial extension as compared with triaxial compression, i.e. Habib

(11), Bishop and Eldin (10), Kirkpatrick (13), Wu, Loh and Malvern (18), and Haythornthwaite (7), are thought to have involved considerable stress variation. It is suggested that these investigations have measured too much the characteristics of the corresponding test apparatus and too little of the true properties of sand. The use of different apparatus, i.e. Kirkpatrick's thick cylinder and standard triaxial tests, in predicting the effect of the stress state on the strength of sand cannot be recommended.

In addition to experimental evidence, the following argument is advanced in support of the relatively high friction angle obtained in triaxial extension: Consider two elements of like sand subjected to the same major and minor principal stresses.

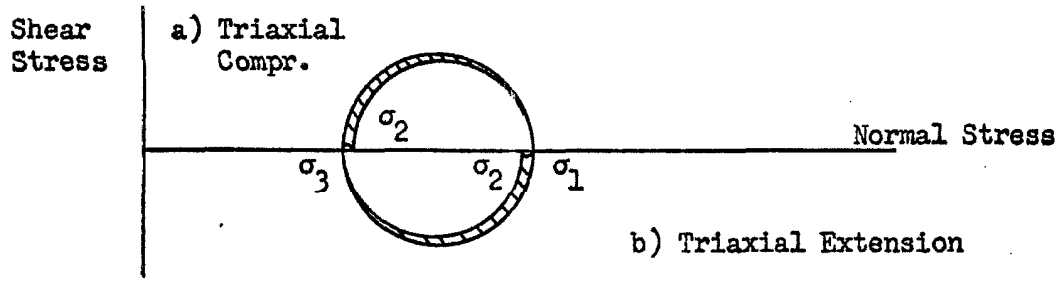

Figure 9.2 Mohr's Circles of Stress for Triaxial Compression and Triaxial Extension

The intermediate principal stress for element A, Figure 9.2 a), is equivalent to the minor principal stress while the intermediate principal stress for element B, Figure 9.2 b), is equivalent to the major principal stress. The shear stress obtained by averaging over all planes is equivalent in both cases; however, the normal stress obtained by averaging over all planes is significantly higher for element B in triaxial extension.

If failure were to occur according to the Mohr-Coulomb concept then both elements would yield at the same friction angle--the maximum ratio of shear to normal stress occurring on a particular plane being identical in both cases. On the other hand, if failure is attributed to shearing on many planes then the ratio of shear to normal stress on a variety of planes, i.e. stress distribution, becomes important. Since the first element is associated with a higher ratio of average shear to normal stress, yield occurring apart from the Mohr-Coulomb concept will occur with a higher friction angle in extension. This simplified physical argument may be extended to other stress states; however, equations based on experimental evidence and including variation in the third stress invariant are best adapted for analysis, i.e. Equation 8.65 for the particular conditions of this study.

The recent work of Rowe and Barden (46) in reducing end plate friction in standard triaxial compression tests on sand has produced some interesting results. In comparison with fixed end specimens later and multiple failure surfaces were observed, lower peak point friction angles measured, and smoother stress-strain response recorded. The author considers the lower friction angle obtained for free ended specimens as due to less variance from the ideal triaxial compression stress state. Normally, the effects of stress concentration are expected to reduce the apparent friction angle except for the single case of the triaxial compression test. It would be most interesting to see the results of free and fixed end triaxial extension tests compared. On the basis of this study, the free end triaxial extension

test will indicate significantly higher and more realistic friction angles.

Additional work is thought necessary along the foregoing lines prior to reaching definite conclusions. Assuming, however, that triaxial compression and extension apparatus can be designed to eliminate end plate friction and still provide for stability, such tests can be recommended in conjunction with more complex apparatus for stress-strain studies. For example, the functions $b_1(n)$ and $b_2(n)$ of Equation 8.66 (obtained from three-dimensional apparatus) might be practically determined for a particular sand over a wide range in initial porosity.

This study did not consider plane strain in detail; however, experimental evidence was inadvertently obtained for a special case. Figures 7.44, 7.45 and 7.46 indicate that a state of plane strain was nearly obtained from spherical compression to yield for $0.2 \leq I_3^* \leq 0.6$. Stress corrected results at yield, Figures 8.17 and 8.18, indicate $I_3^* = 0.3$, $\beta = 0.2$, $I_2^* = 0.145$ and $\Phi = 50°$. Stress-strain results are approximately given for plane strain under radial compression stress by Figure 7.45. The 12° higher angle of friction in comparison with triaxial compression is of special interest.

Local failure, Figure 6.23, was observed in only one experiment of this entire investigation. Even the standard triaxial compression tests, Figure 7.3, performed on this sand at comparable porosities and states of stress exhibited bulging failure. The unique failure plane concept associated with the Mohr-Coulomb failure law must be rejected on the basis of this study. A noted occurrence of a progressive zone

of failure is considered the result either of stress concentration or of non-homogenities occurring within the material.

Kjellman (47) presented a stimulating paper on the topic "Do Slip Surfaces Exist?" and generally concluded that they do not. This paper was overly simplified in several respects and the author cannot agree with much of the discussion advanced. The conclusion doubting the slip-surface concept is, however, considered valid.

A major question still remains in regard to the effect of stress-strain history on first yield. Bishop and Eldin (10), using standard triaxial apparatus, indicate little effect of stress history on the strength of sand over a wide range in initial porosity. The author believes that a unique first yield surface does not exist for a particular sand in principal stress space independent from stress-strain history prior to yield. Magnitudes of possible deviation cannot be advanced on the basis of this study and it is possible that under certain conditions such deviations may be negligible as compared with the accuracy of measurement practically obtainable.

10. CONCLUSIONS AND RECOMMENDATIONS

10.1 CONCLUSIONS

1. Physical tests are particularly useful in obtaining a general stress-strain relationship for sand if the state of stress is homogeneous and subject to complete control.

2. The use of invariant functions allows for the reduction of variables in planning experimental work and in analysis of results.

3. The most desirable stress paths in obtaining a general stress-strain relationship are those three obtained by holding two stress invariant functions constant and varying the third.

4. A judicious selection of invariant functions and corresponding stress paths is most properly made with reference to the physical behavior of the material. In this case the variables I_1, I_2* and I_3* were considered appropriate.

5. Sand samples subjected only to spherical stress were essentially elastic. Sand subjected to deviatoric stress became increasingly anisotropic toward yield and was essentially inelastic.

6. Anisotropic sand subjected to spherical stress became less anisotropic with increasing cycles of stress.

7. Due to the anisotropic behavior of sand under deviatoric stress, the use of invariant functions to describe the general stress-strain behavior of sand is in error.

8. The Mohr-Coulomb yield criterion does not completely describe the effect of the stress state on first yield. The friction angle

associated with the triaxial compression stress state is minimum. The unique failure plane concept is rejected.

9. For limited stress-strain history it is possible to obtain a relatively simple yield criterion in invariant form.

10.2 RECOMMENDATIONS

It is recommended that additional work be carried out to improve the design of stress-strain apparatus-innovations in test equipment are highly desired. The equipment of this study was thought to apply a more homogeneous state of stress than previous apparatus; however, this is subject to improvement. Provisions for more accurate measurement of strains (particularly small strains) are also desired. The strain effects attributed to rubber components of the author's apparatus were particularly undesirable.

Specific improvements in the spherical apparatus of this study are recommended as follows:

1. Provide for measurement of axial and transverse strain.
2. Harden the sample membrane in the transverse direction to reduce the effects of rubber penetration. Materials other than latex rubber might be considered.

Specific improvements in the three-dimensional compression apparatus of this study are recommended as follows:

1. Enlarge the base pressure-cell to 14 in. in square dimensions. This requires the construction of a spacer plate and a base pressure-cell.

2. Obtain stronger and more durable side pressure-cells which more closely fit the space allowed. It would be desirable to increase the magnitude of the principal stress to 100 psi. Synthetic rubber cells are recommended.
3. Make provisions for measurement of principal strains apart from those obtained by volumetric displacement.

Further investigations of the spherical stress-strain relationship for a variety of sands are recommended. It is suggested that special care be taken in the measurement of both linear and volumetric strain. A more detailed study of the effects of stress-strain history on the degree of elasticity obtained would be of interest.

Additional work toward obtaining a general stress-strain relationship for sand might well first consider the use of variables and stress paths suggested in this study. The effect of variation in porosity might be determined in detail for particular stress histories. Finally, the difficult problem of developing a stress-strain relationship which would include in considerable detail the effect of stress-strain history should be considered.

A detailed study of the effect of stress-strain history on first yield for various sands would be of practical interest. Care must be taken in developing equipment which is capable of measuring variations due to this effect. The question "Does sand possess a unique first yield envelope independent of stress-strain history?" has not been conclusively answered on the basis of experimental evidence.

APPENDIXES

A1. SUMMARY OF SYMBOLS

A	= area
a, b, c	= constants
$a_0(I_3^*), a_1(I_3^*), a_2(I_3^*)$	= functions of I_3^* defined by Eq. 8.33
$a_3(I_3^*), a_4(I_3^*)$	= functions of I_3^* defined by Eq. 8.43
$a_5(I_3^*), a_6(I_3^*)$	= functions of I_3^* defined by Eq. 8.52
a_n	= n^{th} parameter representing grain shape
B	= matrix defined by Eq. 2.3
$b_1(n), b_2(n)$	= functions of n defined by Eq. 8.66
b_n	= n^{th} parameter representing grain size distribution
b_{ijkL}	= element of B matrix
$C_1(n), C_2(n)$	= spherical stress-strain porosity functions defined by Eq. 8.4
C_{ij}	= coefficient function of invariant stress-strain relationship for sand: (Eq. 3.61, 3.62 and 3.63) = C_{ijC} if $dI_j > 0$, = C_{ijR} if $dI_j < 0$
C_{ly}, C_{uy}, C_{suy}	= first, ultimate yield and static ultimate yield invariant stress-strain functional relationships
C_u	= Hazen's uniformity coefficient
D	= particle size determined by sieving

D_v = volumetric degree of elasticity defined by Eq. 8.18

d_{1y}, d_{uy}, d_{suy} = first yield, ultimate yield and static ultimate yield stress-strain functional relationships

d_{ijkL} = coefficient in generalized Hooke's law for inelastic solid

E = modulus of elasticity

e = (1) base of natural log; and (2) void ratio

f = coefficient of grain to grain friction

$f(\tau_{ij})$, $f(\sigma_1)$ = ideally plastic yield relationships

g_{ij} = constant in generalized Hooke's law for linearly elastic solid

i, j, k, L = subscripts in indical notation

I_{1n}, I_{2n}, I_{3n} = first, second and third normal stress invariants

I_1, I_2, I_3 = first, second and third modified stress invariants

I_2^* = second modified and dimensionless stress invariant = I_2/I_1^2

I_3^* = third modified and dimensionless stress invariant = $3\sqrt{6}\, I_3/I_2^{3/2}$

J_{1n}, J_{2n}, J_{3n} = first, second and third normal strain invariants

J_1, J_2, J_3 = first, second and third modified strain invariants

J_3^* = third modified and dimensionless strain invariant = J_2/J_1^2

L = length

M = $(1+\nu)/E$

m = exponent defined by Eq. 8.32

N = ν/E

$-dn/d\sigma$ = coefficient of compressibility

P = applied force

p = exponent defined by Eq. 8.31

s = yield strength of grain material

u_i, u_j = displacements

V = volume

x_i, x_j = co-ordinates

α = angle of obliquity

β = principal stress ratio in three dimensions = $(\sigma_1-2\sigma_2+\sigma_3)/(\sigma_1-\sigma_3)$

ϵ_3, ϵ_2, ϵ_1 = principal strains arranged in order of magnitude

ϵ_{ij} = component of strain tensor, positive for extension

ϵ_v = volumetric strain

δ_{ij} = Kronecker delta = 1 if i=j, = 0 otherwise

η = porosity

θ = $\cos^{-1} I_3^*$

κ = principal strain ratio in three dimensions = $(\epsilon_1-2\epsilon_2+\epsilon_3)/(\epsilon_1-\epsilon_3)$

ν = Poisson's ratio

σ = spherical stress

σ_3, σ_2, σ_1 = principal stresses arranged in order of magnitude

σ_3^*, σ_2^*, σ_1^* = dimensionless principal stresses, $\sigma_i^* = \sigma_i/I_1$

τ_{ij}, τ_{kL} = component of stress tensor, positive where compressive

τ_{ij}^* = dimensionless component of stress tensor

φ = friction angle = $\sin^{-1} (\sigma_1-\sigma_3)/(\sigma_1+\sigma_3)$

All stresses are effective stresses and positive for compression.

All strains are engineering strains (i.e. $\gamma_{ij} = \frac{\partial u_i}{\partial x_j} + \frac{\partial u_j}{\partial x_i}$) and positive for extension.

Primes represent spherical components of stress and strain.

Double primes represent deviatoric components of stress and strain.

Stars represent dimensionless variables.

Dots over symbols represent derivatives with respect to time.

Stress path notation is given by Table 4.1.

A2. STRAIN EFFECTS--SPHERICAL COMPRESSION APPARATUS

A2.1 RUBBER PENETRATION

A2.11 INTRODUCTION

The importance of membrane penetration was brought to the author's attention by Dr. R. F. Scott. The penetration depends in general upon the relationship between skin thickness and the size of void spaces available for penetration. Previous investigators have considered the effect for relatively thin membranes, i.e. Newland and Alley (34, 35).

The rubber membrane used in the spherical compression tests was approximately 0.032 in. in thickness; a typical sand grain diameter was 0.024 in. Assuming that a typical void space span is approximated by a grain diameter, the ratio of skin thickness to spanned length is on the order of unity. The behavior of this relatively thick membrane was assumed to be that of bearing penetration.

A2.12 RUBBER PENETRATION TESTS

A sheet of rubber approximately 0.051 in. in thickness manufactured in a manner similar to that of the spherical compression membrane was cut to form two discs, each 2.10 in. in diam. These discs were bonded to cylindrical brass loading plates with rubber cement. The flat exposed rubber surfaces were separated using cardboard strips approximately 0.045 in. in thickness, and masking tape was wrapped around the perimeter of the assembly--leaving space for removal of the cardboard strips, Figure A2.1. After removal of the spacer strips, tape

was wrapped around the entire perimeter of the assembly, forming three layers. Upon the incision of a small hole and attachment of a funnel, Figure A2.2, the space between the rubber discs was filled with Ottawa sand and the assembly was vibrated with a rubber mallet to obtain the maximum density possible. A small piece of tape was used to seal the hole upon filling. The loading plates with attached rubber discs, spacer strips, and tape are shown in Figure A2.3.

The apparatus used to stress the sandwich assembly, Figure A2.4, included a bathroom scale, a one-dimensional consolidation device, and a 1/10,000-in. dial gage. A schematic diagram of the test is given in Figure A2.5. The rubber sandwich containing the sand layer was loaded according to the pressures normally used in the spherical compression tests; the time of a particular load application was 2 min.

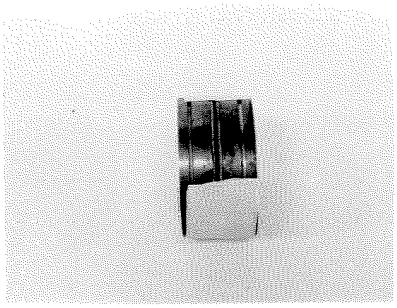

Figure A2.1 Spaced Cylindrical Loading Plates, Rubber-Penetration Test Apparatus

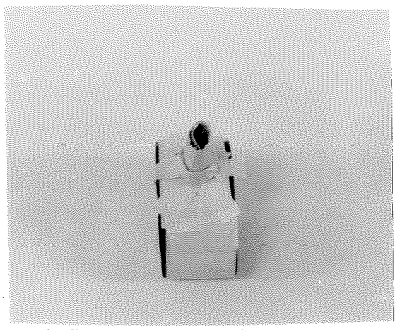

Figure A2.2 Taped Load Plate Assembly Ready for Sand Placement, Rubber-Penetration Test Apparatus

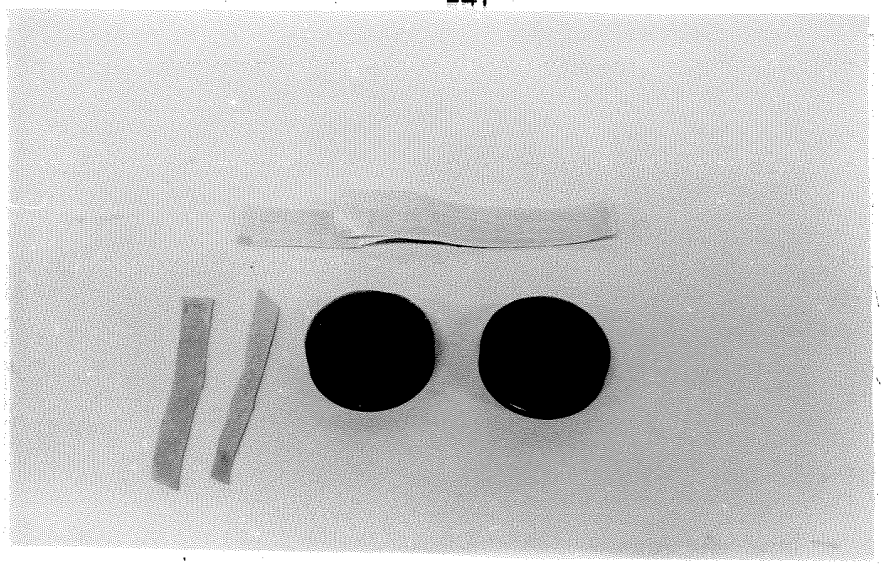

Figure A2.3 Loading Plates with Attached Rubber Discs, Spacer Strips and Masking Tape, Rubber-Penetration Test Apparatus

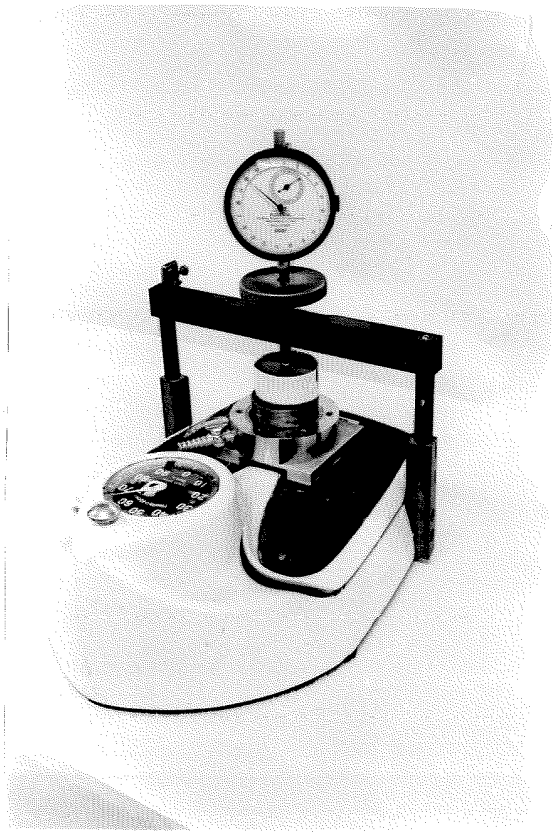

Figure A2.4 Load-Deflection Mechanism, Rubber-Penetration Test Apparatus

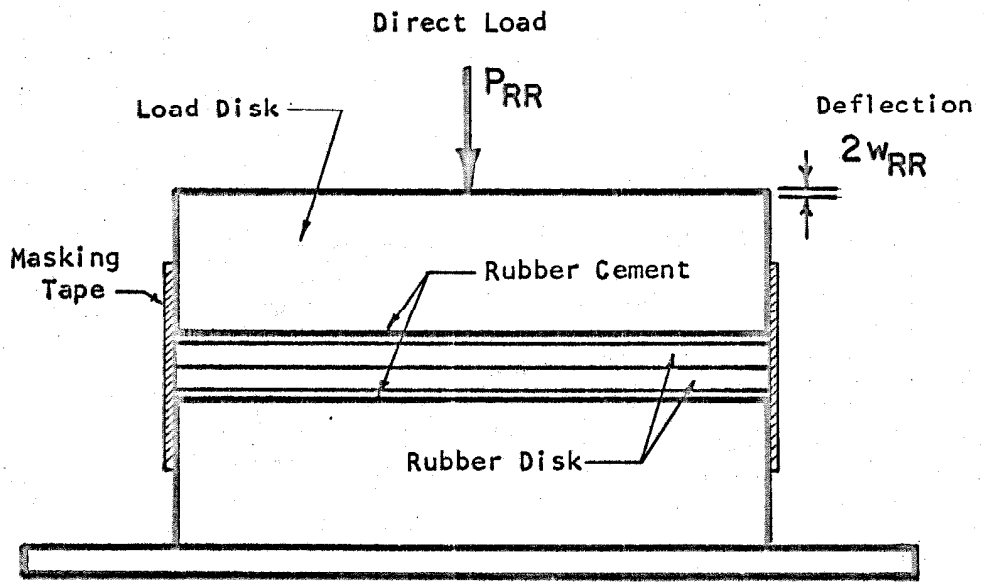

Rubber on Rubber

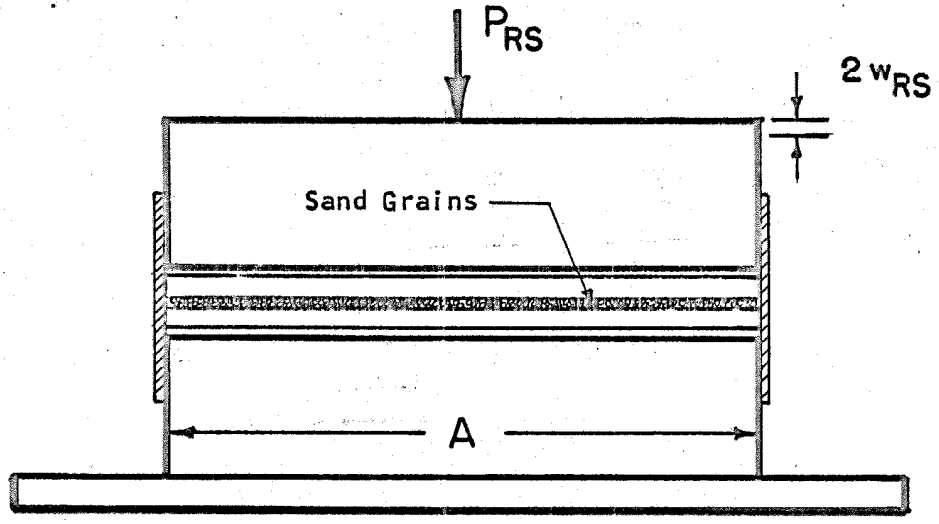

Rubber on Sand

Basis of calculation:

Normal pressure $\sigma = P/A$

Corrected rubber penetration $w_R = w_{RS} - w_{RR}$

Figure A2.5 Schematic Diagram - Rubber Penetration Test

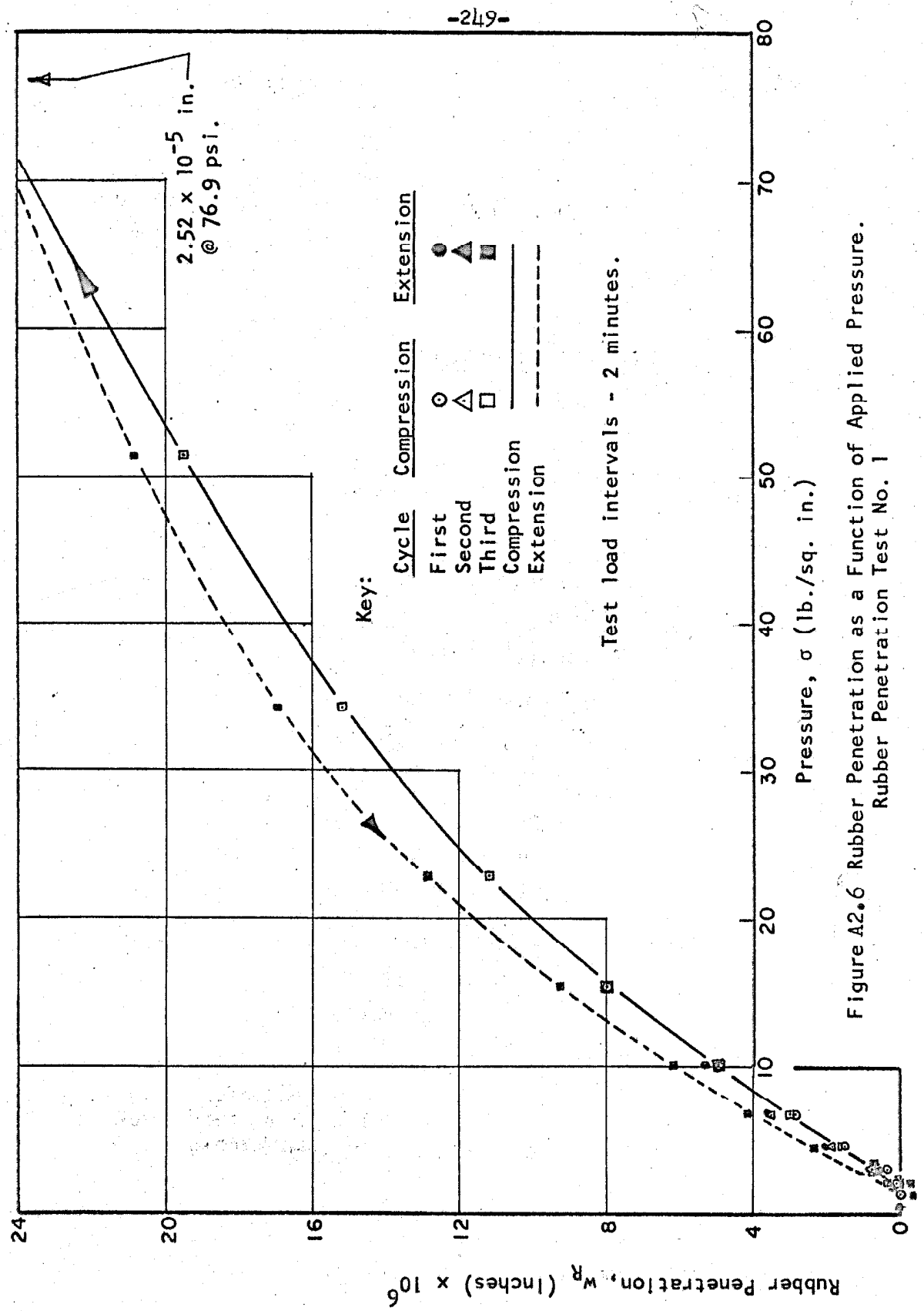

Figure A2.6 Rubber Penetration as a Function of Applied Pressure.
Rubber Penetration Test No. 1

Following a load-deformation test the sand was removed, and an identical load sequence was performed. The rubber penetration value for two sand-rubber surfaces was taken as the difference between the two corresponding test deformation values. This procedure empirically accounted for deformation occurring within the apparatus, and for axial deformations occurring within the rubber due to normal loading and to the lack of sufficient restraint in preventing lateral strains. Figure A2.6 gives rubber penetration W_R obtained as a function of normal pressure σ.

A2.13 RUBBER PENETRATION VOLUME CORRECTION

Based upon the cylindrical dimensions of the spherical compression test sample indicated in Figure A2.7, the rubber-sand surface contact area was estimated to be 653 sq cm.

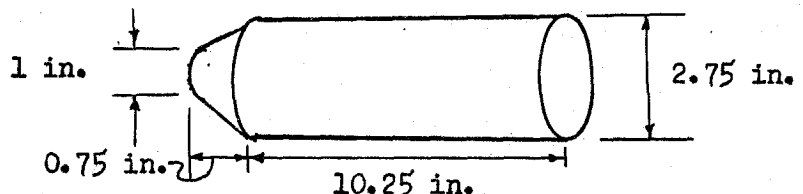

Figure A2.7 Spherical Compression Membrane

Figure A2.8 gives the volume correction based upon Rubber Penetration Test No. 1 as a function of applied pressure.

A2.2 DRAIN LINE COMPRESSION

A2.21 INTRODUCTION

The drain line Q of Figure 5.1 was enclosed within the spherical compression chamber during a stress-strain test and deformed

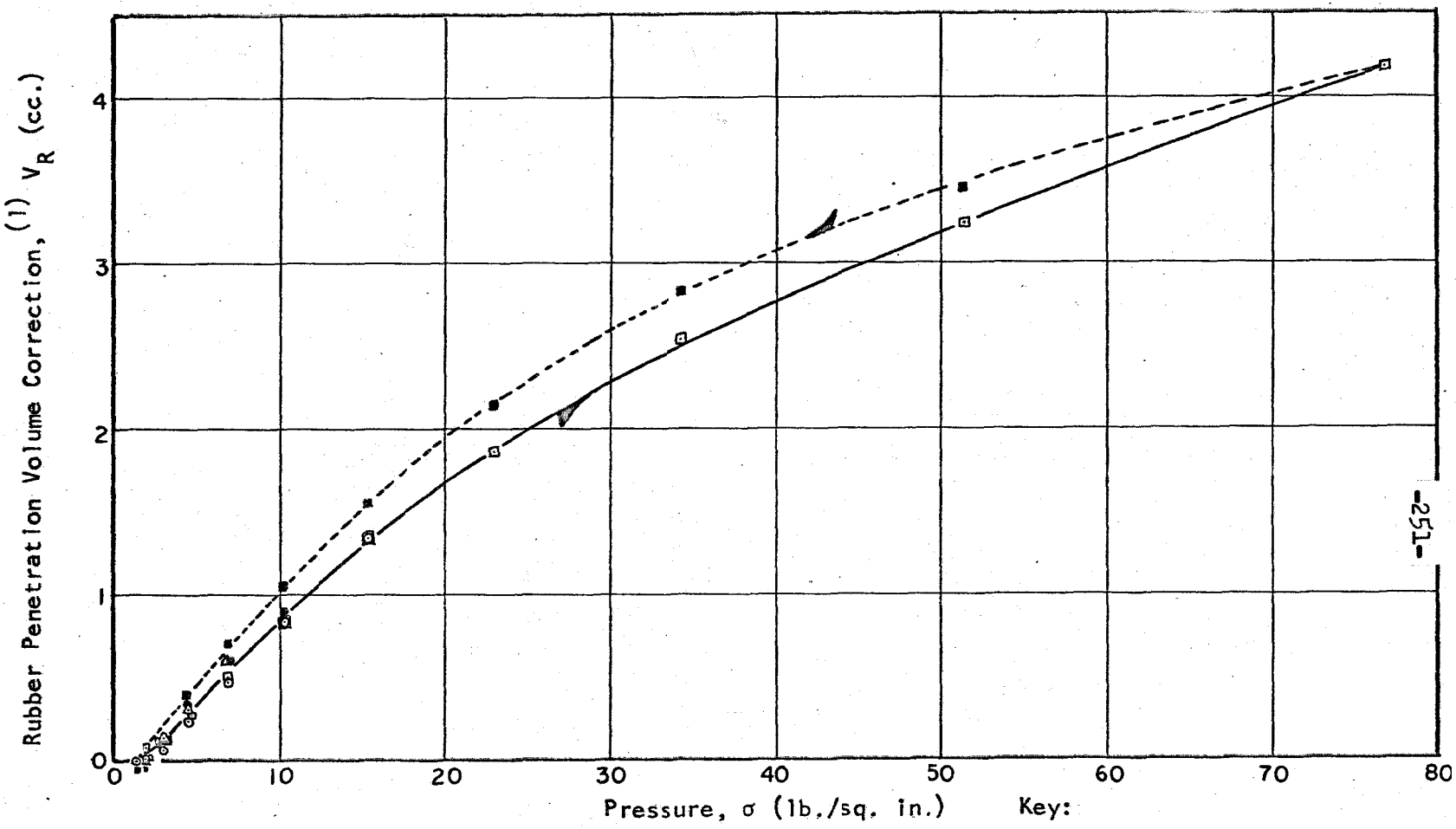

(1) Based on Rubber Penetration Test No. 1 and spherical compression sample surface area of 653 sq. cm.

Figure A2.8 Rubber Penetration Volume Correction as a Function of Applied Pressure for use in Spherical Compression Tests.

due to changes in applied pressure. The effect of drain line compression was determined as described below.

A2.22 DRAIN LINE COMPRESSION TEST

The spherical compression apparatus was prepared as for a stress-strain experiment, and the sample drainage cap S was connected to the internal base drain fitting P. The burette Y was filled with water and valves Z, I, W, J, X and N were opened in sequence momentarily to completely fill the measurement system. The burette was refilled and the compression apparatus assembled as usual. Upon filling the compression chamber with water, valve D was closed and air pressure was applied through valve A. Drain line volume change was recorded at burette Y under pressures to 70 psi. At 70 psi the total drain line compression from atmospheric pressure was 0.13 cc, and the behavior over the entire range of loading was essentially linear and elastic.

A2.3 TEMPERATURE CHANGE

The volume of water contained within a typical test specimen was approximately 350 cc, and the volume of the piping system was approximately 70 cc--thus forming a total measurement system volume of approximately 420 cc. A temperature change of 1°C corresponded to a calculated volume change of approximately 0.11 cc neglecting entrapped air and apparatus deformation.

A3. STRESS EFFECTS--SPHERICAL COMPRESSION APPARATUS

The test sample was covered in major part (99%) by the latex membrane, and sand skeleton deformation occurred essentially in union with that of the membrane boundary. Upon the application of spherical pressure to the specimen, the sample and membrane were strained simultaneously--the sand skeleton accepting the major load. In order to estimate the load carried by the rubber sheath it was necessary first to obtain an approximate stress-strain relationship for the rubber.

A3.1 TENSILE TEST OF A RUBBER STRIP

A sheet of rubber 0.117 cm in thickness was manufactured in a manner similar to that for the membrane itself, and was cut in rectangular form approximately 5 cm in width by 30 cm in length. Four pieces of 1/4-in. thick plywood approximately 5 cm sq were cut, and two pieces were bonded to each end of the rubber strip with rubber adhesive. A C-clamp was then applied to each end, holding the rubber fixed between

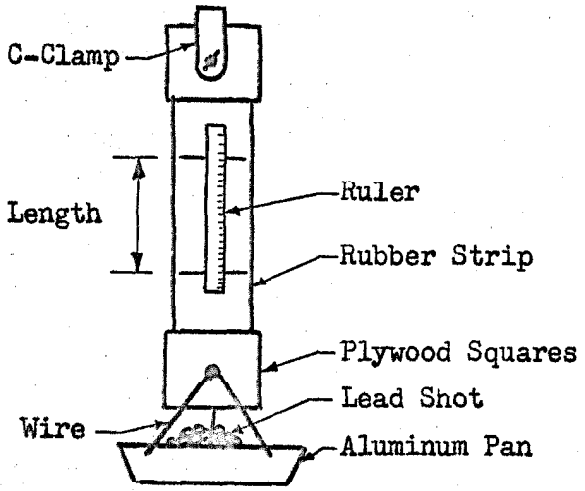

Figure A3.1 Schematic Diagram of Tensile Test Apparatus

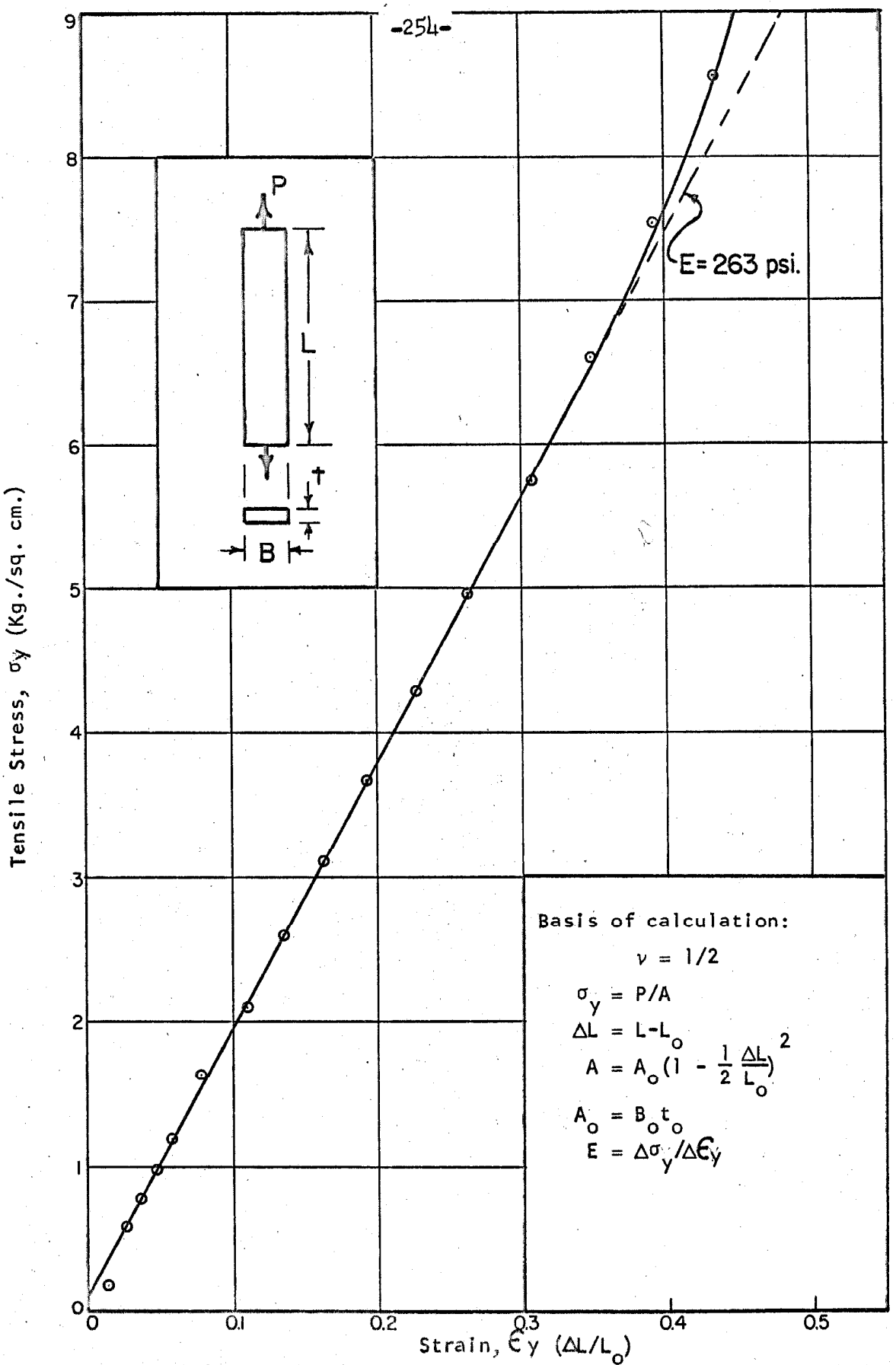

Figure A3.2 Tensile Stress as a Function of Strain - Latex Strip.

the plywood pieces. One day was allowed for curing. Two marks were made with india ink 5 cm apart and normal to the longitudinal axis of the strip. The strip was loaded with lead shot and the deformations measured with a ruler. Figure A3.1 shows a schematic diagram of the apparatus, and the method of calculation and test results are illustrated by Figure A3.2.

A3.2 STRESS CORRECTION DUE TO MEMBRANE BEHAVIOR

Consider the ideal sketch of a cylindrical test sample shown in Figure A3.3 a) subjected to an external spherical state of stress.

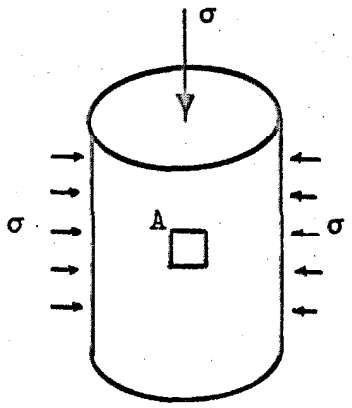

a) Cylindrical Sheathed Sample

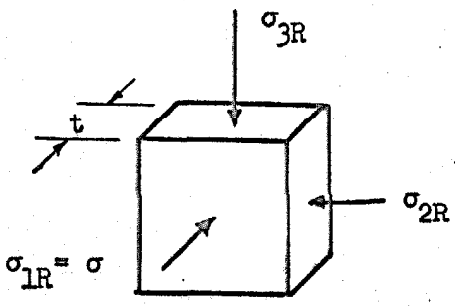

b) Rubber Skin Element A

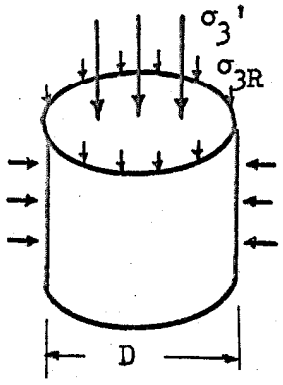

c) Vertical Equilibrium

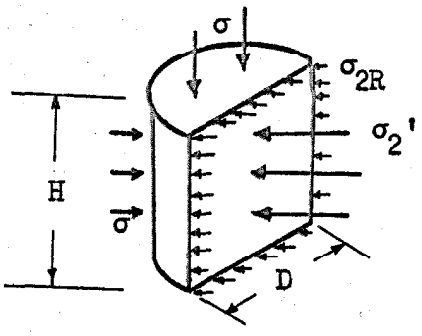

d) Horizontal Equilibrium

Figure A3.3 Rubber-Sand Interaction, Cylindrical Sample under Spherical Stress

If the membrane is thin relative to the size of the test sample then a statement of vertical force equilibrium, Figure A3.3 c) gives

$$\sigma_3' \frac{\pi D^2}{4} + \sigma_{3R} \pi D t = \sigma \frac{\pi D^2}{4} \qquad (A3.1)$$

where

σ_3' = avg normal stress supported by sand on horiz planes

σ_{3R} = avg normal stress supported by rubber skin on horiz planes

D = diameter of cylindrical sample

t = thickness of sample membrane

from which it follows that

$$\sigma_3' = \sigma - \frac{4t}{D} \sigma_{3R} \qquad (A3.2)$$

A statement of horizontal force equilibrium, Figure A3.3 d) gives

$$\sigma_2' DH + \sigma_{2R}(2Ht + 2Dt) = \sigma DH \qquad (A3.3)$$

where

σ_2' = avg normal stress supported by and on vertical planes

σ_{2R} = avg normal stress supported by rubber skin on vertical planes

H = height of test cylinder

from which

$$\sigma_2' = \sigma - (\frac{2t}{D} + \frac{2t}{H}) \sigma_{2R} \qquad (A3.4)$$

According to Equations A3.2 and A3.4 the average vertical and horizontal sand skeleton stresses are equal if $\sigma_{2R} = \sigma_{3R}$ and if the ratio D/H = 1. It should be realized that all non-spherical membrane shells will, however, lead to the development of certain non-uniform sand skeleton stresses even though the average stresses may be equivalent.

The particular sample shape used in the spherical compression test apparatus was not a perfect cylinder, and the ratio D/H ≐ 1/4.

Upon evaluation of σ_{2R}, a solution for σ_2' and σ_3' may be obtained. For the rubber skin element A shown in Figure A3.3 b) Hooke's law states that

$$-\epsilon_{1R} = \frac{\sigma_{1R}}{E} - \frac{\nu}{E}\sigma_{2R} - \frac{\nu}{E}\sigma_{3R} \tag{A3.5}$$

$$-\epsilon_{2R} = \frac{\sigma_{2R}}{E} - \frac{\nu}{E}\sigma_{1R} - \frac{\nu}{E}\sigma_{3R} \tag{A3.6}$$

$$-\epsilon_{3R} = \frac{\sigma_{3R}}{E} - \frac{\nu}{E}\sigma_{2R} - \frac{\nu}{E}\sigma_{1R} \tag{A3.7}$$

where ϵ_{1R}, ϵ_{2R} and ϵ_{3R} represent tensile rubber strains, and E and ν represent the modulus of elasticity and Poisson's ratio for rubber respectively. Addition of Equations A3.5, A3.6 and A3.7 gives

$$\epsilon_{1R} + \epsilon_{2R} + \epsilon_{3R} = -\left(\frac{1-2\nu}{E}\right)(\sigma_{1R} + \sigma_{2R} + \sigma_{3R}) \tag{A3.8}$$

Assuming that Poisson's ratio for rubber is 1/2 it follows that

$$\epsilon_{1R} + \epsilon_{2R} + \epsilon_{3R} = 0 \tag{A3.9}$$

Equations A3.5, A3.6 and A3.7 may then be written in the form

$$\sigma_{3R} = \sigma_{1R} - \frac{2}{3}(2\epsilon_{3R} + \epsilon_{2R})E \tag{A3.10}$$

$$\sigma_{2R} = \sigma_{1R} - \frac{2}{3}(2\epsilon_{2R} + \epsilon_{3R})E \tag{A3.11}$$

If the soil structure is assumed to deform isotropically and the membrane boundary is assumed to follow the soil structure, it follows that

$$\epsilon_{2R} = \epsilon_{3R} = \frac{\epsilon_v}{3} \tag{A3.12}$$

where ϵ_v is the volumetric strain of the soil skeleton, and since $\sigma_{1R} = \sigma$ then Equations A3.10 and A3.11 may be reduced to

$$\sigma_{2R} = \sigma_{3R} = \sigma - \frac{2E}{3}(\epsilon_v) \qquad \text{(A3.13)}$$

and finally substituting Equation A3.13 into Equations A3.2 and A3.4 gives

$$\sigma_3' = \sigma - \frac{4t}{D}(\sigma - \frac{2E}{3}\epsilon_v) \qquad \text{(A3.14)}$$

$$\sigma_2' = \sigma - (\frac{2t}{D} + \frac{2t}{H})(\sigma - \frac{2E}{3}\epsilon_v) \qquad \text{(A3.15)}$$

Using the value E = 263 psi obtained from the tensile test of a rubber strip and the dimensions of the spherical compression membrane, D = 2.75 in., t = 0.032 in. then finally results in

$$\sigma_3' = 0.954\,\sigma + 8.13\,\epsilon_v \qquad \text{(A3.16)}$$

$$\sigma_2' = 0.971\,\sigma + 5.15\,\epsilon_v \qquad \text{(A3.17)}$$

from which it is possible to determine average soil skeleton stresses as corrected for the stress effect of the rubber membrane.

A4. CHAMBER VOLUME DETERMINATION--SPHERICAL COMPRESSION APPARATUS

The volume of water necessary to fill the spherical compression chamber, excluding that of the sample membrane and supplementary attachments, was required in order that the total sample volume could be determined by displacement occurring within the compression chamber. The sample membrane T of Figure 5.1 was attached in the usual manner to the internal supply fitting K, and the split-cylinder base EE was inserted under the membrane. Valve R was closed and the internal drain line Q was connected to the internal base drain fitting and to the sample drainage cap S. The compression chamber was assembled and placed upon the metric scale, the usual attachments being made. The relief valve D was opened, and water was allowed to reach the base of the chamber through valve F. The total weight of the compression chamber and its contents was recorded as well as the volume of the fill reservoir. The chamber fill valve F was then opened allowing de-aired and distilled water to enter the chamber. Upon filling, valve F was then closed. Again the total weight of the compression chamber and its contents was recorded as well as the volume of the fill reservoir. The temperature was also noted. The difference between the initial and final weights of de-aired, distilled water at this particular temperature provided the most accurate measure of chamber volume excluding the usually included accessories. The difference in fill reservoir volume before and after filling served as a check. The results of two tests are given in Table A4.1.

Table A4.1 Spherical Compression Chamber
Volume Determination

Test Number		1	2
Wt of water req'd to fill chamber, gm	W_{cc}	4159.6	4159.7
Temperature, °C	T	26	26
Density of water, gm/cc	γ_w	0.9968	0.9968
Calc'd vol of water req'd to fill chamber, cc	V_{cc}	4173	4173

Assuming the chamber volume at 26°C was 4173.00 cc, chamber volumes were estimated for various temperatures as follows:

$$V_T = V_{26°C} + 2\alpha \Delta T V_{26°C} = V_{26°C}(1 + 2\alpha \Delta T)$$

where

V_T = chamber volume at temperature T

$V_{26°C}$ = chamber volume at temperature 26°C

α = linear coefficient of expansion of lucite cylinder

ΔT = change in temperature from 26°C

The results of volume calculations at various temperatures using $\alpha = 5 \times 10^{-5}/°C$ are presented graphically in Figure A4.1. Also included are the corresponding weights of de-aired, distilled water.

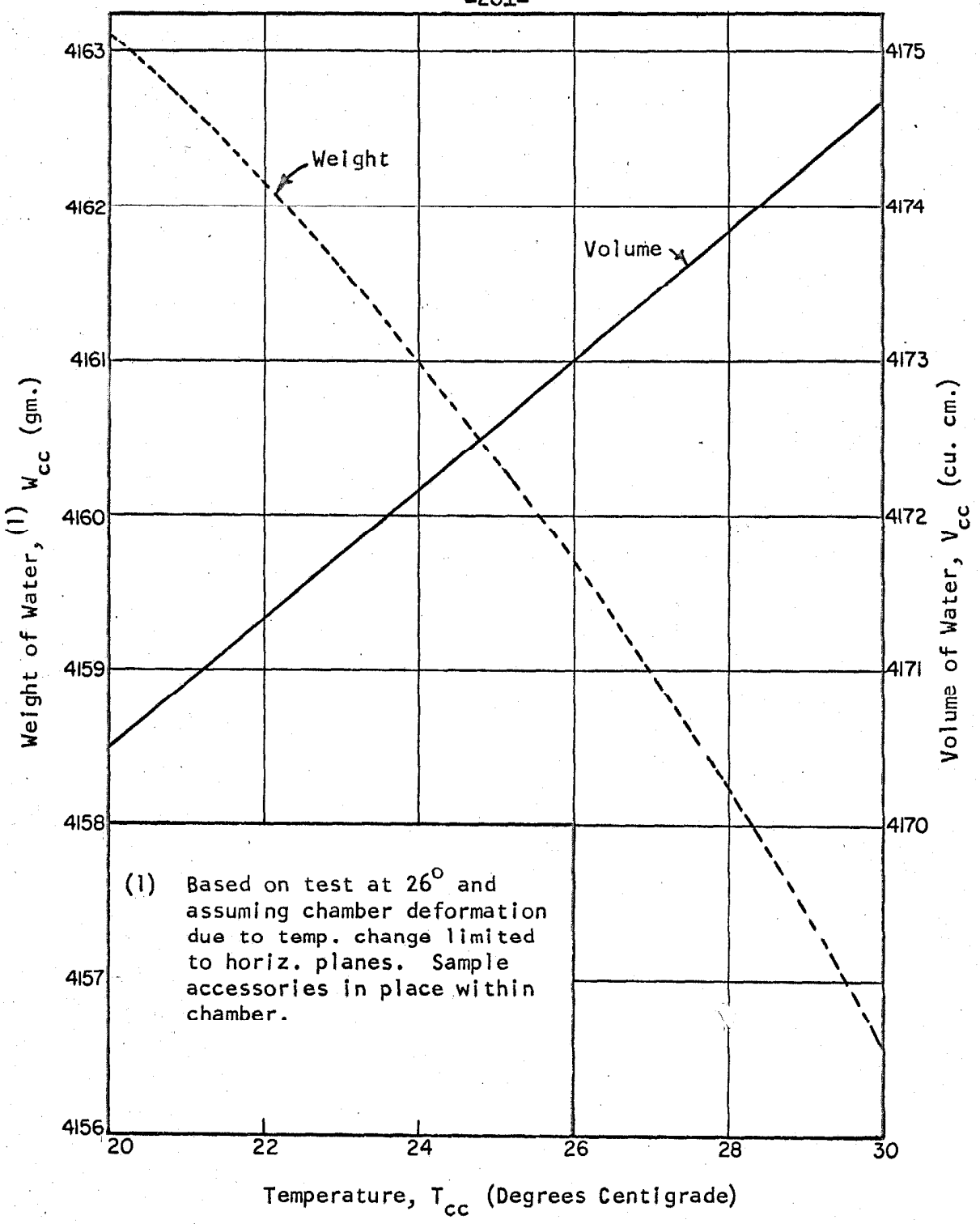

Figure A4.1 Weight and Volume of Distilled Water Required to Fill Spherical Compression Chamber as a Function of Temperature.

A5. COMPLETE DATA--SPHERICAL COMPRESSION EXPERIMENT NO. 6

Initial Data

Weight dry sand, 177.4 gm

Test sample under vacuum 4.5 psi, temperature 25.5°C

Compression chamber volume:

	Chamber Weight + Ballast 1, gm	Fill Reservoir Volume, cc
Before fill	604.0	4000
After fill	3748.5	835

Sample saturation:

	Chamber Weight + Ballast 2, gm	Sample Supply Reservoir Volume, cc
Before fill	244.0	300 150 450
After fill	579.0	150 0 411
After percolation	588.0	

Burette readings:

After percolation	2.73 cc
I. P. stress-strain test	7.07 cc

Final Data

	Chamber Weight + Ballast 3, gm	Fill Reservoir Volume, cc
Before emptying	3762.0	700
After emptying	621.0	3885

Specimen removed from compression chamber:

Weight of wet sample + membrane	2183.0 gm
Weight of membrane	58.8 gm

Table A5.1 Stress-Strain Data--Spherical Compression Experiment No. 6

Time min	Press. σ, psi	Bur.Read. V_B, cc	Time min	Press. σ, psi	Bur.Read. V_B, cc	Time min	Press. σ, psi	Bur.Read. V_B, cc	Time min	Press. σ, psi	Bur.Read. V_B, cc
0(1)	4.5	7.07	50	6.8	7.60	106	22.8	4.85	162	15.2	5.65
2	3.0	7.50	52	10.1	6.90	108	15.2	5.74	164	10.1	6.56
4	2.0	7.95	54	6.8	7.57	110	10.1	6.62	166	6.8	7.32
6	1.3	8.30	56	10.1	6.88	112	15.2	5.82	168	4.5	7.92
8	2.0	8.02	58(2)	15.2	6.03	114	10.1	6.62	170	3.0	8.43
10	3.0	7.60	60	10.1	6.84	116	6.8	7.40	172	2.0	8.93
12	4.5	7.12	62	15.2	6.02	118	10.1	6.70	174	1.3	9.28
14	6.8	6.55	64	22.8	5.07	120	6.8	7.40	176	2.0	9.00
16	10.1	5.81	66	15.2	5.97	122	4.5	8.01	178	3.0	8.58
18	15.2	4.91	68	22.8	5.07	125	6.8	7.47	180	4.5	8.07
20	22.8	3.85	70	34.2	3.91	127	4.5	8.02	182	6.8	7.50
22	34.2	2.59	72	22.8	4.97	129	3.0	8.54	184	10.1	6.75
24	51.3	1.15	75	34.2	3.91	131	2.0	9.04	186	15.2	5.88
		(7.08)	77	51.3	2.61	133	1.3	9.40	188	22.8	4.92
26	76.9	5.46	79	34.2	3.78	135	2.0	9.10	190	34.2	3.78
		(1.17)	81	51.3	2.61	137	3.0	8.68	192	51.3	2.50
28	51.3	2.50	83	76.9	1.10	139	4.5	8.20	195	76.9	1.00
30	34.2	3.73	85	51.3	2.43	141	6.8	7.61	197	51.3	2.32
32	22.8	4.85	88	76.9	1.10	143	10.1	6.87	199	34.2	3.52
34	15.2	5.85	90	51.3	2.40	145	15.2	6.00	201	22.8	4.62
36	10.1	6.72	92	34.2	3.61	147	22.8	5.02	203	15.2	5.60
38	6.8	7.49	94	51.3	2.45	149	34.2	3.87	205(3)	10.1	6.48
40	4.5	8.10	96	34.2	3.64	151	51.3	2.56	207	6.8	7.25
42	3.0	8.60	98	22.8	4.73	153	76.9	1.08	209	4.5	7.85
44	4.5	8.17	100	34.2	3.70	155	51.3	2.39	211	3.0	8.36
46	6.8	7.60	102	22.8	4.75	158	34.2	3.60	213(4)	4.5	7.93
48	4.5	8.14	104	15.2	5.72	160	22.8	4.70	5800(5)	4.5	6.97

Temperature = (1) 24.7°C; (2) 25.4°C; (3) 26.2°C; (4) 26.2°C; (5) 25.0°C

A6. CALCULATION OF TEST RESULTS--SPHERICAL COMPRESSION EXPERIMENT NO. 6

Initial Data

Weight solids, $W_s = 1778.4$ gm

Volume solids, $V_s = \frac{W_s}{\gamma_s} = \frac{1778.4 \text{ gm}}{2.65 \text{ gm/cc}} = 671.1$ cc

Sample volume by weight measurement (use):

Wt chamber water at 25.5°C (Figure A4.1), $W_{cc} = 4160$ gm

Wt chamber water excl. sample, $W_{cs} = 3748.5 - 604.0 = 3144.5$ gm

Wt water displ. by sample, $W_{ss} = W_{cc} - W_{cs} = 1015.5$ gm

Sample volume, $V = \frac{W_{ss}}{\gamma_w} = \frac{1015.5 \text{ gm}}{0.9968 \text{ gm/cc}} = 1018.8$ cc

Sample volume by volume measurement (check only):

Vol chamber water at 25.5°C (Figure A4.1), $V_{cc} = 4173$ cc

Vol chamber water excl. sample, $V_{cs} = 4000 - 835 = 3165$ cc

Sample volume, $V = V_{cc} - V_{cs} = 1008$ cc

Water volume by weight measurement (use):

Wt water accepted by sample through percolation,

$$W_w = 588.0 - 244.0 = 344.0 \text{ cc}$$

Volume of water, $V_w = \frac{W_w}{\gamma_w} = \frac{344.0}{0.9968} = 345.1$ cc

Volume water by volume measurement (check only):

Vol water accepted by sample upon filling,

$$V_w = 300 + 150 + 450 - (150 + 0 + 411) = 339 \text{ cc}$$

Void volume, $V_v = V - V_s = 1018.8 - 671.1 = 347.7$ cc

Physical properties:

Porosity, $n = \frac{V_v}{V} = \frac{347.7}{1018.8} = 0.341$

Void ratio, $e = \frac{V_v}{V_s} = \frac{347.7}{671.1} = 0.518$

Degree of saturation, $S = \frac{V_w}{V_v} = \frac{345.1}{347.7} = 99.3\%$

Dry density, $\gamma_d = \frac{W_s}{V} = \frac{1778.4}{1018.8} = 1.746$ gm/cc

Final Data

Sample volume by weight measurement (use):

Wt chamber water at 25.0°C (Figure A4.1), $W_{cc} = 4160.36$ gm

Wt chamber water excl. sample, $W_{cs} = 3762.0 - 621.0 = 3141.00$ gm

Wt water displ. by sample, $W_{ss} = W_{cc} - W_{cs} = 1019.36$ gm

Sample volume, $V = \frac{W_{ss}}{\gamma_w} = \frac{1019.36}{0.99707} = 1022.4$ cc

Sample volume by volume measurement (check only):

Vol chamber water at 25.0°C (Figure A4.1), $V_{cc} = 4173$ cc

Vol chamber water excl. sample, $V_{cs} = 3885 - 700 = 3185$ cc

Sample volume, $V = V_{cc} - V_{cs} = 988$ cc

Volume water by final sample weights:

Wt of wet sand, $W = 2183.0 - 58.8 = 2124.2$ gm

Wt of water, $W_w = W - W_s = 2124.2 - 1778.4 = 345.8$ gm

Vol of water, $V_w = \frac{W_w}{\gamma_w} = \frac{345.8}{0.99707} = 346.8$ cc

Void volume, $V_v = V - V_s = 1022.4 - 671.1 = 351.3$

Physical properties:

Porosity, $n = \frac{V_v}{V} = \frac{351.3}{1022.4} = 0.344$

Void ratio, $e = \frac{V_v}{V_s} = \frac{351.3}{671.1} = 0.523$

Degree of saturation, $S = \frac{V_w}{V_v} = \frac{346.8}{351.3} = 98.7\%$

Dry Density, $\gamma_d = \frac{W_s}{V} = \frac{1778.4}{1022.4} = 1.739$ gm/cc

Stress-Strain Data

Initial point volumes, $\sigma = 4.5$ psi:

Sample vol, $V_{IP} = V_0 + \Delta V_{BO} = 1018.8 + (7.07 - 2.73) = 1022.74$ cc

where V_0 = sample vol immediately after percolation

ΔV_{BO} = burette vol change to the initial point

Void vol, $V_{VIP} = V_{IP} - V_s = 1022.74 - 671.10 = 351.04$ cc

Stress-strain calculations:

Table A6.1 illustrates the method of calculation used in order to obtain porosity n and volumetric compressibility $-\Delta V/V\,\Delta\sigma$ as a function of spherical stress σ. The burette volume change $\sum \Delta V_B$ was obtained by differencing the burette readings V_B, Table A5.1, from the base point at 1.3 psi. The rubber penetration volume corrections V_R were obtained from Figure A2.8, interpolation being required where the loading program varied from that of the rubber penetration test.

Final point volumes, $\sigma = 4.5$ psi:

The sample volume obtained under final data is comparable with that given by the stress-strain table.

Table A6.1 Calculation of Stress-Strain Results--Spherical Compression Experiment No. 6

Press. σ psi	Bur. Vol. Chg. $\sum\Delta V_B$ ccx10^2	Rub. Pen. Corr. V_R ccx10^2	Corr. Vol. Chg. $\sum\Delta V$ ccx10^2	Inc. Vol. Chg. ΔV ccx10^2	Inc. Press. $\Delta\sigma$ psi	Tot. Samp. Vol. V cc	$V\Delta\sigma$ ccxpsi	Vol. Comp. $-\frac{\Delta V}{V\Delta\sigma}$ $(psi)^{-1}$x10^5	Void Vol. V_v cc	Porosity $n=\frac{V_v}{V}$ x10^5
4.5	-123	29	- 94			1022.14			351.04(1)	34344
3.0	- 80	18	- 62	32	- 1.50	1022.46	- 1534	20.86	351.36	34364
2.0	- 35	8	- 27	35	- 1.00	1022.81	- 1023	34.21	351.71	34387
1.3	0(2)	0	0	27	- 0.67	1023.08	- 686	39.39	351.98	34404
2.0	- 28	5	- 23	-23	0.67	1022.85	685	33.56	351.75	34389
3.0	- 70	12	- 58	-35	1.00	1022.50	1023	34.21	351.40	34367
4.5	-118	29	- 89	-31	1.50	1022.19	1533	20.22	351.09	34347
6.8	-175	54	- 121	-32	2.25	1021.87	2299	13.97	350.77	34326
10.1	-249	86	- 163	-42	3.37	1021.45	3442	12.20	350.35	34299
15.2	-339	133	- 206	-43	5.06	1021.02	5166	8.32	349.92	34272
22.8	-445	186	- 259	-53	7.59	1020.49	7746	6.84	349.39	34237
34.2	-571	249	- 322	-63	11.39	1019.86	11616	5.42	348.76	34197
51.3	-715	323	- 392	-70	17.09	1019.16	17417	4.02	348.06	34152
76.9	-877	418	- 459	-67	25.63	1018.49	26104	2.57	347.39	34108
51.3	-744	348	- 396	63	-25.63	1019.12	-26120	2.41	348.02	34149
34.2	-621	282	- 339	57	-17.09	1019.69	-17427	3.27	348.59	34186
22.8	-509	216	- 293	46	-11.39	1020.15	-11620	3.95	349.05	34216
15.2	-409	155	- 254	39	- 7.59	1020.54	- 7748	5.03	349.44	34241
•	•	•	•	•	•	•	•	•	•	•
•	•	•	•	•	•	•	•	•	•	•
6.8	-269	68	- 201	41	- 3.37	1021.07	- 3441	11.92	349.97	34275
4.5	-209	41	- 168	33	- 2.25	1021.40	- 2298	14.36	350.30	34296
3.0	-158	21	- 137	31	- 1.50	1021.71	- 1533	20.22	350.61	34316
4.5(3)	-201	41	- 160	-23	1.50	1021.48	1532	15.01	350.38	34301

(1) Initial point, stress-strain test
(2) Base point for volume change summation
(3) Final point for stress-strain calculations

A7. SUPPLEMENTAL THREE-DIMENSIONAL COMPRESSION APPARATUS PHOTOGRAPHS

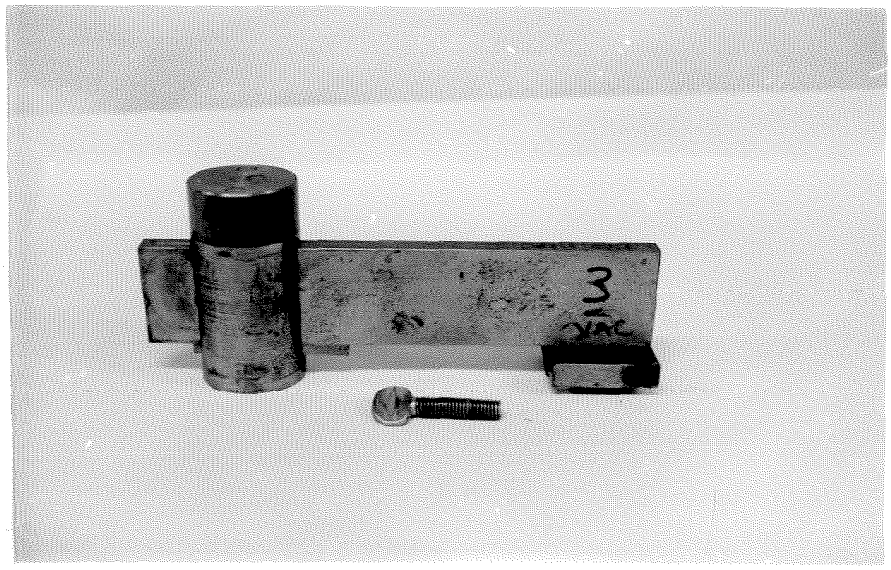

Figure A7.1 Piston Assembly, Three-Dimensional Compression Apparatus

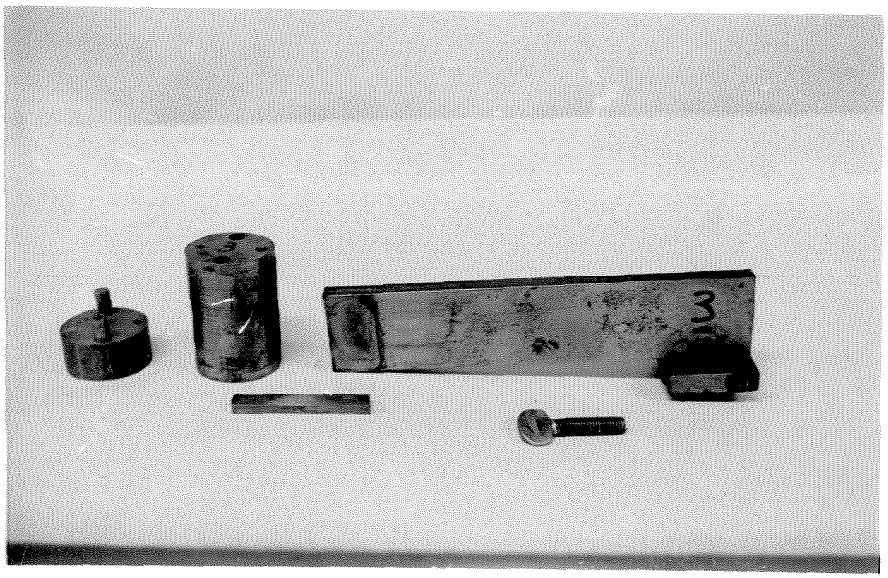

Figure A7.2 Piston Assembly Components: Spacer Cylinder, Base Cylinder, Clamp Bar, Rectangular Piston, Clamp Bolt, Three-Dimensional Compression Apparatus

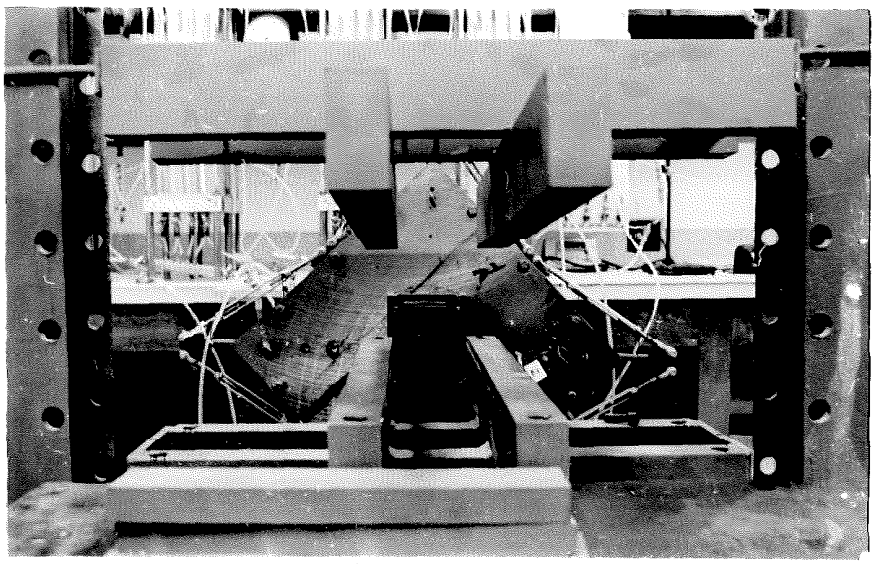

Figure A7.3 Press Frame, Three-Dimensional Compression Apparatus

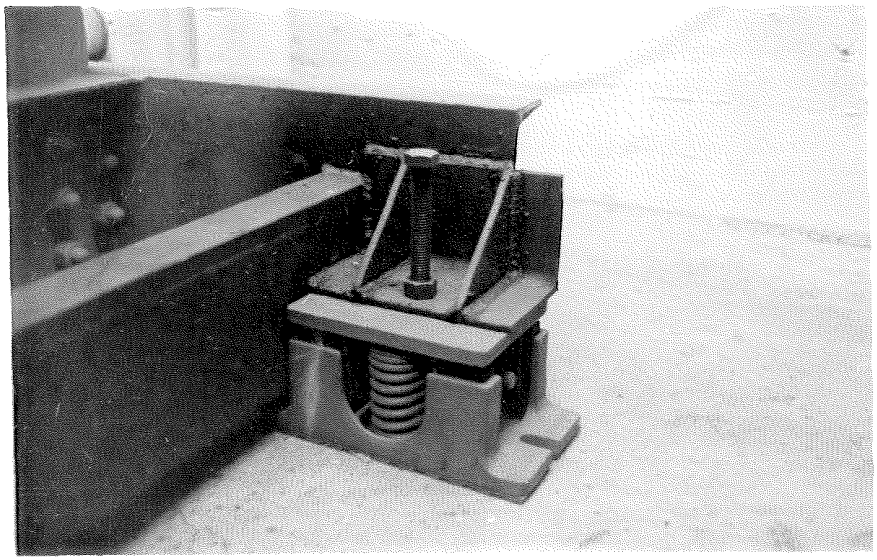

Figure A7.4 Vibration Isolator, Three-Dimensional Compression Apparatus

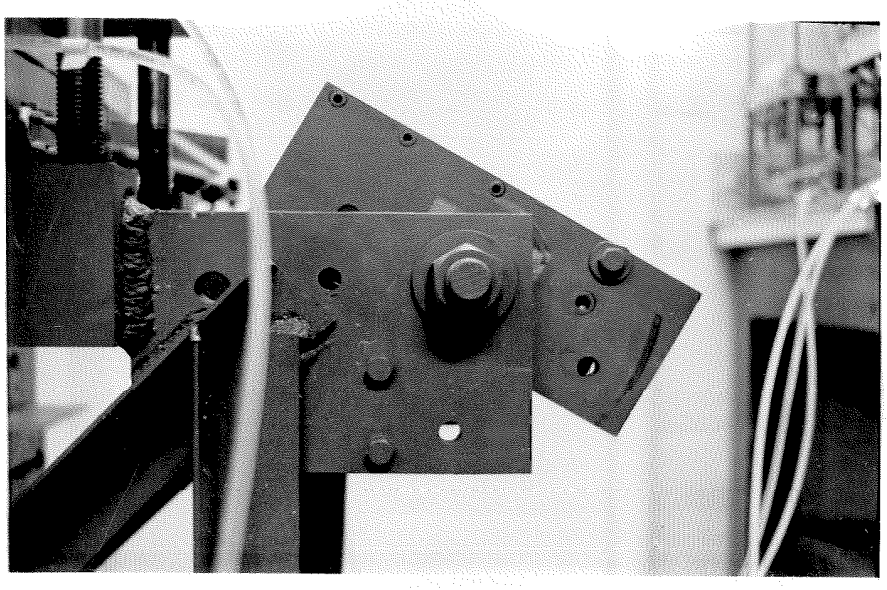

Figure A7.5 Saturation-Rotation Device, Side View, Three-Dimensional Compression Apparatus

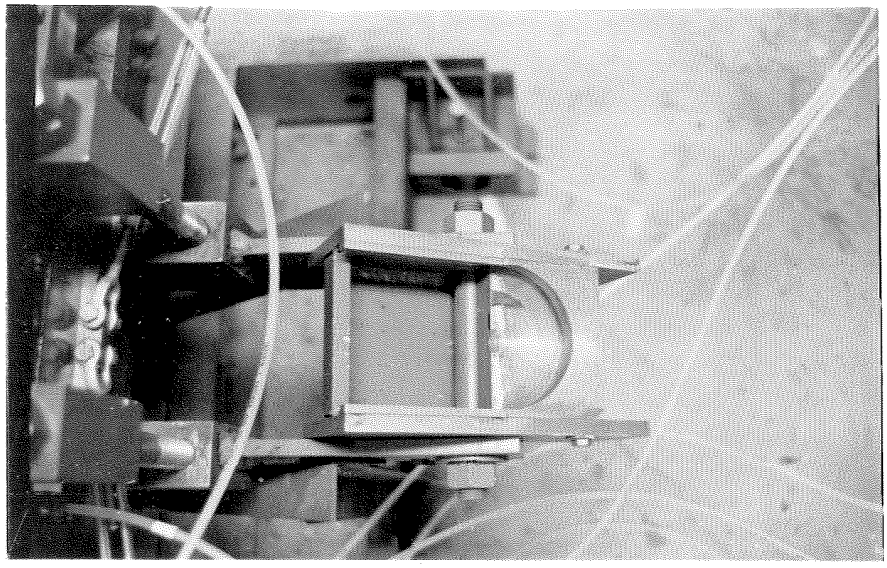

Figure A7.6 Saturation-Rotation Device, Top View, Three-Dimensional Compression Apparatus

Figure A7.7 Attached Manifold, Pressure-Volume Tank No. 1, Three-Dimensional Compression Apparatus

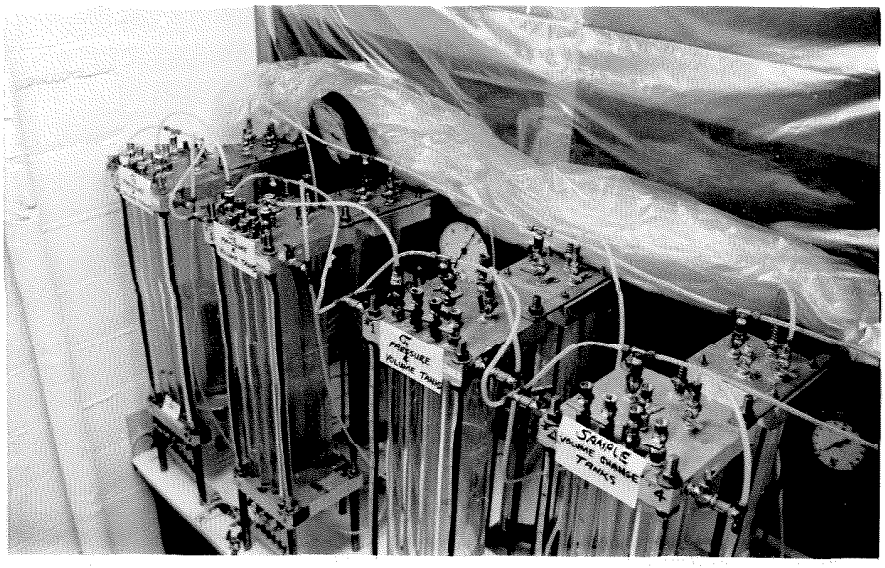

Figure A7.8 Piping Detail at Top of Pressure-Volume Tanks, Three-Dimensional Compression Apparatus

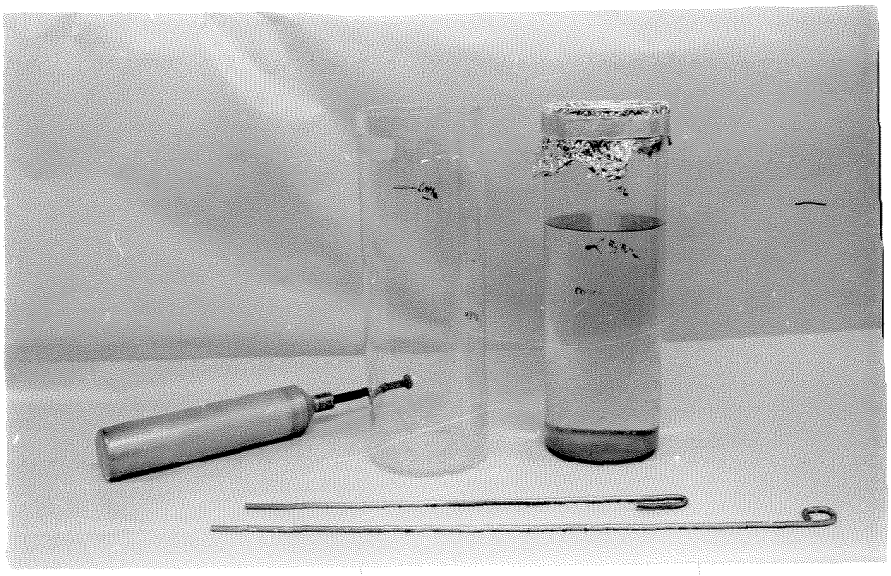

Figure A7.9 Aluminum Mold, Dipping and Coagulant Tanks and Stirring Rods, Side Pressure-Cell Latex Equipment

Figure 7.10 Side Pressure-Cell with Attached Aluminum Valve Core, Three-Dimensional Compression Apparatus

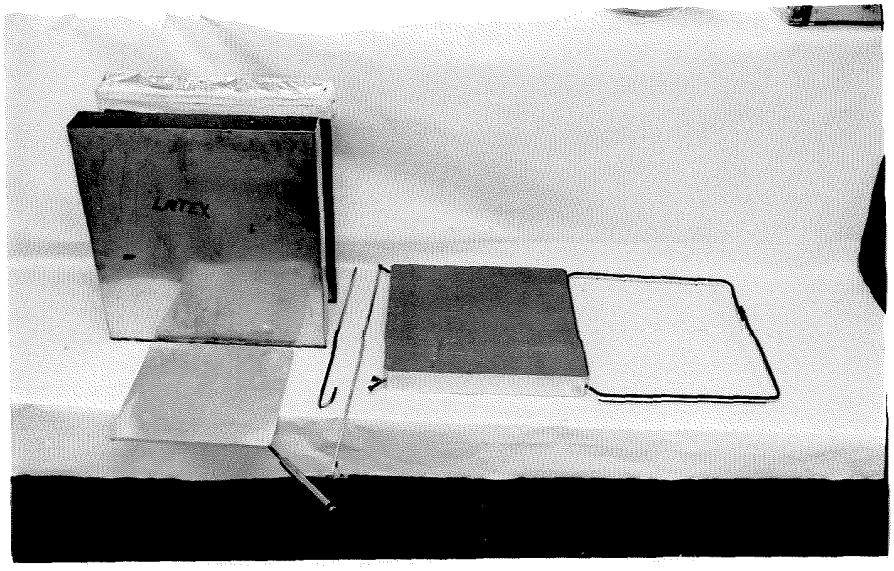

Figure A7.11 Stainless Dipping and Coagulant Tanks, Base Pressure-Cell and Sample Membrane Molds, and Stirring Rods, Latex Equipment

Figure A7.12 Sample Membrane, Three-Dimensional Compression Apparatus

A8. STRAIN EFFECTS--THREE-DIMENSIONAL COMPRESSION APPARATUS

A8.1 RUBBER PENETRATION

The reader is referred to Appendix A2.1 for introductory remarks. For a spherical state of stress the rubber penetration effect in the three-dimensional apparatus was similar to that in the spherical compression apparatus; however, for a deviatoric state of stress each parallel pair of sample faces was subjected to different pressures.

A8.11 RUBBER PENETRATION TESTS

Rubber Penetration Test Nos. 2A and 2B were performed in the fashion of Appendix A2.12 except that the time of load application was 15 min, corresponding to that of the three-dimensional compression tests. In addition, the loading program was modified to correspond to spherical stress cycles from 5 to 30 psi. Figures A8.2 and A83 give rubber penetration W_R as a function of pressure σ for compression and extension from 18 psi respectively.

A8.12 VOLUMETRIC PENETRATION CORRECTION--SPHERICAL STRESS

Based upon the average dimensions of the three-dimensional sample indicated in Figure A8.1, the total rubber-sand surface area for spherical compression was estimated to be 3860 sq cm. Figure A8.4

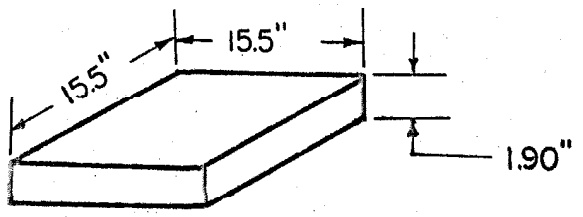

Figure A8.1 Average Dimensions, Three-Dimensional Plate Sample

gives the rubber penetration volume correction V_R as a function of applied pressure σ for compression from 18 psi based on Test 2A. Figure A8.5 gives the rubber penetration volume correction as a function of applied pressure for extension from 18 psi based on Test 2B.

A8.13 VOLUMETRIC PENETRATION CORRECTION--DEVIATORIC STRESS

The side pressure-cells were not in contact over the entire area of the vertical sample faces because of the piston separations. Based upon the overall dimensions of the vertical faces, the surface penetration area corresponding to the principal stress σ_1 and to the principal stress σ_3 was estimated to be 58.9 sq in. Figure A8.6 gives the rubber penetration volume correction V_{R3} as a function of applied pressure σ_3 as based upon Test 2B with pressures decreasing from 18 psi. Figure A8.7 gives the rubber penetration volume correction V_{R1} as a function of applied pressure σ_1 as based upon Test 2A with pressures increasing from 18 psi.

The base pressure-cell was not in contact with the entire lower face of the test specimen due to the provision for shearing deformation. Based upon an area equivalent to twice that of the base pressure-cell, the surface penetration area corresponding to the principal stress σ_2 was estimated to be 288 sq. in. Figure A8.8 gives the rubber penetration volume correction V_{R2} as a function of applied pressure σ_2 based upon Test 2A for pressures increasing from 18 psi, and based upon Test 2B for pressures decreasing from 18 psi.

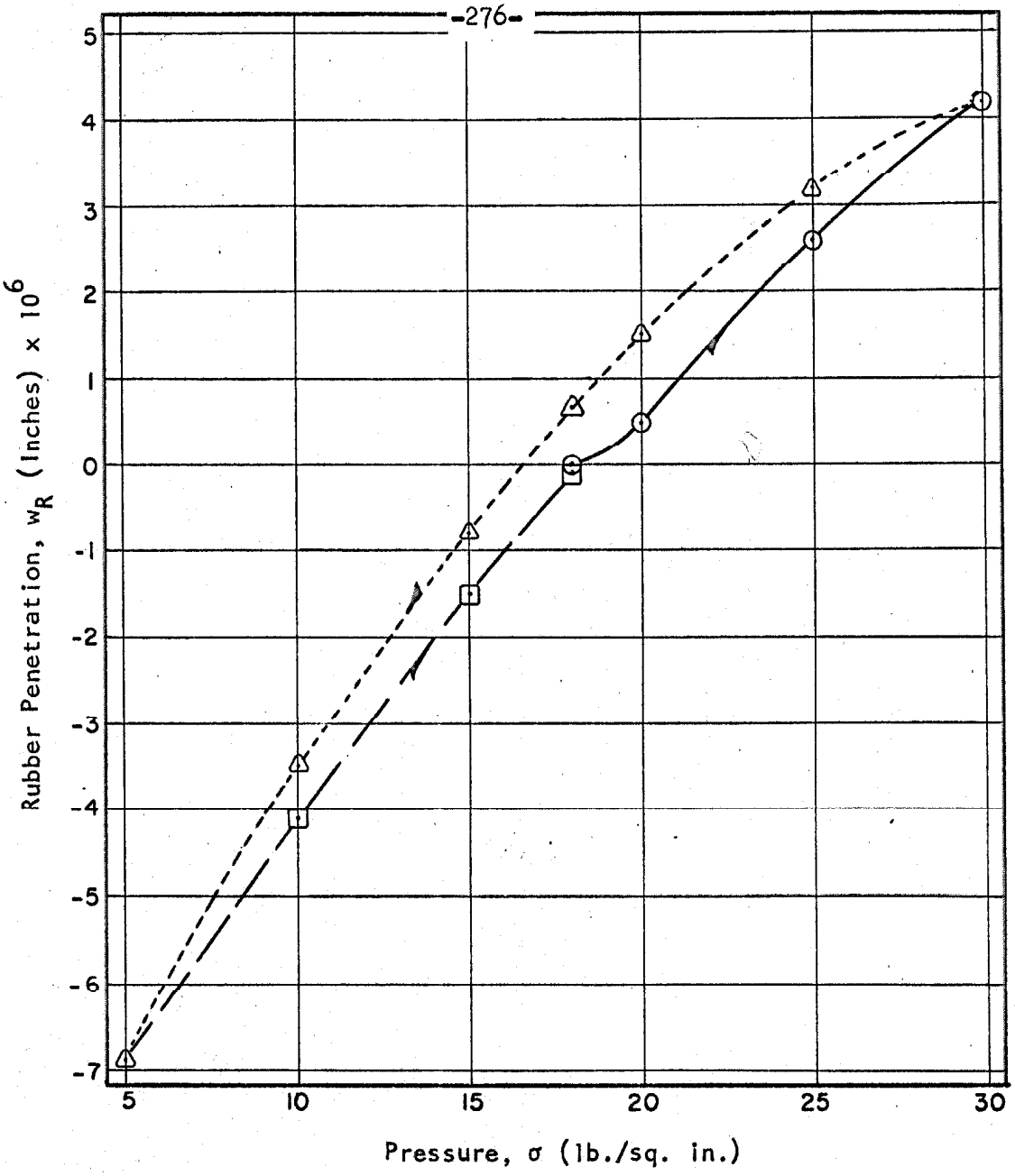

Key: Cycle

⊙ 1 (compression)
△ 2 (extension)
⊡ 3 (compression)

Compression from 18 lb./sq. in. pressure applied 17 hrs. Test load intervals - 15 minutes.

Figure A8.2 Rubber Penetration as a Function of Applied Pressure.
Rubber Penetration Test No. 2A

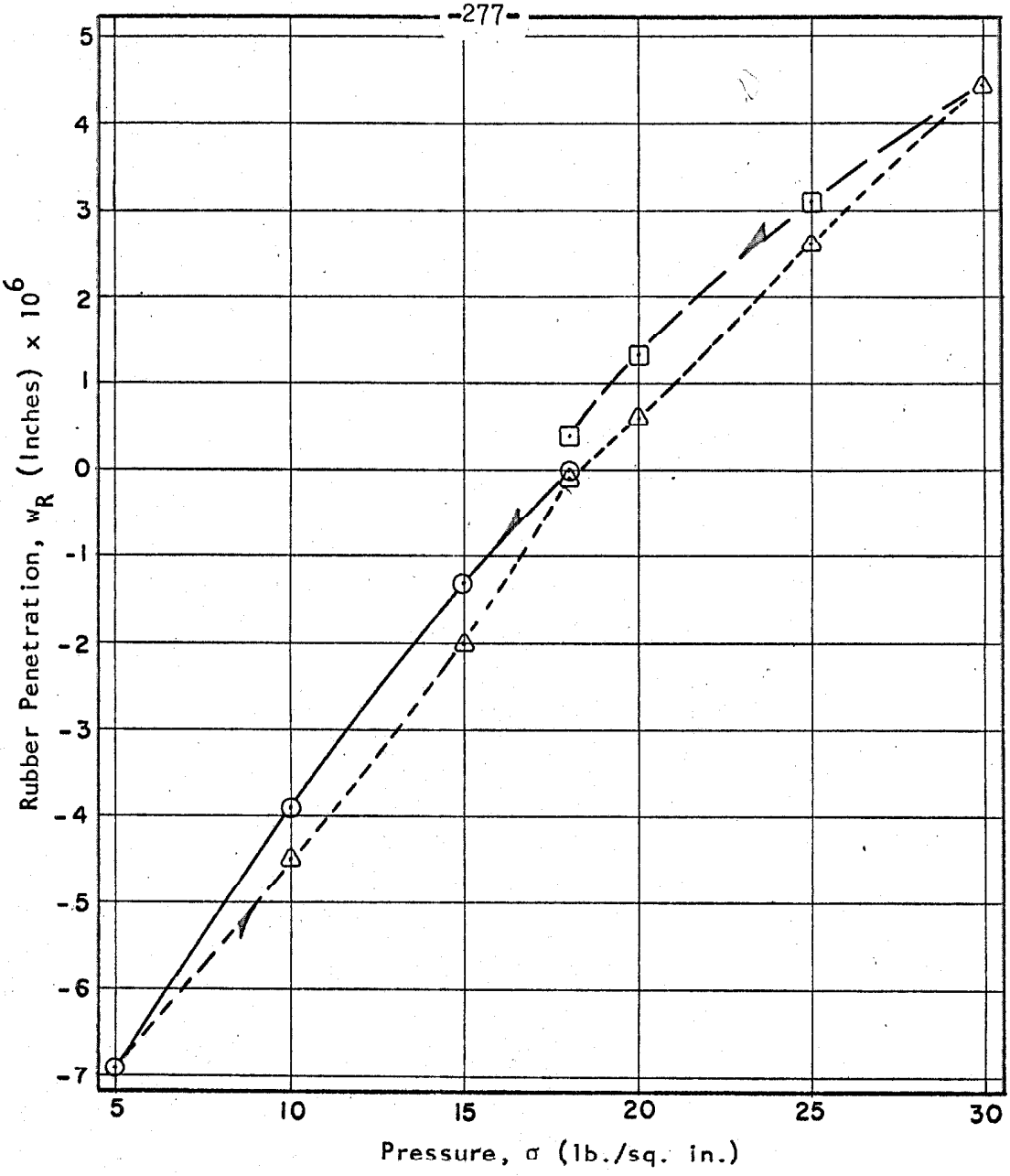

Key: Cycle

⊙ 1 (extension)
△ 2 (compression)
⊡ 3 (extension)

Extension from 18 lb./sq. in pressure applied 17 hrs. Test load intervals - 15 minutes.

Figure A8.3 Rubber Penetration as a Function of Applied Pressure.
Rubber Penetration Test No. 2B

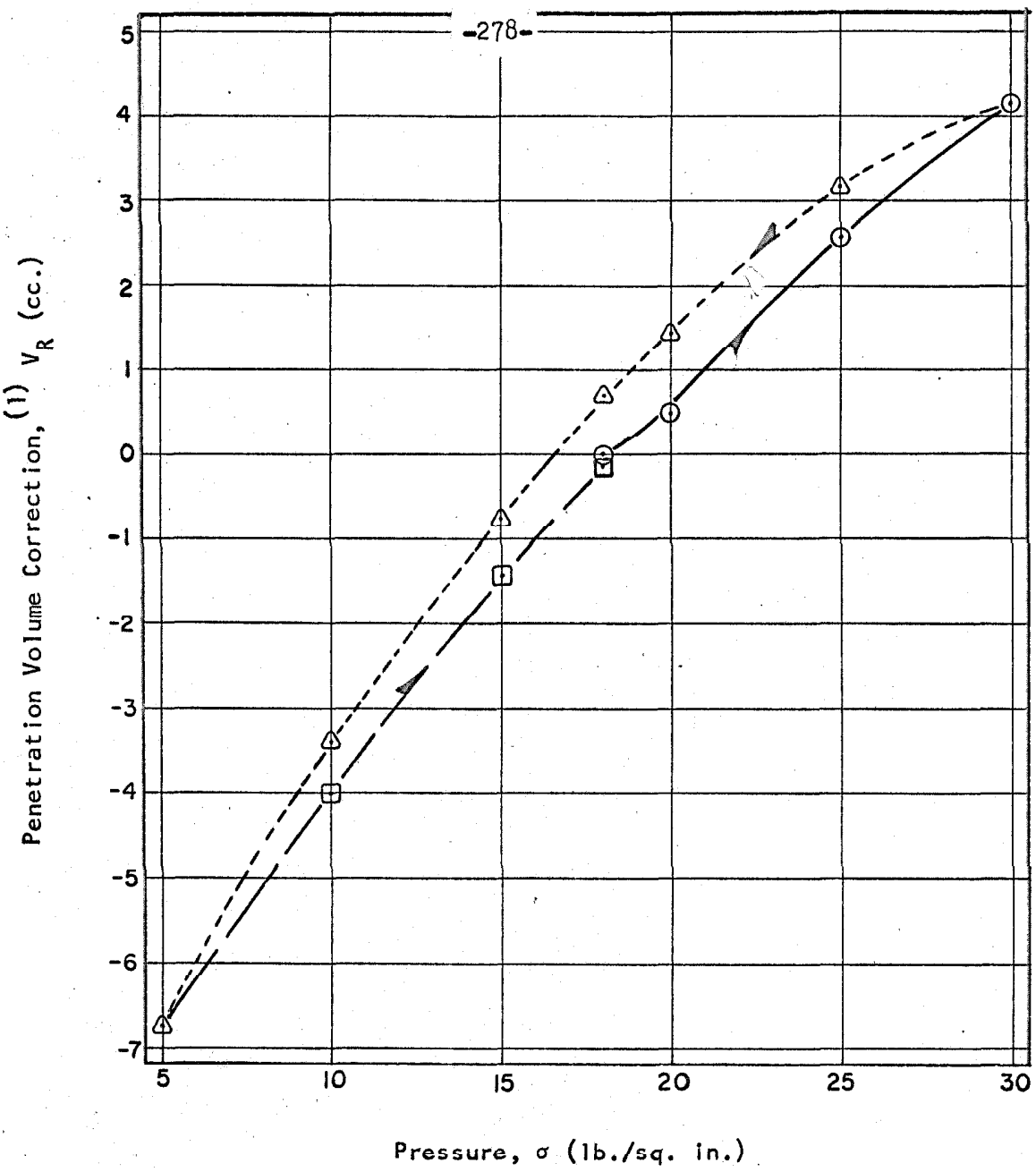

Key: Cycle

⊙ 1 (compression)
△ 2 (extension)
⊡ 3 (compression)

(1) Based on Rubber Penetration Test No. 2A and 3D Compression sample surface area of 3860 sq. cm.

Figure A8.4 Penetration Volume Correction as a Function of Applied Pressure for use in 3-Dimensional Compression Tests.
Compression from 18 lb./sq. in. Spherical Pressure.

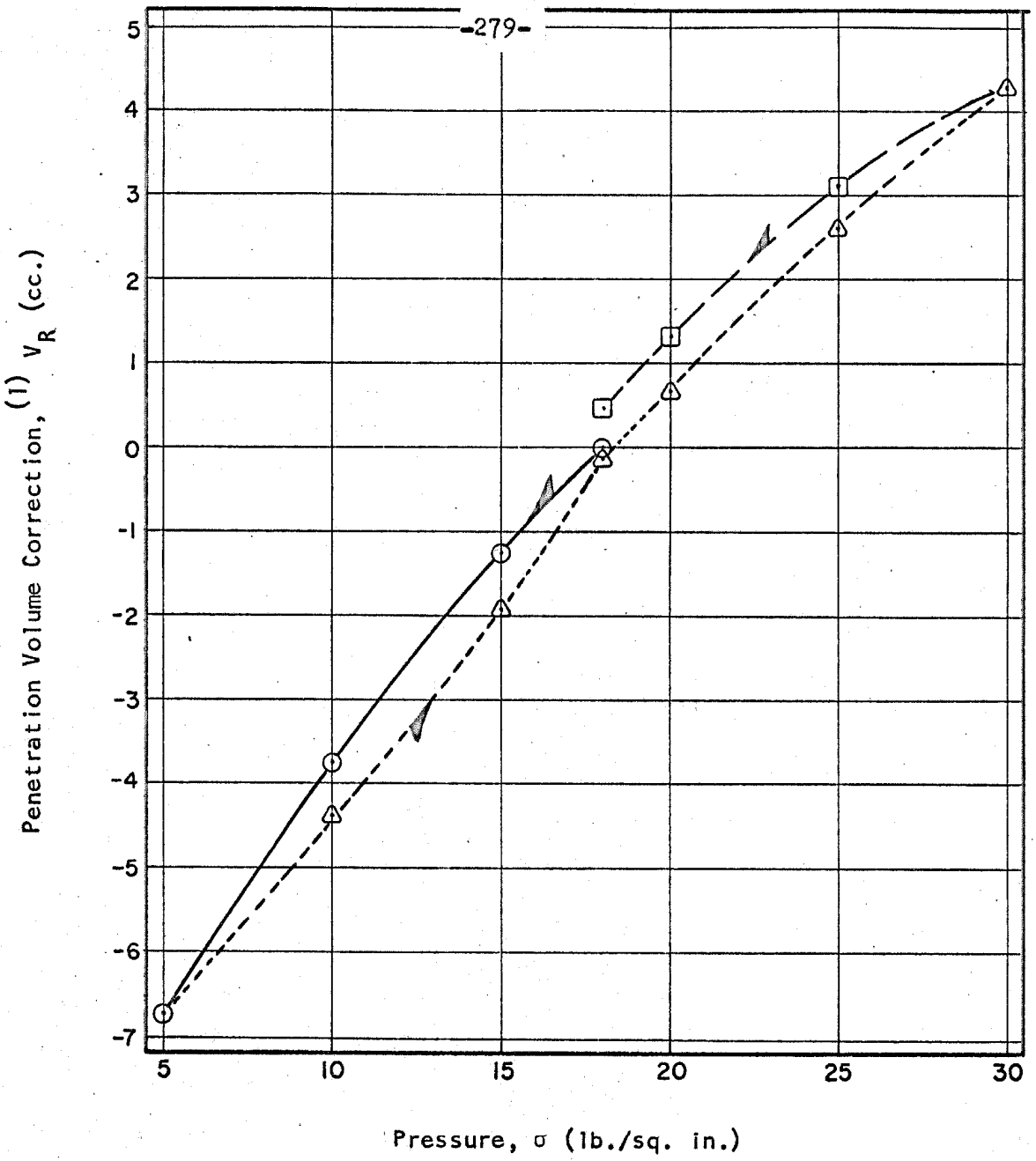

Key: Cycle

⊙ 1 (compression)
△ 2 (extension)
⊡ 3 (compression)

(1) Based on Rubber Penetration Test No. 2B and 3-D Compression sample surface area of 3860 sq. cm.

Figure A8.5 Penetration Volume Correction as a Function of Applied Pressure for use in 3-Dimensional Compression Tests.
Extension from 18 lb./sq. in. Spherical Pressure.

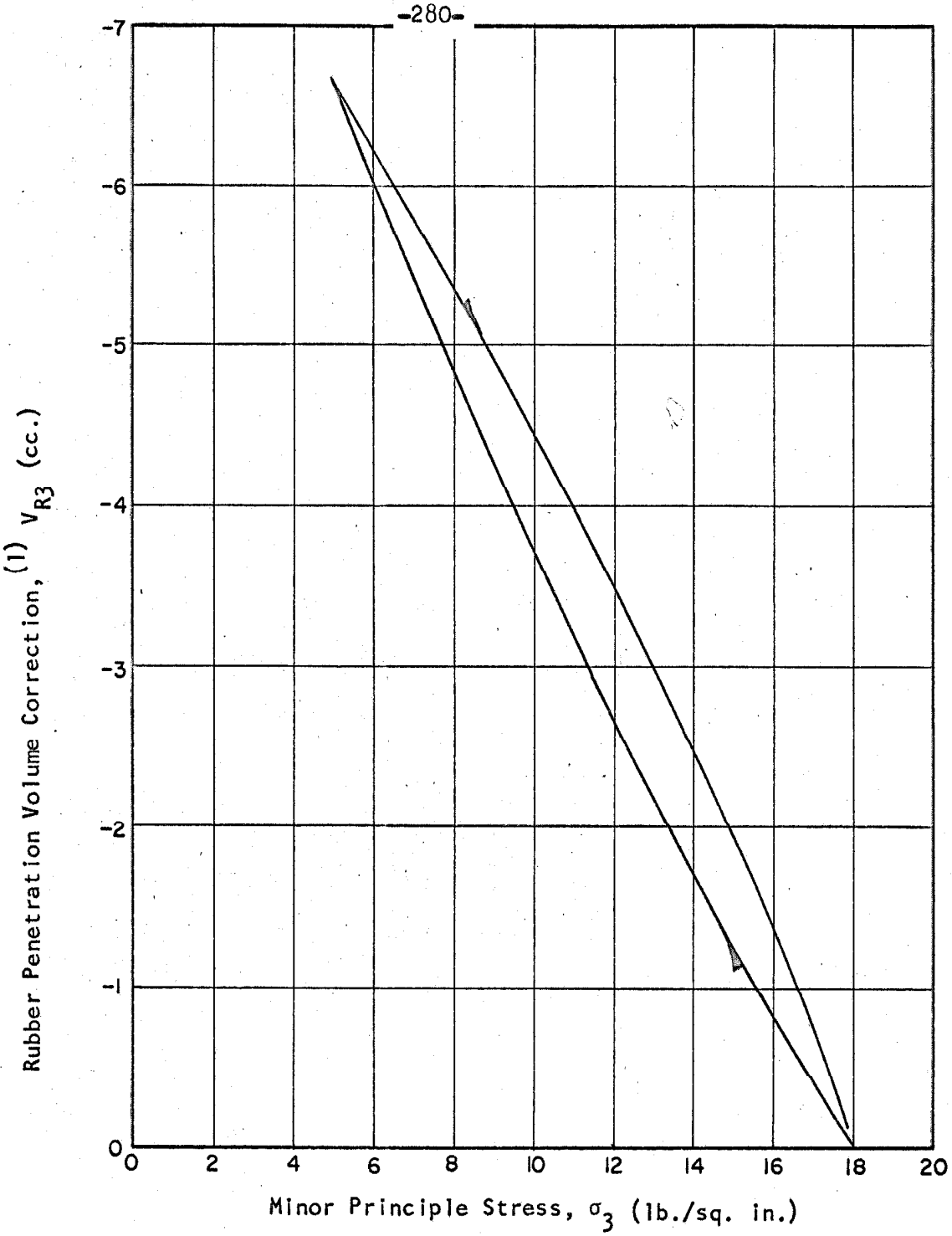

(1) Based on Rubber Penetration Test No. 2B and σ_3 surface area of 58.9 sq. in.
Extension from 18 lb./sq. in. pressure followed by subsequent compression.

Figure A8.6 Rubber Penetration Volume Correction as a Function of Applied Pressure. Minor Principle Stress (σ_3) Surface. 3-D Compression Tests.

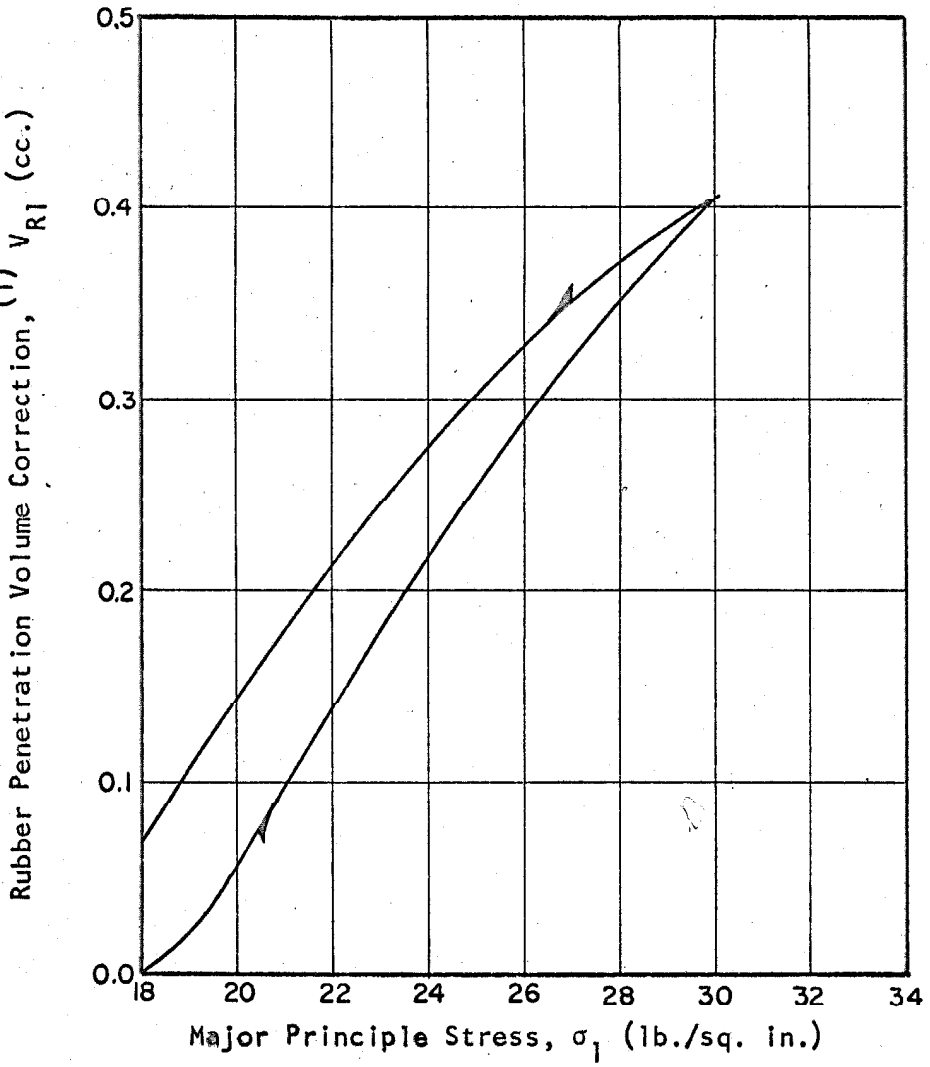

(1). Based on Rubber Penetration Test No. 2A and σ_1 surface area of 58.9 sq. in.

Compression from 18 lb./sq. in. pressure followed by subsequent extension.

Figure A8.7 Rubber Penetration Volume Correction as a Function of Applied Pressure.
Major Principle Stress (σ_1) Surface
3-D Compression Tests.

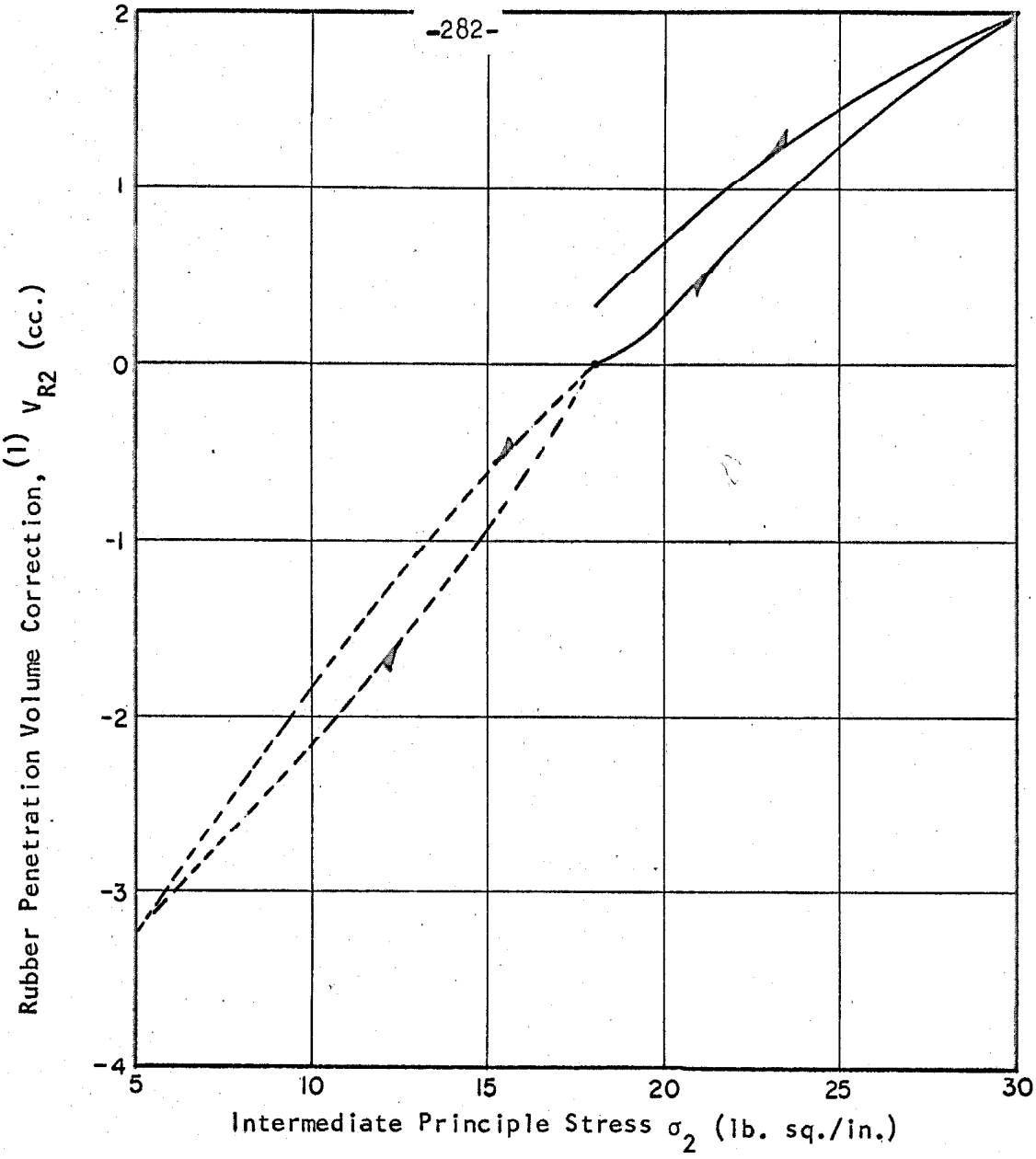

Key: Solid Line - Compression from 18 lb./sq. in. pressure followed by subsequent extension.
Dotted Line - Extension from 18 lb./sq. in. pressure followed by subsequent compression.

(1) Based on Rubber Penetration Test Nos. 2A and 2B and σ_2 surface area of 288 sq. in.

Figure A8.8 Rubber Penetration Volume Correction as a Function of Applied Pressure. Intermediate Principle Stress (σ_2) Surface 3-D Compression Tests.

A8.2 PRESSURE-CELL

Air was trapped initially in pockets between the pressure-cells, the compression chamber and the test sample. As internal pressure was applied to a cell, some air was extruded; and upon reduction of cell pressure, some air returned. With increasing cycles of stress the pressure-cell still exhibited non-linear behavior as the total expulsion of air was not possible; however, the behavior became more elastic and thus was approximately taken into account by calibration. A separate calibration was obtained initially for each experiment through the performance of several spherical compression cycles of stress.

A8.21 PRESSURE-CELL CALIBRATION

After the performance of initial spherical compression cycles, the true volumetric strains may be estimated by correction of the burette readings for rubber penetration, Section A8.12. Assuming an isotropic sample, the three principal strains are identical under spherical compression

$$\epsilon_1 = \epsilon_2 = \epsilon_3 \tag{A8.1}$$

and the volumetric strain is

$$\epsilon_v = \epsilon_1 + \epsilon_2 + \epsilon_3 \tag{A8.2}$$

so it follows that

$$\epsilon_1 = \frac{\epsilon_v}{3}, \quad \epsilon_2 = \frac{\epsilon_v}{3}, \quad \epsilon_3 = \frac{\epsilon_v}{3} \tag{A8.3}$$

Considering the behavior of σ_1 side cells, the corresponding principal strain is given by

$$\epsilon_1 = \frac{\Delta L_1}{L_1} \tag{A8.4}$$

where L_1 is the total length of the sample in the direction of σ_1. The change in length ΔL_1 is given by

$$\Delta L_1 = \frac{\Delta V_1}{A_1} \tag{A8.5}$$

where ΔV_1 is the volume change occurring within incompressible σ_1 cells, and A_1 is the projected area of the sample-cell contact. From Equations A8.4 and A8.5 it follows that

$$\epsilon_1 = \frac{\Delta V_1}{A_1 L_1} \tag{A8.6}$$

The volumetric strain is given by

$$\epsilon_v = \frac{\Delta V}{V} \tag{A8.7}$$

where ΔV is the volume change occurring within the grain skeleton, and V is the total sample volume. Substituting Equations A8.6 and A8.7 into Equation A8.3 then gives

$$\Delta V_1 = (\frac{A_1 L_1}{3V})\Delta V \tag{A8.8}$$

A similar development for the intermediate (base) and minor (side) cells results in

$$\Delta V_2 = (\frac{A_2 L_2}{3V})\Delta V \tag{A8.9}$$

and

$$\Delta V_3 = (\frac{A_3 L_3}{3V})\Delta V \tag{A8.10}$$

For purposes of calculation the following initial dimensions were taken as representative for all tests:

$A_1 = A_3 = 1.90 \times 14.75$ sq in.

$A_2 = 12 \times 12$ sq in.

$L_1 = L_3 = 15.5$ in.

L_2 = 1.90 in.

V = 7300 cc = 446 cu in.

Based upon these dimensions, Equations A8.8, A8.9 and A8.10 are

$$\Delta V_1 = 0.325\Delta V \qquad \text{(A8.11)}$$

$$\Delta V_2 = 0.205\Delta V \qquad \text{(A8.12)}$$

$$\Delta V_3 = 0.325\Delta V \qquad \text{(A8.13)}$$

The differences between volume changes recorded at the three graduated pressure-volume tubes and those given by Equations A8.11, A8.12 and A8.13 were assumed due to the effects of air compressibility and rubber penetration. The pressure-cell contributions are thus

$$-\Delta V_{PC1} = \Delta V_{1B} - 0.325\Delta V \qquad \text{(A8.14)}$$

$$-\Delta V_{PC2} = \Delta V_{2B} - 0.205\Delta V \qquad \text{(A8.15)}$$

$$-\Delta V_{PC3} = \Delta V_{3B} - 0.325\Delta V \qquad \text{(A8.16)}$$

where V_{PCi} represents the volume change correction due to the σ_i cell compressibility and rubber penetration; V_{iB} the recorded volume change at the corresponding graduated pressure-volume tube.

A8.3 TEMPERATURE CHANGE

Neglecting entrapped air, temperature change was calculated to induce volume changes in the various measurement systems as follows:

Measurement System	Volume cc	Volume Change cc/C°
Sample voids	2520	0.7
Side cells (σ_1 or σ_3)	2540	0.7
Base cell (σ_2)	1060	0.3

A9. STRESS EFFECTS--THREE-DIMENSIONAL COMPRESSION APPARATUS

A9.1 MEMBRANE BEHAVIOR

The reader is referred to Appendix A3 for introductory remarks. Upon the occurrence of strain within the three-dimensional test specimen, the membrane accepted a portion of the applied external load, thus modifying the stress taken by the grain skeleton. If the membrane dimensions are large with respect to thickness, the sides of the membrane may be neglected in analysis, and a representative internal element examined, Figure A9.1.

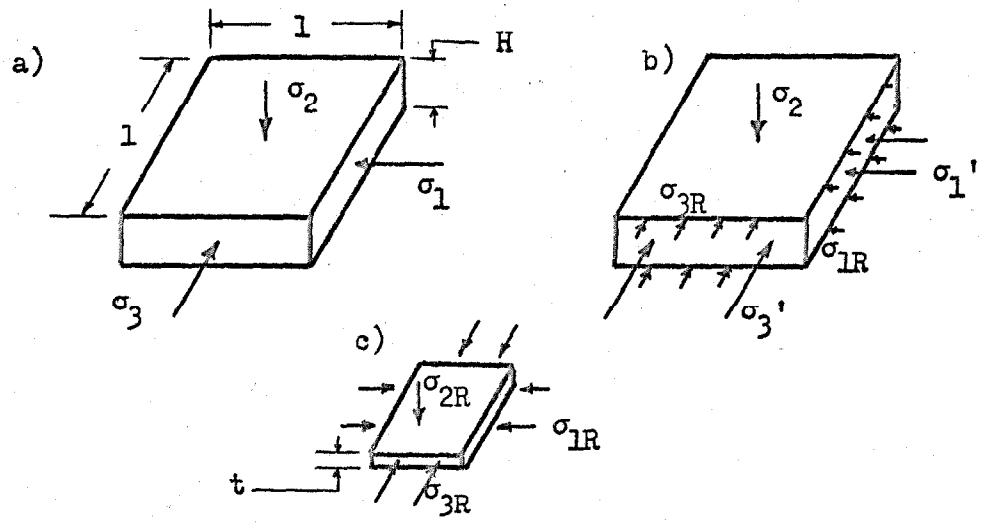

Figure A9.1 Rubber-Sand Interaction, Element of Plate Specimen, Three-Dimensional Compression Test

This element is subjected to the applied principal stresses σ_1, σ_2 and σ_3, as shown in Figure A9.1 a). The sand accepts most of the load through development of the stresses σ_1', σ_3' and σ_2; the rubber skin takes the remainder through the development of the stresses σ_{1R} and σ_{3R}, Figure A9.1 b).

Assuming membrane thickness t small relative to sample thickness H, a statement of equilibrium in the 1 direction is given by

$$\sigma_1 H = \sigma_1' H + \sigma_{1R} 2t$$

or

$$\sigma_1' = \sigma_1 - \frac{2t}{H} \sigma_{1R} \qquad \text{(A9.1)}$$

A corresponding statement of equilibrium in the 3 directions leads to

$$\sigma_3' = \sigma_3 - \frac{2t}{H} \sigma_{3R} \qquad \text{(A9.2)}$$

The rubber stresses, Figure A9.1, are determined by the method of Section A3.2. Equations A3.10 and A3.11 modified for this case are

$$\sigma_{1R} = \sigma_{2R} - \frac{2}{3} (2 \epsilon_{1R} + \epsilon_{3R}) E \qquad \text{(A9.3)}$$

$$\sigma_{3R} = \sigma_{2R} - \frac{2}{3} (2 \epsilon_{3R} + \epsilon_{1R}) E \qquad \text{(A9.4)}$$

Substitution of Equations A9.3 and A9.4 into Equations A9.1 and A9.2 respectively gives

$$\sigma_1' = \sigma_1 - \frac{2t}{H} [\sigma_{2R} - \frac{2}{3} E (2 \epsilon_{1R} + \epsilon_{3R})] \qquad \text{(A9.5)}$$

$$\sigma_3' = \sigma_3 - \frac{2t}{H} [\sigma_{2R} - \frac{2}{3} E (2 \epsilon_{3R} + \epsilon_{1R})] \qquad \text{(A9.6)}$$

Assuming that $\sigma_{2R} = \sigma_2$, $\epsilon_{1R} = \epsilon_1$ and $\epsilon_{3R} = \epsilon_3$, it follows that

$$\sigma_1' = \sigma_1 - \frac{2t}{H} [\sigma_2 - \frac{2}{3} E (2 \epsilon_1 + \epsilon_3)] \qquad \text{(A9.7)}$$

$$\sigma_3' = \sigma_3 - \frac{2t}{H} [\sigma_2 - \frac{2}{3} E (2 \epsilon_3 + \epsilon_1)] \qquad \text{(A9.8)}$$

Using E = 263 psi (from Figure A3.2), and given representative membrane dimensions t = 0.055 in. and H = 1.90 in., the corrected stresses are

$$\sigma_1' = \sigma_1 - 0.0579 [\sigma_2 - 175.3 (2 \epsilon_1 + \epsilon_3)] \qquad \text{(A9.9)}$$

$$\sigma_3' = \sigma_3 - 0.0579 [\sigma_2 - 175.3 (2 \epsilon_3 + \epsilon_1)] \qquad \text{(A9.10)}$$

A9.2 BOUNDARY FRICTION

Silicon grease was applied to the outer surface of the sample membrane to reduce boundary friction. Tests were performed to obtain a measure of the amount of friction actually developed.

A9.21 BOUNDARY FRICTION TESTS

A schematic diagram of the boundary friction test apparatus is given in Figure A9.2. A tee connection was added to the line from pressure-volume tank no. 1 to pressure-cell G1-1 , and a new needle valve BF1 was installed, Figure A9.3. The connecting lines were filled with water and attached to a Statham pressure transducer. The output of the transducer was measured by use of an automatic recorder, Figure A9.4.

Friction tests were carried out following the performance of Test No. $14\text{-}5\text{-}I_{13*R}$, the test specimen remaining in-place within the compression chamber. Initially all pressure-cells were under a pressure of 18 psi. The intermediate σ_2 cell was sealed by closing valve 2-3, Figure 6.2, and the minor σ_3 cells were sealed by closing valves 3-1, 3-2 and 3-3. Pressures were applied to a live σ_{1L} side cell (free to change in volume) and measured at the opposite dead (sealed) σ_{1D} side cell. The difference in pressure (live-dead) was measured, and the corresponding force was considered to be carried in shear by the upper and lower faces of the test specimen.

Initially valve PV1 was closed and all other valves of Figure A9.2 were open. The automatic recorder was switched on and the potential corresponding to 18 psi recorded. Prior to the application of

each load, valve BF1 was closed allowing the live cell (G1-2) pressure to be retorded. Valve PV1-27 was then closed and valve BF1 opened allowing the dead cell pressure to be recorded. The load increment was applied and the dead cell pressure automatically recorded in time. When equilibrium had been established, valve BF1 was closed and valve PV1-27 was opened--recording the live cell pressure once again. This procedure was repeated for each load increment. Normally about 95% of the total pressure change occurred during the load application (1/2 min), and the remaining 5% in from 1 to 2 min.

The ultimate difference between live and dead cell readings from the inked record of potential was compared directly with the difference in live cell (known pressure) readings and the corresponding pressures obtained by proportion. This procedure essentially provided a continuous calibration of the transducer in time. Details of Friction Test Nos. 1, 2, 3A and 3B follow.

Friction Test No. 1

Pressure program: 18, 25, 30, 25, 18 psi

Details: Pistons were rocked at 30 psi

Friction Test No. 2

Pressure program: 18,20,25,30,25,20,18,15,10,5,10,15,18 psi

Details: Pistons were rocked at 30 psi

Friction Test Nos. 3A and 3B

Pressure program: 18,20,25,30,25,18 and 18,15,10,5,10,15,18 psi

Details: Pressures in live and dead cells were equalized following first cycle at 18 psi.

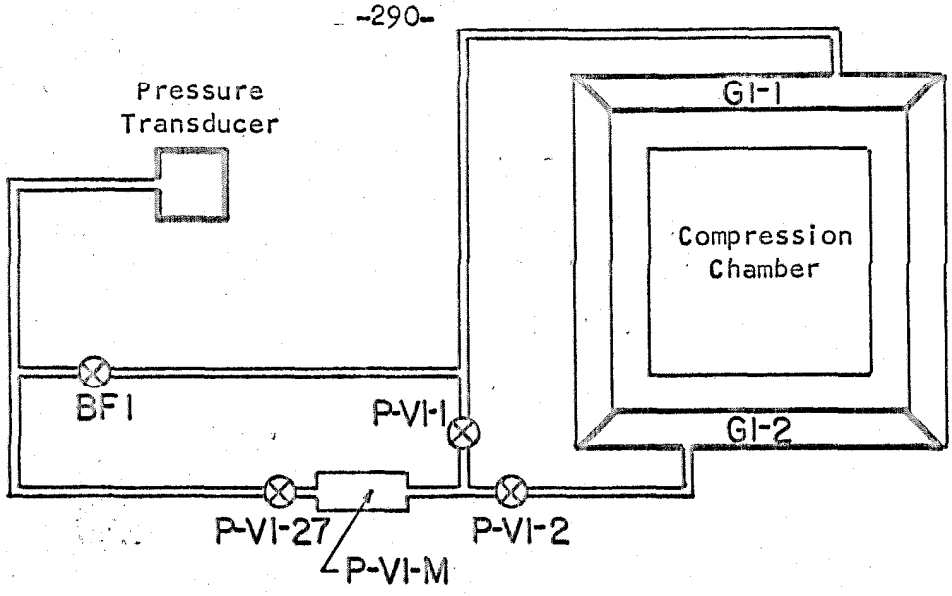

Hydraulic Circuit

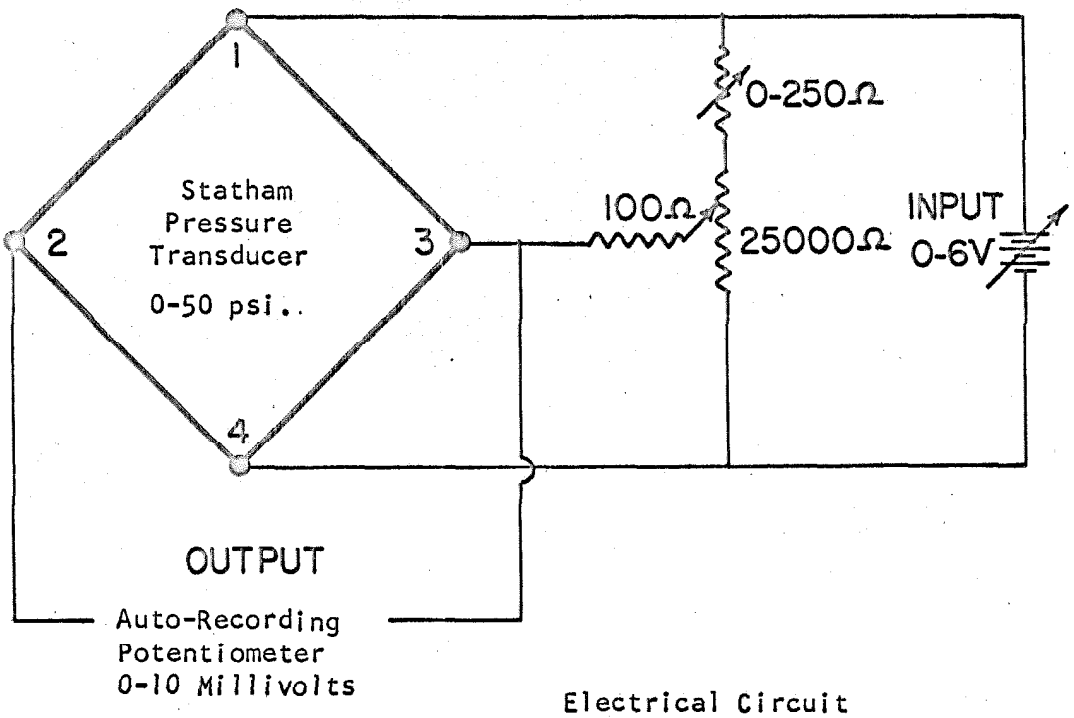

Electrical Circuit

Figure A9.2 Schematic Diagram - Boundry Friction Test Equipment, Three-Dimensional Compression Apparatus

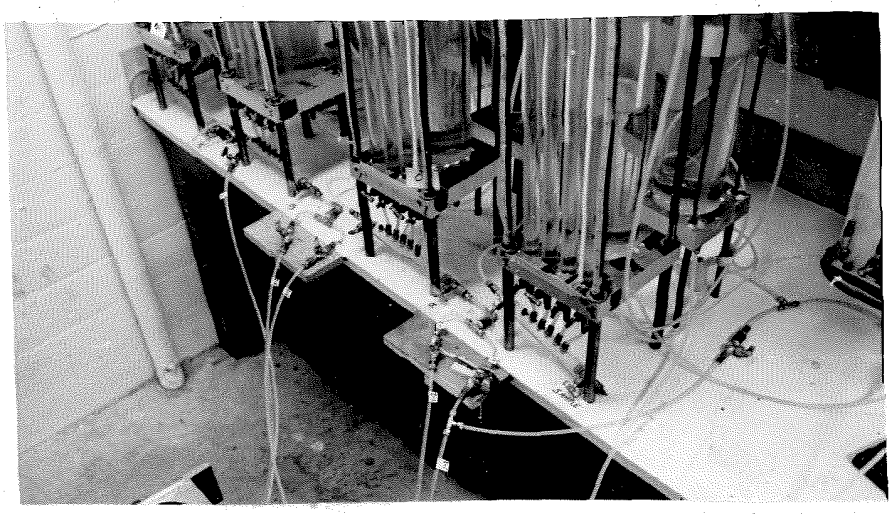

Figure A9.3 Piping Details for Friction Test, Pressure-Volume Tank No. 1

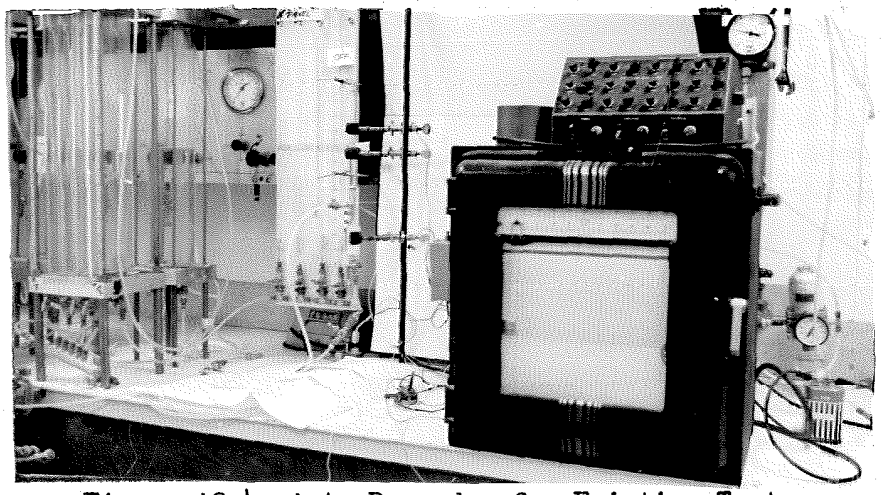

Figure A9.4 Auto-Recorder for Friction Test

A9.22 BOUNDARY SHEAR AS MEASURED BY FRICTION TESTS

A statement of force equilibrium for the plate specimen, Figure A9.5, gives

$$(\sigma_{1L} - \sigma_{1D})(1.90 \times 15.25 = 2\tau(15.25 \times 15.25)$$

or

$$\tau = 0.0872\ (\sigma_{1L} - \sigma_{1D}) \qquad \text{(A9.11)}$$

where τ is the average boundary friction stress developed in psi by a live-dead pressure difference $(\sigma_{1L} - \sigma_{1D})$ in psi. Figure A9.5 illustrates results from friction tests 1, 2, 3A and 3B.

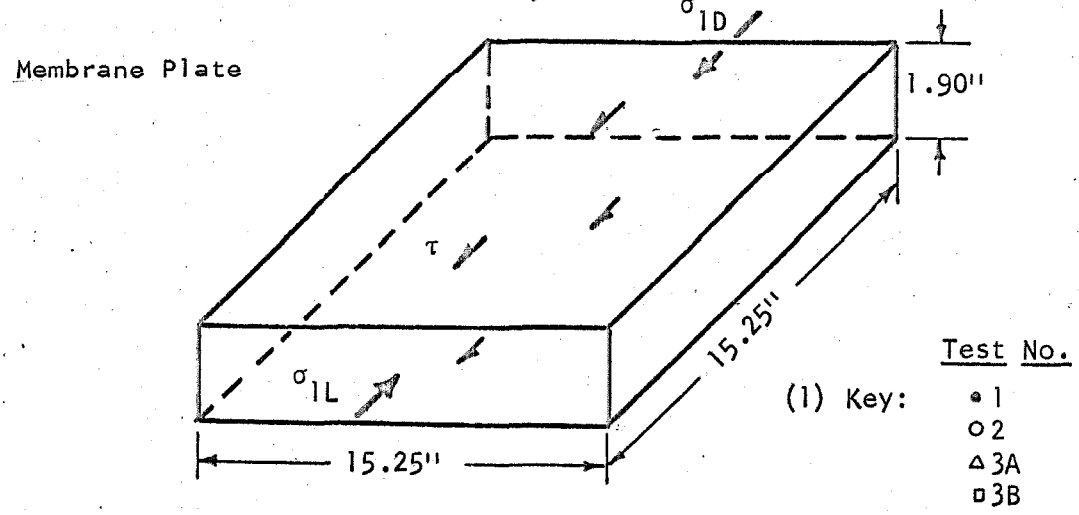

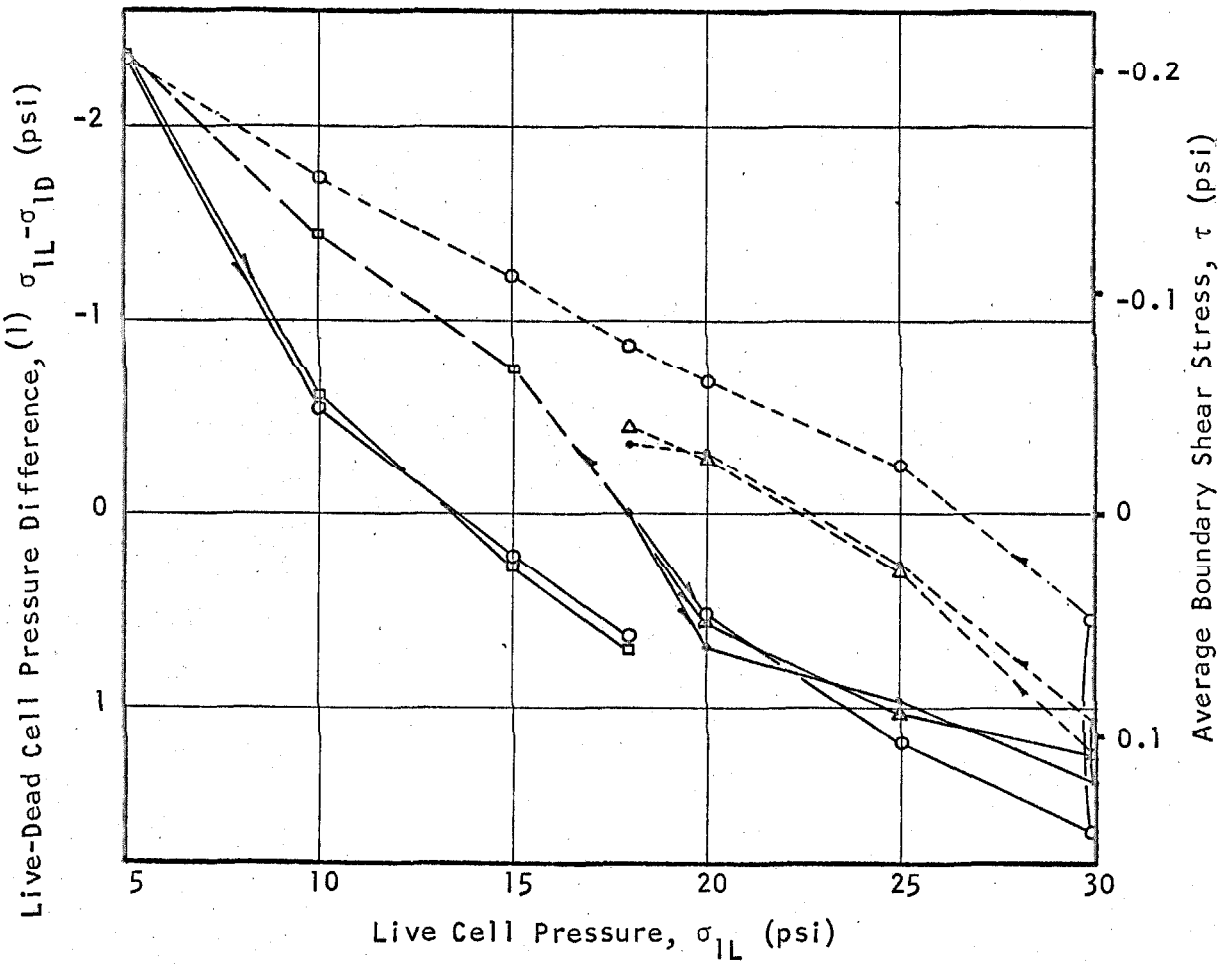

Figure A9.5 Boundary Friction Test Nos. 1, 2, 3 A & B Following Three Dimensional Compression Experiment No. 13.

A10. THE PHOTOGRAPHIC MEASUREMENT OF STRAIN, THREE-DIMENSIONAL COMPRESSION APPARATUS

An unsuccessful attempt was made to photographically measure minor and major principal strains early in the experimental program. For the record, the method of measurement will be briefly described. (See Figure 7.17 for photographic results.)

The sample membrane was marked with india ink to form an orthogonal network of lines 1/2 in. apart and parallel to the major and minor principal stresses. Graph paper lines (10/in.) were superimposed on transparent film by use of a photographic process, and the film was bonded to the inside surface of the lucite cover plate with cellophane tape having adhesive on both sides. A Polaroid camera was attached to the press frame and focused with a closeup lense on the test specimen as viewed through the plexiglas center window. The field of view was approximately 5-1/2 in. sq. Artificial lighting was provided at two sides of the compression chamber.

Photographs were taken using transparency film prior to and following the application of particular load increments. The pictures were mounted in 3-1/4 x 4-in. plastic lantern slide frames for enlarged projection on a glass screen covered with mylar film. Distances from the inked lines on the membrane to the fixed lines on the celluloid film were measured on the screen with a 0.01-in. ruler, and related principal strains were calculated. The enlarged inked lines on the membrane were not initially clear or uniform; and after the membrane was greased several times, the lines became more blurred.

All. AIR VOLUME DETERMINATION--THREE-DIMENSIONAL COMPRESSION APPARATUS

Assuming constant temperature, Boyle's law states that

$$P_A V_A = C \qquad \text{(All.1)}$$

where

P_A = absolute air pressure within test specimen

V_A = air volume contained within test specimen

C = a constant

It follows from differentiation that

$$P_A dV_A + V_A dP_A = 0$$

or

$$V_A = - P_A \frac{dV_A}{dP_A} \doteq - P_A \frac{\Delta V_A}{\Delta P_A} \qquad \text{(All.2)}$$

The air volume apparatus was composed of the volumetric strain burette connected to the voids of the specimen as shown in Figure All.1.

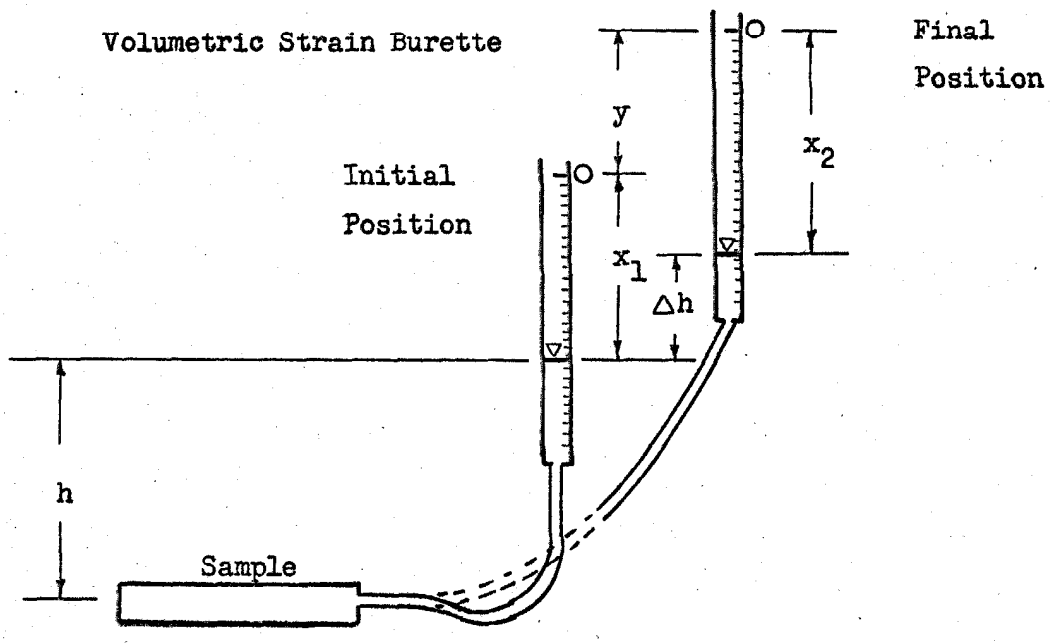

Figure All.1 Air Volume Apparatus

Initially the head of water to the center of the specimen was h. Upon raising the burette a distance y, the head increased by Δh and the burette volume reading changed by $\Delta V = V_{x_2} - V_{x_1}$. Equation A11.2 written in terms of head of water is

$$V_A \doteq \frac{P_A \Delta V}{\gamma_w \Delta P_A / \gamma_w} \qquad \text{(A11.3)}$$

where

$$\frac{P_A}{\gamma_w} = h + \frac{P_B}{\gamma_w} \quad \text{with } P_B = \text{barometric pressure} \qquad \text{(A11.4)}$$

and since

$$\frac{P_A}{\gamma_w} = \Delta h \qquad \text{(A11.5)}$$

it follows from Equation A11.3 that

$$V_A \doteq (h + \frac{P_B}{\gamma_w}) \frac{\Delta V}{\Delta h} \qquad \text{(A11.6)}$$

Assuming a uniform burette cylinder, Figure A11.1 indicates that

$$\Delta h = y - (x_2 - x_1) = [V_y - (V_{x_2} - V_{x_1})] \frac{H}{V} = (V_y - \Delta V) \frac{H}{V} \qquad \text{(A11.7)}$$

where H = length of graduated portion of burette

V = volume capacity of burette

Upon substitution of Equation A11.7 into Equation A11.6 then

$$V_A \doteq (h + \frac{P_B}{\gamma_w}) \frac{\Delta V}{(V_y - \Delta V) \frac{H}{V}} \qquad \text{(A11.8)}$$

Here P_B/γ_w = 1034 cm of water, h = 58 cm, V_y = 25 cc, H = 35 cm, V = 25 cc yielding

$$V_A \doteq \frac{156}{\frac{5}{\Delta V} - 0.2}$$

where V_A is taken to represent the air volume in cc within the test sample, and ΔV is the observed burette volume change in cc corresponding to raising the burette within its holder 35 cm in height (25 cc).

A12. COMPLETE DATA--THREE-DIMENSIONAL COMPRESSION EXPERIMENT NO. 13

Initial Data

Wt of dry sand sample = 28.31 lb

Saturation (9 min)

Initial supply reservoir vol	5080 cc
Final supply reservoir vol	2600 cc

Air volume test

Burette base level	Burette reading
25 cc	7.4 cc
0 cc	5.9 cc
25 cc	7.4 cc
0 cc	5.9 cc

Final Data

Wt wet sand + membrane = 34.95 lb

Wt membrane = 1.23 lb

Stress-Strain Data

Table A12.1 presents data for the initial spherical cycles of stress, and Table A12.2 presents data for the following deviatoric stress cycles.

Table A12.1 Stress-Strain Data--Three-Dimensional Compression
Experiment No. 13, Spherical Stress Cycles

Time min	Pres. σ psi	Pressure-Volume Tube Readings V_{B2} cc	V_{B3} cc	V_{B1} cc	Bur. Read. V_B, cc
	5	80.0	80.0	80.0	25.0
0[1]	10	70.7	71.2	71.0	18.5
5	10	70.0	70.7	70.5	18.5
6	15	60.5	63.8	63.2	13.6
	15	59.2	63.0	62.7	13.8
22	20	50.7	57.3	56.8	10.1
	20	49.8	56.8	56.2	10.1
31	25	42.2	52.4	51.4	6.9
	25	41.5	51.8	51.0	6.8
42	30	35.8	48.0	47.0	4.0
	30	35.0	47.2	46.3	3.8
57	25	39.0	49.5	48.4	5.7
	25	39.0	49.5	48.5	5.8
65	20	43.8	52.4	51.4	8.1
	20	44.0	52.7	51.7	8.2
70	15	50.0	56.1	55.3	11.1
	15	50.5	56.5	55.8	11.3
80	10	58.5	61.8	61.2	14.8
	10	59.2	62.4	61.8	15.1
90	5	71.4	71.5	71.8	20.8
	5	73.1	72.5	72.6	21.2
104	10	64.8	65.6	65.0	15.0
	10	64.2	65.2	64.9	15.0
110	15	57.3	60.0	59.2	10.7
	15	56.8	59.3	59.0	10.6
117[2]	18	52.2	56.5	55.9	8.5
127	18	51.7	56.2	55.8	8.5
1296	17.8	48.8	53.5	53.0	12.7
	18	(80.0)	(80.0)	(80.0)	12.6
1300	20	77.2	78.4	78.3	11.6
	20	70.0	78.2	78.2	11.6
1310[3]	25	70.3	74.9	74.5	9.0
	25	70.0	74.5	74.2	8.9
1316	30	64.9	71.5	70.9	6.3
	30	64.3	71.7	70.4	6.1
1326	25	68.2	73.0	72.4	8.0
	25	68.3	73.0	72.4	8.0
1334	20	73.0	75.2	75.0	10.2
	20	73.1	75.4	75.1	10.3
1340	15	78.5	78.4	78.1	13.0
	15	78.8	78.7	78.4	13.1
1349	10	86.0	83.1	83.1	16.6
	10	86.7	83.7	83.7	16.8
1354	5	97.8	92.0	92.5	22.3
	5	99.0	93.0	93.6	22.7
1363	10	92.0	86.8	87.2	16.9
	10	91.5	86.5	87.0	16.8
1369	15	85.0	82.0	81.8	12.6
	15	84.7	81.5	81.4	12.6
1380	18	80.2	79.0	79.0	10.6
	18	80.0	78.8	78.8	10.5
1368	15	83.0	80.5	80.4	12.2
	15	83.2	80.7	80.5	12.2
1390	10	89.0	84.2	84.5	15.9
	10	89.4	84.6	84.8	16.0
1400	5	98.2	92.0	92.6	21.9
	5	99.0	92.8	93.3	22.1
1405	10	92.0	86.6	86.8	16.3
	10	91.6	86.2	86.4	16.3
1410	15	85.2	81.8	81.6	12.2
	15	85.0	81.5	81.4	12.1
1417	18	80.3	78.8	78.8	10.1
1427[4]	18	80.2	78.5	78.5	10.1

Temperature = (1) 26.9°C; (2) 27.0°C; (3) 24.0°C; (4) 25.5°C

Table A12.2 Stress-Strain Data--Three Dimensional Compression
Experiment No. 13, Deviatoric Stress Cycles

Cell Pressures			Press.-Vol. Tube Readings			Bur.Read.
σ_2 psi	σ_3 psi	σ_1 psi	V_{B2} cc	V_{B3} cc	V_{B1} cc	V_B cc
18.00	18.00	18.00	80.0	80.0	80.0	5.0
17.06	14.74	22.20	80.6	82.2	76.5	4.7
			80.7	82.2	76.3	4.7
16.67	13.39	23.94	81.0	83.7	74.5	4.5
			81.0	83.9	74.0	4.5
16.37	12.35	25.27	81.2	85.3	72.5	4.4
			81.3	85.4	72.3	4.4
16.12	11.48	26.40	81.5	87.2	70.5	4.3
			81.6	87.7	69.8	4.2
15.90	10.71	27.39	81.8	89.4	68.0	4.2
			81.8	89.8	67.7	4.2
15.70	10.01	28.29	82.0	92.1	65.3	4.3
			82.0	93.5	63.5	4.2
15.52	9.37	29.11	82.2	95.2	62.0	4.5
			82.2	94.7	61.5	4.5
15.35	8.77	29.88	82.6	100.2	57.3	5.1
			82.8	103.1	54.7	5.2
15.18	8.22	30.60	83.0	106.0	52.2	5.9
			83.0	107.0	51.5	5.9
15.03	7.69	31.28	83.4	114.0	45.5	7.5
			83.8	132.8	27.6	9.0
				(80.0)	(80.0)	
14.89	7.18	31.93	84.0	85.5	75.0	11.1
			84.6	96.0	67.0	12.9
14.75	6.70	32.55	85.0	102.0	62.5	15.2
			85.5	117.3	50.4	18.2
				(80.0)	(80.0)	(0.0)
14.62	6.24	33.14	86.0	90.0	73.0	4.0
			86.7	104.0	62.7	7.5
				(80.0)	(80.0)	(0.0)
14.49	5.80	33.72	87.0	90.0	73.0	4.2
			88.0	109.8	58.8	9.8
				(80.0)	(80.0)	(0.0)
14.37	5.37	34.27	88.5	95.0	70.0	7.0
			89.9	122.5	51.0	15.1
				(80.0)	(80.0)	(0.0)
14.25	4.95	34.80	90.5	105.0	64.0	10.8
			92.8	152.0	28.5	23.7
				(80.0)	(80.0)	(0.0)

Table A12.2 continued

Cell Pressures			Press.-Vol. Tube Readings			Bur.Read.
σ_2 psi	σ_3 psi	σ_1 psi	V_{B2} cc	V_{B3} cc	V_{B1} cc	V_B cc
			94.3	146.0 (80.0)	35.2 (80.0)	25.0
14.37	5.37	34.27	94.2	80.2	79.6	25.3
			94.2	80.2	79.6	25.3
14.49	5.80	33.72	94.2	79.8	79.8	25.1
			94.2	79.8	79.8	25.1
14.62	6.24	33.14	94.0	79.0	80.0	24.8
			94.0	79.0	80.0	24.8
14.75	6.70	32.55	94.0	78.5	80.4	24.5
			94.0	78.4	80.3	24.4
14.89	7.18	31.93	93.8	78.0	80.7	24.0
			93.8	78.0	80.7	24.0
15.03	7.69	31.28	93.7	77.2	80.8	23.5
			93.7	77.2	80.8	32.5
15.18	8.22	30.60	93.7	76.0	81.2	22.8
			93.7	76.0	81.2	22.8
15.35	8.77	29.88	93.6	74.8	81.8	21.9
			93.5	74.0	81.8	21.6
15.52	9.37	29.11	93.3	73.2	82.2	20.9
			93.3	73.2	82.2	20.9
15.70	10.01	28.29	93.1	71.3	82.9	19.5
			93.1	70.7	83.1	19.1
15.90	10.71	27.39	92.8	68.6	83.9	17.6
			92.8	68.6	83.9	17.6
16.12	11.48	26.40	92.3	64.4	85.5	14.6
			92.2	63.0	85.7	13.8
16.37	12.35	25.27	92.0	60.3	87.0	11.5
			92.0	60.3	87.0	11.5
16.67	13.39	23.94	91.3	52.3	89.8	6.2
			91.1	49.5	90.3	4.9 (25.0)
17.06	14.74	22.20	90.5	40.5	94.2	18.9
			90.1	38.0	95.2	17.4
18.00	18.00	18.00	86.0	0.5	113.8	-1.8 (10.0)
			86.0	-3.0	115.0	6.5

A13. CALCULATION OF TEST RESULTS--THREE-DIMENSIONAL COMPRESSION

EXPERIMENT NO. 13

Initial Data

Wt of dry sand sample, $W_s = 28.31$ lb

Vol solids, $V_s = \frac{W_s}{\gamma_s} = \frac{28.31 \times 453.6 \text{ gm}}{2.65 \text{ gm/cc}} = 4846$ cc

Water vol based on initial fill (check only)

$$V_w = 5080 - 2600 = 2480 \text{ cc}$$

Air volume determination (Appendix A11)

$$V_A = \frac{156}{\frac{5}{x} - 0.2} = \frac{156}{\frac{5}{7.4-5.9} - 0.2} = 50 \text{ cc}$$

where x = vol change (cc) for 25 cc equivalent head change

Final Data (use)

Wt wet sand, $W = 34.95 - 1.23 = 33.72$ lb

Wt water, $W_w = W - W_s = 33.72 - 28.31 = 5.41$ lb $= 5.41 \times 453.6 = 2454$ gm

Vol water, $V_w = \frac{W_w}{\gamma_w} = \frac{2454}{1} = 2454$ gm

Vol voids, $V_v = V_w + V_A = 2454 + 50 = 2504$ cc

Total vol, $V = V_v + V_s = 2504 + 4846 = 7350$ cc

Porosity, $n = \frac{V_v}{V} = \frac{2504}{7350} = 0.341$

Void ratio, $e = \frac{V_v}{V_s} = \frac{2504}{4846} = 0.517$

Degree of saturation, $S = \frac{V_w}{V_v} = \frac{2454}{2504} = 98\%$

Stress-Strain Data

Table A13.1 deals with the initial spherical stress cycles. The burette volume change $\Sigma\Delta V_B$ and the graduated pressure-volume tube volume changes $\Sigma\Delta V_{B1}$, $\Sigma\Delta V_{B2}$ and $\Sigma\Delta V_{B3}$ were obtained by differencing the volume readings given in Table A12.1 from the initial point. The volume change $\Sigma\Delta V$ was obtained by adding the rubber penetration correction V_R from Figure A8.4 to the burette volume change $\Sigma\Delta V_B$. Pressure-cell volume change corrections $\Sigma\Delta V_{PCi}$ were calculated by subtracting the graduated tube volume changes $\Sigma\Delta V_{Bi}$ from the sample volume change contributions $\Sigma\Delta V_i$. Section A8.2 gave $\Sigma\Delta V_2 = 0.205\ \Sigma\Delta V$ and $\Sigma\Delta V_1 = \Sigma\Delta V_3 = 0.325\ \Sigma\Delta V$. Figures A13.1, A13.2 and A13.3 present plots of pressure-cell corrections as a calibration for the deviatoric stress test. The calculation of volumetric compressibility is not shown--the method being almost identical to that given by Table A6.1.

Table A13.2 deals with the deviatoric stress cycles. The burette volume change $\Sigma\Delta V_B$ and the graduated pressure-volume tube volume changes $\Sigma\Delta V_{B1}$, $\Sigma\Delta V_{B2}$ and $\Sigma\Delta V_{B3}$ were obtained by differencing the volume readings given in Table A12.2 from the initial point. The pressure-cell corrections V_{PC2}, V_{PC3} and V_{PC1} were obtained by projection of the plots given by Figures A13.1, A13.2 and A13.3 from 18 psi. Corrected pressure-cell volume changes $\Sigma\Delta V_i$ were obtained by addition of the pressure-cell corrections to the graduated tube volume changes $\Sigma\Delta V_{Bi}$. Principal strains were calculated from

$$\epsilon_1, \epsilon_3 = \frac{\Sigma\Delta V_{1,3}}{A_1 L_1} = \frac{\Sigma\Delta V_{1,3}}{[(1.90 \times 14.75)(15.5)]16.387} = 1.428 \times 10^{-4}\ \Sigma\Delta V_{1,3}$$

$$\epsilon_2 = \frac{\Sigma\Delta V_2}{A_2 L_2} = \frac{\Sigma\Delta V_2}{[(12 \times 12)(1.90)]16.387} = 2.23 \times 10^{-4}\ \Sigma\Delta V_2$$

Rubber penetration corrections for volumetric strain V_{R3}, V_{R1} and V_{R2} were taken from Figures A8.6, A8.7 and A8.8 respectively, and added to $\Sigma\Delta V_B$ to obtain the corrected volume change $\Sigma\Delta V$. Volumetric strain was calculated by $\epsilon_v = \Sigma\Delta V/V$. In this case V was taken constant and equal to the initial volume for the deviatoric test (7302.4 cc), thus $\epsilon_v = 1.369 \times 10^{-4}\ \Sigma\Delta V$. The initial volume was calculated from the final volume determination, accounting for the total volume change occurring in the deviatoric test (7350-47.6 = 7302.4 cc).

Tables A13.3 and A13.4 present the two different methods used in calculation of the strain invariants. In Table A13.3, volumetric strain is calculated as the sum of the three principal strains obtained from Table 13.2. In Table A13.4, the volumetric strain from Table A13.2 is used in conjunction with the principal strains ϵ_2 and ϵ_3. Here the major principal strain is calculated by $\epsilon_1 = \epsilon_v - (\epsilon_2 + \epsilon_3)$. The second modified strain invariant was calculated by

$$J_2 = \frac{1}{3}[(\epsilon_1 - \epsilon_2)^2 + (\epsilon_2 - \epsilon_3)^2 + (\epsilon_1 - \epsilon_3)^2]$$

and the third modified and dimensionless strain invariant J_3^* was calculated from $k = 1 - 2[(\epsilon_1 - \epsilon_2)/(\epsilon_1 - \epsilon_3)]$ in conjunction with Figure 3.2 where the analogous terms were $k = -\beta$ and $J_3^* = I_3^*$.

Table A13.1 Calculation of Stress-Strain Results--Three-Dimensional Compression Experiment No. 13, Initial Spherical Stress Cycles and Pressure-Cell Calibration

Pres σ	Bur. Vol. Chg. $-\Sigma\Delta V_B$	Rub. Pen. Corr. V_R	Corr. Vol. Chg. $-\Sigma\Delta V$	σ_2 Pressure-Cell			σ_3 Pressure-Cell			σ_1 Pressure Cell		
				Tube $-\Sigma\Delta V_{B2}$	Sample $-\Sigma\Delta V_2$	Corr. $\Sigma\Delta V_{PC2}$	Tube $-\Sigma\Delta V_{B3}$	Sample $-\Sigma\Delta V_3$	Corr. $\Sigma\Delta V_{PC3}$	Tube $-\Sigma\Delta V_{B1}$	Sample $-\Sigma\Delta V_1$	Corr. $\Sigma\Delta V_{PC1}$
psi	cc x 10	cc x 10	cc x 10	cc x 10	cc x 10	cc x 10	cc x 10	cc x 10	cc x 10	cc x 10	cc x 10	cc x 10
5	0	0	0	0	0	0	0	0	0	0	0	0
10	65	27	38	100	8	92	93	12	81	95	12	83
15	112	53	59	208	12	196	170	19	151	173	19	154
20	149	76	73	302	15	287	232	24	208	238	24	214
25	182	95	87	385	18	367	282	28	254	290	28	262
30	212	109	103	450	21	429	328	33	295	337	33	304
25	192	99	93	410	19	391	305	30	275	315	30	285
20	168	83	85	360	17	343	273	28	245	283	28	255
15	137	60	77	295	16	279	235	25	210	242	25	217
10	99	32	67	208	14	194	176	22	154	182	22	160
5	38	0	38	69	8	61	75	12	63	74	12	62
10	100	27	73	158	15	143	148	24	124	151	24	127
15	144	53	91	232	19	213	207	30	177	210	30	180
18	165	67	98	283	20	263	238	32	206	247	32	215
18	124	67	57	312	12	300	265	19	246	270	19	251
20	134	76	58	342	12	330	283	19	264	288	19	269
25	161	95	66	412	14	398	320	21	299	328	21	307
30	189	109	80	469	16	453	354	26	328	366	26	340
25	170	99	71	429	15	414	335	23	312	346	23	323
•	•	•	•	•	•	•	•	•	•	•	•	•
•	•	•	•	•	•	•	•	•	•	•	•	•
15	128	53	75	280	15	265	258	24	234	265	24	241
10	90	27	63	218	13	205	219	20	199	222	20	202
5	29	0	29	122	6	116	137	9	128	137	9	128
10	87	27	60	196	12	184	203	20	183	206	20	186
15	129	53	76	262	16	246	250	25	225	256	25	186
18	149	67	82	310	17	293	280	27	253	285	27	258

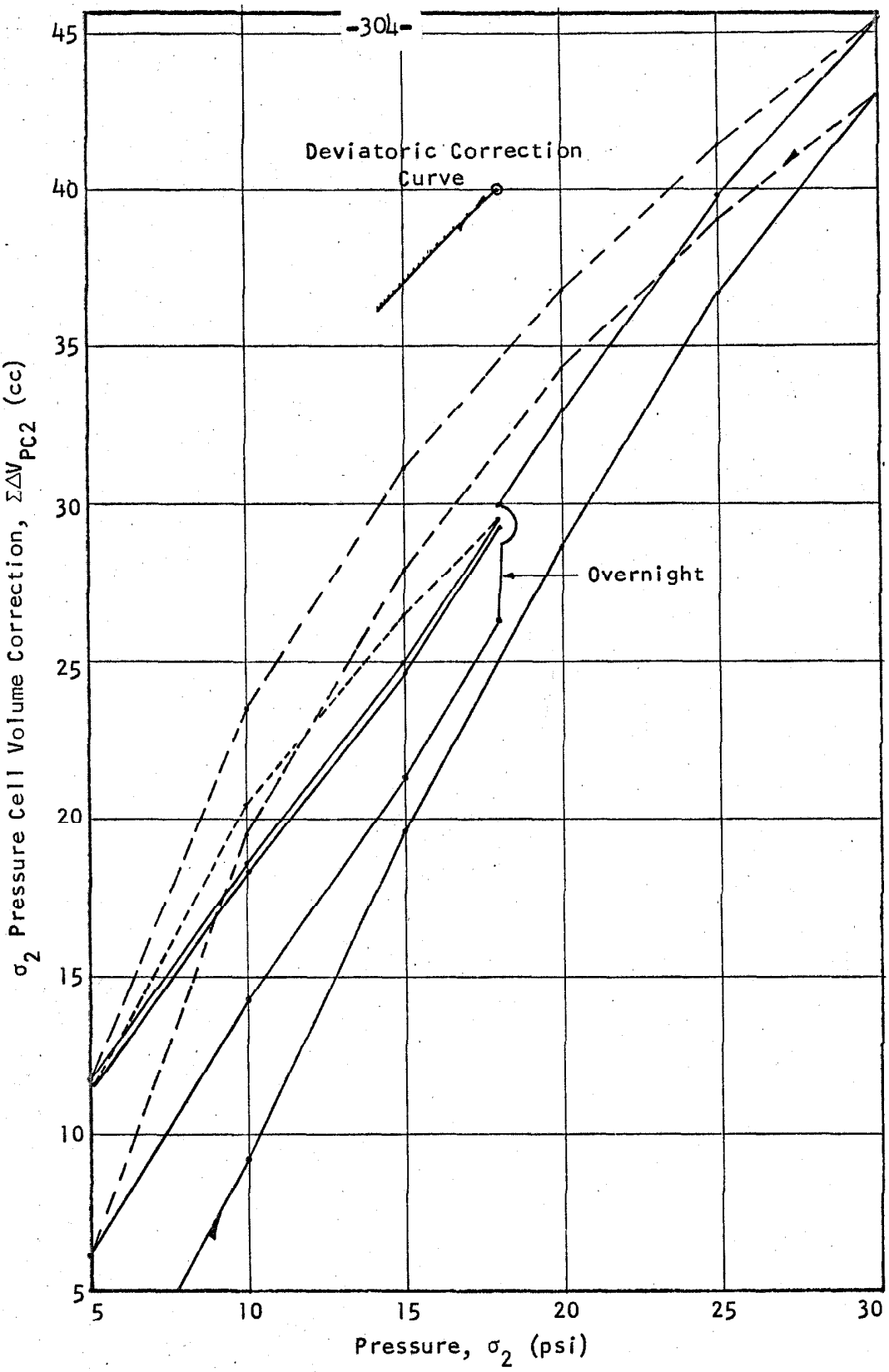

Figure A13.1 σ_2 Pressure-Cell Volume Correction as a Function of Pressure, Experiment No. 13.

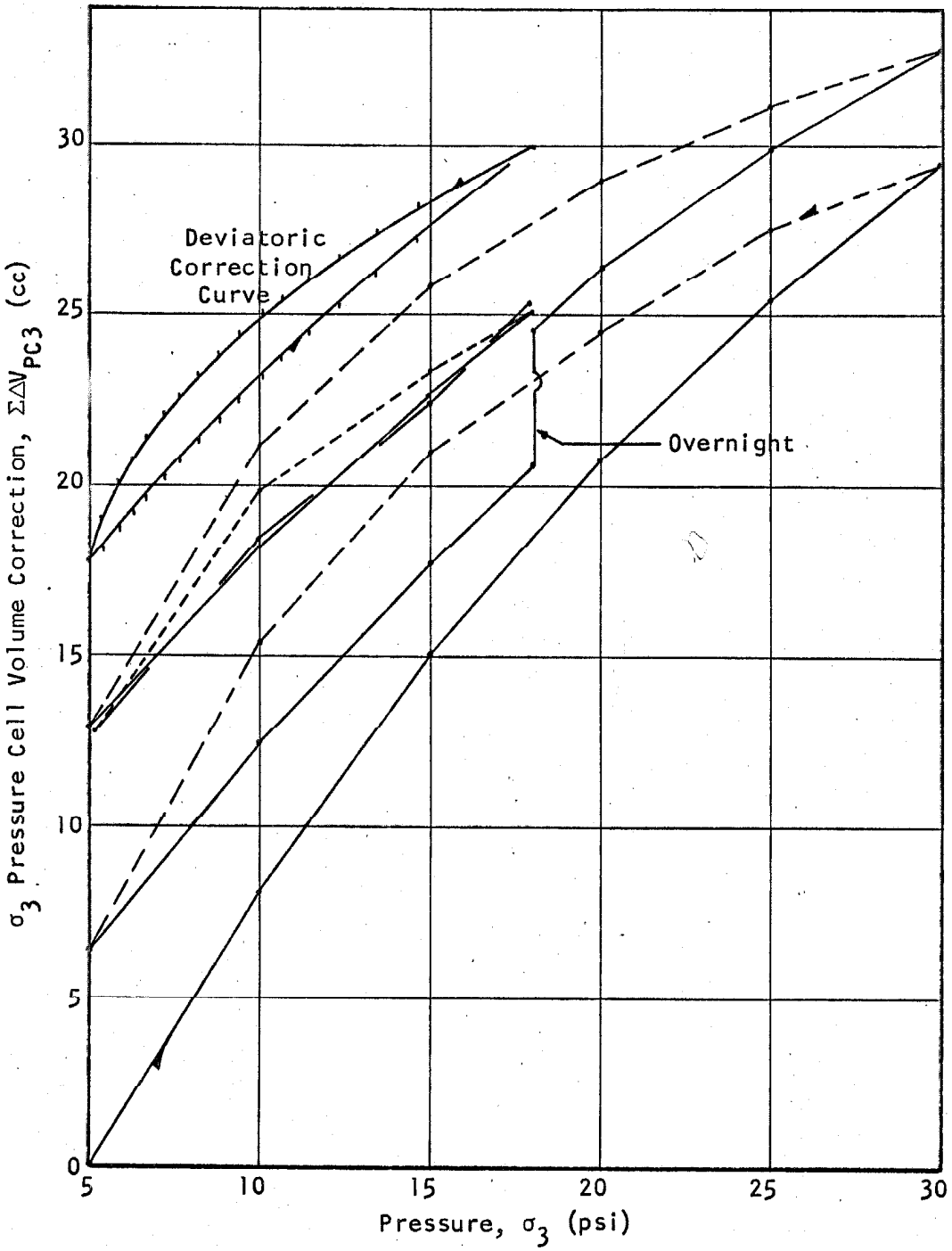

Figure A13.2σ_3 Pressure-Cell Volume Correction as a Function of Pressure, Experiment No. 13.

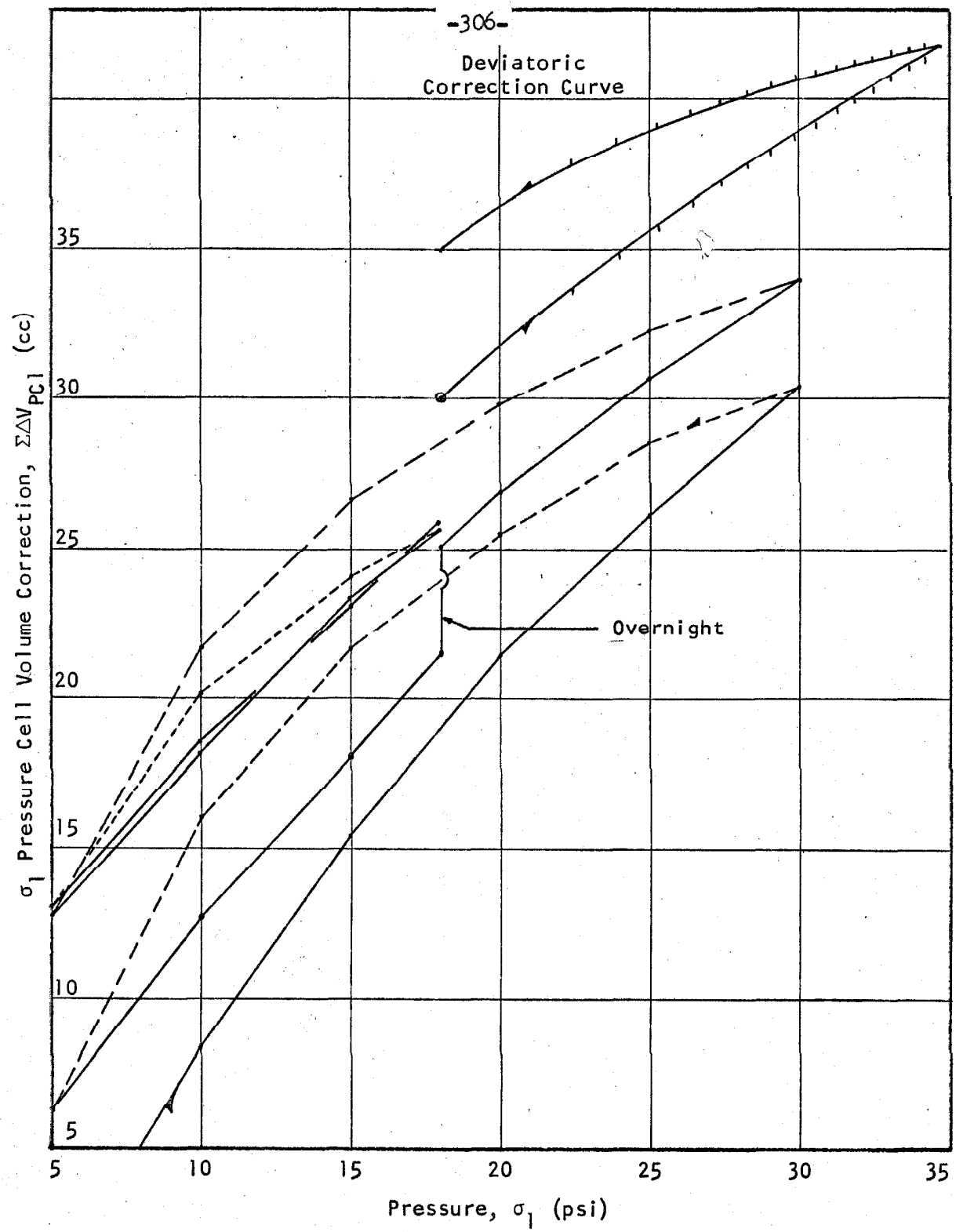

Figure A13.3 σ_1 Pressure-Cell Volume Correction as a Function of Pressure, Experiment No. 13.

Table A13.2 Calculation of Principal Strains--Three-Dimensional Compression Experiment No. 13, Deviatoric Stress Cycles: I_1 = 54 psi, I_3* = 0.6

	Pressure-Cell No. 2				Pressure-Cells No. 3				Pressure-Cells No. 1				Volumetric Strain					
I_2^* x10^2	$\Sigma\Delta V_{B2}$ cc x10	$-V_{PC2}$ cc x10	$\Sigma\Delta V_2$ cc x10	ϵ_2 x10^4	$\Sigma\Delta V_{B3}$ cc x10	$-V_{PC3}$ cc x10	$\Sigma\Delta V_3$ cc x10	ϵ_3 x10^4	$-\Sigma\Delta V_{B1}$ cc x10	V_{PC1} cc x10	$-\Sigma\Delta V_1$ cc x10	$-\epsilon_1$ x10^4	$\Sigma\Delta V_B$ cc x10	V_{R2} cc x10	V_{R3} cc x10	V_{R1} cc x10	$\Sigma\Delta V$ cc x10	ϵ_v x10^4
0	0	0	0	0	0	0	0	0	0	0	0	0	0	0	0	0	0	0
1	7	10	-3	-1	22	18	4	1	37	38	-1	0	-3	-2	-1	1	-5	-1
2	10	13	-3	-1	39	26	13	2	60	49	11	2	-5	-3	-2	2	-8	-1
3	13	17	-4	-1	54	33	21	3	77	58	19	3	-6	-3	-2	3	-8	-1
4	16	19	-3	-1	77	40	37	5	102	66	36	5	-8	-4	-3	3	-12	-2
5	18	21	-3	-1	98	46	52	7	123	72	51	7	-8	-4	-3	3	-12	-2
6	20	23	-3	-1	135	50	85	12	165	78	87	12	-8	-5	-4	4	-13	-2
7	22	25	-3	-1	147	56	91	13	185	82	103	15	-5	-5	-4	4	-10	-1
8	28	26	2	0	231	62	169	24	253	88	165	24	2	-5	-4	4	-3	0
9	30	28	2	0	270	68	202	29	285	92	193	28	9	-6	-5	4	2	0
10	38	30	8	2	528	74	451	65	524	97	427	70	40	-6	-5	4	33	5
11	46	32	4	3	688	80	608	87	654	100	554	79	79	-6	-5	5	72	10
12	55	33	22	5	901	87	814	116	820	105	715	102	132	-7	-6	5	124	17
13	67	35	32	7	1141	93	1048	150	993	108	885	126	207	-7	-6	5	199	27
14	80	36	44	10	1439	100	1339	191	1205	112	1093	156	305	-7	-6	5	297	41
15	99	37	62	14	1864	110	1745	250	1495	114	1381	197	456	-8	-6	5	447	61
16	143	38	105	23	3244	122	3122	446	2458	118	2340	334	943	-8	-7	5	933	128
15	142	37	105	23	3246	118	3128	447	2462	118	2344	335	946	-8	-7	5	936	128
14	142	36	106	24	3242	112	3130	447	2460	116	2344	335	944	-7	-6	5	936	128
•	•	•	•	•	•	•	•	•	•	•	•	•	•	•	•	•	•	•
•	•	•	•	•	•	•	•	•	•	•	•	•	•	•	•	•	•	•
2	111	13	98	22	2939	38	2901	414	2355	85	2270	324	742	-3	-3	3	740	101
1	101	10	91	20	2824	27	2797	399	2306	78	2228	318	666	-2	-2	3	665	91
0	60	0	60	13	2474	0	2474	353	2108	50	2058	294	475	0	0	1	476	65

Table A13.3 Calculation of Strain Invariants Based on ϵ_1, ϵ_2, ϵ_3 Three-Dimensional Compression Experiment No. 13, Deviatoric Stress Cycles

I_2^* x 10^2	ϵ_v x 10^4	ϵ_2 x 10^4	ϵ_3 x 10^4	ϵ_1 x 10^4	J_2 x 10^8	$\frac{\epsilon_1 - \epsilon_2}{\epsilon_1 - \epsilon_3}$	k	$-J_3^*$
0	0	0	0	0	0			
1	0	-1	1	1	2.7			
2	0	-1	2	-2	8.7	0.25	-0.50	-0.74
.	.	.	.	.	.	.	.	.
.	.	.	.	.	.	.	.	.
13	31	7	150	-126	38.1	0.48	-0.04	-0.07
14	45	10	191	-156	60.2	0.48	-0.04	-0.07
15	67	14	250	-197	100.0	0.47	-0.06	-0.10
16	135	23	446	-334	305.0	0.46	-0.08	-0.14
15	135	23	447	-335	306.5	0.46	-0.08	-0.14
14	136	24	447	-335	306.4	0.46	-0.08	-0.14
.	.	.	.	.	.	.	.	.
.	.	.	.	.	.	.	.	.
2	112	22	414	-324	272.7	0.47	-0.06	-0.10
1	101	20	399	-318	257.3	0.47	-0.06	-0.10
0	72	13	353	-294	209.5	0.47	-0.06	-0.10

Table A13.4 Calculation of Strain Invariants Based on ϵ_v, ϵ_2, ϵ_3 Three-Dimensional Compression Experiment No. 13, Deviatoric Stress Cycles

0	0	0	0	0	0			
1	-1	-1	1	-1	2.7	0	-1.00	-1.00
2	-1	-1	2	-2	8.7	0.25	-0.50	-0.75
.	.	.	.	.	.	.	.	.
.	.	.	.	.	.	.	.	.
13	27	7	150	-130	39.2	0.49	-0.02	-0.03
14	41	10	191	-160	61.6	0.48	-0.04	-0.07
15	61	14	250	-203	102.7	0.48	-0.04	-0.07
16	128	23	446	-341	310.3	0.46	-0.08	-0.14
15	128	23	447	-342	311.8	0.46	-0.08	-0.14
14	128	24	447	-343	312.6	0.46	-0.08	-0.14
.	.	.	.	.	.	.	.	.
.	.	.	.	.	.	.	.	.
2	101	22	414	-335	280.7	0.48	-0.04	-0.07
1	91	20	399	-328	264.4	0.48	-0.04	-0.07
0	65	13	353	-301	214.0	0.48	-0.04	-0.07

REFERENCES

1. Reynolds, O., "On the Dilatancy of Media Composed of Rigid Particles in Contact", Phil. Mag. (5), 20, 46, pp. 469-481, (1885).

2. Kezdi, Arpad, Earth Pressure Theories, Berlin: Springer-Verlag, (1962).

3. Coulomb, C. A., "Essai sur une application des regles des maximis et minimis a quelques problemes de statique relatifs a l'architecture", Mem. Acad. Roy. Pres. divers Sav., Vol. 7, Paris, (1776).

4. Rankine, W. J. M., "On the Stability of Loose Earth", Philosophical Transactions, Royal Soc., London, Vol. 147, (1857).

5. Mohr, O., Technische Mechanik, Berlin: Wilhelm Ernst and Sohn, (1906).

6. Capper, P. L., and W. F. Cassie, Mechanics of Engineering Soils, 2nd ed., New York: McGraw-Hill, (1953).

7. Haythornthwaite, R. M., "Mechanics of the triaxial Test for Soils", Proc. ASCE, Jour. Soil Mech. and Found. Div., Vol. 86, No. SM5, pp. 35-62, October, (1960).

8. Kjellman, W., "Report on an Apparatus for Consummate Investigation of the Mechanical Properties of Soils", Proc. 1st Int. Conf. S.M. and F.E., Vol. 2, pp. 16-21, (1936).

9. Wilson, G., and J. L. E. Sutton, "A Contribution to the Study of the Elastic Properties of Sand", Proc. 2nd Int. Conf. S.M. and F.E., Vol. 1, pp. 197, (1948).

10. Bishop, A. W., and A. K. G. Eldin, "The Effect of Stress History", Proc. 3rd Int. Conf. S.M. and F.E., Vol. 1, pp. 100-105, (1953).

11. Habib, P., "Influence de la variation de la contrainte principale moyenne sur la resistance au cisaillement des sols" (Influence of the Variation of the Intermediate Principal Stress upon the Shearing Strength of Soils), Proc. 3rd Int. Conf. S.M. and F.E., Vol. 1, pp. 131, (1953).

12. Jakobson, B., "Some Fundamental Properties of Sand", Proc. 4th Int. Conf. S.M. and F.E., Vol. 1, pp. 167-171, (1957).

13. Kirkpatrick, W. M., "The Condition of Failure for Sands", Proc. 4th Int. Conf. S.M. and F.E., Vol. 1, pp. 172-178, (1957).

14. Peltier, M. R., "Recherches Experimentales sur la Courbe Intrinseque de Rupture des Sols Pulverulents" (Experimental Investigations on the Intrinsic Rupture Curve of Cohesionless Soils), Proc. 4th Int. Conf. S.M. and F.E., Vol. 1, pp. 179-182, (1957).

15. Roscoe, K. H., A. N. Schofield, and C. P. Wroth, "On the Yielding of Soils", Geotechnique, Vol. 8, No. 1, pp. 22-53, March, (1958).

16. Hvorslev, M. Juul, "Physical Components of the Shear Strength of Saturated Clays", Proc. ASCE Res. Conf. on Shear Strength of Cohesive Soils, pp. 169-273, June, (1960).

17. Chaplin, T. K., "Compressibility of Sands and Settlements of Model Footings and Piles in Sand", Proc. 5th Int. Conf. S.M. and F.E., Vol. 2, pp. 33-40, (1961).

18. Wu, T. H., A. K. Loh, and L. E. Malvern, "Study of Failure Envelope of Soils", Proc. ASCE, Jour. Soil Mech. and Found. Div., Vol. 89, No. SM1, pp. 145-181, February, (1963).

19. Hoshino, K., "A Fundamental Theory of Plastic Deformation and Breakage of Soil", Proc. 2nd Int. Conf. S.M. and F.E., Vol. 1, pp. 93, (1948).

20. Hoshino, K., "A General Theory of Mechanics of Soils", Proc. 4th Int. Conf. S.M. and F.E., Vol. 1, pp. 160-166, (1957).

21. Hoshino, K., "An Analysis of the Volume Change, Distortional Deformation and Induced Pore Pressure of Soils under Triaxial Loading", Proc. 5th Int. Conf. S.M. and F.E., Vol. 1, pp. 151-157, (1961).

22. Newmark, Nathan M., "Failure Hypotheses for Soils", Proc. ASCE Res. Conf. on Shear Strength of Cohesive Soils, pp. 17-32, June, (1960).

23. Meyerhof, G. G., "Soil Properties and Their Measurement", Proc. 5th Int. Conf. S.M. and F.E., Vol. 2, pp. 809-818, (1961).

24. Kondner, Robert L., "Hyperbolic Stress-Strain Response: Cohesive Soils", Proc. ASCE, Jour. Soil Mech. and Found. Div., Vol. 89, No. SM., pp. 115-143, (1963).

25. Prager W., and P. G. Hodge, Theory of Perfectly Plastic Solids, New York: Wiley, (1951).

26. Coleman, J. D., "Suction and the Yield and Failure Surface for Soil in Principal Effective Stress Space", Geotechnique, Vol. 10, No. 4, pp. 181-183, December, (1960).

27. Coleman, J. D., and Kenneth Russam, "Some Uses of Stress and Strain Invariants in the Thermodynamic Study of Soil Moisture", Geotechnique, Vol. 11, No. 1, pp. 29-36, March, (1961).

28. Hu, L. W., "Plastic Stress-Strain Relations and Hydrostatic Stress", Proc. 2nd Symp. on Naval Struct. Mech., pp. 194-201, (1960).

29. Haythornthwaite, R. M., "Stress and Strain in Soils", Proc. 2nd Symp. on Naval Struct. Mech., pp. 185-193, (1960).

30. Haythornthwaite, R. M., "Range of Yield Condition in Ideal Plasticity", Proc. ASCE, Jour. Eng. Mech. Div., Vol. 87, No. EM6, pp. 117-133, December, (1961).

31. de Wet, J. A., "The Use of the Energy Concept in Soils Mechanics", Proc. 5th Int. Conf. S.M. and F.E., Vol. 1, pp. 403-406, (1961).

32. Takagi, Shunsuke, "Plane Plastic Deformation of Soils", Proc. ASCE, Jour. Eng. Mech. Div., Vol. 88, No. EM3, pp. 107-151, June, (1962).

33. Deresiewicz, H., "Mechanics of Granular Matter", Advances in Applied Mechanics, Vol. 5, pp. 233-306, New York: Academic Press, Inc., (1958).

34. Newland, P. L., and B. H. Allely, "Volume Changes in Drained Triaxial Tests on Granular Materials", Geotechnique, Vol. 7, pp. 17-34, (1957).

35. Newland, P. L., and B. H. Allely, "Volume Changes During Undrained Triaxial Tests on Saturated Dilatant Granular Materials", Geotechnique, Vol. 9, pp. 174-182, (1959).

36. Rowe, P. W., "The Stress-Dilatancy Relation for Static Equilibrium of an Assembly of Particles in Contact", Proc. Royal Soc. of London, Series A, No. 269, pp. 500-527, Aug.-Oct., (1962).

37. Laszlo, F., "Stability of Granular Masses", Proc. ASCE, Jour. Eng. Mech. Div., Vol. 88, No. EM6, pp. 115-140, December, (1962).

38. Timoshenko, S., and J. N. Goodier, Theory of Elasticity, 2nd ed., pp. 372-382, New York: McGraw-Hill, (1951).

39. Gemant, A., Frictional Phenomena, pp. 411-431, New York: Chemical Publishing Co., (1950).

40. Sokolnikoff, I. S., Mathematical Theory of Elasticity, 2nd ed., New York: McGraw-Hill, (1956).

41. Love, A. E. H., A Treatise on the Mathematical Theory of Elasticity, 4th ed., pp. 92-100, London: Cambridge Univ. Press, (1927).

42. Lode, Von W., "Versuche uber den Einfluss der mittleren Hauptspannung auf das Fliessen der Metalle Eisen, Kupfer und Nickel", Zeitschrift fur Physik, Vol. 36, pp. 913-939, (1926).

43. Balla, A., "Stress Conditions in the Triaxial Compression Test", Proc. 4th Int. Conf. S.M. and F.E., Vol. 1, pp. 140-143, (1957).

44. Bjerrum, L., and O. Kummeneje, "Shearing Resistance of Sand Samples with Circular and Rectangular Cross Section", Norwegian Geotechnical Institute Publication, NR 44, (1961).

45. Bishop, A. W., and D. J. Henkel, The Measurement of Soil Properties in the Triaxial Test, London: Arnold, (1957).

46. Rowe, Peter W., and Laing Barden, "Importance of Free Ends in Triaxial Testing", Proc. ASCE, Jour. Soil Mech. and Found. Div., Vol. 90, No. SM1, pp. 1-26, January, (1964).

47. Kjellman, W., "Do Slip Surfaces Exist?", Geotechnique, Vol. 5, pp. 18-22, (1955).